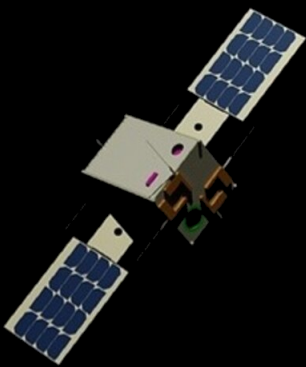


MSc Thesis

On the Design of a Propulsion
System for the Lunar Meteoroid
Impact Observer (LUMIO)

F. A. Nett



MSc Thesis

On the Design of a Propulsion System for the Lunar Meteoroid Impact Observer (LUMIO)

by

F. A. Nett

to obtain the degree of Master of Science
at the Delft University of Technology,
to be defended publicly on Wednesday, 13 October 2021 at 09:30.

Student number:	4717481
Project duration:	February 15, 2021 – October 13, 2021
Examination committee:	Dr. A. Cervone Academic supervisor
	Dr. J. Guo Chairman
	Ir. R. Noomen External member

An electronic version of this thesis is available at <http://repository.tudelft.nl/>.



Preface

This document contains my thesis on the design of a custom propulsion system for the Lunar Meteoroid Impact Observer, conducted in fulfilment of the master of science programme at TU Delft, faculty of Aerospace Engineering. Over a period of roughly an academic year of full-time research, I expanded my knowledge of and my pre-existing interest into the topic of space (micro-)propulsion, an exciting field with important applications for advancing science, by conducting a literature study, generating the designs, and writing this document. I would like to express my sincere gratitude to my supervisor Dr. Angelo Cervone for his guidance and valuable insights. His commitment to the field of micro-propulsion, the faculty and his students is apparent and is greatly appreciated by me. I also want to thank my wonderful family for supporting me during my studies, especially during the Covid-19 pandemic during which this project took place. Finally, it is worth mentioning that towards the end of this project, Dr. Cervone and I collaborated on a paper containing parts of this work, to be presented at the International Astronautical Congress of 2021 in Dubai, United Arab Emirates, titled "Propellant Line Dimensioning for 'Green' CubeSat Mono-Propellant Propulsion Systems". This is an exciting way to conclude my MSc studies, and I am grateful for the opportunity.

F. A. Nett
Delft, September 2021

Contents

Summary	ix
List of Figures	xv
List of Tables	xix
Nomenclature	xxiii
List of Symbols	xxv
1 Introduction	1
1.1 Other CubeSat Missions Beyond Earth Orbit	3
1.2 Research Objectives and Research Questions	4
1.3 Synopsis	5
2 Literature Review	7
2.1 Ideal Rocket Theory	7
2.2 State-of-the-Art of CubeSat and Microspacecraft Propulsion Technology	9
2.2.1 Characterising Technologies	9
2.2.2 Technology Selection	11
2.3 Propellants	13
2.3.1 Chemical Mono-Propellants	13
2.3.2 Resistojet Propellants	14
2.3.3 Cold Gas Propellants	14
2.3.4 Material Compatibility of Selected Propellants	15
2.4 Feed System Layout	17
2.5 Feed System Types	19
2.5.1 Gas-Fed Systems	19
2.5.2 Pump-Fed Systems	21
2.6 Pipe Flow Pressure Loss and Fluid Hammer	26
2.6.1 Straight, Smooth, Circular Tubes	27
2.6.2 Rapid Contraction and Expansion	27
2.6.3 Bends	27
2.6.4 Fluid Hammer	29
2.7 Passive Flow Control Device	31
2.7.1 Uncoupled Passive Flow Control Device	31
2.7.2 Passive Flow Control Device Coupled to the Pump and Thrusters (TVO condition)	32
2.7.3 Passive Flow Control Device Coupled to the Pump only (TVC condition)	33
2.8 Propellant Tank Design	34
2.8.1 Cylindrical Tank Design for the Concept Design Stage	34
2.8.2 Cuboid Tank Design for the Detailed Design Stage	35
2.8.3 Tank Materials	36
2.8.4 Propellant Management Devices	36
2.8.5 Heat Loss and Heating	40
2.9 Commercial-Off-The-Shelf and Experimental CubeSat Propulsion Systems and Components	42
2.9.1 Thrusters	42
2.9.2 Regulator Valves	45
2.9.3 Start/Stop Valves	46
2.9.4 Isolation Valves	47
2.9.5 Latch Valves	48
2.9.6 Fill/Drain Valves	49

2.9.7	Filters	50
2.9.8	Sensors	51
2.9.9	Complete Propulsion Systems	52
3	Concept Design	55
3.1	Design Specifications	55
3.2	Thruster Selection	57
3.2.1	Main Propulsion System Thrusters	57
3.2.2	Reaction Control System Thrusters	58
3.2.3	Discussion of Chosen Thrusters	59
3.3	Thruster Data, Propellants and Pressurants	61
3.3.1	Bradford-ECAPS HPGP 1 N Thruster: Propellant LMP-103s	61
3.3.2	Aurora ARO Thruster: Water Propellant.	61
3.3.3	Additional Assumptions on the ARO Thruster.	62
3.3.4	Selected Pressurant Gas for Concepts: Nitrogen.	63
3.4	Main Propulsion System Propellant Storage & Feed Concepts	64
3.4.1	Pressure Regulated Concept	64
3.4.2	Blow-down Type Concept	66
3.4.3	Pump-Fed Concept.	67
3.5	Reaction Control System Propellant Feed & Storage System Concepts	71
3.5.1	Pressure Regulated Concept	71
3.5.2	Blow-Down Concept	72
3.5.3	Pump-Fed Concept.	73
3.6	Concept Selection	76
3.6.1	Selection of MPS Concept	76
3.6.2	Selection of RCS Concept	77
3.7	Discussion of Selected Concepts	80
4	Detailed Design	81
4.1	Propellant Tank	83
4.1.1	Propellant Management Devices	83
4.1.2	Main Propulsion System Propellant Tank	86
4.1.3	Reaction Control System Propellant Tank.	91
4.1.4	Radiative Heat Loss, Pressurant Gas Expansion and Heating.	93
4.2	Pump-PFCD-Thruster-Regulator System for MPS	95
4.2.1	Thrust Level.	95
4.2.2	Passive Flow Control Device Dimensioning Considerations	95
4.2.3	Pump Requirements and Final Selection	96
4.2.4	Pump-PFCD-Thruster Working Points.	98
4.2.5	Throttling	99
4.3	COTS Component Selection, Integration and Digital Mockup	101
4.3.1	Main Propulsion System Components	101
4.3.2	Reaction Control System Components	102
4.3.3	Integration into Spacecraft Bus	105
4.4	Pressure Drop and Fluid Hammer.	107
4.4.1	Main Propulsion System	107
4.4.2	Conclusion Pressure Loss	109
4.4.3	Feed Line Mass Estimate	110
4.4.4	Fluid Hammer.	110
4.5	Summary of Final Designs and Requirements Compliance	112
4.5.1	Requirements Compliance of the Main Propulsion System	114
4.5.2	Requirements Compliance of the Reaction Control System	116
4.5.3	ECSS and Miscellaneous Requirements	118
4.5.4	Requirements Compliance Discussion	120

4.6	Comparison of Designs to Commercial-off-the-Shelf Systems	121
4.6.1	Commercial-off-the-Shelf System Selection.	121
4.6.2	Comparing Custom Designs to COTS Systems	121
4.6.3	Conclusions on the Comparisons	122
5	Conclusions and Recommendations	125
5.1	Conclusions.	125
5.2	Recommendations	128
	Bibliography	I
A	Requirements	IX
A.1	Main Propulsion System Requirements	IX
A.2	Reaction Control System Requirements	XII
A.3	ECSS Requirements	XIV
A.3.1	Sourced From Tailored Requirements of ECSS-E-ST-35-01C.	XIV
A.3.2	Sourced From Tailored Requirements of ECSS-E-ST-35C Rev. 1.	XIV
A.4	Miscellaneous Requirements	XV
B	State-of-the-Art Propulsion Systems and Thrusters (COTS and Experimental)	XVII
C	Flightworks, inc. Magnetically Coupled Micro-Gear Pumps	XXI
D	CubeSat Standard	XXIII
D.1	12U CubeSat Design Specifications (Outer Dimensions)	XXIV
D.2	12U CubeSat Design Specifications (Extra Volume)	XXV
E	Finite Element Analysis Results	XXVII
E.1	Main Propulsion System	XXVIII
E.1.1	Design Iteration: Reduction of Wall Thickness	XXIX
E.1.2	Sensitivity Analysis for FE-Analysis	XXX
E.2	Reaction Control System.	XXXVI
E.2.1	Sensitivity Analysis for FE-Analysis	XXXVII

Summary

The Lunar Meteoroid Impact Observer (LUMIO) is a CubeSat measuring 3x2x2 CubeSat Units (U) - 12 U - proposed by a consortium of TU Delft, Politecnico di Milano and others to observe, quantify and characterise the impacts of meteoroids on the Lunar far side. Making these observations, the spacecraft will complement Earth-based observations on Near Earth Objects impacting the Lunar near side and improve understanding of the Lunar meteoroid environment. Selected as ex-aequo winner of the Lunar CubeSats for Exploration competition hosted by the European Space Agency, the phase 0 study was conducted to assess its scientific relevance and technical feasibility which resulted in a positive outcome; similarly, the phase A study concluded positively in March of 2021. The spacecraft will be brought into a Lunar parking orbit by a TBD mothership, from where after separation it will independently transfer into a quasi-halo orbit around the Earth-Moon L2 point using its Main Propulsion System (MPS), where the operational phase will take place. For orbital transfer, station-keeping and disposal, the Δv budget has been set at 203 m-s⁻¹; for de-tumbling and reaction wheel de-saturation, the worst-case total impulse budget of the Reaction Control System (RCS) has been conservatively estimated as 170 N-s regardless of thruster placement. To fulfil the purpose of the MPS and RCS, Commercial-Off-The-Shelf (COTS) solutions exist, however often with limited options for customisation. The research objectives of this thesis are to first of all achieve a complete custom design of the LUMIO propulsion system utilising COTS thrusters that fulfils all requirements and secondly to achieve better performance as compared to selected baseline COTS systems judged on the metrics wet mass, volume, power consumption and thrust level.

Prior to this project, a review of scientific literature was conducted on the current state-of-the-art of propulsion systems for CubeSats and microspacecraft. Here, first, 107 experimental and commercially available systems were considered to preliminarily select the most feasible technologies to fulfil the roles of LUMIO's MPS and RCS. This trade-off resulted in the selection of the Chemical Mono-Propulsion (CMP) technology for the MPS and both Cold Gas Thruster (CGT) and Electrothermal (Resistojet) (ETR) technologies for the RCS. Since the requirements have not changed significantly since the literature review phase, this selection is chosen as final. The CMP technology was chosen as most suitable for the MPS due to its specific impulse in the range of 125 - 258 s in combination with the propellant mass to propulsion system wet mass fraction typically resulting in Δv values sufficient for LUMIO, with most of the systems considered populating the higher end of the presented range for specific impulse. The technologies CGT and ETR were selected due to their typical thrust level ranges of 10 mN - 3.6 N and 0.129 mN - 30 mN, respectively, where most systems considered populate the lower ends of the ranges. Furthermore, the CGT and ETR systems considered are characterised by specific impulse values ranging from 30 - 110 s and 48 - 150 s, respectively. Through studying the commercially available propulsion systems CHIPS by VACCO and the MRS-142 CHAMPS by Aerojet Rocketdyne, the experimental hybrid propulsion system by NASA/JPL for interplanetary CubeSat missions and finally the experimental propulsion system of NASA's Green Propellant Infusion Mission, it was concluded that a propulsion system consists of at least but may not be limited to thrusters, propellant/pressurant tanks, Propellant Management Devices (PMD), pressure regulator valves, latch valves, start/stop valves, isolation valves, filters, lines, heaters, pressure transducers and thermocouples.

The selected COTS thruster for the MPS is the ECAPS HPGP 1N thruster by Bradford ECAPS due to its high specific impulse of 231 s, highest TRL of 9 and high volumetric specific impulse. The thruster generates 0.25 N - 1.00 N of thrust at inlet pressure values of 5.50 bar - 22.00 bar. For the RCS, the selection process resulted in the Aurora Resistojet One (ARO) being the most feasible option, due to its high specific impulse of 100 s and the high storage density of its water-based propellant. This thruster generates 1 mN - 4 mN of thrust at an assumed 0.25 - 1.00 bar of thruster inlet pressure and 5 W - 20 W of electric input power. The CGT thrusters for the RCS were both designed for use with gaseous Nitrogen propellant, which at a storage temperature of 300 K and pressure of 50 bar would result in an excessively high required storage volume exceeding the volume requirements for the RCS. Other

popular propellants for the CGT technology include refrigerant R134a or Butane, storable in the liquid phase at 300 K and at acceptable values for pressure. Due to the only propellant specified for use in the thrusters considered being gaseous Nitrogen however, these thrusters were deemed infeasible. The propellant for the ECAPS HPGP 1N thruster is LMP-103s, an ADN-based "green" mono-propellant; for the ARO thruster, the chosen propellant is water as an unspecified "water based propellant" is described by Aurora. Both propellants were determined acceptable considering the requirements, as they are not considered toxic by REACH regulations.

The first step of the propulsion system design process is the concept design phase, consisting of generation and selection of feed system concepts. Here, for both MPS and RCS, a regulated type, a blow-down type and a pump-fed concept was generated. In a regulated type system, propellant and pressurant gas are stored in separate tanks, with a pressure regulating valve between both tanks. This has the advantage of constant propellant tank pressure, typically lower as compared to in a blow-down type system, and can enable constant thruster inlet conditions. Alternatively, propellant and pressurant can be stored in the same tank, using a regulator valve between the tank outlet and the thruster(s) instead. In a blow-down type system, propellant and pressurant gas are typically stored together in the propellant tank and as propellant is expended, the tank pressure drops. This type of concept has the advantage of typically lower complexity and mass as compared to pressure regulated type systems. The pump-fed concept operates similar to a blow-down type system, however a pump is used to provide a pressure differential between the tank and the thruster. Pump-fed systems have the advantage of typically very low propellant tank pressure and therefore light tanks, additionally constant thruster inlet conditions can be achieved similar to a pressure regulated type system, by increasing the pump power over the lifespan of the propulsion system. The most feasible concept for each role (MPS and RCS) was selected based on the metrics total system mass, total system volume, power consumption, thrust level and propellant tank pressure. Here, each concept was awarded positively for a low value for all metrics except thrust level. For the MPS, this selection resulted in a pump-fed system due to its lowest total required volume and lowest required propellant tank pressure; the mass was similar to that of the blow-down type concept and lower compared to that of the regulated type system due to the latter requiring a pressure regulating valve (with typically high mass) between the pressurant and propellant tank. For the RCS, a blow-down type system was chosen due to its lower tank pressure as compared to the regulated type concept and more margin above the propellant vapour pressure as compared to the pump-fed concept.

The design process continues with the detailed design phase, where the first step is to generate the propellant tank design, including mechanical design of the tank and a preliminary design of PMD. For both systems, a conformal tank design was chosen due to the low required tank pressure and highest achievable volumetric efficiency using a cuboid shape for both MPS and RCS. The tank pressure for the MPS is low due to using a pump, the BOL tank pressure for the RCS is set at 1 bar due to a blow-down type feed system being chosen and the inlet pressure of the ARO thruster being 1 bar. The selected tank material for both MPS and RCS is Ti-6Al-4V due to its material compatibility with LMP-103s and water, its superior specific strength properties and similar specific stiffness as compared to stainless steels. The MPS propellant tank is constrained by the height of the spacecraft bus (2U) and 1 U of width due to payload reservations, the free design parameter taken here is therefore the tank length. Assuming isothermal expansion, varying the tank length changes the BOL/EOL pressurant gas volume ratio and therefore the BOL/EOL pressure ratio, influencing bending stress and out-of-plane displacements of the tank walls for a given tank wall thickness, using thin plate theory and assuming all wall edges being simply supported. Out-of-plane displacements of 1 mm were selected conservatively as maximum allowable value. This proved to be design driving - the tank wall thickness required to achieve compliant displacements was higher as compared to the wall thickness required for allowable stress. An optimum for tank length was found using the grid search method, where the wall thickness of each wall for each tank length increment was calculated, resulting in a tank length of 136 mm for the selected width of 94.5 mm and height of 199 mm, all dimensions referring to internal dimensions. Here furthermore a volume penalty was respected, introduced by the PMD: changing the tank length influences vane and fillet volume, in turn influencing the inside volume of the tank. The resulting top/bottom wall thickness is 2.74 mm, side walls 4.47 mm and front/rear walls 3.08 mm, resulting in a tank dry mass of 2.246 kg. The design was verified by FE-analysis in Ansys Workbench, and stresses and displacements

were sufficiently low to apply a design iteration subtracting 1 mm of wall thickness for each wall pair, resulting in an updated tank dry mass of 1.679 kg, a reduction of 25.253%. The RCS tank design in turn was constrained by the BOL/EOL pressure ratio inside the tank where the initial pressure was set at 1.000 bar to accommodate for the maximum thruster inlet pressure and the final pressure set at 0.274 bar to comply with minimum required thrust of 1 mN including a pressure drop margin of 0.024 bar, for the BOL condition no margin was provided in order to prevent excessive inlet pressure of the thruster (assumed BOL inlet pressure of 1 bar). This resulted in an ullage fraction of 27.4% and interior dimensions are 94.5 mm width, 94.5 mm height and 32.344 mm length. Due to the required tank inner geometry being known, the required wall thickness was simply solved for, similarly to the method used for the MPS tanks, using thin plate theory and assuming simply supported tank wall edges. Wall thickness for the sides is 0.495 mm however selected as 1.000 mm and front/rear is 1.450 mm. A tank dry mass of 250.480 g results. Again, FE-analysis in Ansys Workbench was used for verification of the design, however no iterations were made due to the tank dry mass being a smaller fraction of the total propulsion system wet mass as compared to the MPS. FE-analysis was performed using an automatically generated mesh using triangular elements with a minimum of two elements in thickness direction. A preliminary design of the PMDs was generated for both the MPS and RCS tanks. Due to the tanks being of conformal geometry, surface tension devices were selected instead of membrane-type PMD. For both MPS and RCS a sponge-type PMD is used to hold sufficient on-demand propellant for a selected time interval of firing, to be re-filled by vanes. The hold volume of the sponges is assumed to be equal to the free volume in between the sponge plates, using a conservative safety factor of 2 on the hold volume. The sponges will be refilled using single vane-type PMD in ribbon orientation meaning parallel to the tank walls. The width and the wall spacing of the ribbon-type PMD are preliminary set at 1 cm. For the MPS, one vane is placed on the narrow tank side, traveling around the entire inner tank and feeding into the sponge at the tank outlet. Two vanes are placed on the wider tank sides, feeding towards the vane connected to the sponge. For the RCS, a similar configuration is chosen however only two vanes being used in total, all meeting at the sponge and at the opposite end of the tank. Performance of the vanes was calculated assuming choked flow along the vanes. The firing time to calculate the sponge hold volume is 60 s for the MPS and 201.810 s for the RCS, based on a maximum reaction wheel momentum dump of 120 mN-m-s (40 mN-m-s assumed over every body axis). The choked flow along the vanes results in a mass flow rate of $0.035 \text{ kg}\cdot\text{s}^{-1}$ for the MPS and $0.024 \text{ kg}\cdot\text{s}^{-1}$ for the RCS, theoretically enabling constant firing even without the sponges, as mass flow rates are $7.946 \text{ E-4 kg}\cdot\text{s}^{-1}$ for 2 thrusters firing at 0.45 N for the MPS and $4.079 \text{ E-6 kg}\cdot\text{s}^{-1}$ for 1 thruster firing at 4 mN at BOL for the RCS. Finally, fillets were added to all wall edges using a conservatively selected radius of 10 mm. This has two functions in a real scenario: decreasing stress concentrations at the wall edges and preventing excessive fluid build-up around the edges. The total added mass of the sponge is 61 g for the MPS and 9 g for the RCS. The total vane mass is 32 g for the MPS and 7 g for the RCS. The addition of fillets introduced 163 g of mass for the MPS and 84 g for the RCS. Finally, the tanks are covered with 40 layers of MLI, namely crinkled aluminised mylar, weighing 73 g for the MPS and 18 g for the RCS, assuming an effective emissivity of 0.001 for both tanks. A worst-case estimate for radiative heat loss resulted in roughly 6 E-2 W of required heating power for the MPS tank and roughly 1.5 E-2 W for the RCS tank. Another mode of heat loss for the tanks is the expansion of pressurant gas over the propulsion system lifetime. A worst-case estimate assuming isentropic expansion is used resulting in required heating power during firing of roughly E-1 W during firing for the MPS and E-4 W for the RCS.

The next step in the detailed design phase is the pump selection for the MPS, which includes considerations for the thrust level and a custom regulator valve design. For the RCS, this step is skipped. For pump selection, three thrust levels at different thruster inlet pressure values are considered: minimum (5.500 bar, 0.250 N; 13.750 bar, 0.625 N; 22.000 bar, 1.000 N). A shortlist of five micro-gear pumps by Flightworks, Inc. providing the highest pressure differential of all pumps listed is created. A constant thrust level is selected over the lifespan of the spacecraft. Therefore, at End-Of-Life (EOL) condition, the pump must provide a higher pressure differential as compared to Beginning-Of-Life (BOL) conditions. It is already observed that with the low EOL tank pressure of 0.741 bar, the maximum thrust is unattainable with any of the shortlisted pumps. The pump outlet to pump inlet are linked by a Passive Flow Control Device (PFCD) with an orifice diameter of 500 micron in order to set the pump working point. Orifice lengths from 25 mm to 150 mm are considered in steps of 25 mm to find the influence of

PFCD flow rate to its provided differential pressure. Limiting the PFCD dimensions, an orifice length of 50 mm is chosen. PFCD flow rates of below approximately $150 \text{ ml}\cdot\text{min}^{-1}$ are observed to be insufficient to provide a sufficient pressure drop for any of the selected thrust levels, eliminating three pumps from the shortlist. The two remaining pumps provide the same pressure differential of 12.066 bar, sufficient for a constant nominal thrust force selected as 0.450 N. Of these pumps, the lighter pump is selected with still sufficient flow rate at maximum differential pressure of $270 \text{ ml}\cdot\text{min}^{-1}$. This selected pump is model 2222-M04C58. The pump-PFCD system is considered for both Thruster Valves Open (TVO) and Thruster Valves Closed (TVC) conditions to determine the thrust level. At TVC condition, the pump is chosen to operate at constant rotational velocity as compared to the TVO condition. This means that for the TVC condition more mass flow flows through the PFCD resulting in a higher pressure differential, which may exceed pump specifications if the thrust level is not selected properly. Furthermore, due to the throttling requirement of $\pm 10\%$ of nominal thrust, the constant feed pressure towards the regulator valve must be higher than the nominal value. For a nominal thrust level of 0.45 N, all conditions were met - pressure corresponding to a thrust of 0.45 N plus the pressure drop margin of 0.024 bar will not result in excessive pump pressure differential at TVC condition, and some margin from the maximum specified pump pressure differential is present. Therefore, 0.45 N is selected as nominal thrust level for the MPS. Finally, in order to enable throttling, a regulator valve is required in front of each thruster. Due to lack of COTS options, a custom design using the specifications of the MEMS pressure regulator module by GOMSpace/NanoSpace AB as baseline is made, essentially resulting in an upscaled version of this valve, weighing 15 g.

The third step in the detailed design phase is the selection of COTS components, integration of all components and generating a Digital Mockup (DMU). The LUMIO spacecraft bus consists of $3 \times 2 \times 2$ U, where the scientific payload occupies three CubeSat units arranged in the longest direction due to the large inlet baffles designed to reduce incoming stray light. At the rear of the spacecraft (the opposite end of the inlet of the optical system which is pointed at the Lunar surface), the outer, rearward-pointing surfaces of three CubeSat units are unoccupied, where four "tuna can" volumes are available for mounting hardware outside of the typical CubeSat bus volume. The two MPS thrusters are placed inside two of these "tuna cans", diagonally opposed, the "tuna can" volume on the last free surface houses the four RCS thrusters. The nozzles of these thrusters are pointing in Y and Z directions of the CubeSat body reference frame. The placement of the MPS and RCS thrusters puts a useful constraint on the design and placement of other propulsion system components, namely determining the endpoints of the feed system lines and constraining the available build volume for all other components. For the MPS, the Omnidea Hydrazine FDV is selected as fill/drain valve and is connected to the propellant tank using its own port. Redundant pressure transducers are placed just downstream of the tank outlet port towards the feed system to measure tank pressure, the GP:50 miniature 7000 is selected due to its low mass. Thermocouples are RS Pro K-Type. From VACCO, the miniature latch valve V1E10728-01 is selected due to being the lightest version compatible with LMP-103s. The pump as mentioned before is the Flightworks, Inc. 2222M04C58 micro-gear pump. The regulator valves and PFCD from this design step stage are also included. Thrusters are the Bradford/ECAPS HPGP 1 N as mentioned before. For the RCS, a modified VACCO F1D10807-02 is used, scaled down to suit the reduced flow rate, and a FDV by VACCO. The same pressure transducers and thermocouples as for the MPS are used. The latch valve is based on the Moog Latching Valve, an experimental Xenon gas latch valve. Finally, the Aurora Resistojet One (ARO) thrusters are used as mentioned before.

The final step in the detailed design phase is approximating the pressure drop over the feed systems and estimating the worst-case magnitude of fluid hammer pressure surges. For approximating pressure drop, a line inner diameter of 3 mm was used for the MPS and 1 mm for the RCS. After interconnection of all components using propellant feed lines, the segment lengths and bends were known. For the MPS, a pressure drop between pump and regulator of 226.117 Pa was approximated. Between tank and pump, 190.663 Pa resulted and 15.672 Pa between regulator outlet and thruster valve resulted. For the RCS, a total approximated pressure drop of 20.711 Pa resulted. These values of pressure drop are not expected to have a significant influence on the operation of the propulsion system - the approximated values are below the conservatively assumed margin 0.024 bar used in the design. Total feed line lengths (including flow paths through bends and junctions) are 363.448 mm for the MPS and 118.604 mm for the RCS, resulting in a line mass of 20 g for the MPS and 1 g for the RCS. Finally,

fluid hammer was considered using the Joukowski equation to consider a worst-case scenario. The estimated magnitude is 1.026 bar for the MPS and 0.078 bar for the RCS, deemed insignificant.

After the designs were finalised, they were compared to COTS systems. For the MPS, the selected baseline is the Aerojet Rocketdyne MPS-135, as using the other candidates (Busek AMAC and NanoAvionics EPSS) would have resulted in excessive propulsion system wet mass for the Δv requirement, this was estimated using a propellant mass/wet mass fraction ratio ϕ . For the RCS, the same method was used, and the only resulting feasible COTS system is the Aurora ARM, infeasible systems are GOMSpace/Nanoprop 6DOF and the VACCO MiPS CGT. Metrics for comparison are wet mass, volume, power consumption and thrust level. For both the MPS and RCS, wet mass and volume were estimated higher than those of the COTS versions, attributed mostly to a higher level of integration achieved in the COTS systems. Comparing power consumption for the MPS is somewhat inconclusive as it depends on the numbers of thrusters used in the COTS system, which has a total of 8 thrusters in the chosen configuration of two systems. For the RCS, the same power consumption is observed as both the COTS system and the custom solution utilise the same thruster (ARO), which are compared on basis that they are both operated from their maximum thrust level of 4 mN at BOL down to 1 mN at EOL. Finally, the total thrust level of the custom MPS is 0.9 N and for the COTS system it varies from 2 N to 8 N - again, this comparison is somewhat inconclusive as it depends on the number of thrusters used. For the RCS, the same thrust levels are observed.

List of Figures

1.1	Illustrations of CubeSat spacecraft buses.	1
1.2	Mission phases of the Lunar Meteoroid Impact Observer.	2
1.3	Examples of CubeSat missions beyond Earth orbit.	3
2.1	Thrust force versus specific impulse of state-of-the-art CubeSat and small spacecraft thrusters.	10
2.2	Thrust force versus electric power consumption of state-of-the-art CubeSat and small spacecraft propulsion systems.	10
2.3	Propellant mass fraction versus specific impulse and achievable Δv , own work.	11
2.4	Feed system layout examples.	17
2.5	Feed system layout examples, continued.	18
2.6	Simplified diagrams of pressurisation methods for a propellant feed system using pressurant gas, draw.io.	19
2.7	Gas density (isothermal, at 300 K) for pressure values ranging from 1 to 50 bar.	20
2.8	Lunar Flashlight Propulsion Module.	21
2.9	Simplified diagram of pump-fed propulsion system between tank and thruster valves, including recirculation loop and Passive Flow Control Device (stations 2, 3, 4, 5), draw.io.	21
2.10	Pump characteristic and Passive Flow Control Device baseline.	22
2.11	Characteristics of Flightworks, Inc. pump model 2222-M04C58, Python/Matplotlib.	23
2.12	Reynolds number as function of pipe diameter, Python/Matplotlib.	26
2.13	Diagrams for abrupt cross-sectional changes in flows.	27
2.14	Cross-section of flow through a circular tube downstream of a bend, own work.	28
2.15	Dean number as function of constant Reynolds number and bend radius/pipe diameter ratios, Python/Matplotlib.	29
2.16	Bend pressure loss friction factors as function of Reynolds number and constant bend radius/pipe diameter ratios, Python/Matplotlib.	29
2.17	PFCD schematic with local station numbers, draw.io.	31
2.18	PFCD performance example for various mass flow rates of propellant LMP-103s at 300 K, fixed high-pressure side pressure, orifice length of 0.1 m, Python/Matplotlib.	32
2.19	PFCD performance example for various mass flow rates of propellant LMP-103s at 300 K, fixed high-pressure side pressure, orifice length of 0.01 m, Python/Matplotlib.	32
2.20	Cylindrical tank shape used for the concept design stage, draw.io.	34
2.21	Thin, rectangular plate.	35
2.22	Results of thin plate relations for deformations and stresses, Python/Matplotlib.	36
2.23	Examples for non-capillary Propellant Management Devices.	37
2.24	Examples for capillary Propellant Management Devices classified as full-communication devices.	38
2.25	Sponge- and ribbon-vane-type Propellant Management Devices inside the Lunar Flashlight Propulsion Module.	38
2.26	Vane-type and fillet PMD illustrations.	40
2.27	Effective emissivity of aluminised Mylar blankets	41
2.28	Main Propulsion System thruster options.	43
2.29	Main Propulsion System thruster options, continued.	43
2.30	Reaction Control System thruster options.	44
2.31	Regulator valve options.	45
2.32	Start/stop valve options.	46
2.33	Isolation valve options.	47
2.34	Latch valve options.	48
2.35	Fill/drain valve options.	49

2.36 Filter options.	50
2.37 Sensor options.	51
2.38 Complete COTS Main Propulsion System options.	53
2.39 Complete COTS Reaction Control System options.	54
3.1 Ideal required heating power (I) and specific impulse (r) for the Aurora ARO at an expansion ratio of 25, thrust force of 4 mN, Python/Matplotlib.	63
3.2 Selected Flightworks, inc. magnetically coupled micro-gear pump model 2212-M04C49 for the Main Propulsion System concept.	68
3.3 Selected Flightworks, inc. magnetically coupled micro-gear pump model 2212-M03C01 for the Reaction Control System concept.	73
4.1 Hydraulic diagram for the Main Propulsion System, draw.io.	82
4.2 Hydraulic diagram for the Reaction Control System, draw.io.	82
4.3 BOL tank pressure, ullage fraction and pressurant gas mass as function of tank length, Python/Matplotlib.	87
4.4 Von Mises stresses in tank walls at centre of plate as function of tank length, Python/Matplotlib. 87	
4.5 Required tank wall thickness for maximum displacement, Python/Matplotlib.	88
4.6 Final required wall thickness considering maximum displacements, Python/Matplotlib.	88
4.7 Von Mises stress and displacements for the RCS propellant tank, at the centre of the plates, Python/Matplotlib.	91
4.8 Recirculation loop pressure drop as function of volumetric flow rate for different thruster pressure values, Python/Matplotlib.	96
4.9 Recirculation loop Reynolds number and Darcy-Weissbach friction factor as function of volumetric flow rate for different thruster pressure values, Python/Matplotlib.	97
4.10 Pump-PFCD operating point for a constant thrust force of 0.5 N, Python/Matplotlib.	98
4.11 PFCD pressure at all stations for a constant thrust force of 0.5 N, Python/Matplotlib.	99
4.12 Spacecraft bus including "black box" payload, Inventor 2022.	101
4.13 Digital Mockups of Main Propulsion System Components, 1, Inventor 2022.	102
4.14 Digital Mockups of Main Propulsion System Components, 2, Inventor 2022.	102
4.15 Digital Mockups of Main Propulsion System Components, 3, Inventor 2022.	103
4.16 Digital Mockups of Reaction Control System Components, 1, Inventor 2022.	104
4.17 Digital Mockups of Reaction Control System Components, 2, Inventor 2022.	104
4.18 Digital Mockups of Reaction Control System Components, 3, Inventor 2022.	104
4.19 Complete propulsion system integrated into the 12U spacecraft bus, Inventor 2022.	105
4.20 Main Propulsion System DMU, two views, Inventor 2022.	106
4.21 Reaction Control System DMU, two views, Inventor 2022.	106
4.22 Line segments and components of the Main Propulsion System for approximating pressure drop, draw.io.	108
4.23 Approximated pressure per station for the Main Propulsion System, Python/Matplotlib.	109
4.24 Line segments and components of the Reaction Control System for approximating pressure drop, draw.io.	110
4.25 Approximated pressure per station for the Reaction Control System, Python/Matplotlib.	111
D.1 CubeSat Design Specifications for a 12U CubeSat.	XXIV
D.2 CubeSat Design Specifications for CubeSats with extra volume.	XXV
E.1 Von Mises stresses. Maximum: 153.460 MPa, minimum: 0.344 MPa, ANSYS 2019.	XXVIII
E.2 Deformations. Maximum: 0.407 mm, minimum: 8.769 E-5 mm, ANSYS 2019.	XXVIII
E.3 Von Mises stresses after the first design iteration. Maximum: 349.540 MPa, minimum: 0.816 MPa, ANSYS 2019.	XXIX
E.4 Deformations after the first design iteration. Maximum: 0.883 mm, minimum: 1.467 E-4 mm, ANSYS 2019.	XXIX
E.5 Main Propulsion System tank FE-analysis Stress result for 3 mm element size, ANSYS 2019.	XXX
E.6 Main Propulsion System tank FE-analysis Deformation result for 3 mm element size, ANSYS 2019.	XXX

E.7 Main Propulsion System tank FE-analysis Stress result for 5 mm element size, ANSYS 2019.	XXXI
E.8 Main Propulsion System tank FE-analysis Deformation result for 5 mm element size, ANSYS 2019.	XXXI
E.9 Main Propulsion System tank FE-analysis Stress result for 10 mm element size, ANSYS 2019.	XXXII
E.10 Main Propulsion System tank FE-analysis Deformation result for 10 mm element size, ANSYS 2019.	XXXII
E.11 Main Propulsion System tank FE-analysis Stress result for 3 mm element size, after the wall thickness reduction iteration, ANSYS 2019.	XXXIII
E.12 Main Propulsion System tank FE-analysis Deformation result for 3 mm element size, after the wall thickness reduction iteration, ANSYS 2019.	XXXIII
E.13 Main Propulsion System tank FE-analysis Stress result for 5 mm element size, after the wall thickness reduction iteration, ANSYS 2019.	XXXIV
E.14 Main Propulsion System tank FE-analysis Deformation result for 5 mm element size, after the wall thickness reduction iteration, ANSYS 2019.	XXXIV
E.15 Main Propulsion System tank FE-analysis Stress result for 10 mm element size, after the wall thickness reduction iteration, ANSYS 2019.	XXXV
E.16 Main Propulsion System tank FE-analysis Deformation result for 10 mm element size, after the wall thickness reduction iteration, ANSYS 2019.	XXXV
E.17 Von Mises stresses. Maximum: 56.557 MPa, minimum: 0.081 MPa, ANSYS 2019.	XXXVI
E.18 Deformations. Maximum: 0.267 mm, minimum: 6.327 E-5 mm, ANSYS 2019.	XXXVI
E.19 Reaction Control System tank FE-analysis Stress result for 1 mm element size, ANSYS 2019.	XXXVII
E.20 Reaction Control System tank FE-analysis Deformation result for 1 mm element size, ANSYS 2019.	XXXVII
E.21 Reaction Control System tank FE-analysis Stress result for 3 mm element size, ANSYS 2019.	XXXVIII
E.22 Reaction Control System tank FE-analysis Deformation result for 3 mm element size, ANSYS 2019.	XXXVIII
E.23 Reaction Control System tank FE-analysis Stress result for 10 mm element size, ANSYS 2019.	XXXIX
E.24 Reaction Control System tank FE-analysis Deformation result for 10 mm element size, ANSYS 2019.	XXXIX

List of Tables

2.1	Summary of technologies considered for technology selection.	12
2.2	Dry and wet mass data of found propulsion systems and corresponding propellant mass fraction ϕ	12
2.3	Propellant mass and tank volume (Equation (2.38)) required for different chemical monopropellants considering a spacecraft wet mass of 26 kg and a Δv of 203 m-s ⁻¹ as per the requirements in Appendix A, lowest mentioned specific impulse value considered.	14
2.4	Typical liquid RCS propellants for ETR technology at a thrust of 10 mN, storage temperature of 300 K, nozzle expansion ratio of 25, chamber temperature of 750 K, chamber pressure of 11 bar.	16
2.5	Typical RCS propellants for CGT technology at a thrust of 10 mN, nozzle expansion ratio of 25, chamber temperature of 300 K, chamber pressure of 1 bar.	16
2.6	Relevant properties of Helium and Nitrogen for feed system design at 300 K.	20
2.7	Coefficients for the Flightworks, Inc. pump model 2222-M04C58 characteristic line offset.	23
2.8	Approximate test data for determining NPSH of Flightworks, Inc. micro-gear pumps.	25
2.9	Material properties of a Ti-6Al-4V alloy.	34
2.10	Materials compatible with propellant LMP-103s.	37
2.11	Comparison of Propellant Management Device types	39
2.12	Thruster options for the Main Propulsion System.	42
2.13	Relevant thruster data for the Reaction Control System trade-off.	44
2.14	Regulator valve options.	45
2.15	Start/stop valve options.	46
2.16	Isolation valve options.	47
2.17	Latch valve options.	48
2.18	Fill/drain valve options.	49
2.19	Filter options.	50
2.20	Sensor options.	51
2.21	Main Propulsion System COTS candidates.	53
2.22	Main Propulsion System COTS candidates.	54
3.1	Design specifications for MPS and RCS concept generation, requirements from Appendix A.	56
3.2	Main Propulsion System thruster trade-off table.	57
3.3	Reaction Control System thruster trade-off table.	59
3.4	Relevant thruster data for concept generation.	60
3.5	Properties of propellant LMP-103s, interpolated for conditions at 300 K; gas properties for assumed decomposition temperature of 1873.15 K.	61
3.6	Properties of water at 300 K and 1 bar, gas properties at 729 K and 1 bar.	61
3.7	Aurora ARO Thruster properties at nominal conditions.	62
3.8	Aurora ARO Thruster properties at throttled conditions.	63
3.9	Example pressurant gas mass calculation for Helium and Nitrogen gas.	63
3.10	Pressure regulated concept for high and low regulated pressure for the Main Propulsion System.	65
3.11	Properties of blow-down type concepts, for each tank (low duty cycle, isothermal expansion at 300 K).	66
3.12	Pump selection criteria for the Main Propulsion System concept.	67
3.13	Pump characteristics of selected Flightworks, inc. micro-gear pump.	68
3.14	Pump-fed concept for the Main Propulsion System.	69
3.15	MPS pump-fed concept calculation steps in PFCD.	70
3.16	Pressure regulated concept for the Reaction Control System.	71

3.17 Blow-down concept for the Reaction Control System.	72
3.18 Pump selection criteria for the Reaction Control System concept.	73
3.19 2212M03C01 pump data.	74
3.20 Pump-fed concept for the Reaction Control System.	74
3.21 RCS pump-fed concept calculation steps in PFCD.	75
3.22 Relevant data for MPS trade-off.	76
3.23 Trade-off for selecting the most feasible Main Propulsion System concept.	77
3.24 Relevant data for RCS trade-off.	78
3.25 Trade-off for selecting the most feasible Reaction Control System concept.	79
4.1 Vane-type Propellant Management Device design. Surface tension values taken at 25 deg. C, closest available to 300 K.	84
4.2 Sponge-type Propellant Management Device design for worst-case scenario.	85
4.3 Input parameters for the Main Propulsion System tank detail design.	86
4.4 Optimisation results for MPS propellant tank dimensioning using thin plate theory.	89
4.5 Design iteration: reducing wall thickness of the MPS propellant tank: relevant changes.	90
4.6 Sensitivity analysis on the FE-analysis of the Main Propulsion System tank.	90
4.7 Sensitivity analysis on the FE-analysis of the Main Propulsion System tank after the wall thickness reduction iteration.	91
4.8 Thruster and tank conditions (1 thruster firing).	92
4.9 Dimensioning results for RCS propellant tank.	92
4.10 Sensitivity analysis on the FE-analysis of the Reaction Control System tank.	93
4.11 Results for approximate heating required for MPS and RCS.	94
4.12 Thrust level options for the Main Propulsion System.	95
4.13 Shortlist of pumps, data for highest rotational velocity, highest pressure differential attainable. Selected pump marked in bold. Infeasible pumps marked in italics.	97
4.14 Pump-PFCD-Thruster system at BOL, EOL conditions for TVC and TVO conditions.	99
4.15 Custom regulator valve design.	100
4.16 Operating conditions for one thruster.	100
4.17 Required input data for pressure drop approximation for the Main Propulsion System, steady state TVO situation at EOL.	107
4.18 Feed line segments and their pressure drop for the Main Propulsion System. Each station refers to the downstream end of the component.	108
4.19 Required input data for pressure drop approximation for the Reaction Control System, steady state thruster firing at BOL.	109
4.20 Feed line segments and their pressure drop for the Reaction Control System. Each station refers to the downstream end of the component.	110
4.21 Feed line mass estimate for the Main Propulsion System and the Reaction Control System.	111
4.22 Fluid hammer calculations.	111
4.23 Summary of specifications of the Main Propulsion System and the Reaction Control System.	112
4.24 Mass budget for the Main Propulsion System.	112
4.25 Mass budget for the Reaction Control System.	113
4.26 Power budget for the Main Propulsion System.	113
4.27 Power budget for the Reaction Control System.	113
4.28 Requirements compliance check for the MPS. Y = Yes, N = No, TBD = To Be Determined. Requirements PROP.010 - PROP.080.	114
4.29 Requirements compliance check for the MPS. Y = Yes, N = No, TBD = To Be Determined. Requirements PROP.090 - PROP.180	115
4.30 Requirements compliance check for the MPS. Y = Yes, N = No, TBD = To Be Determined. Requirements PROP.190 - PROP.200	116
4.31 Requirements compliance check for the RCS. Y = Yes, N = No, TBD = To Be Determined. Requirements RCS.030 - RCS.070.	116
4.32 Requirements compliance check for the RCS. Y = Yes, N = No, TBD = To Be Determined. Requirements RCS.080 - RCS.170.	117

4.33 Requirements compliance check for the RCS. Y = Yes, N = No, TBD = To Be Determined. Requirements RCS.180 - RCS.200.	118
4.34 Requirements compliance check for the MPS and RCS. Y = Yes, N = No, TBD = To Be Determined. Requirements ECSS.020 until ECSS.080.	118
4.35 Requirements compliance check for the MPS and RCS. Y = Yes, N = No, TBD = To Be Determined. Requirements ECSS.090 until ECSS.140.	119
4.36 Requirements compliance check for the MPS and RCS. Y = Yes, N = No, TBD = To Be Determined. Requirements PLD.150 and SYS.040 until SYS.060.	119
4.37 Comparing the custom design to the commercial-off-the-shelf version. Main Propulsion System.	122
4.38 Comparing the custom design to the commercial-off-the-shelf version. Reaction Control System.	122

Nomenclature

Acronym	Description
ADN	Ammonium Dinitramide
AFRL	Air Force Research Laboratory (US)
ARM-A	Aurora Attitude Control Module
ARO	Aurora Resistojet One
AMAC	Advanced Monopropellant Application for CubeSats
ASCENT	Advanced Spacecraft Energetic Non-Toxic
BoPET	Biaxially-oriented Polyethylene Terephthalate
BOL	Beginning Of Life
CBP	Chemical Bi-Propellant
CGT	Cold Gas Thruster
CHAMPS	CubeSat High Impulse Adaptable Monopropellant Propulsion System
CHIPS	CubeSat High Impulse Propulsion System
CMP	Chemical Mono-Propulsion
COPV	Composite Overwrapped Pressure Vessel
COTS	Commercial-off-the-shelf
CRES	Corrosion Resistant
CSD	Chemical Solid
DMU	Digital Mockup
ECHA	European Chemical Agency
ECSS	European Cooperation for Space Standardization
EDP	Electrodynamic PPT/VAT/MNS
EE	Expulsion Efficiency
EOL	End Of Life
ESA	European Space Agency
ESE	Electrostatic Electropray/FEEP/Colloid
ESEOD	Equivalent Sharp Edge Orifice Diameter
ESH	Electrostatic Hall-effect
ESI	Electrostatic Ion
ETR	Electrothermal (Resistojet)
FDV	Fill/Drain Valve
FE	Finite Element
FEEP	Field Effect Electric Propulsion
FI	Finland
GPIM	Green Propellant Infusion Mission
H	Heater
HAN	Hydroxylammonium Nitrate
HPGP	High Performance Green Propellant
IPA	Isopropyl Alcohol
ITAR	International Traffic in Arms Regulations
JPL	Jet Propulsion Laboratory
LEO	Low Earth Orbit
LFM	Lunar Flashlight Mission
LFPM	Lunar Flashlight Propulsion Module
LUMIO	Lunar Meteoroid Impact Observer

Acronym	Description
MarCO	Mars Cube One
MEMS	Micro Electromechanical System
MEOP	Maximum Expected Operating Pressure
MiPS	(ADN) Micro Propulsion System
MLI	Multi Layer Insulation
MLV	Moog Latching Microvalve
MMH	Monomethylhydrazine
MNS	Magnetic Nozzle System
MON	Mixed Oxides of Nitrogen
MPS	Main Propulsion System
NASA	National Aeronautics and Space Administration (US)
NC	Normally Closed
NEO	Near Earth Objects
NIST	National Institute of Standards and Technology (US)
NLM	National Library of Medicine (US)
NPSH	Net Positive Suction Head
NO	Normally Open
NTO	(Di)nitrogen Tetroxide
PFCD	Passive Flow Control Device
PMD	Propellant Management Device
PPT	Pulsed Plasma Thruster
PT	Pressure Transducer
PTFE	Polytetrafluoroethylene
RCS	Reaction Control System
REACH	Registration, Evaluation, Authorisation and Restriction of Chemicals
ROD	Review-of-Design
SBIR	Small Business Innovation Research
SC	Spacecraft
SE	Sweden
SMIM	Stable Manifold Injection Manoeuvre
STA	Solution Treated & Aged
TBC	To Be Confirmed
TBD	To Be Determined
TC	Thermocouple
TRL	Technology Readiness Level
TVC	Thruster Valves Closed
TVO	Thruster Valves Open
U	CubeSat Unit
UDMH	Unsymmetrical Dimethylhydrazine
US	United States of America
VAT	Vacuum Arc Thruster
WC	Tungsten Carbide

List of Symbols

Symbol	Description	Unit
<i>Greek</i>		
α	Pump flow rate characteristic slope	ml-min ⁻¹ - psi ⁻¹
γ	Specific heat ratio	-
Γ	Van den Kerckhove parameter	-
δ	Displacement	m
Δp	Pressure differential or drop	Pa, bar, psid
Δv	Velocity increment	m-s ⁻¹
ε	Emissivity	-
ζ	Flexural rigidity	N-m
η	Efficiency	-
ν	Dynamic viscosity	Pa-s
ρ	Density	kg-m ⁻³
σ	Stress	Pa
ζ	Surface tension (absolute)	N-m ⁻¹
τ	Valve response time	s
Υ	Stefan-Boltzmann constant (5.670 E-8 W-m ⁻² -K ⁻⁴)	W-m ⁻² -K ⁻⁴
ϕ	Propellant/wet mass fraction	-
Φ	Fill ratio	-
ψ	Minimisation objective function	Pa
ω	Pump rotational velocity	min ⁻¹ , rad- s ⁻¹
<i>Latin</i>		
a_n	Polynomial fit coefficients (n = 0, 1, 2)	ml-min, ml, ml-min ⁻¹
a	Wave celerity	m-s ⁻¹
A	Area	m ²
c	Specific heat	J-mol ⁻¹ -K ⁻¹
C	Constant	-
D	Diameter	m
De	Dean number	-
E	Young's modulus	Pa
EE	Expulsion efficiency	-
f	Darcy-Weissbach friction factor	-
F	Force	N
g_0	Gravitational acceleration at Earth, sea-level (9.80665 m-s ⁻²)	m-s ⁻²
I	Impulse	s, N-s
j	Load factor	-
K	Friction factor	-
K_{con}	Friction factor for rapid contraction	-
K_{exp}	Friction factor for rapid expansion	-

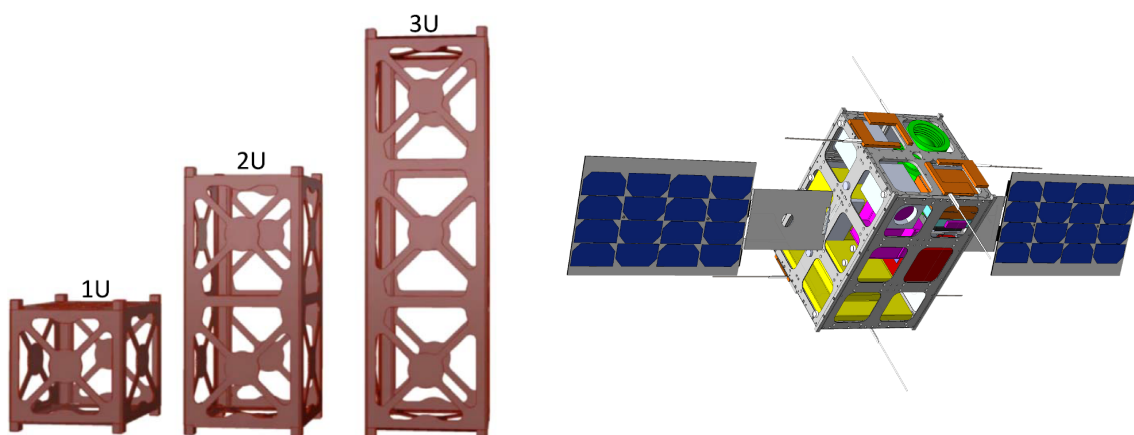
Symbol	Description	Unit
<i>Latin</i>		
<i>l</i>	Length	m
<i>L</i>	Latent heat	J·kg ⁻¹
<i>m</i>	Mass flow	kg·s ⁻¹
<i>M</i>	Mass	kg, g·mol ⁻¹
<i>M</i>	Bending moment	N·m
<i>NPSH</i>	Net Positive Suction Head	m
<i>p</i>	Pressure	Pa
<i>P</i>	Power	W
<i>q</i>	Wave propagation velocity	m·s ⁻¹
<i>r</i>	Radius	m
<i>R</i>	Gas constant	J·kg ⁻¹ ·K ⁻¹
<i>R̄</i>	Universal gas constant (8.3145 J·mol ⁻¹ ·K ⁻¹)	J·mol ⁻¹ ·K ⁻¹
<i>Re</i>	Reynolds number	-
<i>t</i>	Thickness	m
<i>T</i>	Temperature	K
<i>v</i>	Velocity	m·s ⁻¹
<i>V</i>	Volume	m ³
<i>Ṽ</i>	Volumetric flow rate	ml·min ⁻¹
<i>w</i>	Jet velocity	m·s ⁻¹
<i>Subscripts</i>		
<i>a</i>	Available	
<i>b</i>	burn	
<i>be</i>	Bend	
<i>bu</i>	Burst	
<i>boil</i>	Boiling point	
<i>BOL</i>	Beginning Of Life	
<i>c</i>	Curved	
<i>ch</i>	Chamber	
<i>ca</i>	Cavitation	
<i>con</i>	Contraction	
<i>e</i>	Exit	
<i>el</i>	Electric	
<i>exp</i>	Expansion	
<i>EOL</i>	End Of Life	
<i>f</i>	Final	
<i>fil</i>	Fillet	
<i>g</i>	Gas	
<i>h</i>	Hydraulic	
<i>ha</i>	(Fluid) hammer	
<i>he</i>	Heating	
<i>i</i>	Initial, inner	
<i>in</i>	Inlet	
<i>is</i>	Isentropic	
<i>l</i>	Liquid	
<i>max</i>	Maximum	
<i>min</i>	Minimum	
<i>mo</i>	Molar	
<i>MPS</i>	Main Propulsion System	
<i>o</i>	Outer	
<i>old</i>	Old	
<i>new</i>	New	

Symbol	Description	Unit
	<i>Subscripts</i>	
<i>p</i>	Propellant	
<i>p</i>	At constant pressure	
<i>PFCD</i>	Passive Flow Control Device	
<i>pla</i>	Plates	
<i>pres</i>	Pressurant	
<i>pump</i>	Pump	
<i>req</i>	Required	
<i>RCS</i>	Reaction Control System	
<i>s</i>	Straight	
<i>sp</i>	Specific	
<i>st</i>	Surface tension	
<i>spc</i>	Spacecraft	
<i>spo</i>	Sponge	
<i>sto</i>	Storage	
<i>t</i>	Throat, total	
<i>tip</i>	Tip	
<i>tank</i>	Tank	
<i>tube</i>	Tube	
<i>T</i>	Thrust	
<i>u</i>	Ultimate (1.25 load factor)	
<i>us</i>	Usable	
<i>v</i>	At constant volume (gas)	
<i>va</i>	Vane	
<i>vap</i>	Vaporisation	
<i>vm</i>	Von mises	
<i>w</i>	Wet	
<i>wa</i>	Wave	
<i>wall</i>	Wall	
<i>y</i>	Yield (1.10 load factor)	

Introduction

Since its inception in 1999 at Stanford University and California Polytechnic State University, the CubeSat standard has become a popular spacecraft platform for universities, research institutes and industry. Due to standardisation of CubeSat technology and the availability of Commercial-Off-The-Shelf (COTS) components, CubeSats offer an affordable alternative with shorter lead times to traditionally larger and more costly spacecraft. Comprising one or more CubeSat Units (U) each measuring 10x10x10 cm - example configuration shown in Figure 1.1a - these spacecraft are typically launched in a piggyback arrangement alongside larger payloads and/or other CubeSats. Usually CubeSats find their deployment in Low Earth Orbit (LEO) with applications such as technology demonstration or Earth imaging, as discussed by Poghosyan and Golkar in 2017 [2]. Furthermore, a yearly increasing number of patent filings and scientific papers published related to CubeSat technology since 1999 has been observed by Villela et al. in 2019 [3], indicating a growing popularity of the CubeSat standard.

Where most CubeSats launched to date lack an active propulsion system, significantly limiting their lifetime and operational envelope, more ambitious missions have been undertaken and are planned. One such mission is the Lunar Meteoroid Impact Observer (LUMIO, shown in Figure 1.1b), proposed by a consortium of TU Delft, Politecnico di Milano and others. Equipped with optical instrumentation, this 12U CubeSat with a maximum wet mass of 26 kg is planned to observe, quantify and characterise the impact flashes from meteorites on the Lunar far side as discussed by Speretta et al. in 2018 [4] and Cervone et al. in 2020 [5]. Scientific data obtained from this mission will compliment Earth-based observations on near Earth objects impacting the Lunar near side and will ultimately assist in better understanding the composition and formation of our solar system.



(a) CubeSat units in 1, 2 and 3 U configurations, cropped from [2]. (b) The Lunar Meteoroid Impact Observer spacecraft configuration, cropped from [4].

Figure 1.1: Illustrations of CubeSat spacecraft buses.

Selected as ex-aequo winner of the SysNova Lunar CubeSats for Exploration by ESA, an independent phase 0 study was conducted by ESA's Concurrent Design Facility to assess its scientific relevance and technical feasibility, resulting in a positive outcome. Subsequently, the phase A study was conducted and concluded with positive outcome in March of 2021. LUMIO's mission phases are presented in Figure 1.2: after launch, the spacecraft will piggyback on a yet to be determined (TBD) mothership to a selenocentric parking orbit. Once arrived in this parking orbit, LUMIO will separate from the mothership and will independently perform an orbital transfer manoeuvre into a quasi-halo orbit around the Earth-Moon system L2 point, where the operational phase will take place consisting of scientific and navigation cycles for at least one year. Finally, after completion of the operational phase, all spacecraft systems will be decommissioned and the spacecraft will perform an End-Of-Life (EOL) disposal manoeuvre. For orbital transfer, station-keeping and disposal, the required total amount of Δv is determined as 203 m-s^{-1} including margins, to be delivered by the Main Propulsion System (MPS). For de-tumbling and reaction wheel de-saturation, an estimated worst-case total impulse of 170 N-s including margins is required to be delivered by the Reaction Control System (RCS), regardless of RCS thruster placement as stated in the propulsion system requirements in Appendix A.

This thesis delineates the design of a custom propulsion system to fulfil the aforementioned purposes and specifications, and will discuss the performance of this system as compared to selected commercially available systems. Prior to this thesis, a literature study was conducted on the current state-of-the-art of CubeSat and microspacecraft propulsion systems, where 107 commercially available and experimental systems were considered to select the most feasible propulsion technologies. A preliminary trade-off of most feasible technologies was performed and resulted in the selection of the Chemical Mono-Propulsion (CMP) technology for the MPS; for the RCS, both Cold Gas Thruster (CGT) and Electrothermal (Resistojet) (ETR) technologies were selected. Since the requirements for LUMIO's propulsion system have not changed significantly between the end of the literature study phase and the start of this project, this selection is chosen as final. This thesis will contribute to the greater pool of knowledge by presenting design steps for custom CubeSat propulsion systems, which may be advantageous to space engineers and student teams working on similar missions given the observed growing numbers of already completed and planned CubeSat missions deployed beyond Earth orbit.

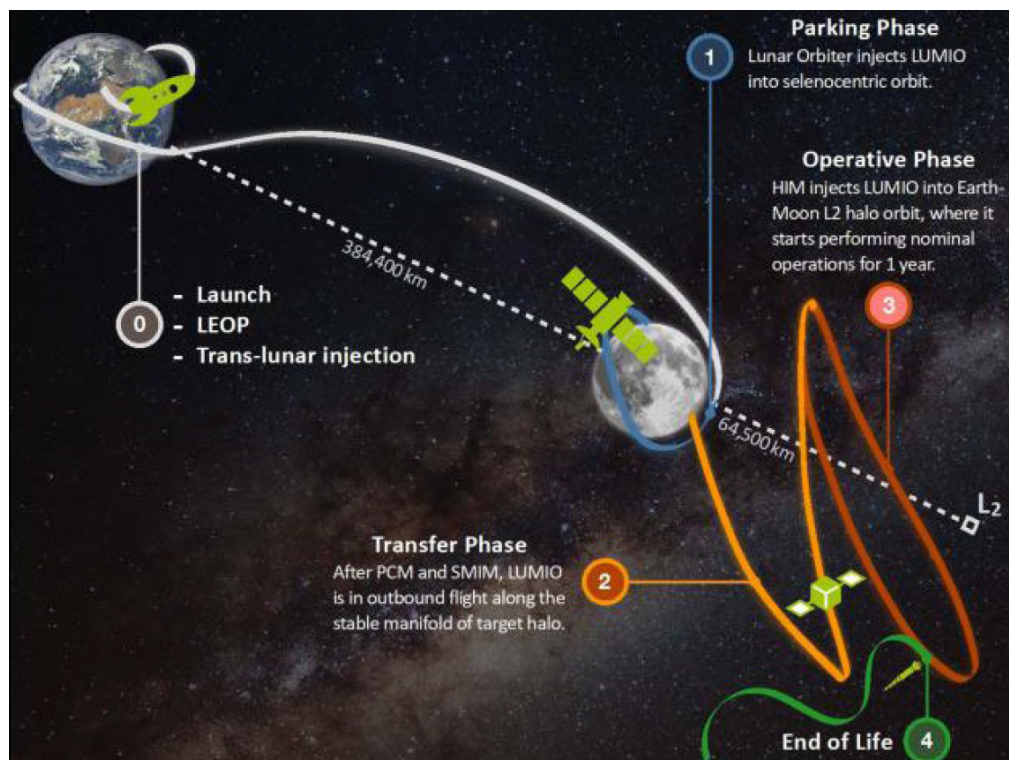
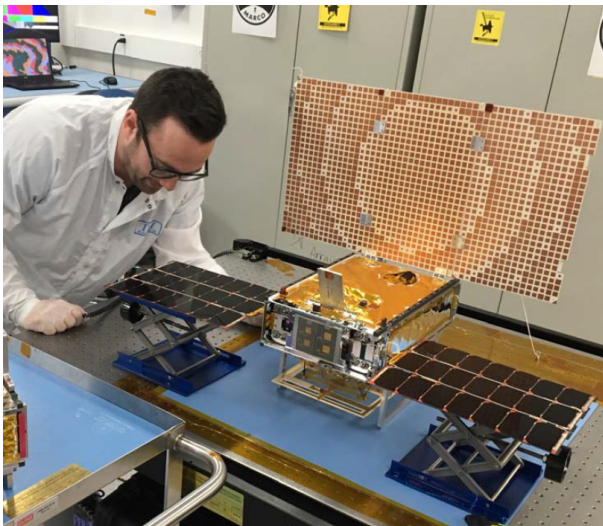


Figure 1.2: Mission phases of the Lunar Meteoroid Impact Observer, cropped from [5].

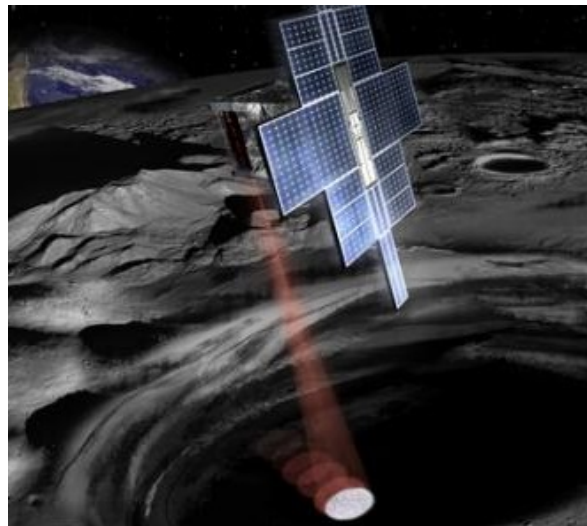
1.1. Other CubeSat Missions Beyond Earth Orbit

Two comparable missions to LUMIO are the NASA/JPL Mars Cube One (MarCO, Figure 1.3a) and Lunar Flashlight missions (Figure 1.3b). The former was launched in 2018 and was the first CubeSat mission beyond Earth orbit. The two 6U CubeSats equipped with UHF and X-band antennae successfully served as bent-pipe communications relay for the Insight lander during its critical Entry, Descent and Landing phase on Mars. Piggybacking alongside the Insight lander, the two CubeSats were deployed into a heliocentric Mars fly-by trajectory during which trajectory corrections and reaction wheel de-saturation manoeuvres were performed by a cold gas propulsion system developed by VACCO. This system used refrigerant R236fa as propellant, providing 40 m/s of Δv for a spacecraft wet mass of 14 kg as discussed by Asmar and Matousek in 2016 [6]. The Lunar Flashlight mission is equipped with instrumentation to search for mineral deposits and water ice on the Lunar south pole. This 6U CubeSat is planned for launch in 2021 alongside the Artemis-I spacecraft and will be deployed in a Lunar polar orbit. Propulsion is provided by the Lunar Flashlight Propulsion Module (LFPM), developed by Georgia Institute of Technology in cooperation with NASA's Marshall Space Flight Centre. This module utilises four thrusters with 'green' mono-propellant AF-M315E to independently perform orbital manoeuvres and RCS duties, delivering a total impulse of 1800 N-s to the spacecraft with a wet mass of 5.5 kg, as discussed by Andrews et al. in 2020 [7] and Huggins et al. in 2021 [8].

Both these missions show contributions to science beyond Earth orbit which would not be possible without employing active propulsion systems. The systems used were designed for significantly differing purposes, use differing technologies and show differing characteristics, further underlining the need for custom propulsion systems.



(a) A technician inspecting a Mars Cube One spacecraft, seen with X-band antenna and solar panels deployed, cropped from [9].



(b) The Lunar Flashlight spacecraft observing a Lunar crater (artist's impression), cropped from [10].

Figure 1.3: Examples of CubeSat missions beyond Earth orbit.

1.2. Research Objectives and Research Questions

The objective of this project is:

1. To achieve a complete design of the LUMIO propulsion system that fulfils all requirements
2. To achieve a better performing system than the selected baseline COTS systems

In order to achieve these objectives and to guide this project, research questions are formulated. These are:

1. What are the most relevant performance and design metrics for the LUMIO propulsion system?
 - (a) If these metrics have an order of importance, what is the order?
2. What are feasible concepts for the propulsion system of LUMIO?
 - (a) What are feasible COTS systems for the propulsion system of LUMIO and what are their characteristics?
 - (b) What COTS systems are chosen as the baseline to compare the in-house designed system to and what are their characteristics?
 - (c) What are the most feasible propulsion system concepts for the in-house design of LUMIO and what are their characteristics?
3. What is the detailed design for the propulsion system of LUMIO?
 - (a) What are the characteristics of this design?
 - (b) How will this system be integrated into the spacecraft?
 - (c) How will the system performance and health be monitored on-orbit?
 - (d) How does this design compare to the COTS baseline systems?
 - (e) What are the most critical requirements for this design?

1.3. Synopsis

The layout of this document is as follows:

- **Chapter 1 - Introduction**

This chapter serves to provide background on the LUMIO mission, to show two examples of comparable missions, and to present research objectives, research questions and the synopsis of the document.

- **Chapter 2 - Literature Review**

The purpose of this chapter is to present the relevant findings from the literature review phase and additional fundamentals added during the thesis phase required for generating the design of LUMIO's propulsion system. This chapter presents ideal rocket theory, the summarised propulsion technology selection process that took place during the literature review phase, different feed system types, pressure loss and fluid hammer in pipe flow, typical propellants for the selected technologies, mechanical relations for tank design, tank materials, and design steps for propellant management devices. Finally, a selection of COTS propulsion systems, thrusters, valves, filters and sensors is presented.

- **Chapter 3 - Concept Design**

In this chapter, first, COTS thrusters are selected for both the MPS and RCS, followed by concept generation of pressurant gas-fed and pump-fed systems. Finally, a trade-off is performed to select the most feasible feed system type.

- **Chapter 4 - Detailed Design**

Knowing the thrusters and feed system types for the MPS and RCS, this chapter contains the design of all custom components and selection of the remaining components: valves, filters, sensors and heaters. The custom components designed here are propellant tanks including Propellant Management Devices and the flow control device for the pump-fed MPS. Furthermore, this chapter presents a digital mockup of the complete propulsion systems for the MPS and RCS and an approximation of pressure loss over the feed systems is made. Finally, requirements compliance is discussed and a comparison between the custom designs and selected COTS systems is made.

- **Chapter 5 - Conclusions and Recommendations**

In this chapter, first, the conclusions drawn are presented by answering the research questions presented in chapter 1. Subsequently, recommendations are given for the work presented and for future work.

2

Literature Review

This chapter discusses the relevant findings from scientific literature during the literature review phase and the thesis phase, including the fundamental theory required for generating the propulsion system design. Furthermore, COTS components and propulsion systems are presented.

First, general relations with respect to thrust force, achievable impulse delivered and achievable velocity changes for a rocket propulsion system are presented. Furthermore, relevant relations from Ideal Rocket Theory (IRT) are considered, relating to flow inside a de Laval nozzle. Secondly, the state-of-the-art of CubeSat and microspacecraft propulsion technology is discussed, including the selection of the most feasible propulsion technologies for LUMIO's MPS and RCS. Thirdly, typical propellants utilised for the selected technologies are discussed and compared. Fourthly, four state-of-the-art COTS and experimental space propulsion systems are considered to determine the typically required components for a propulsion system design. Fifthly, pressurisation systems are considered: pressurant gas-fed and pump-fed systems are discussed. Sixthly, pressure losses in straight, bent, contracting and expanding pipe segments are discussed. Seventhly, propellant tank design is discussed, including wall stress relations and PMD design. Eighthly and finally, COTS and experimental CubeSat propulsion systems and components are presented, to be used in the concept and detailed design for the propulsion system.

2.1. Ideal Rocket Theory

As discussed in George Sutton's Rocket Propulsion Elements, 1992 [11], the thrust force F_T in N of a rocket engine in vacuum is described as:

$$F_T = wm + p_e A_e \quad (2.1)$$

where w is the average gas velocity across the nozzle exit plane in $\text{m}\cdot\text{s}^{-1}$, m is the propellant mass flow in $\text{kg}\cdot\text{s}^{-1}$, p_e is the gas pressure at the exit plane in Pa and A_e is the exit plane area in m^2 . Total impulse I_t in N-s delivered by a rocket engine is described as:

$$I_t = \int F_T dt \quad (2.2)$$

Consider the definition of specific impulse I_{sp} in s:

$$I_{sp} = \frac{I_t}{g_0 M_p} = \frac{\int_0^t F_T dt}{g_0 \int_0^t m dt} \quad (2.3)$$

where M_p is the propellant mass in kg and g_0 is the gravitational acceleration at Earth, sea level ($9.80665 \text{ m}\cdot\text{s}^{-2}$). Ignoring any transients, the thrust F_T of a rocket engine in vacuum can thus also be described as:

$$F_T = I_{sp} g_0 m \quad (2.4)$$

Specific impulse is an important parameter for determining the ideal total attainable velocity change Δv in $\text{m}\cdot\text{s}^{-1}$ in a trajectory, as described by Tsiolkovsky's rocket equation:

$$\Delta v = I_{sp} g_0 \ln \frac{M_i}{M_f} \quad (2.5)$$

where M_i is the mass of the vehicle at the start of the manoeuvre and M_f is the vehicle mass at the end of the manoeuvre. Finally, the ideal exhaust velocity w for propellant gas passing through a de Laval nozzle is calculated according to:

$$w = \sqrt{\frac{2\gamma}{\gamma-1} \frac{\bar{R}}{M_{mo}} T_{ch} \left[1 - \left[\frac{p_e}{p_c} \right]^{\frac{\gamma-1}{\gamma}} \right]} \quad (2.6)$$

where γ is the exhaust gas ratio of specific heats, \bar{R} is the universal gas constant defined as $8314.4626 \text{ J}\cdot\text{K}^{-1}\cdot\text{kmol}^{-1}$, M_{mo} is the molar mass in $\text{g}\cdot\text{mol}^{-1}$, T_{ch} is the chamber temperature in K, p_e is the pressure across the nozzle exit plane and p_c is the chamber pressure, both in Pa. Using a known nozzle area ratio $A_e A_t^{-1}$, the exit-to-chamber pressure ratio of the rocket engine can be solved for using the following relation:

$$\frac{A_e}{A_t} = \frac{\Gamma}{\sqrt{\frac{2\gamma}{\gamma-1} \left[\frac{p_e}{p_c} \right]^{\frac{2}{\gamma}} \left[1 - \left[\frac{p_e}{p_c} \right]^{\frac{\gamma-1}{\gamma}} \right]}} \quad (2.7)$$

here, the dimensionless "Van den Kerckhove" parameter Γ was introduced, which is a function of the ratio of specific heats γ and is defined as:

$$\Gamma = \sqrt{\gamma} \left[\frac{2}{\gamma+1} \right]^{\frac{\gamma+1}{2(\gamma-1)}} \quad (2.8)$$

The critical mass flow m in $\text{kg}\cdot\text{s}^{-1}$, where the flow becomes sonic at the throat, is calculated using:

$$m = \frac{\Gamma p_c A_t}{\sqrt{\frac{\bar{R}}{M_{mo}} T_c}} \quad (2.9)$$

where A_t is the nozzle throat area in m^2 . Through combination of Equation 2.1, Equation 2.6 and Equation 2.9, the throat area of a thruster can be calculated for a given thrust force, chamber pressure, specific heat ratio, pressure ratio and area ratio. It is observed that the chamber temperature T_{ch} is eliminated from the equation:

$$A_t = \frac{F_T}{p_c \Gamma \sqrt{\frac{2\gamma}{\gamma-1} \left[1 - \left[\frac{p_e}{p_c} \right]^{\frac{\gamma-1}{\gamma}} \right]} + \frac{A_e}{A_t} p_c \frac{p_e}{p_c}} \quad (2.10)$$

Finally, as in this project also resistojet thrusters are considered, the power required to vaporise the propellant inside a resistojet and heat it to operating temperatures P_{el} in W is described by:

$$P_{el} = m (c_{p,l}(T_{boil} - T_i) + L_h + c_{p,g}(T_{ch} - T_{boil})) \quad (2.11)$$

where $c_{p,l}$ is the specific heat at constant pressure for the liquid phase, T_{boil} is the boiling point of the propellant at chamber pressure, T_i is the initial propellant temperature, L_h is the latent heat of vaporisation for the propellant in $\text{J}\cdot\text{kg}^{-1}$, $c_{p,g}$ is the specific heat at constant pressure for the gaseous phase. Temperatures are in K and values for specific heat in $\text{J}\cdot\text{kg}^{-1}\cdot\text{K}^{-1}$.

2.2. State-of-the-Art of CubeSat and Microspacecraft Propulsion Technology

During the literature review project, the state-of-the-art of propulsion systems and thrusters for CubeSats and microspacecraft was studied. For this, first, a comparison of 107 propulsion systems and thrusters designed for CubeSat and small spacecraft was made based on thrust force, specific impulse, electric power consumption and propellant mass fraction of propulsion system wet mass. The systems were divided in the following classifications:

- Cold Gas Thruster (CGT)
- Chemical Mono-Propellant (CMP)
- Chemical Bi-Propellant (CBP)
- Chemical Solid (CSD)
- Electrothermal Resistojet (ETR)
- Electrostatic Ion thrusters (ESI)
- Electrostatic Hall-effect thrusters (ESH)
- Electrostatic Electrospray/Field Effect Propulsion (FEEP)/Colloid, grouped as ESE
- Electrodynamic Pulsed Plasma Thrusters (PPT)/Vacuum Arc Thrusters (VAT)/Magnetic Nozzle Systems (MNS), grouped as EDP

Classification was done based on the grouping handled by Fortescue and Stark in 1992 [12] and Kristina Lemmer in 2017 [13]. The systems and thrusters were taken from technology reviews in scientific literature, namely Jürgen Müller in 2010 [14], Khary Parker in 2016 [15], Kristina Lemmer in 2017 [13], Tummala and Dutta in 2017 [16], Weston et al. in 2018 [17] and finally Krejci and Lozano in 2018 [18]. Over the course of the literature study, additional systems and thrusters were found in literature and commercial listings and were added as well.

2.2.1. Characterising Technologies

A comprehensive list of these systems and thrusters is presented in Appendix B, numbered and sorted by classification.

Figure 2.1 shows a log-log plot of specific impulse on the x-axis and thrust force on the y-axis, with 3- σ confidence ellipses to indicate regions of typical performance for each type. Here, typically low thrust force but high specific impulse is observed for electric propulsion technology except for electrothermal technology. Chemical systems are observed to be characterised by higher thrust force, however lower specific impulse as compared to electrostatic and electrodynamic technologies.

Figure 2.2 shows thrust force on the x-axis versus electric power consumption on the y-axis for the electric propulsion systems considered, also in log-log scale. Here it is observed, that ETR and ETH technologies are characterised by the highest thrust force; ETH furthermore is the technology with typically the highest power consumption.

Finally, Figure 2.3 shows the propellant mass fraction of propulsion system wet mass ϕ on the x-axis versus specific impulse on the y-axis, parameters used are shown in Table 2.2. Here, achievable total impulse and Δv contours are added to show the capability of systems considered. For the CMP systems shown, it is important to note that the systems considered are very small, causing a low value of ϕ . It is assumed, that for larger systems such as for LUMIO, of which the propulsion system wet mass may become as high as 6 kg, the ratio ϕ increases due to only an increase in tank dimensions. Another important note here is, that during the literature study phase, the spacecraft wet mass was still set at 24 kg in contrast to the current value of 26 kg (Appendix A.1), however this difference is considered insignificant for the purpose of technology selection. The contour lines were calculated using Equation 2.12 and Equation 2.13 for Δv and I_t , respectively.

$$\Delta v = I_{sp} g_0 \ln \frac{M_{w,spc}}{M_{w,spc} - M_{w,p} \phi} \tag{2.12}$$

$$I_t = \int_{t_0}^{t_1} F_T dt = \int_{t_0}^{t_1} m I_{sp} g_0 dt = m I_{sp} g_0 t_1 = m I_{sp} g_0 \frac{M_p}{m} = I_{sp} g_0 M_{w,p} \phi \tag{2.13}$$

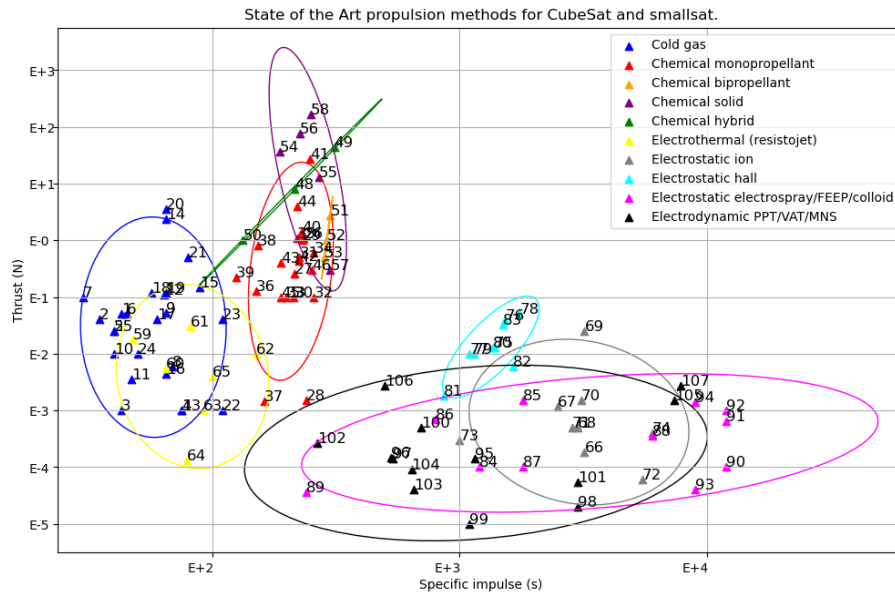


Figure 2.1: Thrust force versus specific impulse of state-of-the-art CubeSat and small spacecraft thrusters [7, 13, 14, 16–37], Python/Matplotlib.

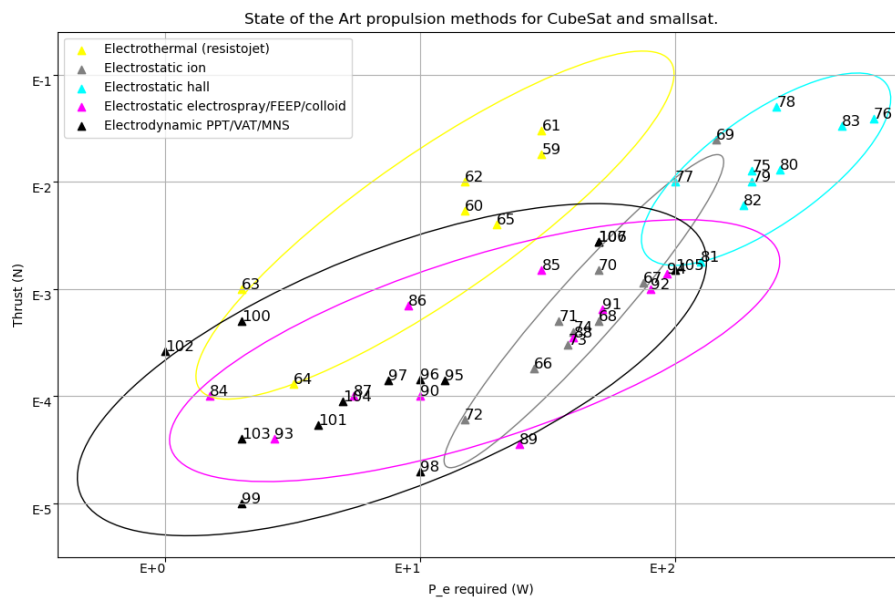


Figure 2.2: Thrust force versus electric power consumption of state-of-the-art CubeSat and small spacecraft propulsion systems [7, 13, 14, 16–37], Python/Matplotlib.

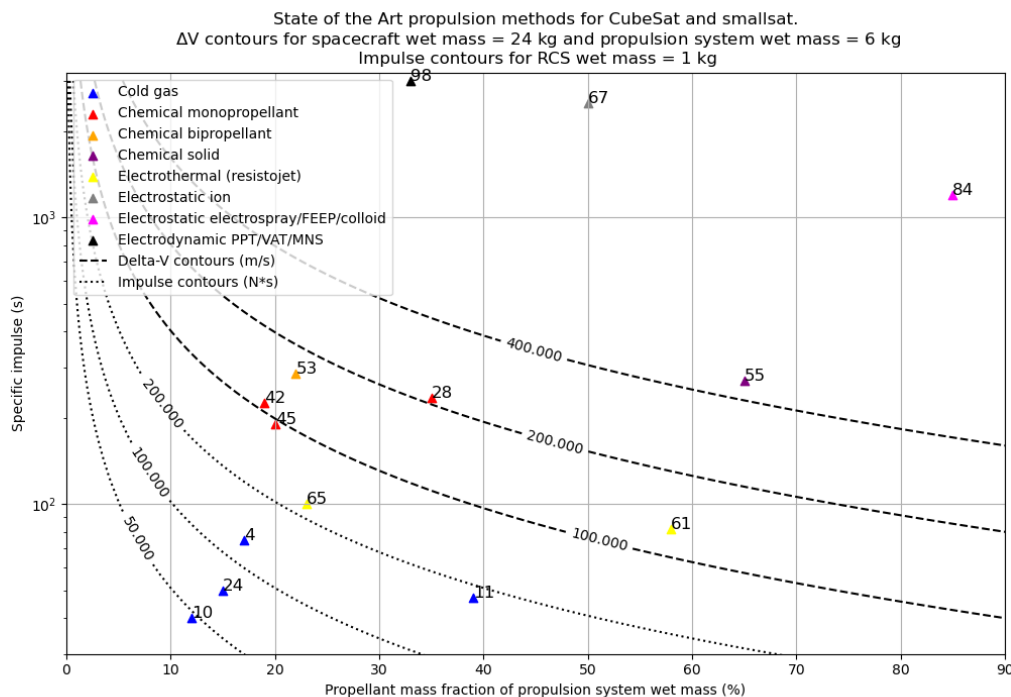


Figure 2.3: Propellant mass fraction versus specific impulse and achievable Δv [7, 13, 14, 16–37], Python/Matplotlib.

2.2.2. Technology Selection

Table 2.1 shows a summary of the technologies considered.

Main Propulsion System

For the MPS, the CMP technology was selected: for this technology, a specific impulse range of 125–258 s is observed, with most of the systems populating the higher end of the range as seen in Figure 2.1; thrust values range from 1.44 mN to 26.9 N with most systems populating the range from roughly 100 mN to 1 N as seen in Appendix B rows 26 - 47. Furthermore, the attainable Δv as shown in Figure 2.3 was deemed acceptable. All other technologies were considered infeasible for the MPS: CGT is infeasible due to its typically unacceptably low specific impulse; CHB is not considered due to the low representation in literature; CBP was not considered due to its low representation in literature; CSD was not considered due to its typical lack of throttling ability; all electric propulsion methods (types starting with E) are infeasible due to their typically low thrust level: LUMIO's MPS thrusters are required to each deliver a thrust force of 100 mN - 1 N (Appendix A.1). Furthermore, these technologies pose a challenge for use in LUMIO due to their typically high electric power consumption.

Reaction Control System

For the RCS, CGT and ETR were selected due to their typical thrust levels being acceptable: systems with 10 mN thrust are observed for CGT, systems with thrust levels between 0.129 mN and 30 mN are observed for ETR. Furthermore, specific impulse ranging from 30 - 110 s for CGT and 48 -150 s for ETR seem to be acceptable considering Figure 2.3, showing close to 200 N-s of total impulse being attainable for CGT, for ETR this is over 200 N-s. CMP, CHB, CBP and CSD are not considered due to their typically high thrust level as compared to the required level of 1-10 mN (Appendix A.2); ESI, ESE, EDP were not considered due to their low thrust level and ESH was not considered due to its thrust-to-power ratio being worse than that of ETR and its excessively high power consumption for the systems considered.

Table 2.1: Summary of technologies considered for technology selection.

Type	# Sys-tems	Rows in App. B	F_T range	I_{sp} range (s)	P_{el} range (W)	Feasible?
CGT	25	1 - 25	10 mN - 3.6 N	30 - 110	n/a	RCS
CMP	22	26 - 47	1.44 mN - 26.9 N	125 - 258	0.2-37	MPS
CHB	3	48 - 50	0.5 N - 44 N	133-311	n/a	No
CBP	3	51 - 53	0.5 N - 2.7 N	285 - 300	n/a	No
CSD	5	54 - 58	0.3 N - 169 N	187 - 300	n/a	No
ETR	7	59 - 65	0.129 mN - 30 mN	48 - 150	2 - 30	RCS
ESI	9	66 - 74	0.06 mN - 25 mN	1,000 - 6,000	28 - 145	No
ESH	9	75 - 83	1.8 mN - 50 mN	865 - 1,650	100 - 600	No
ESE	11	84 - 94	0.04 mN - 1.5 mN	240 - 12,000	1.5 - 93	No
EDP	13	95 - 107	0.01 mN - 2.77 mN	266 - 7,852	2 - 100	No

Table 2.2: Dry and wet mass data of found propulsion systems and corresponding propellant mass fraction ϕ .

Type	ID, Name	I_{sp} (s)	Dry mass (kg)	Prop. mass (kg)	Wet mass (kg)	ϕ	Ref.
CGT	#4 - CubeSat MEMS (NanoSpace)	75	0.25	0.05	0.3	17%	[15]
CGT	#10 - MiPS (VACCO)	40	0.403	0.053	0.456	12%	[14]
CGT	#11 - PUC (CU Aerospace)	47	0.45	0.27	0.72	38%	[15]
CGT	#24 - NanoProp 6DOF (GOMSpace)	50	0.682	0.122	0.804	15%	[19]
CMP	#28 - MPS-130 (Aerojet)	235	1.1	0.6	1.7	35%	[22]
CMP	#42 - AMAC (Busek)	225	1.2	0.29	1.49	19%	[15]
CMP	#45 - Argomoon (Vacco)	190	1.43	0.42	2.065	20%	[26]
CBP	#53 - PM200 (Hyperion Tech.)	285	1.1	0.31	1.41	22%	[31]
CSD	#55 - STAR 4G (ATK)	269	0.52	0.98	1.5	65%	[14]
ETR	#61 - CHIPS (CU Aerospace)	82	0.5	0.7	1.2	58%	[15]
ETR	#65 - ARM-A (Aurora)	100	0.23	0.07	0.3	23%	[33]
ESI	#67 - BIT-3 (Busek)	2,500	1.5	1.5	3	50%	[15]
ESE	#84 - S-iEPS (MIT)	1,200	0.018	0.1	0.118	85%	[15]
EDP	#98 - μ CAT (GWU)	3,000	1	0.5	1.5	33%	[15]

2.3. Propellants

As discussed in the previous section, the selected technologies for LUMIO's propulsion system are CMP, CGT and ETR. This section discusses the literature review findings on the propellants relevant for these technologies. An important consideration for propellants is furthermore the material compatibility, which describes whether the propellant will not degrade in contact with a given material and furthermore whether the given material will not degrade when in contact with the propellant, discussed only for the selected propellants, in the last subsection.

2.3.1. Chemical Mono-Propellants

Hydrazine propellants have significant space propulsion heritage and as a popular mono-propellant its major advantages are being Earth-storable and being characterised by modest specific impulse ranging from 225-250 s with a density of 1.00 g-cc^{-1} . Major disadvantages of hydrazine however are high toxicity, low vapour pressure and a high risk of auto-combustion at room temperature and pressure as described by Kristina Lemmer in 2017 [13]. A possible outlawing of this propellant is indicated by the European Chemical Agency (ECHA) after their listing of Hydrazine as a "substance of high concern", furthermore handling of this propellant is costly due to all aforementioned problems as discussed by Gohardani et al. in 2014 [38]. Significant efforts were undertaken for development of safer alternatives to Hydrazine, most notably on Ammonium Dinitramide (ADN) and Hydroxylammonium Nitrate (HAN) based propellants.

In the US, efforts by the Air Force Research Laboratory (AFRL) focused on development of HAN-based propellants, resulting in the propellant AF-M315E. Also called "Advanced Spacecraft Energetic Non-Toxic" (ASCENT) propellant, this propellant is characterised by specific impulse ranging from 250 s - 257 s and a density of 1.47 g-cc^{-1} as described by Sackheim and Masse in 2014 [39] and Ronald Spores in 2015 [21].

In Europe, efforts were focused on ADN-based mixtures, most notably by the Swedish Defence Research Agency and Bradford bECAPS (Sweden), resulting in propellants LMP-103s and FLP-106. LMP-103s is so far observed as the most popular of this new generation of "green" mono-propellants, with significant flight heritage of the specially designed Bradford ECAPS High Performance Green Propellant (HPGP) 1N thrusters utilising this propellant having reached TRL 9; 12 systems featuring 46 of such thrusters are on orbit as of 2021 as stated by Bradford ECAPS in a news release in 2021 [40]. LMP-103s is characterised by a specific impulse of 245 s - 253 s and a density of 1.26 g-cc^{-1} as discussed by Sackheim and Masse in 2014 [39] and Gohardani et al. in 2014 [38].

For both AF-M315E and LMP-103s, significantly higher volumetric specific impulse (ρI_{sp}) performance is observed as compared to Hydrazine, however typically much higher required temperature for decomposition. This temperature is in the order of 1,600 degrees Celsius for the ECAPS HPGP 1N thruster as specified by Persson et al. in 2012 [41] as compared to hydrazine for which chamber temperatures of 850-1,150 degrees Celsius are typical as discussed by Gohardani et al. in 2014 [38], translating to much more stringent material and thermal management requirements for the thruster hardware and higher required catalyst bed pre-heating power.

In Table 2.3, a comparison based on the aforementioned data from literature is presented, considering LUMIO's requirements (Appendix A). It is observed that AF-M315E scores favourable as it results in the lowest values for required propellant mass and tank length. For both LMP-103s and AF-M315E, the total amount of propellant can be stored in cylindrical tanks of less than 3U of volume. For Hydrazine, much worse volumetric specific impulse performance is observed, resulting in the largest required tank length. The required cylindrical tank length for a given radius is calculated according to Equation 2.38.

Table 2.3: Propellant mass and tank volume (Equation (2.38)) required for different chemical mono-propellants considering a spacecraft wet mass of 26 kg and a Δv of 203 m-s⁻¹ as per the requirements in Appendix A, lowest mentioned specific impulse value considered.

Quantity	Hydrazine	LMP-103s	AF-M315E
I_{sp}	225 s	245 s	250 s
ρ_p	1,004 kg-m ⁻³	1,238 kg-m ⁻³	1,470 kg-m ⁻³
ρI_{sp}	225.9 g-s-cc ⁻¹	303.3 g-s-cc ⁻¹	367.5 g-s-cc ⁻¹
M_p	2.285 kg	2.107 kg	2.066 kg
V_p	2.276 E-3 m ³	1.702 E-3 m ³	1.406 E-3 m ³
Total cylindrical tank length (radius 0.048 m)	0.346 m	0.267 m	0.226 m

2.3.2. Resistojet Propellants

In contrast to the mono-propellants mentioned in Section 2.3.1, no decomposition of the propellant takes place inside resistojet thrusters. The energy required to accelerate the propellant through the nozzle originates from both the potential energy (feed pressure) and the electrical (typically resistive) heating of the propellant. Typically, a liquid propellant is used, for which a low molar mass is desirable in achieving a high exhaust velocity as seen in Equation 2.6. Additionally, a low latent heat of vapourisation is desirable from a power consumption perspective as seen in Equation 2.11.

A selection of typical resistojet propellants observed from Appendix B and publications by Jürgen Müller in 2000 [42] and Tummala and Dutta in 2017 [16] is presented in Table 2.4. Here, calculations are made using relations presented in Section 2.1, assuming storage temperature $T_{storage}$ of 300 K, a nozzle area ratio of 25, chamber temperature T_c of 750 K, storage and chamber pressure p_c of 11 bar and finally a thrust level F_T of 10 mN. For these constant properties, it is observed that water has the best volumetric specific impulse performance due to its density being significantly higher at only a small difference in molar mass as compared to Ammonia. This can most clearly be seen by observing the required spherical tank inner diameter D_i which is 6.96 cm for Ammonia, 6.20 cm for water in comparison to the higher values 7.35 cm and 8.57 cm of Methanol and Butane, respectively.

A major disadvantage of water however is its comparably high required heating power, with its latent heat of vapourisation ΔH_{vap} being significantly higher than that of the other propellants. It is important to note, that the propellant gas specific heats are assumed constant in these calculations at the vaporisation temperature. Increasing the chamber temperature therefore would further decrease the accuracy of the model. All losses in this theoretical model are neglected and therefore these calculations only serve to allow for a preliminary comparison between propellants. It can be concluded from this model however, that water and Ammonia are the best performing resistojet propellant due to their high volumetric specific impulse and significantly lower required storage volume as compared to Methanol and Butane.

2.3.3. Cold Gas Propellants

Similar to resistojet thrusters, no decomposition takes place in a Cold Gas Thruster (CGT) either, however the energy to accelerate the propellant through the nozzle purely originates from potential energy, namely the storage pressure of the propellant, as discussed by Jürgen Müller in 2000 [42, 43]. Characterised by limited specific impulse performance however also by low power consumption and low complexity due to not requiring a catalyst or thruster heaters, CGT are a popular choice for RCS in spacecraft. Similar to resistojet thrusters, exhaust velocity of a CGT is a function of molar mass, being proportional to the inverse of the square root of propellant molar mass as observed from Equation 2.6. Therefore, a propellant with low molar mass is desirable, however propellants with low molar mass may result in excessive storage volume unless the propellant is storable in the liquid phase. Furthermore, spacecraft contamination issues may arise from using gaseous non-benign propellants with low molar mass leaking into the spacecraft, where the likelihood of leakage problems is related to the inverse of molar mass. Popular propellants may therefore considering aforementioned desirable characteristics be gaseous Nitrogen or liquid Ammonia.

Table 2.5 shows a selection of CGT propellants, considering the requirements for LUMIO's RCS (Appendix A). Storage and chamber temperature T_{sto} and T_{ch} are both assumed constant at 300 K to grant comparative measure, storage pressure p_{sto} is set at 11 bar to enable storage of all propellants are in the liquid phase, except for Nitrogen which is stored at 50 bar in the supercritical phase to achieve higher density. Here it is observed, that in order to achieve the required total impulse delivered, gaseous Nitrogen propellant is infeasible for LUMIO due to its low density and resulting high required storage volume, observed from the high spherical tank inner diameter D_i of 19.830 cm. However, the propellants able to be stored in liquid phase are feasible given their required storage volume. Here, Ammonia performs best with the lowest required propellant mass and lowest propellant volume, due to its comparatively low molar mass and resulting highest specific impulse.

2.3.4. Material Compatibility of Selected Propellants

As propellant LMP-103s was selected for the MPS and water was selected as propellant for the RCS, the compatibility with metals is required to be known. LMP-103s is compatible with the materials Ti-6Al-4V and stainless steels for storage of propellant as stated by Persson et al. in 2019 [23]. Stainless steel alloys such as 304 type alloys are known for their corrosion-resistant properties to water as discussed by Kumar et al. in 2005 [44] and are used in applications where corrosion resistance is important such as piping for water cooling systems in nuclear reactors as discussed by [45]. Therefore, stainless steels are assumed compatible with water for the purpose of LUMIO's propulsion system.

The alloy Ti-6Al-4V is used in a wide range of applications from aerospace tank materials as discussed by Persson et al. to biomedical applications where it is used for its corrosion resistance as discussed by Kumar et al. in 2010 [46]. Therefore, the materials Ti-6Al-4V and stainless steels (e.g. 304, 304L, 301) are assumed fully compatible with the propellants LMP-103s and water for the purpose of LUMIO's propulsion system.

For components where less strength is required, such as PMDs, Aluminium alloys may be of interest. These however are not compatible with LMP-103s as stated by [47], and therefore will not be considered for the MPS. Due to corrosion risks being present for Aluminium alloys in contact with water as discussed by Liu et al. in 2016 [48], these alloys are also not considered for the RCS.

Finally, as discussed by Friedhoff, et al. of Bradford/ECAPS in 2017, the ECAPS HPGP 1N thruster utilising LMP-103s propellant is equipped with a series redundant solenoid valve using Polytetrafluoroethylene (PTFE) seats. For valve selection therefore the acceptable materials for use with LMP-103s are taken as Ti-6Al-4V, CRES variants and PTFE.

Table 2.4: Typical liquid RCS propellants for ETR technology at a thrust of 10 mN, storage temperature of 300 K, nozzle expansion ratio of 25, chamber temperature of 750 K, chamber pressure of 11 bar [42, 49].

Quantity	Ammonia	Water	Methanol	Butane
Required	10.62 bar	1 bar	1 bar	2.58 bar
p_{sto}				
Chosen	11 bar	11 bar	11 bar	11 bar
p_{sto}				
ρ	598.20 kg-m ⁻³	882.62 kg-m ⁻³	660.32 kg-m ⁻³	494.33 kg-m ⁻³
M_{mo}	17.03 g-mol ⁻¹	18.02 g-mol ⁻¹	32.04 g-mol ⁻¹	58.12 g-mol ⁻¹
R_g	488.22 J-kg ⁻¹ -K ⁻¹	461.40 J-kg ⁻¹ -K ⁻¹	259.50 J-kg ⁻¹ -K ⁻¹	143.06 J-kg ⁻¹ -K ⁻¹
$c_{p,l}$	4,744.57 J-kg ⁻¹ -K ⁻¹	4,181.52 J-kg ⁻¹ -K ⁻¹	2,496.88 J-kg ⁻¹ -K ⁻¹	2,278.39 J-kg ⁻¹ -K ⁻¹
L_{vap}	1,159,700 J-kg ⁻¹	2,437,300 J-kg ⁻¹	1,173,533 J-kg ⁻¹	385,409 J-kg ⁻¹
$c_{p,g}$	2,172.64 J-kg ⁻¹ -K ⁻¹	1,930.45 J-kg ⁻¹ -K ⁻¹	1,460.67 J-kg ⁻¹ -K ⁻¹	2,146.77 J-kg ⁻¹ -K ⁻¹
T_{vap}	301.17 K	457.21 K	413.51 K	357.05 K
γ	1.29	1.31	1.22	1.07
Γ	0.67	0.67	0.65	0.62
$p_e p_{ch}^{-1}$	2.774 E-3	2.549 E-3	3.595 E-3	6.014 E-3
A_t	5.137 E-9 m ²	5.186 E-9 m ²	4.973 E-9 m ²	4.586 E-9 m ²
w	1,549.271 m-s ⁻¹	1,483.544 m-s ⁻¹	1,176.818 m-s ⁻¹	964.3152 m-s ⁻¹
m	6.214 E-6 kg-s ⁻¹	6.496 E-6 kg-s ⁻¹	8.080 E-6 kg-s ⁻¹	9.584 E-6 kg-s ⁻¹
I_{sp}	164.107 s	156.986 s	126.207 s	106.402 s
ρI_{sp}	98.169 g-s-cc ⁻¹	138.559 g-s-cc ⁻¹	83.337 g-s-cc ⁻¹	52.598 g-s-cc ⁻¹
I_t	170 N-s	170 N-s	170 N-s	170 N-s
P_{el}	13.300 W	23.773 W	15.743 W	13.024 W
M_p	0.106 kg	0.110 kg	0.137 kg	0.163 kg
D_i	6.96 cm	6.20 cm	7.35 cm	8.57 cm

Table 2.5: Typical RCS propellants for CGT technology at a thrust of 10 mN, nozzle expansion ratio of 25, chamber temperature of 300 K, chamber pressure of 1 bar [42, 49].

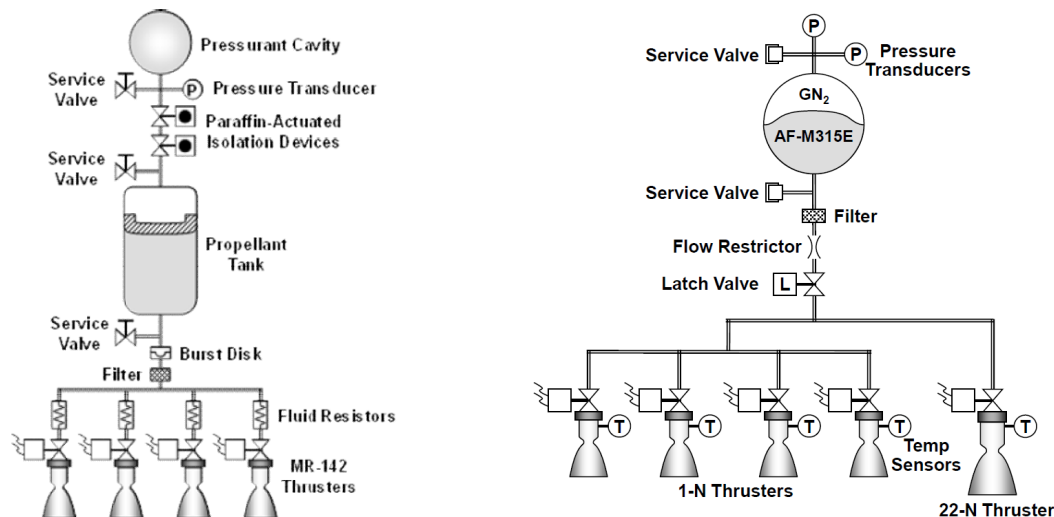
Quantity	Nitrogen	Butane	Ammonia	R134a
M_{mo}	28.01 g-mol ⁻¹	58.12 g-mol ⁻¹	17.03 g-mol ⁻¹	102.03 g-mol ⁻¹
Required	n/a	2.576 bar	10.62 bar	7.028 bar
p_{sto}				
Chosen	50.000 bar	11.000 bar	11.000 bar	11.000 bar
p_{sto}				
Phase	Supercritical	Liquid	Liquid	Liquid
Reactivity	Inert	Reactive	Reactive	Reactive
ρ	56.154 kg-m ⁻³	572.160 kg-m ⁻³	600.010 kg-m ⁻³	1,202.100 kg-m ⁻³
$c_{p,g}$	1,039.670 J-kg ⁻¹ -K ⁻¹	1,702.510 J-kg ⁻¹ -K ⁻¹	2,172.640 J-kg ⁻¹ -K ⁻¹	407.450 J-kg ⁻¹ -K ⁻¹
γ	1.400	1.092	1.290	1.250
Γ	0.685	0.627	0.665	0.658
$p_e p_{ch}^{-1}$	1.852 E-3	4.856 E-3	2.757 E-3	3.416 E-3
A_t	5.878 E-8 m ²	5.108 E-8 m ²	5.651 E-8 m ²	5.556 E-8 m ²
w	721.306 m-s ⁻¹	607.157 m-s ⁻¹	978.191 m-s ⁻¹	408.968 m-s ⁻¹
m	1.349 E-5 kg-s ⁻¹	1.545 E-5 kg-s ⁻¹	9.825 E-6 kg-s ⁻¹	2.338 E-5 kg-s ⁻¹
$I_{sp,th}$	75.610 s	66.005 s	103.790 s	43.607 s
$\rho I_{sp,th}$	4.246 g-s-cc ⁻¹	37.765 g-s-cc ⁻¹	62.275 g-s-cc ⁻¹	52.420 g-s-cc ⁻¹
I_t	170 N-s	170 N-s	170 N-s	170 N-s
M_p	0.229 kg	0.263 kg	0.167 kg	0.398 kg
D_i	19.830 cm	9.571 cm	8.101 cm	8.580 cm

2.4. Feed System Layout

Four propulsion systems in literature were considered to determine the typical layout of a spacecraft propulsion system: the MRS-142 CubeSat High Impulse Adaptable Monopropellant Propulsion System (CHAMPS), the custom propulsion system for the Green Propellant Infusion Mission (GPIM) developed by Aerojet Rocketdyne, the CubeSat High Impulse Propulsion System (CHIPS) system developed by VACCO/CU and finally an experimental hybrid propulsion system utilising gaseous oxygen as oxidiser by NASA/JPL.

The MRS-142 CHAMPS is a commercial system developed by Aerojet Rocketdyne as discussed by Schmuland et al. in 2012 [50]. This system, as its name implies, is adaptable to different CubeSat configurations by offering a 1 U and 2 U version, accommodating for different Δv requirements. The MRS-142 CHAMPS utilises Hydrazine propellant and operating in blow-down mode. The hydraulic diagram is presented in Figure 2.4a, showing a piston-type PMD in the propellant tank, being pressurised by pressurant gas stored in an external pressurant tank. Furthermore, series redundant isolation valves are shown between the pressurant tank and propellant tank, further downstream between propellant tank and thrusters, a burst disk is placed. These devices are placed for launch safety considerations and ensure that the propellant is unpressurised during ground operations and launch. It can furthermore be seen that a filter is placed behind the burst disk to filter out any burst disk debris or debris originating from other components. A pressure transducer is placed after the pressurant tank, enabling pressure measurements of pressurant gas. Service valves are placed on the lines enabling filling and draining of pressurant and propellant. It is observed that no latch valve is present in this system.

As discussed by Spores et al. in 2015 [21], the GPIM mission initiated by NASA's Space Technology Mission Directorate demonstrated an on-board green propellant propulsion system developed by Aerojet Rocketdyne, shown in Figure 2.4b. Similar to the MRS-142 CHAMPS, this system operates in blow-down mode however storing both propellant and pressurant inside the same tank, separated by an elastomeric diaphragm. It is observed that next to four smaller GR-1 thrusters serving as RCS demonstrators, a larger GR-22 thruster is used as primary divert thruster. The system is observed to not employ a single-use isolation valve, instead a latching valve is placed downstream of the propellant system in case of any valve leakage. Similar to CHAMPS, pressure transducers, service valves are observed, with the addition of thermocouples to measure temperature. The authors did not address the purpose of these thermocouples.

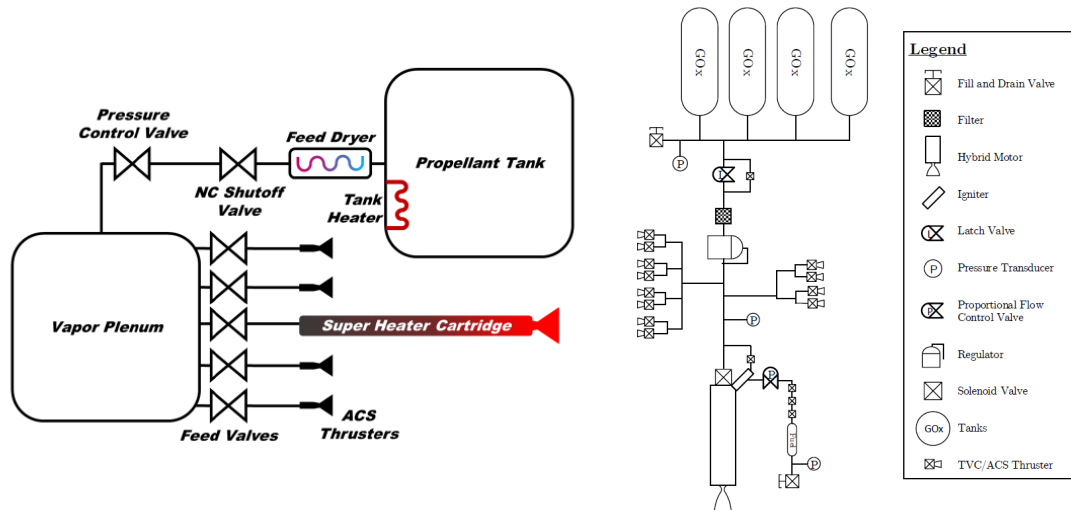


(a) Aerojet Rocketdyne MRS-142 CHAMPS schematic, cropped from [50]. (b) Green Propellant Infusion Mission propulsion system schematic, cropped from [21].

Figure 2.4: Feed system layout examples.

The CHIPS system (Figure 2.5a) was developed in co-operation between VACCO and CU Aerospace, as discussed by Hejmanowski et al. in 2015 and 2016 [51, 52]. The purpose of the system is to provide significant attitude changes and provide Δv for station-keeping to CubeSats. Refrigerants R134a and R236fa can both be used as propellants, stored in the liquid phase. By heating, some propellant is vaporised and fed into a vapour plenum at a desired pressure, regulated by a pressure regulator valve. No latching and isolation valves are observed to be included.

at NASA/JPL, an experimental hybrid propulsion system for interplanetary CubeSat (Figure 2.5b) was developed by Jens et al. [28]. The system uses gaseous oxygen as oxidiser, stored inside COPVs at 689 bar. The oxidiser is simultaneously used as propellant for RCS thrusters. Similar to aforementioned systems, fill/drain valves, filters, latch valves, a pressure regulator, pressure transducers and solenoid valves are observed to be included.



(a) VACCO/CU CHIPS schematic, cropped from [52].

(b) NASA/JPL experimental Hybrid propulsion system, cropped from [28].

Figure 2.5: Feed system layout examples, continued.

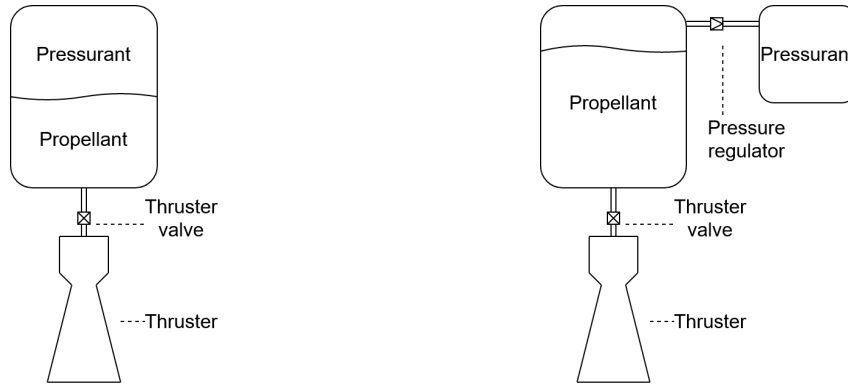
Inferred from the aforementioned COTS and experimental propulsion systems is that a typical propellant storage and feed system for small spacecraft and CubeSats may consist of the following components:

- Propellant tanks
- Pressurant tanks
- Propellant Management Devices (PMD)
- Valves
 - Fill/drain valves
 - Isolation valves
 - Latch valves
 - Start/stop valves
 - Regulator valves
- Feed lines
- Filters
- Heaters
- Sensors
 - Thermocouples (temperature measurements)
 - Pressure transducers (pressure measurements)

2.5. Feed System Types

For feeding propellant from the propellant tank to the thruster, gas-fed systems and pump-fed systems can be considered. First, gas-fed systems are discussed and subsequently, pump-fed systems are discussed.

2.5.1. Gas-Fed Systems



(a) Blow-down type system.

(b) Regulated type system.

Figure 2.6: Simplified diagrams of pressurisation methods for a propellant feed system using pressurant gas, draw.io.

As discussed by Elliot Ring in 1964 [53] and George Sutton in 1992 [11], two pressurisation methods exist using pressurant gas, namely a blow-down type system and a regulated type system. In a blow-down type system (Figure 2.6a), the propellant and pressurant gas are typically stored together in the same tank. As propellant is expelled, the tank pressure decreases, resulting in thruster inlet conditions changing over time. Advantages are lower complexity as compared to the regulated type system, however possibly higher propellant tank mass. In a pressure regulated system (Figure 2.6b), the pressurant is typically stored under high pressure in a separate tank and a regulator valve ensures constant propellant tank pressure and constant thruster inlet conditions. In principle, the pressurant gas and propellant may also be stored in the same tank and a regulator valve can be integrated between the tank outlet and the thrusters. Storing pressurant gas and propellant in separate tanks however has the advantage of lower propellant tank pressure which may result in lower propellant tank mass. A disadvantage is that extra complexity and possibly extra mass is introduced by the required regulator valve and a separate pressurant tank. When using pressurant gas in blow-down configuration (where pressurant gas initially occupies the available ullage volume and in final conditions occupies the entire tank volume), the pressurant mass M_{pres} in kg is defined using the ideal gas law at final conditions:

$$M_{pres} = \frac{p_{tank,f} V_{tank}}{R_g T_f} \quad (2.14)$$

where $p_{tank,f}$ is the tank pressure at final conditions in Pa, V_{tank} is the tank volume in m^3 , R_g is the gas constant of the pressurant gas in $J \cdot kg^{-1} \cdot K^{-1}$ and T_f is the temperature in K inside the tank at final conditions. Assuming low duty cycle operation, where heat is constantly exchanged with the surroundings, the pressure at final conditions is calculated using the following isothermal relation:

$$p_f = p_i \frac{V_{gas,i}}{V_{gas,f}} \quad (2.15)$$

Here, the gas volume values result from the fill ratio Φ_0 which is a function of the selected pressure ratio of the system:

$$\Phi_0 = 1 - \frac{p_{pres,f}}{p_{pres,i}} \quad (2.16)$$

Using the tank volume, this fill ratio is then used to determine the available propellant volume V_p and pressurant gas volume V_{pres} :

$$V_p = V_{tank} \Phi_0; \quad V_{pres} = V_{tank} (1 - \Phi_0) \quad (2.17)$$

For a pressure regulated configuration, i.e. where pressurant gas initially occupies the separate pressure vessel and at final conditions occupies the volume of both tanks, the pressurant mass is described as:

$$M_{pres} = \frac{\rho_{pres,tank,prop,f} V_{tank,prop}}{1 - \frac{\rho_{pres,tank,pres,f}}{\rho_{pres,tank,prop,i}}} \quad (2.18)$$

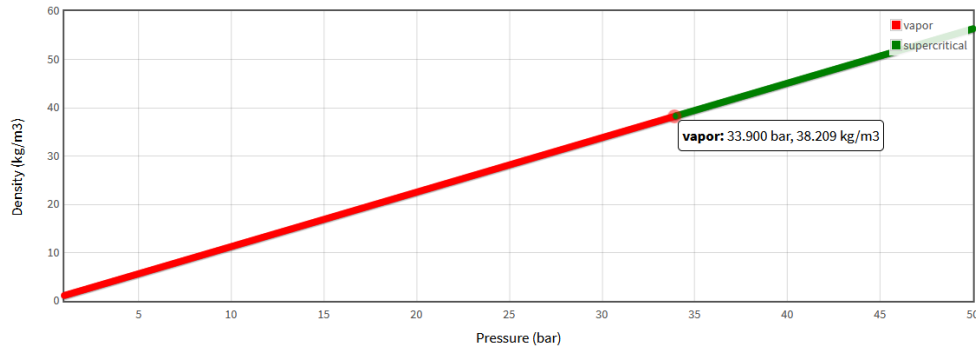
where $\rho_{pres,tank,prop,f}$ is the ullage pressure inside the propellant tank at final conditions, $V_{tank,prop}$ is the propellant tank volume, $\rho_{pres,tank,pres,i}$ is the pressurant gas density inside the pressurant tank at initial conditions and finally, $\rho_{pres,tank,pres,f}$ is the same density however at final conditions, all in $\text{kg}\cdot\text{m}^{-3}$.

Pressurant Gas

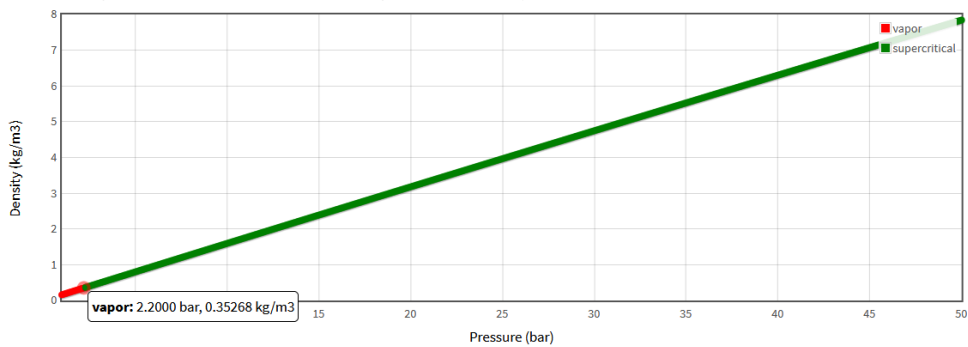
Typically, Helium or Nitrogen gas is used to pressurise spacecraft propulsion systems due to being chemically inert, i.e. they do not react with the propellant. Furthermore, in case of leakage, these gases have a lower risk of spacecraft contamination as compared to non-inert gases, as discussed by Elliot Ring in 1964 [53]. The relevant properties for Helium and Nitrogen gas are presented in Table 2.6. For the concept design phase, these properties are assumed to remain constant with temperature. Figure 2.7 shows the density of Nitrogen and Helium at 300 K between 1 and 50 bar, here it is observed that for Nitrogen, the phase change from vapour to supercritical occurs at approximately 33.90 bar and for Helium this occurs at approximately 2.20 bar. At this point, the ideal gas law is not valid anymore, however for the presented pressure range the density is observed to be related mostly linearly to pressure (Figure 2.7) and therefore during the concept design phase, the ideal gas law is assumed valid for these gases in the presented pressure range.

Table 2.6: Relevant properties of Helium and Nitrogen for feed system design at 300 K [49].

	M_{mo} (g/mol)	R_g (J·kg ⁻¹ ·K ⁻¹)	$c_{p,g}$ (J·kg ⁻¹ ·K ⁻¹)	c_v (J·kg ⁻¹ ·K ⁻¹)	γ (-)
Helium	4.0026	2,077.264	5,193.129	3,115.865	1.667
Nitrogen	28.0134	296.803	1,039.673	742.870	1.400



(a) Nitrogen, phase change to super-critical phase occurring at approximately 33.90 bar.

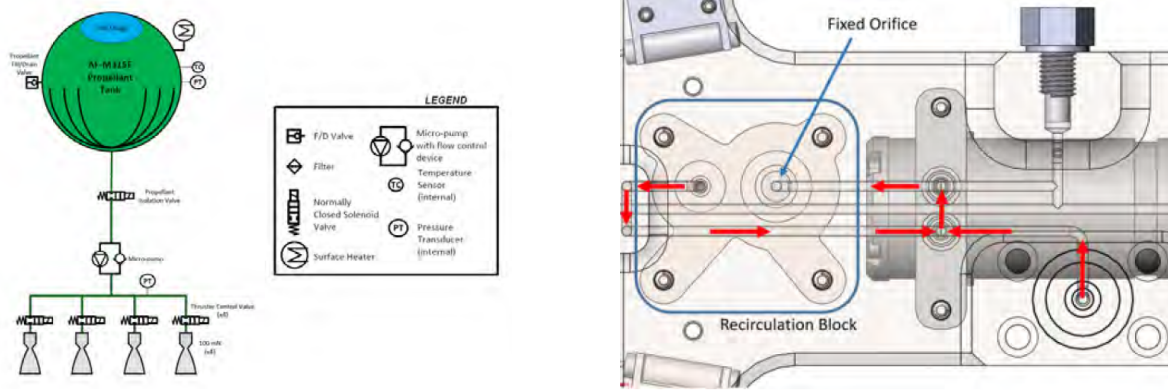


(b) Helium, phase change to super-critical phase occurring at approximately 2.20 bar.

Figure 2.7: Gas density (isothermal, at 300 K) for pressure values ranging from 1 to 50 bar, captured from [49].

2.5.2. Pump-Fed Systems

From 2008 to 2020, the US Small Business Innovation Research (SBIR) fund awarded several contracts to the company Flightworks Inc., US, to develop electric micro-gear pumps for spacecraft propulsion applications as stated by the US SBIR fund [54] and discussed by Besnard et al. in 2019 [55]. Such a pump produced by Flightworks, Inc. is used for the Lunar Flashlight Propulsion Module (LFPM) of the LFM spacecraft to be launched in 2021, which is used for both Δv and RCS purposes. Using such a pump results in lower required propellant storage pressure, lowering fracture criticality of the propellant tank and enabling the production thereof using Additive Manufacturing (AM) technology. Manufacturing of the propulsion system structure and manifolds using AM has resulted in a high level of component integration and elimination of approximately 40 custom-designed components as discussed by Huggins et al. in 2021 [8] and Andrews et al. in 2020 [7]. Flightworks, inc. offers three series of pumps: C-series (low flow coreless gear pumps), X-series (brushless gear pumps) and M-series (magnetically coupled gear pumps). The latter is of most interest for the MPS of LUMIO, because the actual pump head component is magnetically coupled to the motor instead of mechanically, eliminating the need for shaft seals, furthermore enabling a wide range of working fluids for aerospace applications as concluded from product datasheets published by Flightworks, inc. [56]. A list of all 43 M-series pumps is included in Appendix C, for continuous operation using heavy fuel of roughly $2 \text{ E-3 Pa}\cdot\text{s}$ of dynamic viscosity.



(a) Hydraulic diagram, showing a heated propellant tank with gas ullage (blue), pump with a flow control device, valves and four thrusters. (b) Recirculation loop showing the pump inlet and outlet ports, propellant tank port (right lower corner) and a flow control device (fixed orifice).

Figure 2.8: Lunar Flashlight Propulsion Module, cropped from [8].

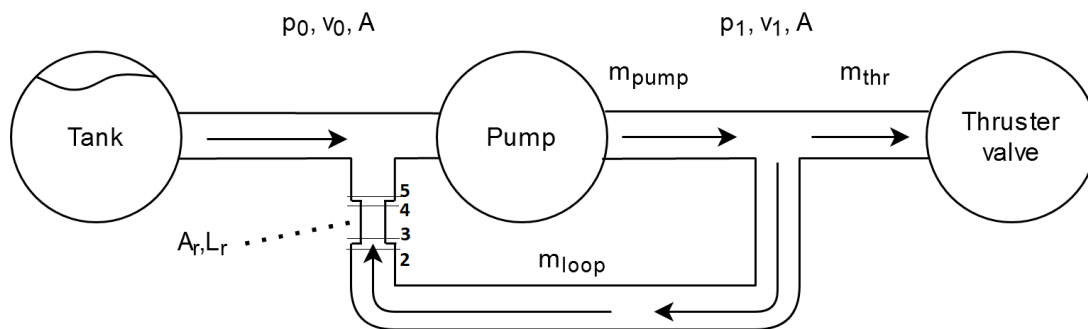


Figure 2.9: Simplified diagram of pump-fed propulsion system between tank and thruster valves, including recirculation loop and Passive Flow Control Device (stations 2, 3, 4, 5), draw.io.

For commercially available pumps, usually a pump characteristic is provided, in the case of the Flightworks, inc. pumps, these characteristics relate the volumetric flow rate to the pressure differential across the inlet and outlet ports for different rotational velocities of the pump, example shown in Figure 2.10a. In order to design a propulsion system using such a pump, working points of the pump can be chosen for constant thruster inlet conditions by properly designing the system for both BOL and EOL conditions, where at EOL the tank pressure is lower than at BOL. Either a pressure regulator valve can be placed such that it regulates the pump outlet pressure to achieve a desirable operating point, or a

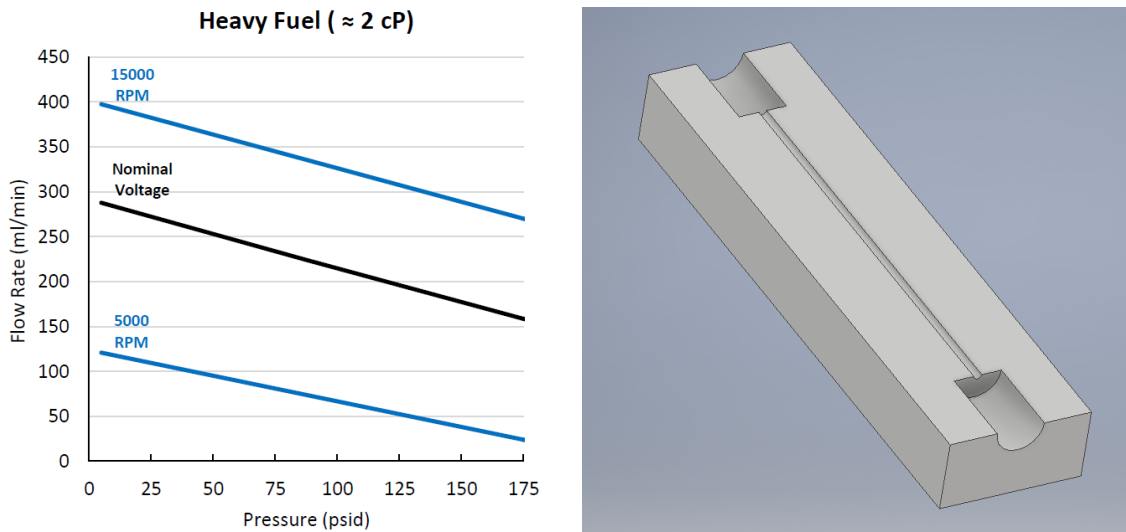
Passive Flow Control Device (PFCD) inside a recirculation loop can be used, as done in the LFPM. The PFCD effectively fulfils two functions: first, it generates a pressure drop over its length as function of PFCD mass flow, through which in combination with the thruster inlet conditions the working point of the pump can be set. Secondly, as the required volumetric flow rate by the thrusters may be below that of the operational envelope of the chosen pump, any excess part of the pump flow can be routed through the PFCD back towards the pump inlet.

A schematic of the pump-PFCD-thruster valve system is presented in Figure 2.9, where the PFCD is shown at stations 2, 3, 4 and 5. The theory required to design the PFCD is presented in Section 2.7. Inside the propellant tank, some gas is required to occupy the ullage volume to prevent a vacuum forming and to prevent vaporisation of propellant. A baseline illustration for the PFCD is presented in Figure 2.10b below. For each station, the flow velocity and static pressure are calculated. The pressure drops occurring at each station are calculated using relations Equation 2.25 and Equation 2.26 discussed in the next section. Finally, the required hydraulic power P_h in W to be provided by the pump is described by

$$P_h = \dot{V} \Delta p \quad (2.19)$$

where \dot{V} is the volumetric flow rate in $m^3 \cdot s^{-1}$ and Δp is the pressure differential across the pump inlet and outlet ports in Pa. Pump hydraulic power is in turn related to the pump required electric power $P_{e,pump}$ in W in the following way, where η_{pump} is the dimensionless pump efficiency factor, typically dependent on the pump flow rate:

$$P_{e,pump} = \frac{P_h}{\eta_{pump}} \quad (2.20)$$

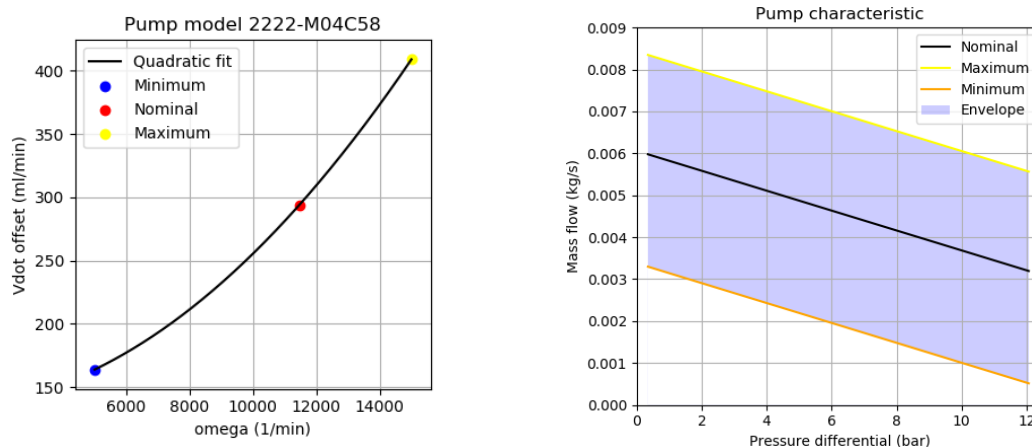


(a) Pump characteristic of the Flightworks, inc. 2222M04C58 pump for heavy fuel, cropped from [56]. (b) Passive Flow Control Device baseline, lengthwise cross-sectional view, Inventor 2022.

Figure 2.10: Pump characteristic and Passive Flow Control Device baseline.

Pump Characteristic Calculations

Considering a specific pump rotational velocity ω , the provided pressure differential and flow rate at this rotational velocity are assumed to behave according to a linear characteristic line. For constant thrust over the spacecraft lifetime, the pump is required to provide a higher pressure differential over time. Before thruster firing can commence, the pump is required to spool up to the required rotational velocity which is a function of the current tank pressure and the selected thrust level, this condition is called Thruster Valves Open (TVO). Spooling up occurs while thruster valves are closed, the Thruster Valves Closed (TVC) condition. For the required rotational velocity at the TVC condition it is evaluated



(a) Quadratic fit for volumetric flow rate offset. Offsets calculated using the end points of the provided characteristics. (b) Generated pump characteristic. Units converted for convenience, assuming incompressible propellant LMP-103s at 300 K.

Figure 2.11: Characteristics of Flightworks, Inc. pump model 2222-M04C58, Python/Matplotlib.

if the maximum specified differential pressure is within the pump specifications. This subsection describes how the relevant equations relating pump rotational velocity to provided pressure differential and volumetric flow rate are obtained. The pump characteristic of each Flightworks, Inc. pump contains three lines: minimum, nominal and maximum rotational velocity (example in Figure 2.10a), of which the begin and endpoints are visually determined. To simplify the calculations, the lines are assumed to be of constant slope, equal to the slope of the line corresponding to nominal operation. This slope is calculated using the finite difference formula, using the begin and endpoint of the nominal line. Subsequently, the offset of this constant slope line is determined by the pump rotational velocity. The lines correspond to the following format, using the units $\text{ml}\cdot\text{min}^{-1}$ for the volumetric flow rate \dot{V} and psi for the pressure differential Δp :

$$\dot{V} = \dot{V}_0(\omega) + \alpha \Delta p \quad (2.21)$$

$$\dot{V}_0(\omega) = a_0 \omega^2 + a_1 \omega + a_2 \quad (2.22)$$

For the three given lines, the flow rate offset values are calculated using the end point of each line and it is observed that the relationship is not linear. Because three datapoints are present, a second order polynomial fit was chosen to relate the flow rate to rotational velocity, shown in Figure 2.11a. The generated pump characteristic on which working points are to be plotted is shown in Figure 2.11b. The coefficients of the quadratic fit are shown in Table 2.7. The slope α is equal to $-0.794 \text{ ml}\cdot\text{min}^{-1}\cdot\text{psi}^{-1}$. To find the working point of the pump for a given pressure differential and volumetric flow rate, the equation Equation 2.21 is simply solved using the quadratic formula and taking the maximum result.

Table 2.7: Coefficients for the Flightworks, Inc. pump model 2222-M04C58 characteristic line offset.

a_0	a_1	a_2
1.236 E-6 ml-min	-2.241 E-4 ml	1.342 E+2 ml-min ⁻¹

Net Positive Suction Head Requirements

If at any point in the feed system the pressure is equal to or lower than the vapour pressure of the working fluid, cavitation may occur. The greatest risk occurring is inside the pump, where e.g. close to parts moving at high velocity, local low-pressure regions form, causing propellant to vaporise and form bubbles which violently implode. These implosions may damage the pump, cause vibrations and the shockwaves may propagate downstream, damaging other components. In order to prevent this, the available Net Positive Suction Head (NPSH) of the pump must be above the required NPSH, which is a characteristic of the pump and depends on pump flow rate. The available value is denoted as NPSH_a and the required value as NPSH_{req} . As no information about the NPSH of the Flightworks, Inc. micro-gear pumps is available, a conservative approach is used. As described by Besnard et al.

in 2019 [55], qualification tests were performed on some of their magnetically decoupled models for use in an MMH/MON-25 propulsion system, however not specifying any model designation. Data from these tests will be used to form a conservative estimate of the minimum required pump inlet pressure in LUMIO's propulsion system. NPSH is calculated as:

$$NPSH = \frac{p_{in,pump} - p_{vap}}{\rho g_0} \quad (2.23)$$

The test data is presented in Table 2.8. The fluid density and vapour pressure are determined using the pump inlet temperature as reference temperature. Where a pump inlet temperature is provided, this value will be used. Otherwise, the propellant tank temperature will be used, in this case marked by an asterisk (*). Data for pressure in the tests is interpreted visually and is therefore not completely accurate. As no problems of cavitation were mentioned in the publication, the lowest reported pump inlet pressure for each test is taken to calculate the NPSH. Finally, if the values for NPSH calculated here would correspond to the NPSH_r for LMP-103s at 300 K, a minimum required pump inlet pressure p_i for LUMIO's propulsion system is calculated. The fluid properties of Acetone are taken from the National Library of Medicine [57] and fluid properties for MON-3 and MON-25 are taken from the 1977 propellant manual published by the (US) Air Force Rocket Propulsion Laboratory [58].

The first pump tested was a "micropump" for 100-200 lbf class thrusters, using Acetone as MON-25 simulant at "ambient temperatures" (assumed 300 K) to validate pump performance. A steady-state pump inlet pressure of 30 psi (≈ 2.068 bar) was observed. The pump was used to supply 250-300 ml·min⁻¹ of fluid at a differential pressure of 250 - 365 psid (≈ 17.237 - ≈ 25.166 bar), a much higher differential pressure than those observed in Appendix C. It is however important to note that the fluid viscosity of Acetone is significantly lower than that of LMP-103s: approximately 3.000 E-4 Pa·s according to the National Library of Medicine [57] as compared to approximately 3.000 E-3 Pa·s for LMP-103s (Table 3.5). The other pump tested was a "200 lbf thrust-class medium pump", tested first in a hot fire test at "ambient temperatures" again assumed 300 K, using MMH/MON-3 propellants, later a test using "thermally conditioned" MMH/MON-25 propellants at approximately 243 K was performed: first in a closed-loop setting, subsequently as hot-fire. Only data for the MON-3 and MON-25 propellants (oxidisers) from the latter tests was considered, as four data points seem sufficient. No flow rates were reported for this pump, however pressure differentials of up to 430 psi (≈ 29.648 bar) were observed in the MON-3 hot fire tests, using the same pump type as for the MON-25 propellant. For the thermally conditioned tests, a pump inlet temperature for the MON-25 pump was specified, namely -15 deg. C (≈ 258 K).

As observed from Table 2.8, the calculated values for NPSH and p_{in} differ significantly. However, as discussed before, no cavitation was reported anywhere in the publication. Therefore, the lowest calculated value for NPSH of 4.694 m and corresponding $p_{in,pump}$ for propellant LMP-103s is deemed acceptable, namely 0.717 bar.

Tao et al. in 2018 [59] describe the dimensionless "head coefficient" C_{ca} using which the pump cavitation characteristics can be decoupled from the test conditions:

$$C_{ca} = \frac{2g_0 NPSH}{\omega^2 r_{tip}^2} \quad (2.24)$$

where g_0 is the gravitational acceleration at Earth, sea-level (9.80665 m·s⁻²), ω the pump rotational velocity in rad·s⁻¹ and r_{tip} the tip radius of the pump head in m. In the pump test paper by Besnard however, only a rotational velocity was reported for test 1, namely 12,500 RPM. No data on this regard was reported for the others. No data on tip radius or other pump dimensions was presented either. However, all pumps offered by Flightworks, inc. M-series pumps, including the one in the test, have an outer diameter of 22 mm as per their datasheets [56]. Using this value, a tip radius is assumed, assuming two pump gears are used with each a diameter of half the outer diameter of the pump. This results in an assumed tip radius of 5.5 mm, with which the dimensionless head coefficient can be calculated, resulting in a value of 8.657 for test 1. It must be noted however, that for these tests, cavitation was not discussed and the chosen pump inlet pressure in the tests was not driven by cavitation requirements. Therefore, some margin may be present. This coefficient will later be used to compare the results of the pump working points to.

Table 2.8: Approximate test data for determining NPSH of Flightworks, Inc. micro-gear pumps ([55]). Data for Acetone from [57], data for MON-3 and MON-25 data from [58].

Parameter	Test 1 (Ambient Acetone closed loop)	Test 2 (Ambient MON-3 hot fire)	Test 3 (Cold MON-25 closed loop)	Test 4 (Cold MON-25 hot fire)
Working fluid	Acetone	MON-3	MON-25	MON-25
Pump inlet temperature	300 K*	300 K*	258 K	258 K
Pump inlet pressure	2.068 bar	5.516 bar	1.724 bar	1.379 bar
Fluid density	784.5 kg-m ⁻³	1,448.0 kg-m ⁻³	1,475.0 kg-m ⁻³	1,475.0 kg-m ⁻³
Fluid vapour pressure	0.308 bar	0.960 bar	0.700 bar	0.700 bar
Resulting <i>NPSH</i>	22.877 m	32.084 m	7.077 m	4.694 m
Calculated $p_{in,pump}$ for LMP-103s	2.922 bar	4.039 bar	1.006 bar	0.717 bar
Rotational velocity	12,500 RPM	n/a	n/a	n/a
Assumed tip radius	5.50 mm	n/a	n/a	n/a
C_{ca}	8.657	n/a	n/a	n/a

2.6. Pipe Flow Pressure Loss and Fluid Hammer

Viscous effects cause flow through smooth, circular tubes to experience pressure loss. This section describes analytical methods to approximate these losses for straight segments, contractions, expansions and bends. As discussed by Assefa and Kaushal, 2015 [60], this pressure loss can be approximated using the Darcy-Weissbach relation:

$$\Delta p = f \frac{l}{D} \frac{1}{2} \rho v^2 \quad (2.25)$$

where f is the dimensionless friction factor, l the pipe length in m, D the pipe diameter in m, ρ the density of the medium in $\text{kg}\cdot\text{m}^{-3}$ and v the velocity of the medium in $\text{m}\cdot\text{s}^{-1}$. An alternative form of this relation is also used, where the friction factor and length-to-diameter ratio are replaced by a factor K , as discussed by Benedict et al. in 1966 [61]:

$$\Delta p = K \frac{1}{2} \rho v^2 \quad (2.26)$$

To determine the flow regime relevant to the propulsion system design, the dimensionless Reynolds numbers is calculated as function of pipe diameter using Equation 2.27:

$$Re = \frac{\rho v D}{\nu} \quad (2.27)$$

where ν is the dynamic viscosity of the medium in $\text{Pa}\cdot\text{s}$. It is assumed that the MPS uses two thrusters simultaneously delivering 1 N of thrust each with a specific impulse of 200 s, consuming propellant LMP-103s with a density of $1236.520 \text{ kg}\cdot\text{m}^{-3}$ and a dynamic viscosity of $3.000 \text{ E-3 Pa}\cdot\text{s}$. For the RCS, four thrusters are assumed to be simultaneously firing at 10 mN of thrust each with 100 s of specific impulse, consuming water propellant with a density of $996.560 \text{ kg}\cdot\text{m}^{-3}$ and a dynamic viscosity of $1.000 \text{ E-3 Pa}\cdot\text{s}$. The plot in Figure 2.12 shows the flow for both the MPS and RCS will remain in the laminar regime ($Re < 2,100$) for pipe diameters no smaller than $500 \mu\text{m}$. As pipe diameter increases, the fluid flow velocity is proportional to D^{-2} , so the Reynolds number is proportional to D^{-1} causing the observed shape of Figure 2.12.

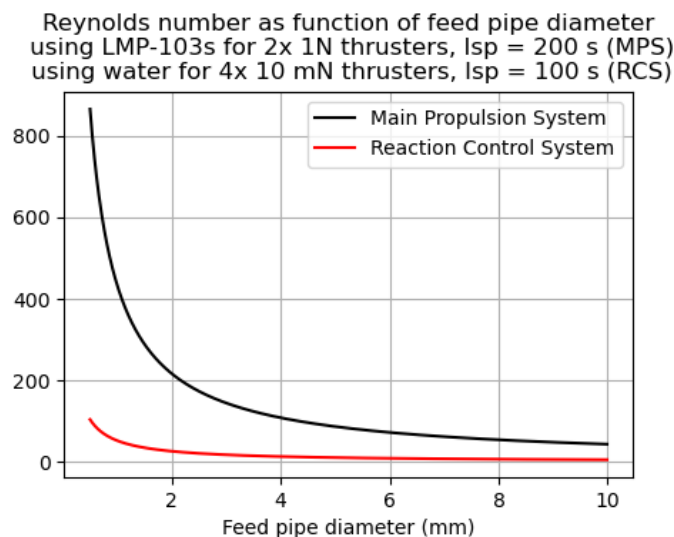


Figure 2.12: Reynolds number as function of pipe diameter, Python/Matplotlib.

2.6.1. Straight, Smooth, Circular Tubes

As discussed by Assefa and Kaushal, 2015 [60], for laminar flows, i.e. at $Re \leq 2,100$, the Hagen and Poiseuille relation can be used:

$$f = \frac{64}{Re} \quad (2.28)$$

For turbulent and transitional flow at $2,100 < Re \leq 2 \cdot 10^4$, the first Blasius correlation can be used to calculate the friction factor:

$$f = 0.316Re^{-0.25} \quad (2.29)$$

For turbulent flow for $Re > 2 \cdot 10^4$, the second Blasius correlation can be used:

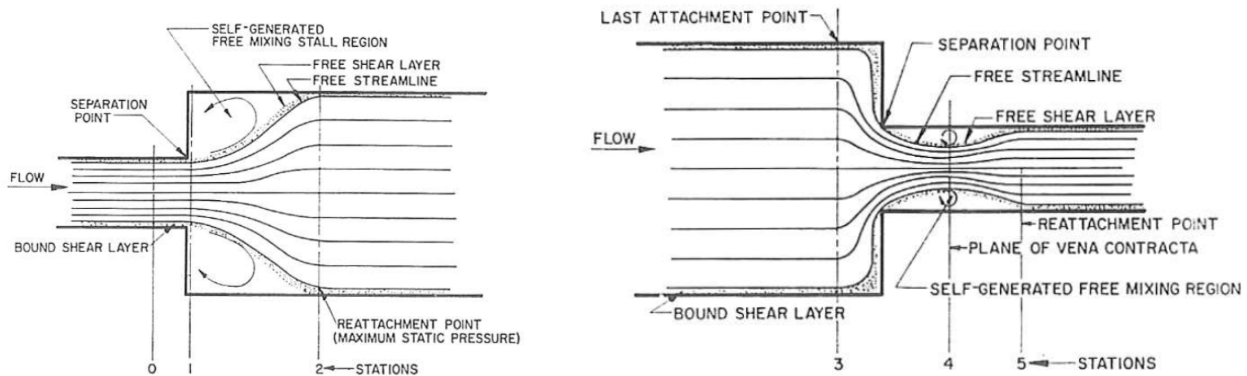
$$f = 0.185Re^{-0.2} \quad (2.30)$$

2.6.2. Rapid Contraction and Expansion

As discussed by Benedict et al., 1966 [61], for rapid expansion, the factor K in Equation 2.26 can be taken as K_{exp} , defined as:

$$K_{exp} = \left(1 - \frac{A_0}{A_2}\right)^2 \quad (2.31)$$

where areas A_0 and A_2 are illustrated in Figure 2.13a. Here, the area A_2 is taken where the flow is fully re-attached, assuming that this cross-section matches the large pipe cross-section. The area A_0 is taken right before the separation point, assuming that this cross-section matches the small pipe cross-section. For rapid contraction, the factor K_{con} is used instead. Consider Figure 2.13b, here it is seen that first an acceleration of the flow occurs towards the vena contracta, followed by expansion. From both instances a pressure drop occurs results, however difficult to describe analytically. Benedict confidently proposes a conservative empirical value of $K_{con} = 0.5$ to arrive at an acceptable first order approximation. Due to no other sources found for more accurate however still simple estimates for this loss were found, this approximation is used.



(a) Situational diagram for rapid expansion of a flow.

(b) Situational diagram for rapid contraction of a flow.

Figure 2.13: Diagrams for abrupt cross-sectional changes in flows, cropped from [61].

2.6.3. Bends

Two types of in-plane bends exist, namely regular bends and elbow bends. In literature, an elbow bend is considered an exceptional case of an in-plane bend and applies to R_{be}/D_p ratios below 5, where R_{be} is the bend radius and D_p is the internal pipe diameter, as discussed by Spedding et al. in 2004 [62]. Pressure loss in curved pipes is a topic discussed extensively in literature, some examples throughout the years are the works by Beij in 1938, Itō in 1960 and Crawford in 2005: in 1938, K. Hilding Beij published a research paper on pressure loss through 90 degree steel pipe bends with a diameter of 4 inches and bend radii varying from 6 to 80 inches for Reynolds numbers in the order of $E+5$ and therefore including both regular and elbow bends [63]. In 1960, H. Itō published measurements and empirical formulas on pressure loss in smooth pipe bends, considering both regular and elbow bends [64]. In 2005, Naomi Crawford published her PhD thesis on pressure losses at bends and junctions,

conducting measurements, simulations and discussing empirical relations however also focusing on higher Reynolds numbers, around the order of $E+5$, also including elbow bends [65].

Spedding et al. have published a paper in 2004 [62], discussing works and results from the previous authors and others, additionally discussing results from their own experiments and explaining theory concerning these losses. Laminar flow traveling through a regular bend experiences pressure loss due to secondary flow patterns in the form of two helical vortices arising over the bend (Figure 2.14), experiencing viscous losses, caused by two effects. The first effect is due to centrifugal acceleration: the faster moving core part of the flow is forced to the outer wall when flowing through a bend. The second effect is due to the faster moving lower pressure region in the core of the flow attracting fluid from the outer parts of the flow where velocity is lower and pressure is higher. In the case of an elbow bend, two additional effects come into play. The first is caused by flow separation at the inner wall of the bend, leaving a turbulent area close to the inner wall around the bend. The second is due to fluid impingement on the outer wall of the bend.

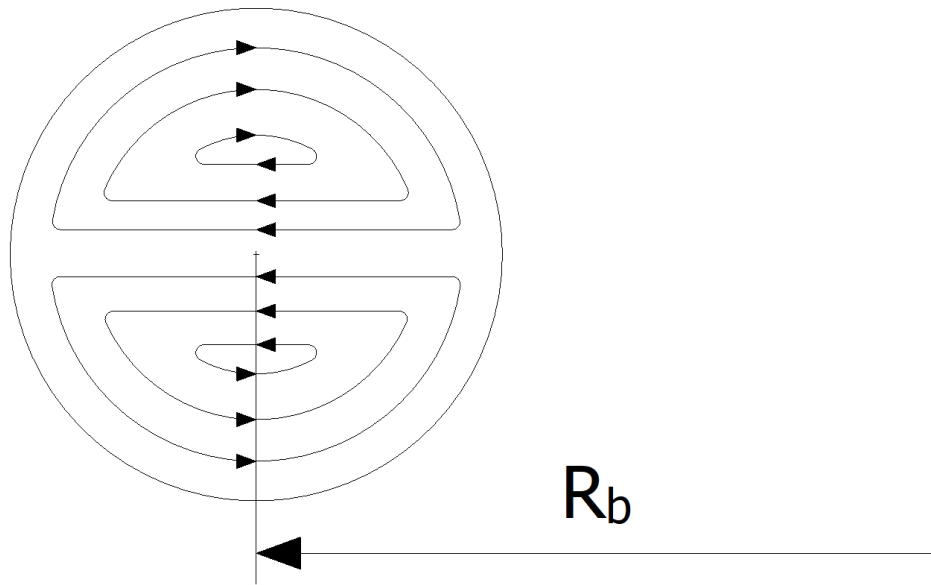


Figure 2.14: Cross-section of flow through a circular tube downstream of a bend, Inventor 2022.

The relevant conclusions from the aforementioned works is that empirical relations for pressure loss in laminar flow regimes with low error exist. For elbow bends however, no relations were presented for the Reynolds numbers as encountered in this project (Figure 2.12). Therefore, the pressure losses in elbow bends at the Reynolds numbers relevant to this project are simply approximated by regular in-plane bends to arrive at a first order approximation of pressure losses. In order to approximate pressure loss due to bends, first, the Dean number De is calculated, relating the flow regime to the bend properties and the Reynolds number:

$$De = Re \left(\frac{D_p}{D_{be}} \right)^{0.5} \quad (2.32)$$

For laminar flow at $11.6 < De < 2,000$, the following relation by White is proposed as the most reliable, according to Spedding et al. the data correlates to experimental data with underprediction of 1% at low De numbers and overprediction of 2.5% at higher De numbers. It is presented as the ratio of the friction factor for a straight pipe f_s and friction factor for a curved pipe f_c :

$$\frac{f_s}{f_c} = 1 - \left(1 - \left(\frac{11.6}{De} \right)^{0.45} \right)^{\frac{1}{0.45}} \quad (2.33)$$

For $De \leq 11.6$, f_c is assumed to equal f_s . In order to obtain the curved friction factor, the relation is simply inverted. The Dean number behaviour as function of Reynolds number and R_{be}/D_p ratio (=

$2(D_p/D_{be})^{-1}$) is shown in Figure 2.15 below. The friction factor behaviour is shown in Figure 2.16 below. It is observed, that for the low Reynolds numbers relevant to LUMIO’s MPS and RCS, the bend ratio has an influence of approximately a maximum factor of 1.5 between the smallest and largest bend ratios. In case pressure loss is not of significant magnitude and therefore not critical in the design, integration of components can be done with more freedom, with more freedom in choice of pipe bend radius.

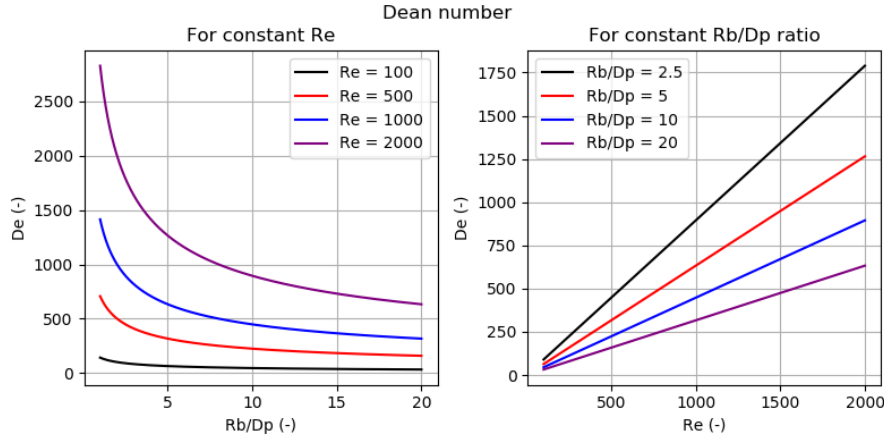


Figure 2.15: Dean number as function of constant Reynolds number and bend radius/pipe diameter ratios, Python/Matplotlib.

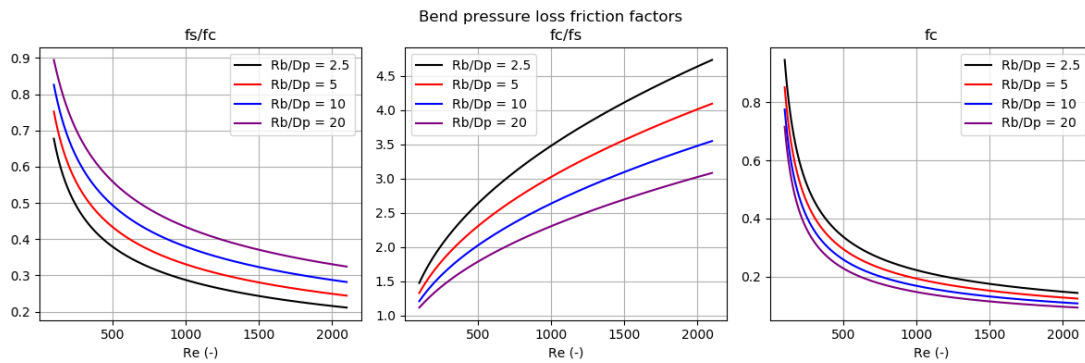


Figure 2.16: Bend pressure loss friction factors as function of Reynolds number and constant bend radius/pipe diameter ratios, Python/Matplotlib.

2.6.4. Fluid Hammer

Fluid hammer is a phenomenon that may occur at rapid opening or closing of a valve, in a spacecraft this may happen during priming of the propulsion system or during closing of any valve in the system. This phenomenon is characterised by a pressure wave traveling from the valve being operated towards an upstream boundary (in case of valve closure), reflecting off of said boundary and traveling back to the valve. This time depends on the wave celerity of the fluid. It is a complex phenomenon difficult to model, as discussed by Prickett et al. in 1992, Lecourt and Steelant in 2007, and Lema et al. in 2011 [66–68]. Effects such as elasticity of feed lines and multiphase effects in the flow significantly complicate modeling. However, Lema et al. propose two simple equations to approximate the magnitude of these effects. The first applies to rapidly closing valves ($\tau_{cl} < 2l/a_p$), where τ_{cl} is the valve (closing) response time, l refers to the pipe segment length and a_p is the wave celerity of the fluid. In this case, a "savage perturbation" takes place, of which the magnitude of this perturbation Δp_{ha} in Pa is approximated by the Joukowski equation:

$$\Delta p_{ha} = \rho_p v a_p \tag{2.34}$$

here, ρ_p is the fluid density in $\text{kg}\cdot\text{m}^{-3}$ and v is the flow velocity in $\text{m}\cdot\text{s}^{-1}$. The equation was derived by Joukowsky from the conservation of mass and momentum. The important assumption here are inelastic feed lines and that all kinetic energy of the flow is instantaneously converted into pressure. For the situation with slower closing valves, where $\tau_{cl} > 2L/a_p$, the "slow perturbation" applies, the magnitude of which is approximated by:

$$\Delta p_h = \frac{2\rho_p l v}{\tau_{cl}} \quad (2.35)$$

here, the fluid wave celerity was substituted for using $a_p = 2s/\tau$, assuming that the wave travels from the valve to an upstream boundary and back during valve closing time.

2.7. Passive Flow Control Device

As mentioned in Section 2.5.2, in order to use a pump for LUMIO's propellant feed system, a PFCD is required, fulfilling the functions of creating the desired pressure differential between the pump outlet and inlet and to accommodate any excess mass flow not used by the thrusters. A simple design is chosen, to illustrate how a simple, straightforward component can be used to set the pump working point. This design comprises a straight tube with an orifice to generate a pressure drop as function of the mass flow rate through the PFCD. Instead of using a contracting and subsequent expansion, also a continuous tube of constant diameter could be used to connect the pump outlet and inlet. In this case however, the approximation of junction pressure losses is complicated due to a change of cross-section from the start of the junction to the end of the junction. The advantage of the chosen design is thus a constant feed tube diameter throughout the entire feed system, allowing for a simple preliminary feed system design. Figure 2.17 shows the schematic of the baseline design.

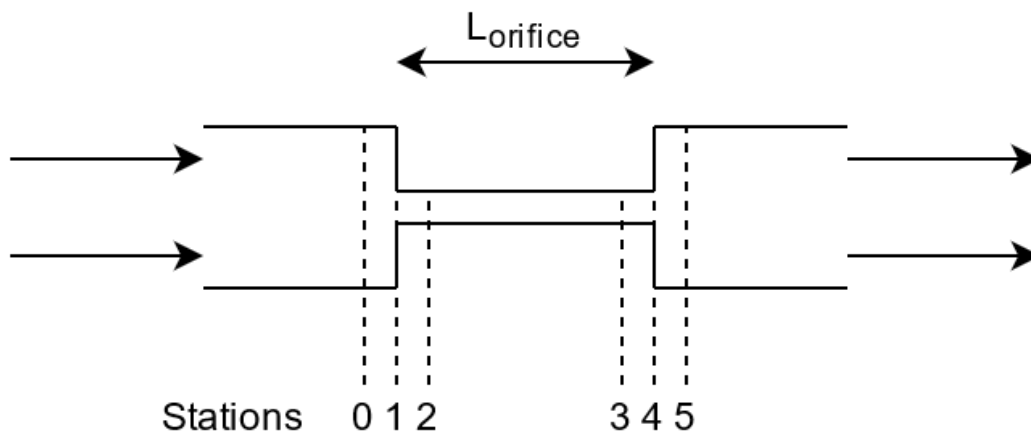


Figure 2.17: PFCD schematic with local station numbers, draw.io.

In this illustration, station 0 corresponds to incoming flow conditions. At station 1, a contraction in flow cross-sectional area occurs, causing an increase in flow velocity and a decrease in static pressure. This change in static pressure is approximated using Bernoulli's equation (Equation 2.36), assuming one-dimensional, incompressible flow:

$$p_0 + \frac{1}{2}\rho v_0^2 = p_1 + \frac{1}{2}\rho v_1^2 \quad (2.36)$$

At station 2, the static pressure has dropped due to rapid contraction, Equation 2.26 is used to approximate the resulting pressure loss, assuming a loss coefficient of $K_{con} = 0.5$ as discussed in Section 2.6.2. Over the length of the orifice $L_{orifice}$, pressure loss due to viscous losses in a smooth, straight, circular tube occur. These are in turn approximated by Equation 2.25 and the friction factor is calculated using Equation 2.28, Equation 2.29 or Equation 2.30, depending on the flow regime (Reynolds number). At station 4, the flow is expanding again, causing velocity to decrease and recovering static pressure, approximated using Equation 2.36. At station 5, a loss of static pressure due to rapid expansion is expected, approximated using Equation 2.26, this time a function of cross-sectional area. The station locations and numbering are placed to accommodate convenient calculation of the static pressure throughout the system. In reality, some stations may coincide.

2.7.1. Uncoupled Passive Flow Control Device

Figure 2.18 shows an example calculation for the pressure at various stations within the PFCD, not yet coupled to the pump, assuming that the pressure is fixed at the high-pressure side of the system. It is observed that for this specific orifice length, the pressure at station 3 (just before pressure recovery) is lower than at station 5, after the expansion pressure loss is applied. This means that the provided pressure drop approximated for the PFCD may be lower than the high-pressure end pressure, and that if the desired pressure drop of the PFCD is close to the sum of the pressure values at the low pressure side of the system (e.g. propellant tank) and the high pressure side of the system (e.g. pump outlet), the

pressure inside the PFCD may become zero, making the solution invalid. In reality however, first, the vapour pressure of the propellant will be reached and the liquid propellant will vaporise, therefore the pressure would not drop to zero - cavitation effects may occur however. For the blue line corresponding to a mass flow rate of $0.004 \text{ kg}\cdot\text{s}^{-1}$, it is seen that the pressure gets close to zero however stays above zero. For the red line corresponding to a mass flow rate of $0.006 \text{ kg}\cdot\text{s}^{-1}$ however, it is observed that the pressure intersects zero between stations 2 and 3 and from this point onward the solution is invalid. Figure 2.19 shows the same calculations however for a much shorter orifice length of 0.01 m . A significantly lower pressure drop is observed.

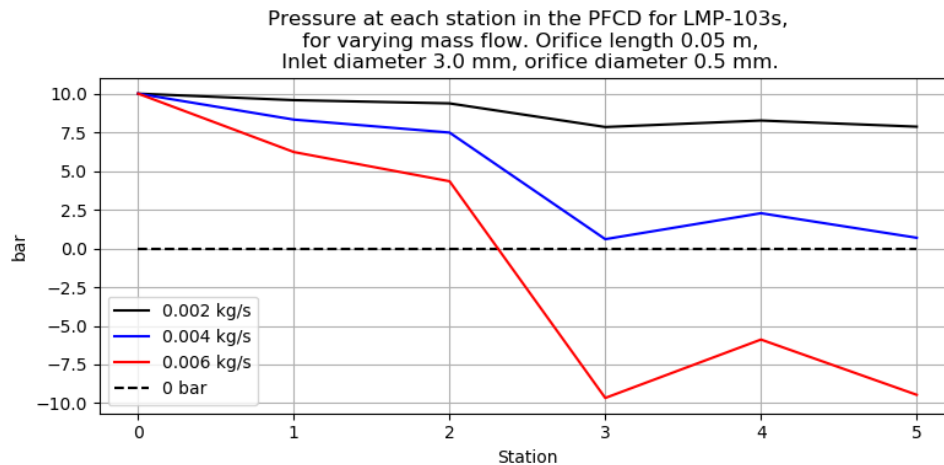


Figure 2.18: PFCD performance example for various mass flow rates of propellant LMP-103s at 300 K , fixed high-pressure side pressure, orifice length of 0.1 m , Python/Matplotlib.

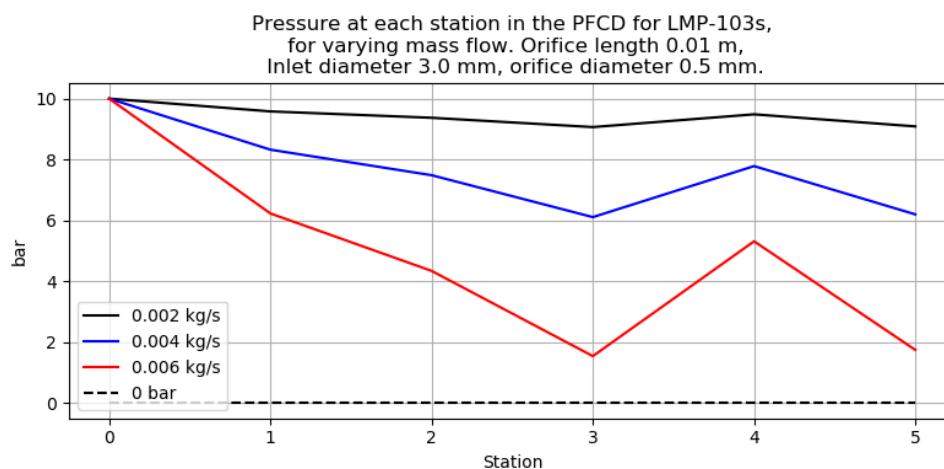


Figure 2.19: PFCD performance example for various mass flow rates of propellant LMP-103s at 300 K , fixed high-pressure side pressure, orifice length of 0.01 m , Python/Matplotlib.

2.7.2. Passive Flow Control Device Coupled to the Pump and Thrusters (TVO condition)

Calculations for PFCD performance become more complicated when the PFCD and pump are coupled, as more equations are introduced. Consider the situation where the PFCD is placed in a recirculation loop between the pump outlet and pump inlet as illustrated in Figure 2.9, with thruster valves opened (TVO condition). For a set rotational velocity of the pump, the flow through the pump will find an equilibrium working point, where the pressure differential and flow rate of the pump equal those of the PFCD. Some of the mass flow will also flow into the thrusters, at a desired pressure. For this rotational

velocity, the relation for pressure differential and flow rate of the pump is known. The numerical solver `fmin` is used in Python, from the SciPy optimization package. The objective function ψ is created (Equation 2.37), returning the absolute difference in pressure differential between the pump and the PFCD, both functions of mass flow m , to be minimised by the function `fmin`. Subsequently, the objective function value is checked to be sufficiently close to zero, meaning that a valid solution is found for the pump equilibrium point. In reality, this value will be zero, however a small numerical error in this theoretical solution is expected which must be insignificant in relation to the actual pressure drop, e.g. a preliminarily chosen order of magnitude of 1 Pa for a pressure drop in the order of E+5 Pa. In Table 4.14 it can be seen that the solver `fmin` works well, and the order of magnitude of the absolute error is E-3 Pa for a pressure drop of magnitude E+5 Pa at BOL, for EOL this is in the order of E-5 Pa for a pressure drop of E+6 Pa. Therefore the algorithm is expected to converge properly and the solution is taken as valid. The objective function is:

$$\psi = |\Delta p_{pump}(m) - \Delta p_{PFCD}(m)| \quad (2.37)$$

here, Δp_{pump} is calculated using the pump characteristic for the desired rotational velocity, Equation 2.21. The value of Δp_{PFCD} is calculated according to the method discussed at the start of this Chapter, and is the sum of the rapid contraction pressure loss, the straight tube viscous loss and finally the rapid expansion loss.

The TVO condition is discussed first as it is more simple to solve than the TVC condition. This is due to the pressure at the high-pressure side of the system being known. This high-pressure side pressure is set equal to the desired thruster inlet pressure and is proportional to the desired thrust level.

2.7.3. Passive Flow Control Device Coupled to the Pump only (TVC condition)

Before thruster firing, the pump will need to accelerate to the required rotational velocity, this will be done with thruster valves closed. For a constant pump rotational velocity, it is expected that during the TVC condition, the mass flow through the system decreases and the differential pressure over the pump increases as compared to the TVO condition where some of the total mass flow is routed towards the thrusters. For the TVC condition, the system working point will be determined to check whether this working point is within the bounds of the pump characteristics (e.g. not exceeding the maximum achievable differential pressure). This condition requires solving for an additional unknown, namely the pressure at the high-pressure side of the system. However, the rotational velocity ω for this condition is already known, providing the pump characteristic, relating pump mass flow to provided pressure differential. In order to solve for the working point here, a custom line search algorithm is employed, operating according to the following steps:

1. Loop through pump pressure differential values on the characteristic line (e.g. 1 bar to 10 bar),
2. Calculate the corresponding pump mass flow rate using the characteristic line and the current pressure differential value,
3. Calculate the high pressure side pressure using the current pressure differential value and the tank pressure (e.g. EOL tank pressure),
4. Evaluate pressure drop over PFCD using the PFCD mass flow rate, which is at TVC condition equal to the pump mass flow rate. Check whether at every point in the PFCD the pressure is above zero, otherwise return an error,
5. Calculate the absolute difference of the current pump pressure differential value and the PFCD pressure drop (Equation 2.37), save in array,
6. Find the minimum value in the aforementioned array, this corresponds to the working point.

2.8. Propellant Tank Design

This section contains the relations required for tank design. First, the cylindrical tank is considered for the concept design stage to arrive at a simple tank design. Subsequently, relations for cuboid tanks are presented, which are used in the detailed design phase. Finally, tank materials are discussed and types of PMD with preliminary design methods are presented.

2.8.1. Cylindrical Tank Design for the Concept Design Stage

In the concept design phase, the cylindrical tank shape is used, as discussed in Chapter 3. Figure 2.20 shows the shape of the tank type used in case a spherical tank is not feasible due to volume restrictions. For simplicity and to allow comparison, only a cylindrical tank design with hemispherical endcaps is chosen for the concept design. The inside volume is:

$$V_{tank} = \pi r^2 l_{tank,i} + \frac{4}{3} \pi r^3 r_{tank,i} \quad (2.38)$$

where $r_{tank,i}$ denotes the inside radius of the hemispherical ends and the cylindrical part, $l_{tank,i}$ denotes the inside length of the cylindrical part, both in m. The material Ti-6Al-4V is chosen for concept generation, due to its high specific strength as discussed by Tam et al. in 1997 [69], assuming the properties shown in Table 2.9.

Table 2.9: Material properties of a Ti-6Al-4V alloy [70].

Quantity	Value
Tensile yield strength $\sigma_{t,y}$	880 MPa
Tensile ultimate strength $\sigma_{t,u}$	950 MPa
Density	4,430 kg-m ⁻³

Hoop stress for a thin-walled (valid for $t \ll 10r$) cylinder can be rewritten for wall thickness:

$$t_y = \frac{p_{tank} r_{tank}}{\sigma_y} j_{bu} j_y; \quad t_u = \frac{p_{tank} r_{tank}}{\sigma_u} j_{bu} j_u \quad (2.39)$$

here, the allowable value for either yield or ultimate stress is used, j_{bu} is the burst safety factor (equal to 2.5 as per PROP.162, RCS.162), j_y is the yield load factor and j_u is the ultimate load factor. The wall thickness is calculated for ultimate stress, as ultimate stress is observed as dimensioning as dimensioning; load factors are chosen as 1.1 for yield, 1.25 for ultimate, 2.5 for burst. Taking tank radius and pressure as constant, the wall resulting wall thickness is compared for both yield and ultimate situations.

$$f\left(\frac{j_b j_y}{\sigma_{t,y}}\right) = f\left(\frac{2.5 \cdot 1.1}{880}\right) = f(3.125E - 3) \quad (2.40)$$

$$f\left(\frac{j_b j_u}{\sigma_{t,u}}\right) = f\left(\frac{2.5 \cdot 1.25}{950}\right) = f(3.289E - 3) \quad (2.41)$$

It is observed that for this material, ultimate stress is dimensioning and therefore yield stress will not be considered in the concept design phase.



Figure 2.20: Cylindrical tank shape used for the concept design stage, draw.io.

2.8.2. Cuboid Tank Design for the Detailed Design Stage

In the detailed design phase, a cuboid tank shape was chosen due to higher volumetric efficiency as compared to a cylindrical tank shape, discussed in Section 4.1.2. For dimensioning such a tank, the relations for bending moment, deflection and stress in a thin rectangular plate with simply supported edges are used as presented by T. H. G. Megson in Aircraft structures for Engineering Students, 5th edition [71]. Consider a thin, rectangular plate with length a and width b , as presented in Figure 2.21 on which a distributed transverse load p (Pa) is applied.

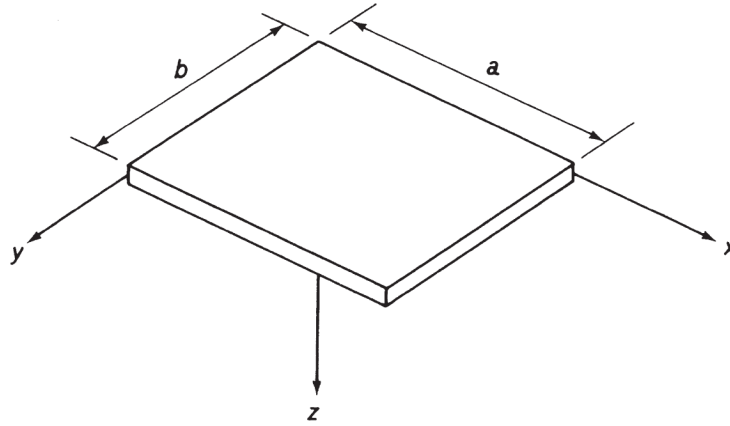


Figure 2.21: Thin, rectangular plate, cropped from [71].

The plate is assumed to be in pure bending. First, the plate flexural rigidity ζ (N-m) is considered:

$$\zeta = \frac{Et^3}{12(1-\nu^2)} \quad (2.42)$$

where E is the Young's modulus of the material, t is the thickness of the plate and ν is the transverse contraction coefficient of the material. For calculating deflections and bending moments of the plate considering simply supported edges, the simplified version of Navier's Fourier series solution is used, considering the first five terms (1, 3, 5, 7, 9). The deflection δ in m is described by:

$$\delta = \frac{16p}{\pi^6 \zeta} \sum_{m=1,3,\dots}^{\infty} \sum_{n=1,3,\dots}^{\infty} \frac{\sin(m\pi x/a) \sin(n\pi y/b)}{mn(m^2/a^2 + n^2/b^2)^2} \quad (2.43)$$

where p is the applied transverse load in Pa, ζ is the plate flexural rigidity in N-m and finally a and b are the plate length and width, respectively, both in m. For the maximum deflection, occurring at the plate's centre ($x = a/2$, $y = b/2$), this becomes:

$$\delta_{max} = \frac{16p}{\pi^6 \zeta} \sum_{m=1,3,\dots}^{\infty} \sum_{n=1,3,\dots}^{\infty} \frac{\sin(m\pi/2) \sin(n\pi/2)}{mn(m^2/a^2 + n^2/b^2)^2} \quad (2.44)$$

The bending moment distributions per unit length \mathcal{M}_x and \mathcal{M}_y in N are described by:

$$\mathcal{M}_x = \frac{16p}{\pi^4} \sum_{m=1,3,\dots}^{\infty} \sum_{n=1,3,\dots}^{\infty} \frac{m^2/a^2 + \nu(n^2/b^2)}{mn(m^2/a^2 + n^2/b^2)^2} \sin(m\pi x/a) \sin(n\pi y/b) \quad (2.45)$$

$$\mathcal{M}_y = \frac{16p}{\pi^4} \sum_{m=1,3,\dots}^{\infty} \sum_{n=1,3,\dots}^{\infty} \frac{\nu(m^2/a^2) + n^2/b^2}{mn(m^2/a^2 + n^2/b^2)^2} \sin(m\pi x/a) \sin(n\pi y/b) \quad (2.46)$$

The bending moments per unit length at the plate's centre (also in N) are described by:

$$\mathcal{M}_x = \frac{16p}{\pi^4} \sum_{m=1,3,\dots}^{\infty} \sum_{n=1,3,\dots}^{\infty} \frac{m^2/a^2 + \nu(n^2/b^2)}{mn(m^2/a^2 + n^2/b^2)^2} \sin(m\pi/2) \sin(n\pi/2) \quad (2.47)$$

$$\mathcal{M}_y = \frac{16p}{\pi^4} \sum_{m=1,3,\dots}^{\infty} \sum_{n=1,3,\dots}^{\infty} \frac{v(m^2/a^2) + n^2/b^2}{mn(m^2/a^2 + n^2/b^2)^2} \sin(m\pi/2) \sin(n\pi/2) \quad (2.48)$$

Finally, the von Mises stress σ_{vm} in Pa is calculated using:

$$\sigma_{vm} = \sqrt{\frac{(\sigma_x - \sigma_y)^2 + (\sigma_y - \sigma_z)^2 + (\sigma_z - \sigma_x)^2}{2}} = \sqrt{\frac{(\sigma_{x,max} - \sigma_{y,max})^2 + \sigma_{y,max}^2 + \sigma_{x,max}^2}{2}} \quad (2.49)$$

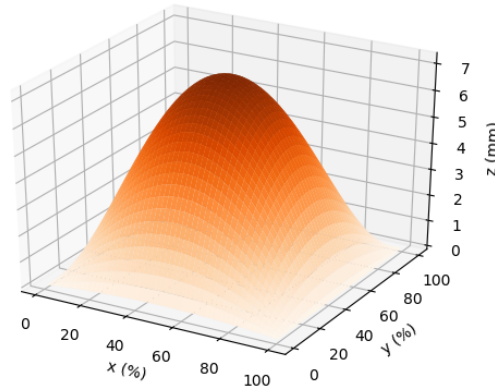
where the stress components at the centre of the plate follow from:

$$\sigma_{x,max} = \frac{6\mathcal{M}_x}{t^2} \quad (2.50)$$

$$\sigma_{y,max} = \frac{6\mathcal{M}_y}{t^2} \quad (2.51)$$

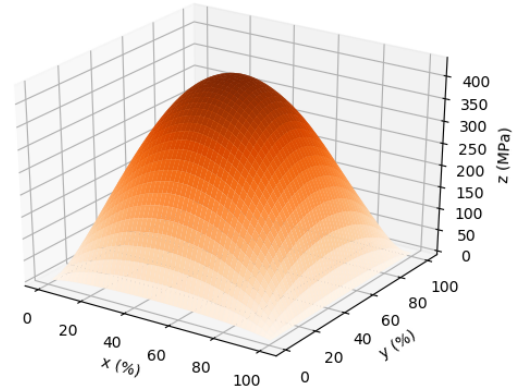
where it must be noted that, as mentioned before, the bending moment distributions per unit length \mathcal{M}_x and \mathcal{M}_y are in N and plate thickness t is in m, resulting in a valid result of $\sigma_{x,max}$ and $\sigma_{y,max}$ in N-m⁻² or Pa. The relations for deformations are demonstrated in Figure 2.22a, stresses shown in Figure 2.22b, visualising that the stresses and deformations are at their maximum at the centre of the plate.

Out-of-plane deformation of thin plate with simply supported edge:
a = 0.1 m, b = 0.15 m, t = 1.0 mm, p = 1.0 bar



(a) Out-of-plane deformations.

Von Mises stress of thin plate with simply supported edges
a = 0.1 m, b = 0.15 m, t = 1.0 mm, p = 1.0 bar



(b) Von Mises stresses.

Figure 2.22: Results of thin plate relations for deformations and stresses, Python/Matplotlib.

2.8.3. Tank Materials

For selecting the tank material, the parameters specific strength and specific stiffness are considered: specific strength is the ratio of stress to density, specific stiffness is the ratio of Young's modulus to density. For both parameters, materials with comparably higher values result in lower tank mass for the same deformations and stresses. For the MPS propellant LMP-103s, material compatibility with the titanium alloy Ti-6Al-4V and stainless steels is stated by Persson et al in 2019 [23]. A selection of these materials is presented in Table 2.10, here it is observed that the material Ti-6Al-4V Solution Treated & Aged (STA) is the most suitable material due to its highest specific strength, the specific stiffness is within a small range for all materials. The RCS propellant is water, and is assumed to be compatible with Ti-6Al-4V as well.

2.8.4. Propellant Management Devices

The integration of Propellant Management Devices (PMD) into a propulsion system serves the primary purpose of providing gas-free propellant expulsion at the outlet port of the tank. As secondary purpose,

Table 2.10: Materials compatible with propellant LMP-103s.

Material	$\sigma_{t,y}$	$\sigma_{t,u}$	E	ρ	$\sigma_{t,u}/\rho$	E/ ρ	Ref.
Ti-6Al-4V (STA)	1,100 MPa	1,170 MPa	114 GPa	4.430 g-cc ⁻¹	264.108 MPa-cc-g ⁻¹	25.734 GPa-cc-g ⁻¹	[72]
AISI 304L	210 MPa	564 MPa	193 GPa	8.000 g-cc ⁻¹	70.500 MPa-cc-g ⁻¹	24.125 GPa-cc-g ⁻¹	[73]
301 Stainless steel	205 MPa	515 MPa	212 GPa	8.030 g-cc ⁻¹	61.134 MPa-cc-g ⁻¹	26.401 GPa-cc-g ⁻¹	[74]

they serve to control the position of the fluid and thereby reduce sloshing. In this study, PMDs are characterised by their mass, volume and Expulsion Efficiency (EE), which is defined as the ratio of usable propellant to total propellant:

$$EE = \frac{M_{p,us}}{M_{p,tot}} \tag{2.52}$$

A high EE is desirable, meaning that only a low fraction of propellant is left as residuals at EOL. Jason Hartwig has published historical reviews on PMD in 2016 and 2017 [75, 76]. The author separates the PMD types by classification of non-capillary PMD and capillary PMD. Here, non-capillary PMD are diaphragms (Figure 2.23a), bladders (Figure 2.23b) and piston-type devices (Figure 2.23c).

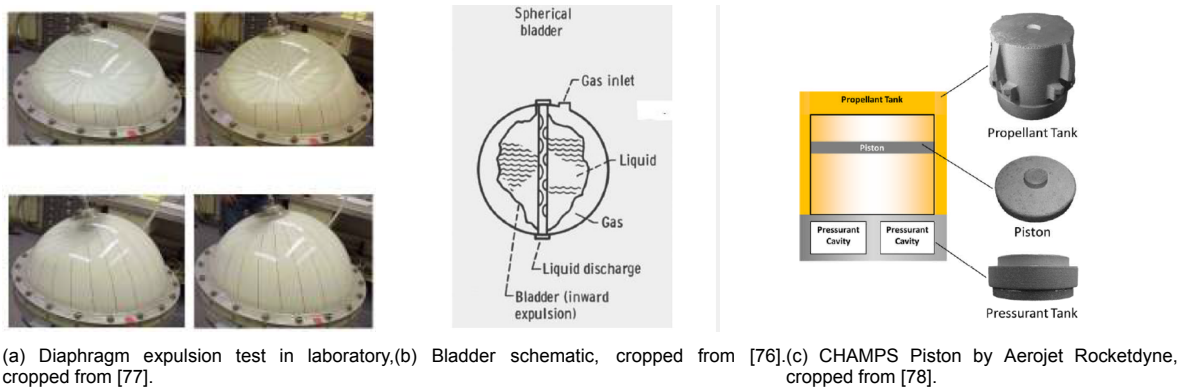


Figure 2.23: Examples for non-capillary Propellant Management Devices.

Capillary PMD types are divided into full-communication devices and partial-communication devices. Of interest for LUMIO are full-communication devices, namely sponges (Figure 2.24a), vanes (Figure 2.24b) and galleries (Figure 2.24c). These devices may be designed such that propellant is gathered from any location inside the tank, which is desirable in the design of LUMIO. In reality, however a combination of PMD can be used to achieve a high degree of communication. Partial communication devices are traps, troughs, vortex suppressors and baffles, these serve mainly to filter gas bubbles and reduce slosh.

Propellant Management Devices in CubeSat Applications

Collicott et al. have discussed the suitability of PMD for smaller spacecraft such as CubeSats with conformal tanks in 2019 [79], proposing surface-tension devices for use in this type of tank. Due to the choice of conformal tanks for both the MPS and RCS, bladder-, diaphragm- and piston-type devices are excluded from consideration. This leaves the options of gallery-, vane- and sponge-type devices. Sponges are placed at the outlet port, to guarantee delivery of a fixed amount of propellant on-demand, to be refilled over time by a vane or gallery type device. It can be seen that between the gallery- and vane-type devices, the vane-type device scores best in all metrics. Since the design of these devices is complicated and difficult to verify, a conservative approach is chosen, using a combination of two

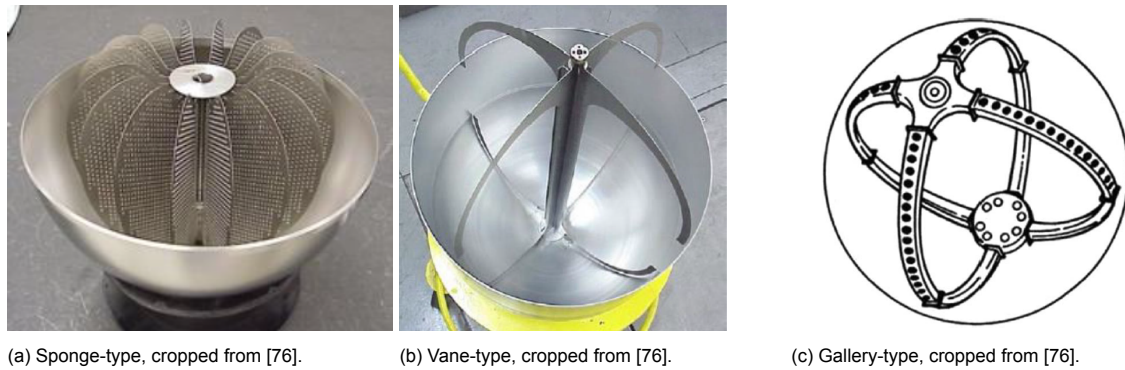


Figure 2.24: Examples for capillary Propellant Management Devices classified as full-communication devices.

PMD. One example of this is the choice of PMD inside the Lunar Flashlight Propulsion Module, where a combination of vane- and sponge-type devices is chosen, with a conservatively estimated EE of 90%. Another CubeSat application is found in the CHAMPS system by Aerojet Rocketdyne, where a piston-type PMD is used to form a hard boundary between the pressurant gas and propellant, shown in Figure 2.23c, discussed by Carpenter et al. in 2017 [78], no data with respect to EE is presented for this system, however.

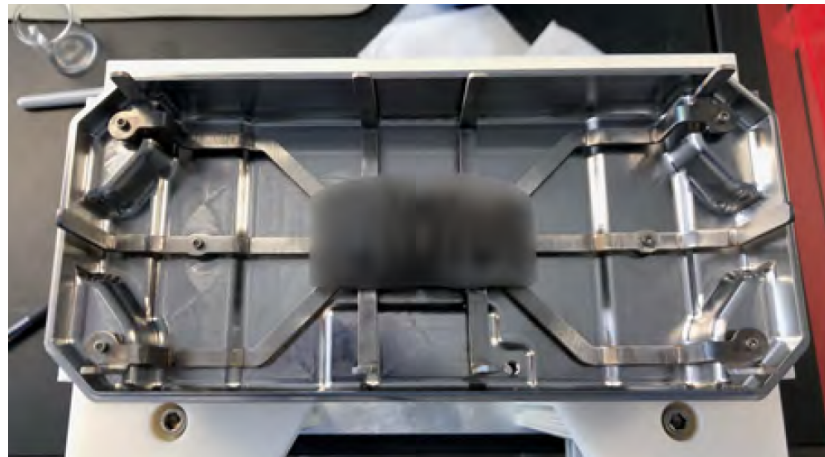


Figure 2.25: Sponge- and vane-type Propellant Management Devices inside the Lunar Flashlight Propulsion Module, cropped from [8].

Comparison of Propellant Management Devices

From the aforementioned works by Hartwig and Collicott, the general properties of six PMD types considering EE, mass, simplicity and suitability for conformal tanks are compared qualitatively in Table 2.11. The first two options are preliminarily discarded due to not being suitable for conformal tanks, the piston-type PMD is discarded due to poor EE. Due to it being unclear whether a gallery or vane-type device is sufficient to provide sufficient propellant on demand, a combination of a sponge and either a gallery or vane is of interest. Due to the vane-type device being more simple as compared to the gallery-type device, the preliminarily selected PMD are a combination of sponge and vane-type devices, as discussed in Section 4.1.1. Finally, in order to prevent propellant from sticking to the edges inside the tank and simultaneously reduce the magnitude of stress concentrations along the tank edges, fillets are preliminarily selected to be added as well.

Sponge Design

Sponge design is performed considering methods presented by Jaekle in 1993 [80]. A sponge requires extensive analysis, e.g. for leakage and dripping under adverse accelerations, which is left out of scope. In order to arrive at a mass and volume estimate for the sponge-type PMD, a conservative design method is used. As recommended by Jaekle, a safety factor of 2 is used on the required

Table 2.11: Comparison of Propellant Management Device types [75, 76, 79].

Type	EE	Mass	Simplicity	Suitable for con-formal tanks
Bladder	Good	Excellent	Good	No
Diaphragm	Excellent	Excellent	Excellent	No
Piston	Poor	n/a	n/a	n/a
Gallery	Excellent	Good	Poor	Yes
Vane	Excellent	Good	Excellent	Yes
Sponge	Good	Poor	Good	Yes

sponge holding volume and the available sponge diameter is calculated using a wall spacing of one inch outside the sponge. The sponge is assumed to hold fluid between its plates with the following fluid volume:

$$V_{ho,spo} = h_{spo}(\pi r_{spo}^2 - N_{pla} l_{pla} t_{pla} - \pi r_{tube,o}^2) \quad (2.53)$$

where h_{spo} is the height of the sponge plates, r_{spo} the radius, N_{pla} is the number of plates around the centre tube, t_{pla} is the thickness of the plates and finally, l_{pla} is the length of each plate, calculated using the following relation:

$$l_{pla} = r_{spo} - r_{tube,o} \quad (2.54)$$

The required sponge holding volume is calculated using the burn time of the thrusters:

$$V_{ho,req} = \frac{t_{bu} m_p}{\rho_p} \quad (2.55)$$

The volume of the sponge material, which needs to be compensated for in propellant tank design, is calculated. The mass simply results from multiplying this volume with the density of the selected material:

$$V_{spo} = h_{spo}(N_{pla} l_{pla} t_{pla} + \pi(r_{tube,o}^2 - r_{tube,o}^2)) \quad (2.56)$$

Vane Design

Similar to sponge design, vane design requires extensive analysis which is left out of scope, and only a simple design is considered in order to arrive at a mass and volume estimate of the device. One method presented by Jaekle, 1991 [81] on approximating a possible upper limit for the flow rate is considered however. Different cross-sectional geometries of vanes are possible as shown in Figure 2.26a. Due to the more easily approximated flow area between the ribbon-type vane PMD and the tank wall, the ribbon-type vane PMD is chosen. First, vane dimensions are assumed. Secondly, a possible upper limit on fluid flow is calculated by calculating the area wave propagation speed q along the vanes. Here, it is assumed that the cross-sectional area of the fluid flow along the vanes is proportional to the square of wave fillet radius R_{wa} . This fillet radius in turn is preliminarily assumed to be equal to the spacing between tank wall and vane:

$$q = \sqrt{\frac{1}{2} \frac{\zeta_{st}}{\rho_p} \frac{1}{R_{wa}}} \quad (2.57)$$

where ζ_{st} is the absolute surface tension of the propellant in N-m⁻¹, ρ_p is the density of the propellant and R_{wa} is the wave fillet radius in m, which will be assumed equal to the vane-wall spacing. Using this velocity, a maximum flow rate at this condition can be calculated per vane:

$$\dot{V}_{va} = q A_{va} \quad (2.58)$$

where for the vane flow area A_{va} , simply the area below the ribbon-type vane and the wall is used, assuming the fluid fills up that space. The fluid forming a fillet-type region outside of this rectangular area is ignored. The volume of the vane material is calculated using:

$$V_{va} = w_{va} t_{va} L_{va} \quad (2.59)$$

here, L_{va} is determined by tank length, and is calculated for the MPS tank in the following way for the short side. For the long side of the tank, a_{tank} is used instead of b_{tank} . For the RCS, $a = b$:

$$l_{va,RCS,shortside} = (b_{tank} - D_{tube,o} - 2d_{va}) + (b_{tank} - 2d_{va}) + 2(L_{tank} - 2d_{va} - 2t_{va}) \quad (2.60)$$

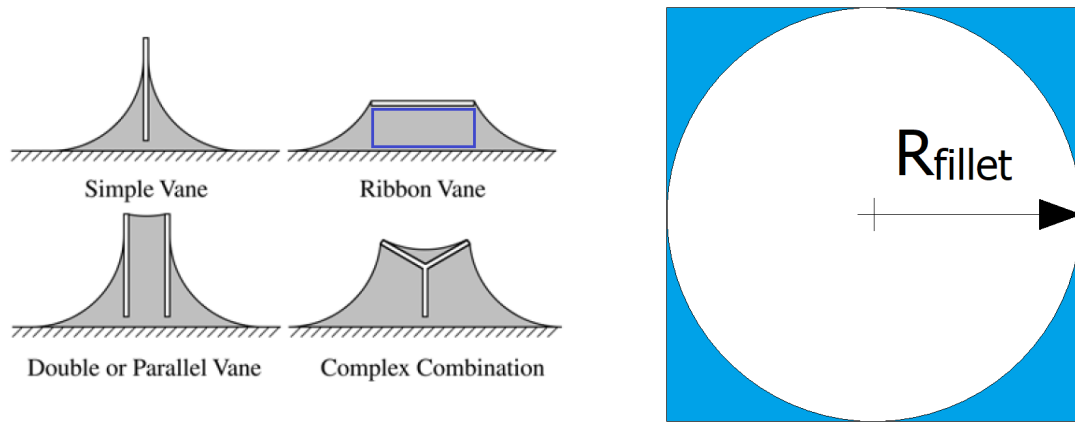
where a_{tank} is the width of the tank, $D_{tube,o}$ is the outer diameter of the tube at the centre of the sponge and d_{va} is the stand-off distance from the tank wall.

Fillet Design

The volume occupied by fillets along four edges is considered by subtracting the area of a circle with radius R_{fil} of a square with lengths $2R_{fil}$ (Figure 2.26b). The fillet volume over one tank axis is therefore:

$$V_{fil} = ((2R_{fil})^2 - \pi R_{fil}^2)L_{fil} \quad (2.61)$$

The total fillet volume along all 12 edges inside the cuboid tank shape results from simply adding the fillet volume for each of the three axes, assuming the difference between this method and separately considering the fillet volume in all eight corners of the tank is negligible.



(a) Different types of vane-type PMD, flow area under ribbon vane(b) Illustration for fillet area calculation, fillet cross-sectional area marked blue, edited from [81].
blue, Inventor 2022.

Figure 2.26: Vane-type and fillet PMD illustrations.

2.8.5. Heat Loss and Heating

Radiative Heat Loss

In the quasi-vacuum of space, the only modes of heat transfer considered are conduction and radiation. Here, radiation is considered for generating an estimate of radiative heat loss \dot{Q} in W, approximated as:

$$\dot{Q} = \varepsilon \gamma T_{wall}^4 A_o \quad (2.62)$$

where ε is the dimensionless emissivity, γ the Stefan-Boltzmann constant ($5.670 \text{ E-}8 \text{ W-m}^{-2}\text{-K}^{-4}$), T_{wall} the outer wall temperature in K and finally A_o the outer surface area of the tank in m^2 . Fortescue et al. described in 2011 [82] a ε of 0.60 for polished Titanium. This can be further reduced by using several layers of insulation blankets with low emissivity. The proposed method by Fortescue et al. is to use several layers of aluminised plastic sheets as Multi Layer Insulation (MLI); these very thin sheets of material are either separated by a low conductance spacer material such as silk or glass-fibre netting to prevent conductance between layers or the sheets are crinkled/dimpled to reduce the surface area of contact. Theoretically, this will allow very low values of emissivity, as shown in Figure 2.27. A popular material for this is Biaxially-oriented Polyethylene Terephthalate (BoPET), colloquially known as "Mylar", with a thin layer of aluminium. As density, the value of Mylar of $1,390 \text{ kg-m}^{-3}$ is taken as reported by the Dupont de Nemours corporation in 2003 [83]. The authors state that in reality these MLI blankets may consist of at least 40 layers of each $10 \text{ }\mu\text{m}$ thickness (according to Figure 2.27 this would theoretically result in an effective emissivity of $\varepsilon = 0.001$).

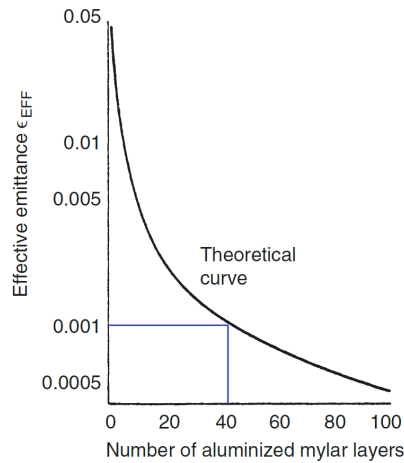


Figure 2.27: Effective emissivity of aluminised Mylar blankets, edited from [82].

Pressurant Gas Expansion

During thruster operation, the pressurant gas will expand to occupy the now vacant volume left behind by the expelled propellant. In reality, the propellant will expand as well, and its temperature will decrease too. However, to achieve a preliminary estimate of required heating power, only the expansion of the pressurant gas is considered. This energy $E_{he,tank}$ in J is calculated as follows:

$$E_{he,tank} = M_{pres} c_{v,pres} \Delta T_{pres} \quad (2.63)$$

where M_{pres} is the pressurant mass in kg, $c_{v,pres}$ is the specific heat capacity considering constant volume for the pressurant gas in $\text{J}\cdot\text{kg}^{-1}\cdot\text{K}^{-1}$ and ΔT_{pres} the temperature difference between BOL and EOL in K. For calculating ΔT_{pres} a worst-case estimate assuming isentropic expansion is assumed:

$$\Delta T_{pres} = T_{BOL} - T_{EOL,is} \quad (2.64)$$

$$T_{EOL,is} = T_{BOL} \left(\frac{p_{EOL}}{p_{BOL}} \right)^{\frac{\gamma-1}{\gamma}} \quad (2.65)$$

Finally, the power $P_{he,tank}$ in W is approximated assuming a linear decrease in temperature between BOL and EOL over the total burn time:

$$P_{he,tank} = \frac{E_{he,tank}}{t_b} \quad (2.66)$$

where t_b is the burn time of the system between BOL and EOL in s.

2.9. Commercial-Off-The-Shelf and Experimental CubeSat Propulsion Systems and Components

This section serves to present a selection of possibly feasible components for the custom propulsion system design and COTS options for full propulsion systems to serve as baseline to compare the final design to. The data for many of these components is sourced from datasheets and web-sources and is therefore treated as unreliable. However, due to lack of reliable, peer-reviewed articles on these specific components, for the sake of generating a theoretical propulsion system design, the data is assumed correct. It is furthermore assumed, that all of these components can be purchased or recreated and are thus available for use in the custom propulsion system design. Leakage rates of components are at MEOP unless indicated otherwise. Fluid compatibility is stated as presented in the datasheet/publication, unless indicated otherwise.

2.9.1. Thrusters

Main Propulsion System Thrusters

Thrusters from manufacturers Bradford ECAPS (Sweden), Aerojet Rocketdyne (US) and Busek (US) are presented in Table 2.12. Thrusters using Hydrazine propellant are not considered as it is listed as a "substance of high concern" by the European Chemicals Agency (ECHA) [84] and this is deemed unacceptable as per requirement PROP.190. The thruster options discussed here utilise either LMP-103s or AF-M315E as propellant, both were developed as an alternative to Hydrazine propellants. LMP-103s (Ammonium Dinitramide, "ADN"-based) has been mostly the focus of the Swedish defense research agency and ECAPS, AF-M315E or "ASCENT" (Hydroxylammonium nitrate, "HAN"-based) was developed by the US Air Force Research Laboratory (AFRL) [38, 39].

A significant difference in I_{sp} is observed between the 100 mN and 1 N thrusters of Bradford ECAPS, even though the same propellant is used (LMP-103s). The 100 mN thruster is characterised by a significantly lower thrust range and I_{sp} as compared to the 1 N thruster. The lower I_{sp} of the 100 mN thruster may be caused by miniaturisation effects causing lower nozzle efficiency, one possible effect may be a reduced effective nozzle cross-sectional area due to a laminar boundary layer forming on the walls at lower Reynolds numbers, typical for lower throat diameters, as discussed by Robert Bayt in 1999 [85].

Table 2.12: Thruster options for the Main Propulsion System.

Name (Manufacturer)	Propellant	I_{sp}	F_T range	$p_{t,in}$	$P_{el,pre}$	TRL	Ref.
HPGP 100 mN (Bradford ECAPS)	LMP-103s	200 s	30 mN - 100 mN	2.3 bar - 4.5 bar	8 W	5	[86]
HPGP 1 N (Bradford ECAPS)	LMP-103s	231 s	250 mN - 1,000 mN	4.5 bar - 22 bar	10 W	9	[40]
GR-1 (Aerojet Rocketdyne)	AF-M315E	231 s	260 mN - 1,420 mN	6.9 bar - 37.9 bar	n/a	n/a	[87]
BGT-X1 (Busek)	AF-M315E	215 s	20 mN - 180 mN	n/a	4.5 W	n/a	[88]
BGT-X5 (Busek)	AF-M315E	225 s	50 mN - 500 mN	6.9 bar - 34.5 bar	20 W	5	[89]



(a) Bradford ECAPS HPGP 100 mN thruster, (b) Bradford ECAPS HPGP 1 N thruster, (c) Aerojet Rocketdyne GR1 thruster, cropped from [86].
cropped from [40].
cropped from [24].

Figure 2.28: Main Propulsion System thruster options.



(a) Busek BGT-X1 thruster, cropped from [88].

(b) Busek BGT-X5 thruster, cropped from [89].

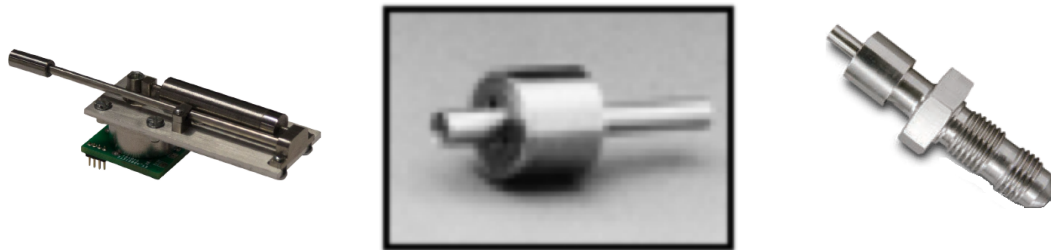
Figure 2.29: Main Propulsion System thruster options, continued.

Reaction Control System Thrusters

Three commercially available microthrusters suitable for LUMIO's RCS are presented in Table 2.13. The Aurora Resistojet One (ARO) thruster was developed by Aurora (Finland) and uses the resistojet technology with an unspecified water-based propellant which for the sake of this project is assumed to be water. The thruster includes a tank available in different sizes, seen in Figure 2.30a. However, the smallest available variant is 20 x 20 x 20 mm, still including a tank. For the design of the RCS, these dimensions are taken even though the tank is not utilised. Moog (US) has developed two Cold Gas Thrusters (CGT) using Nitrogen propellant. The 58X125A thruster is shown in Figure 2.30b and the 58E143 thruster is shown in Figure 2.30c. The latter is characterised by higher mass, lower chamber pressure and lower specific impulse however also by higher thrust.

Table 2.13: Relevant thruster data for the Reaction Control System trade-off.

Name (Manufacturer)	Type ¹	Propellant	I_{sp}	ρI_{sp} ²	F_T range	$p_{t,in}$	$P_{el,fire}$	Mass	Ref.
ARO (Aurora)	ETR	Water-based	100 s	99.656 g-s-cc ⁻¹	0.6 - 4 mN	< 1 bar	2 - 20 W	29 g	[90]
58X125A (Moog)	CGT	GN ₂	65 s	3.650 g-s-cc ⁻¹	4.4 mN	3.447 bar	10 W	9 g	[42]
58E143 (Moog)	CGT	GN ₂	60 s	3.369 g-s-cc ⁻¹	10 mN	1.500 bar	10 W open, 1 W hold	40 g	[91]



(a) Aurora Resistojet One by Aurora with propellant tank, cropped from [90]. (b) Moog 58X125A Nitrogen Cold Gas Thruster, cropped from [14]. (c) Moog 58E143 Nitrogen Cold Gas Thruster, cropped from [91].

Figure 2.30: Reaction Control System thruster options.

¹CGT: Cold Gas Thruster, ETR: Electrothermal resistojet

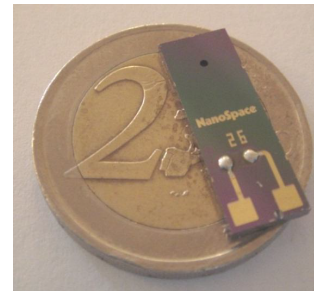
²Calculated using storage density of propellant at 50 bar, 300 K from Table 2.5 for GN₂, for water the values 1 bar and 300 K are used [49].

2.9.2. Regulator Valves

A regulator valve can be used to regulate downstream pressure by flow restriction. This component may be integrated for example in front of a thruster, to achieve throttling, or between the pressurant tank and propellant tank in a regulated-type system with split pressurant/propellant tanks, to achieve constant propellant tank pressure. Valcor offers a line of pressure regulator valves, of which the smallest is shown in Figure 2.31a. Its inlet and outlet pressure ranges are however outside that feasible for LUMIO, namely above 50 bar. MOOG offers the 51E339 Proportional Flow Control Valve, shown in Figure 2.31b. This valve only has a small outlet pressure range, however can accommodate for a large range of inlet pressures. Both of these valves are characterised by significant mass. Rangsten et al. at GOMSpace (formerly NanoSpace AB) have developed the Pressure Regulator Module on a MEMS chip for feeding ion engines. The valve is significantly smaller compared to the other two valves considered here. It is important to note that all of these valves are designed for use with gas flows.

Table 2.14: Regulator valve options.

Parameter	V4000-189-W	51E339	MEMS PRM
Dimensions	n/a	n/a	20 x 7 x 1.2 mm
Mass	179 g	115 g	n/a
Material	Titanium	Stainless steel/Vespel	Silicon
Leak rate internal	n/a	1.000 E-4 sccs He	n/a
Leak rate external	n/a	1.000 E-6 sccs	n/a
Availability	COTS	COTS	COTS
Inlet pressure range	124.016 - 689.476 bar	2.8 - 186 bar	n/a
Outlet pressure range	75.842 - 94.803 bar	0 - 2.8 bar	n/a
MEOP	n/a	186 bar	2 bar
Flow rate	2.458 E-5 - 1.966 E-3 m ³ /s	0 - 30 mg/s Xe at 186 bar	5 - 50 µg/s Xe
Fluid compatibility	He	Xe, He	Xe
Filter	n/a	25 µm inlet filter	n/a
Reference	[92]	[93]	[94]



(a) Valcor V4000-189-W pressure regulator (b) VACCO 51E339 Proportional Flow Control Valve, cropped from [93]. (c) GOMSpace Pressure Regulator Module on a MEMS chip, cropped from [94].

Figure 2.31: Regulator valve options.

2.9.3. Start/Stop Valves

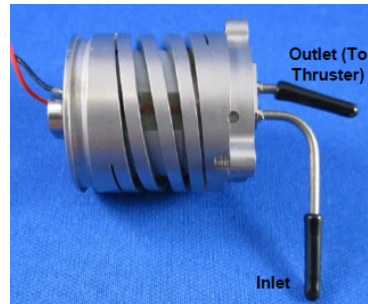
For opening fluid circuits for short periods of time (e.g. flow to a thruster), a normally closed start/stop valve can be used. Marotta has developed a miniature solenoid valve for micropropulsion systems, seen in Figure 2.32a, taken from the corresponding product datasheet [95]. As discussed by Tsay et al. in 2014, Busek has developed a piezo microvalve (Figure 2.32b) for micropropulsion systems with low mass, volume and power consumption in mind, however not much information is public at present. Yang, et al. at NASA/JPL have discussed the development of a piezo microvalve (Figure 2.32c) in 2004 [96]. Relevant characteristics about these valves are shown in Table 2.15. Little information is available about the two latter valves, therefore if these valves are chosen in the design, some assumptions may be required to be made on their characteristics.

Table 2.15: Start/stop valve options.

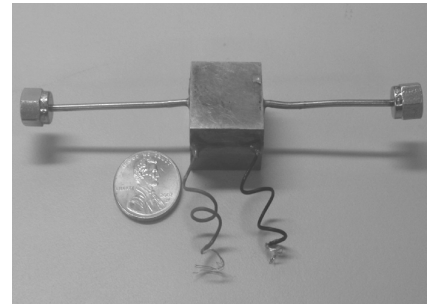
Parameter	Marotta SPV187	Busek Piezo Microvalve	JPL MEMS Piezo Microvalve
Dimensions	31.95 mm length, 17.14 mm largest diameter	n/a	n/a
Mass	45 g	n/a	n/a
Material	CRES 304L	Titanium	Silicon and unspecified metals
Leak rate internal	<1.000 E-4 sccs GHe	n/a	8.333 E-5 sccs GHe
Leak rate external	<1.000 E-6 sccs GHe	n/a	n/a
Availability	COTS	Experimental	Experimental
Port diameter	3.18 mm (outer)	n/a	n/a
Operating pressure	10 bar	3.447 bar	55.158 bar (leak test)
Proof pressure	187.5 bar	n/a	n/a
Burst pressure	312.5 bar	n/a	n/a
Fluid compatibility	N ₂ , inert gas	AF-M315E	Inert gas
Filter	n/a	n/a	n/a
Reference	[95]	[97]	[96]



(a) Marotta SPV187 solenoid valve, cropped from [95].



(b) Busek piezo microvalve, cropped from [98].



(c) NASA/JPL piezo microvalve, cropped from [96].

Figure 2.32: Start/stop valve options.

2.9.4. Isolation Valves

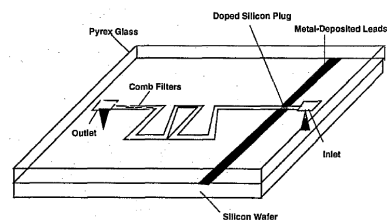
For launch safety considerations, a Normally Closed (NC) isolation valve may be used to isolate the pressurant or propellant from downstream components until the system is primed for operation. These NC valves are initially in the closed position, not allowing any fluid to pass through until the signal is sent for opening. Once the valve is opened, it will permanently remain in the open position. Such a component may typically be placed directly downstream of a pressurant gas reservoir and/or downstream of the propellant tank to isolate these fluids from the rest of the propulsion system. One type of isolation valve is a pyrotechnic valve, where the flow is blocked by a shear plug which is moved out of the way using a squib-type initiator device to drive a ramming component to the plug as described by James Richard in 2014 [99]. Arianespace and Vacco offer such pyrotechnical valves, shown in Figure 2.33a and Figure 2.33b. These devices may however be too large for small propulsion systems such as the ones used in CubeSats. Some development efforts into MEMS isolation valves have been made, where one example is the MEMS pyrovalve developed at NASA/JPL by Mueller et al. in 1999 and 2000 [43, 100], shown in Figure 2.33b. This valve is produced on a Silicon substrate with etched fluid passages and an anodically bonded Pyrex cover, and uses a doped silicon plug blocking the fluid passage. When current passes through the barrier, it melts and allows the flow of fluid with some debris of the barrier flowing down-stream. This is partially mitigated by the comb-type filtering passages, however additional filtering may be required as the authors note that some debris was found downstream of the valve. Typically, actuating pyrotechnic valves require a significant momentary amount of power, e.g. the worst case peak value for the discussed MEMS valve, which is 1 kW. The energy required can however be stored in a capacitor to mitigate this problem. Relevant data on these valves is shown in Table 2.16.

Table 2.16: Isolation valve options.

Parameter	Arianespace MMH Pyrovalve	JPL MEMS isolation valve
Dimensions	n/a	10 x 10 x 5 mm
Mass	< 160 g	n/a
Material	Titanium	Silicon, Pyrex
Leak rate internal	1.000 E-6 sccs GHe	n/a
Leak rate external	1.000 E-6 sccs	n/a
Availability	COTS	Experimental
Port diameter	6.35 mm	n/a
Operating pressure	310 bar	n/ar
Proof pressure	465 bar	n/a
Burst pressure (pre-firing)	1,240 bar	197 bar
Burst pressure (post-firing)	775 bar	n/a
Fluid compatibility	MON, MMH, Hydrazine	n/a
Filter	None	Comb filters
Reference	[101]	[43, 100]



(a) Arianespace pyrovalve, cropped from [101].



(b) MEMS isolation valve developed at NASA/JPL, cropped from [43].

Figure 2.33: Isolation valve options.

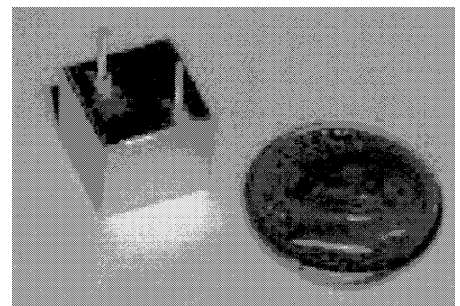
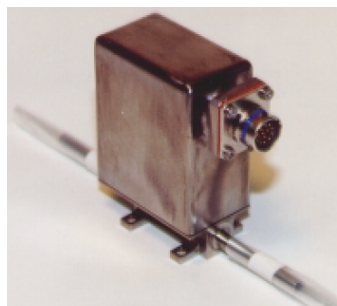
2.9.5. Latch Valves

A latch valve can be used in spacecraft propulsion systems to isolate parts of the system in case of leakage or other situations where isolation after system priming may be required. This type of valve has stable open and close positions, where the valve only momentarily draws power to switch the valve from one position to the other. This type of valve may just like an isolation valve be placed just downstream of a pressurant reservoir or propellant tank, to act as isolation valve, with the additional functionality of closing again.

VACCO offers low pressure and high pressure liquid and gas latch valves for space applications, seen in Figure 2.34a and Figure 2.34b. In collaboration between NASA/JPL and Moog, the Moog Latching Microvalve (MLV) was developed for applications in micropropulsion systems, as discussed by Mueller, et al. in 2001 [102]. The relevant characteristics of these valves are listed in Table 2.17. No data on power consumption for these valves was reported, however it is assumed this is non-critical due to only a momentary pulse of electric energy is required for operation. In case the power budget is exceeded by this, the required energy for switching of the valve position could be taken from a capacitor, similar to the recommendations made by Mueller about the NASA/JPL MEMS isolation valve in 2000 [43].

Table 2.17: Latch valve options.

Parameter	V1E10728-01	V1E10537-01	MLV
Dimensions	79.248 mm (length) x 34.798 mm (diameter)	32.512 x 81.788 x 55.626 mm	10 x 10 x 10 mm
Mass	168 g	340 g	7 g
Material	CRES, PTFE	All Titanium	n/a
Leak rate internal	2.778 E-4 sccs GHe	8.333 E-4 sccs GHe	1.000 E-4 sccs GN ₂
Leak rate external	1.000 E-6 sccs	1.000 E-6 sccs	n/a
Availability	COTS	COTS	Experimental
Port diameter	6.350 mm	6.350 mm	0.250 mm (ESEOD)
Operating pressure	27.579 bar	137.895 bar	20.684 bar
Proof pressure	41.369 bar	310.264 bar	n/a
MEOP	n/a	n/a	68.948 bar
Burst pressure	68.948 bar	517.107 bar	n/a
Fluid compatibility	Water, Hydrazine	Xe, GHe	Xe, GN ₂
Filter	40 µm etched disk	40 µm etched disk	n/a
Reference	[103]	[104]	[102]



(a) VACCO V1E10728-01 low pressure liquid (b) VACCO V1E10537-01 high pressure gas (c) Moog Microvalve, exterior identical to Moog Latching Microvalve, cropped from [102].

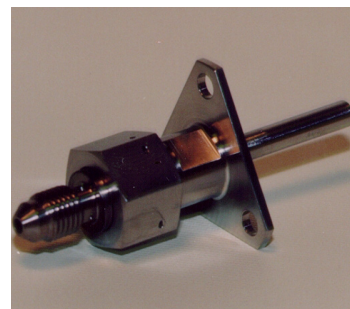
Figure 2.34: Latch valve options.

2.9.6. Fill/Drain Valves

For filling and draining of propellant and pressurant, a Fill/Drain Valve (FDV) can be used. One end can be attached to the tank or to a line connected to the propulsion system circuit. The other end is equipped with a NC valve, opening only when the ground half coupling is attached. Omnidea RTG offers a fill/drain valve for Hydrazine systems, citing flight heritage on NASA's GALILEO mission [105]. Arianespace offers a series of fill/drain valves, variants offered are designed to be compatible with MMH, GHe, MON, GXe, with all however being either a fill or a drain valve. As example, the MMH fill valve is used [101]. Finally, VACCO offers a fill/drain valve for low pressure applications using Titanium 304L CRES and a Tungsten Carbide (WC) ball [106]. For the latter material, no source explicitly stating compatibility with propellant LMP-103s could be found.

Table 2.18: Fill/drain valve options.

Parameter	Omnidea FDV	Hydrazine	Arianespace MMH Fill Valve	VACCO FDV
Dimensions	150 x 150 x 150 mm		109 mm length, other di- mensions n/a	103.759 mm length, 47.498 mm largest diameter
Mass	150 g		90 g	113 g
Material	Ti-6Al-4V, steel	Stainless	Ti-6Al-4V	Ti, WC, 304L CRES
Leak rate internal	< 1.000 E-5 sccs GHe		<2.800 E-4 sccs GHe	<1.000 E-5 sccs GHe
Leak rate external	< 1.000 E-6 sccs GHe		< 1.000 E-6 sccs GHe	<1.000 E-6 sccs GHe
Availability	COTS		COTS	COTS
Port diameter	6.35 mm		6.4 mm	6.35 mm
Operating pressure	28 bar		33 bar	17.237 bar
Proof pressure	n/a		n/a	n/a
Burst pressure	n/a		1,240 bar	n/a
Fluid compatibility listed	Hydrazine, MMH, Kerosene	UDMH, Aerozine,	MMH, NTO, Hydrazine	MMH, Water, IPA, N ₂ O ₄
LUMIO propellant compatible				
Filter	n/a		n/a	n/a
Reference	[105]		[101]	[106]



(a) Omnidea RTG Hydrazine fill/drain valve, (b) Arianespace fill/drain valve, cropped from (c) VACCO fill/drain valve, cropped from [107].
cropped from [105]. [101].

Figure 2.35: Fill/drain valve options.

2.9.7. Filters

Any particulate matter present in fluids flowing through the propulsion system may damage downstream components or reduce the leak tight properties of valves. Therefore, in case components are not equipped with a filter, a separate filter may be required to be included in the flow circuit, typically downstream of any particle containing components such as a tank or particle generating components such as isolation valves. Omnidea RTG offers a propellant filter (Figure 2.36a) with 2 μm mesh filter for Hydrazine, UDMH and MMH propellants with flight heritage on the SAR-Lupe spacecraft. The material of the body is Ti-6Al-4V and the mesh material is stainless steel. Furthermore, a completely stainless steel fabricated pressurant filter (Figure 2.36b) is offered for inert gases, with the same mesh size and flight heritage in the Champ and Grace spacecraft, as presented in their product catalogue [105]. VACCO offers a COTS line of etched disk filters, shown in Figure 2.36c is the example of F1D10807-02, designed for use with Hydrazine propellants. The material is an unspecified Titanium alloy. It is observed that it is the lightest filters out of all options presented here.

Table 2.19: Filter options.

Parameter	Omnidea RTG propellant filter	Omnidea RTG pressurant filter	VACCO F1D10807-02
Dimensions	145 x 26 x 26 mm	50 x 30 x 30 mm	97.5 mm length, 14.0 mm largest diameter
Mass	110 g	76 g	24 g
Material	Ti-6Al-4V, Stainless steel	Stainless steel	Titanium alloy (unspecified)
Leak rate external	0	0	<1.000 E-6 sccs GHe
Availability	COTS, qualification pending	COTS, qualified	COTS, qualification unspecified
Port diameter	6.35 mm (outer)	6.35 mm (outer)	6.35 mm (outer)
Operating pressure	28 bar	350 bar	20.684 bar
Proof pressure	n/a	n/a	68.948 bar
Burst pressure	n/a	n/a	861.845 bar
Fluid compatibility	Hydrazine, UDMH, MMH	Inert gas	Hydrazine
Filter	2 μm mesh	2 μm	15 μm
Reference	[105]	[105]	[108]



(a) Omnidea RTG propellant filter, cropped from [105]. (b) Omnidea RTG pressurant filter, cropped from [105]. (c) VACCO F1D10807-02, cropped from [108].

Figure 2.36: Filter options.

2.9.8. Sensors

In order to measure temperature, a thermocouple can be used. A thermocouple consists of a bi-metallic junction which generates a small potential difference as function of temperature. The reactor temperature inside the Bradford/ECAPS HPGP 1N thruster is measured using an Inconel-covered K-type thermocouple according to Friedhoff et al. in 2017 [109]. RS Pro offers a wide range of thermocouples offering options for sheath materials, temperature ranges and junction type. An example is their mineral insulated K-type thermocouple with Inconel sheath with a temperature range of -40 deg. C to 750 deg. C (Figure 2.37a). The shaft length is however 150 mm, this may not be suitable for LUMIO's propellant tanks. Therefore, customisation of the component will be necessary. In order to measure propellant temperature, this component may be integrated inside the propellant tank. A pressure transducer uses a strain gauge to measure the force exerted on a specific area and thus pressure applied, to be measured by the change in electrical resistance through the gauge. GP:50 offers a line of commercially available pressure transducers for aerospace applications, one example is the 7000 series miniature pressure transducer (Figure 2.37b) with a pressure range of 0-7 bar and an accuracy of 0.25% of the range (1750 Pa accuracy). This component can be integrated inside a propellant or pressurant tank, or installed just downstream of these tanks.

Table 2.20 shows the specifications of the aforementioned sensor options.

Table 2.20: Sensor options.

Parameter	RS Pro K-type thermo-couple	GP:50 Miniature pres-sure transducer 7000
Minimum operating temperature	-40 deg. C	-60 deg. C
Maximum operating temperature	750 deg. C	130 deg. C
Minimum measured pressure	n/a	0 bar
Maximum measured pressure	n/a	7 bar
Sheath material	Inconel	Stainless steel or Titanium
Junction type	K	n/a
Sheath diameter	0.5 mm	4.2 mm
Sheath/probe length	150 mm	< 25.4 mm
Accuracy	n/a	+-.25% of range
Mass	n/a	12 g
Reference	[110]	[111]



(a) RS Pro K-type thermocouple, cropped from [110].



(b) GP:50 Miniature pressure transducer 7000 series, cropped from [111].

Figure 2.37: Sensor options.

2.9.9. Complete Propulsion Systems

The following complete propulsion systems are candidates the final custom design can be compared to for evaluation of performance. First, MPS candidates are shown, subsequently, RCS candidates are shown.

Main Propulsion System

As discussed by Carpenter et al. of Aerojet Rocketdyne in 2013 [78], Aerojet Rocketdyne has developed a line of CubeSat propulsion systems designated "Modular Propulsion Systems", based on the earlier "CubeSat High Impulse Adaptable Modular Propulsion System" (CHAMPS) or "MRS-142", starting in 2011. The systems of interest in this line are the MPS-12X and MPS-13X, where the second digit "2" refers to Hydrazine mono-propellant systems and "3" refers to AF-M315E "green" mono-propellant systems. Other systems with different digits exist, such as electric and cold gas propulsion systems. The third digit, now marked "x", indicates the feed type system, where "0" indicates piston fed systems with condensable pressurant and "5" indicates a pump-fed system with PMD tank. Out of the MPS-12x and MPS-13x series, only the MPS-13X series is considered as Hydrazine propellant is not feasible according to requirement PROP.190 outlawing all propellants indicated as toxic by REACH, including Hydrazine (Appendix A.1). From the publication by Carpenter et al. it is inferred that the MPS-13X series only exists in 1U configuration, however in the datasheets supplied by Aerojet Rocketdyne [22, 112], several versions exist, namely: 1 U, 2 U in length, 4 U in 4x1 cuboid configuration, 6 U in 4x1.5 cuboid configuration and 8 U in 4x2 cuboid configuration. The larger systems in cuboid configuration are all pump-fed whereas the 1U and 2U variants are piston-fed. It is important to note, that these cuboid configurations are infeasible for LUMIO due to payload requirements driven propulsion system requirement PROP.200 (Appendix A.1). Therefore, the only systems considered by Aerojet Rocketdyne are the MPS-135-1U and MPS-135-2U (Figure 2.38a). All these systems furthermore include four thrusters mounted at the corners, indicating the system may serve as both MPS and RCS. According to Carpenter et al., the system was produced using Additive Manufacturing (AM) and features a high level of integration of components, enabling the small system volume. Using a ϕ of 0.507, based on the provided wet mass and propellant mass for the 2 U version, an acceptable wet mass of 4.322 kg results for LUMIO.

According to Tsay et al. in 2017 [25], Busek has developed a "green" mono-propellant thruster system called "Advanced Monopropellant Application for CubeSats" (AMAC), utilising propellant AF-M315E and their BGT-X5 thruster. According to the datasheet [89], the system is scalable, however no data with regards to this was published. The system employs a blow-down concept, utilising a pressurant gas generator system vapourising liquid CO₂, requiring 15 W of heater power. After gas generation, the catalyst bed pre-heater of the thruster requires 15-20 W until firing can commence. No data with regards to propellant mass was published, however from the provided total impulse value and specific impulse, a preliminary estimate of attainable Δv for LUMIO using two of these systems was calculated as 43.895 m·s⁻¹ (Table 2.21), the propellant mass and dry mass here are marked with an asterisk (*) to indicate they were calculated backwards from the total impulse delivered. It is important to note, that using the calculated wet mass fraction ϕ reported here would result in a total propulsion system wet mass of 13.379 kg for LUMIO, making it an unfeasible system for use in LUMIO.

NanoAvionics has developed a modular SmallSat Propulsion System called EPSS, using an ADN-based mono-propellant as stated by NanoAvionics in 2021 [27]. The system is scalable in three steps: 1.5 U, 2 U and 3 U, and according to the manufacturer, the system has flight heritage (e.g. the NanoAvionics M6P 1,2 pathfinder mission). The presented data for the EPSS is only shown for the 2 U configuration (1.5 U and 3 U on request), and using the resulting ϕ of 0.308, a wet mass of 7.588 kg would result for use in LUMIO, making it unfeasible. It is however important to note, that ϕ is expected to increase for larger variants, therefore the 3 U option may be feasible however no data is publicly available for this system. The relevant properties of the aforementioned systems are presented in Table 2.21. Here it can be seen, that only the MPS-135-2U by Aerojet Rocketdyne has an acceptable wet mass after scaling.

Table 2.21: Main Propulsion System COTS candidates.

Parameter	Aerojet Rocketdyne MPS-135-1U	Rock-MPS-135-2U	Busek AMAC	NanoAvionics EPSS
System volume	1U	2U	1U + T ¹	2 U
Number of thrusters	4	4	1	1
Thrust	0.25 - 1.00 N	0.25 - 1.00 N	0.10 - 0.50 N	0.25 - 1.00 N
Specific impulse	206 - 235 s	206 - 235 s	220 - 225 s	220 s
Propellant	AF-M315E	AF-M315E	AF-M315E	ADN
Dry mass	1.060 kg	1.360 kg	1.243*	1.800 kg
Wet mass	1.560 kg	2.760 kg	1.500 kg	2.600 kg
Propellant mass	0.500 kg ²	1.400 kg	0.253 kg*	0.800 g
ϕ	0.321	0.507	0.169	0.308
Total impulse 1 system	1,200 N-s	3,360 N-s	565 N-s	1,700 N-s
Δv attainable ³	90.387 m-s ⁻¹	262.592 m-s ⁻¹	43.895 m-s ⁻¹ ⁴	137.028 m-s ⁻¹
Propellant mass for 203 m-s ⁻¹ of Δv	2.192 kg	2.192 kg	2.285 kg	2.335 kg
Wet mass for 203 m-s ⁻¹	6.840 kg	4.322 kg	13.379 kg	7.588 kg
Power consumption (pre-heating) 1 system	28 W ⁵	28 W	15 - 20 W	n/a
Power consumption (tank heating) 1 system	10 W	10 W	n/a	n/a



(a) Aerojet Rocketdyne MPS-135-2U, cropped from [22]. (b) Busek BGT-X5, cropped from [89]. (c) NanoAvionics EPSS 2 U, cropped from [113].

Figure 2.38: Complete COTS Main Propulsion System options.

¹T = utilising "tuna can" volume

²Datasheet notes 0.50 kg of propellant mass for 1.66 kg wet mass and 1.06 kg dry mass. It is unclear whether this is an error, given that for the 2U system there is no discrepancy.

³Calculated using maximum specific impulse noted and propellant mass, assuming two systems are used, assuming a spacecraft wet mass of 26 kg.

⁴Calculated using propellant mass resulting from total impulse delivered and maximum noted specific impulse.

⁵7 W per thruster

Reaction Control System

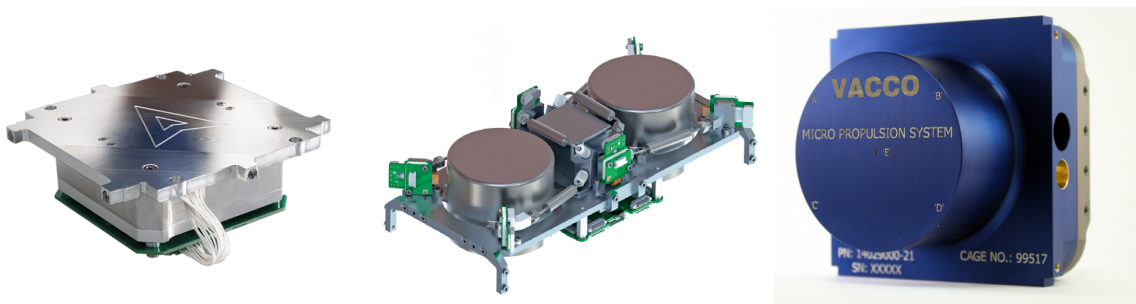
Aurora has developed the ARM-A Attitude Control Module (Figure 2.39a) featuring six resistojet thrusters utilising a water-based propellant according to the datasheet [33]. The module is scalable and the datasheet presents examples of 0.35 U, 1 U and 4 U system volume. For the 1U version, 300 - 600 N-s of total impulse is noted for a maximum wet mass and dry mass of 1.3 kg and 1.0 kg, respectively. The power consumption of this unit is significant, with each of the 6 thrusters using 2-20 W of power.

GOMSpace/NanoProp have developed the NanoProp 6DOF propulsion system (Figure 2.39b), offering 6 MEMS thrusters each configurable to fire at either 1 mN or 10 mN, utilising Butane propellant according to the datasheet [19]. Not much data is published about this system. The system is 2 U wide and 0.55 U deep, this exceeds the volume restrictions for LUMIO's RCS limiting the RCS volume to 1 U (Appendix A.2).

VACCO has developed a cold gas micropropulsion system "End-Mounted Standard MiPS" (Figure 2.39c) featuring four RCS thrusters and one Δv thruster utilising the liquid storable self-pressurising refrigerant R134a as propellant. The system is scalable and utilises the "tuna can" volume in a CubeSat bus. All relevant data found is presented in Table 2.22. It is observed, that the GOMSpace/Nanoprop 6DOF unit is not feasible due to not complying with the impulse requirement of 170 N-s and the volume requirements (Appendix A.2).

Table 2.22: Main Propulsion System COTS candidates.

Parameter	Aurora ARM-A 0.35 U	Aurora ARM-A 1.00 U	GOMSpace/Na- noprop 6DOF	VACCO MiPS CGT
System volume	0.35 U	1.00 U	2 x 0.55 U	0.5 U
Number of thrusters	6	6	6	4
Thrust	0.60 - 4.00 mN	0.60 - 4.00 mN	1 mN or 10 mN	10 mN
Specific impulse	100 s	100 s	50 s	40 s
Propellant	Water-based	Water-based	Butane	R134a
Dry mass	0.230 kg	1.000 kg	0.682 kg	0.501 kg
Wet mass	0.300 kg	1.300 kg	0.804 kg	0.924 kg
Propellant mass	0.070 kg	0.300 kg	0.122 kg	0.423 kg
ϕ	0.233	0.231	0.152	0.458
Total impulse	70 N-s	600 N-s	100 N-s	166 N-s
Propellant mass for 170 N-s of I_t	0.173 kg	0.173 kg	0.347 kg	0.433 kg
Wet mass for 170 N-s of I_t	0.742 kg	0.749 kg	2.283 kg	0.946 kg
Power consumption (firing)	2 - 20 W	2 - 20 W	n/a	10 W



(a) Aurora ARM-A, cropped from [33]. (b) GOMSpace/Nanoprop 6DOF, cropped from [19]. (c) VACCO CGT MiPS Tuna Can, cropped from [114].

Figure 2.39: Complete COTS Reaction Control System options.

3

Concept Design

This Chapter delineates the generation and evaluation of different concepts for LUMIO's propulsion system. The best performing concept will result from a trade-off, and will be developed in more detail in the detail design, discussed in Chapter 4. First, the key design driving requirements are summarised and presented in the form of concept design specifications. Subsequently, for the MPS, the thruster selection follows and propellant storage and feed system options are discussed, concepts are generated and finally, the best concept is selected in the trade-off. This is repeated for the RCS. During this stage, simplified models are used for the purpose of selecting the most feasible feed system type. The effects of cavitation for the pump and any compressibility effects in the pressurant gas are therefore not considered here. Furthermore, cylindrical tank shapes will be used at this stage, and will only be dimensioned on strength, not on stiffness. This is due to the wall thickness dimensioning being more simple for cylindrical tanks as compared to cuboid tanks: for cylindrical shapes, the hoop stress relation can be used (Section 2.8.1), for a cuboid tank shape every wall pair must be considered separately using thin plate theory (Section 2.8.2). Using cylindrical tanks therefore allows for a simple, first order comparison between volume and mass requirements for the propellant and pressurant storage in each concept.

3.1. Design Specifications

In order to generate system concepts, the key design-driving requirements are chosen as design specifications, these are presented in Table 3.1 and are all based on the actual requirements, presented in Appendix A. The full requirements will only be considered after the detailed design is finished in the next chapter. These specifications were selected from the full requirements in order to achieve a first order concept of each system and determine its mass, volume, power consumption, thrust level and maximum required propellant tank pressure. At this stage, no orientation and exact placement of non-payload components is known yet except for three U in length being reserved for the scientific payload as per requirement PLD.150 (Appendix A.4). For generating the concepts and allowing for comparison between concepts, a simple inside volume of each U is assumed to be 10x10x10 cm, during the detailed design phase the CubeSat standard dimensions will be considered in detail.

Table 3.1: Design specifications for MPS and RCS concept generation, requirements from Appendix A.

Specification	MPS	Reference	RCS	Reference
Available build volume	3 x 3U in length	PLD.150	3 x 3U in length	PLD.150
Required Δv delivered	203 m-s ⁻¹	PROP.010, PROP.020		
Required I_t delivered			170 N-s	RCS.030
F_T (thrust) range for each thruster	100 mN - 1,000 mN	PROP.050, PROP.053	1 mN - 10 mN	RCS.050
Number of thrusters	2	PROP.051	4 minimum, preferably 6 or more.	RCS.051
Throttle range	+/- 10% of nominal thrust	PROP.052		
Operational temperature range	278 K - 323 K	PROP.090	278 K - 308 K	RCS.090
Non-operational temperature range	273 K - 313 K	PROP.091	273 K - 313 K	RCS.091
Maximum volume	5 U	PROP.100	1 U	RCS.100
Maximum wet mass	6 kg	PROP.110	1 kg	RCS.110
Max. Firing power	10 W	PROP.120	25 W	RCS.120
Max. Pre-heat power	25 W	PROP.120		
Max. Standby power	1 W	PROP.120	0.5 W	RCS.120
Minimum impulse bit			2 mNs	RCS.140
Maximum pressure all components	50 bar	PROP.160	50 bar	RCS.160
Burst factor pressure vessels	2.5	PROP.162	2.5	RCS.162
Propellant type	Non-toxic (REACH)	PROP.190	Non-toxic (REACH)	RCS.190
Specification	General	Reference		
Spacecraft wet mass $M_{w,spc}$	26 kg	SYS.050		

3.2. Thruster Selection

Before the storage and feed systems can be designed, thrusters need to be selected. This section contains the selection of the most suitable candidate for each role (MPS and RCS), for which first a trade-off is performed. Subsequently, a sensitivity analysis is performed to check the validity of the trade-off. Finally, the properties of the chosen thrusters are discussed.

3.2.1. Main Propulsion System Thrusters

Trade-Off

The relevant properties of the candidates are presented in Table 2.12. The trade-off is presented below, in Table 3.2, showing that the HPGP 1 N thruster by Bradford ECAPS scores best having received the "excellent" score in three criteria, "good" in one criterion and "poor" in one criterion. The runner-up is the HPGP 100 mN, also by Bradford ECAPS, scoring "excellent" in 1 criterion, "good" in 1 criterion and "poor" in three criteria. The selection is based on the following criteria:

- I_{sp} (specific impulse): higher specific impulse means less propellant mass required to achieve the same Δv or total impulse I_t delivered. Values ranging from 200 s to 231 s are observed, values between 200 s and 210 s are assigned the score "poor", values between 211 s and 220 s "good", values above 221 s "excellent".
- F_T (thrust force): higher thrust means shorter transfer times. For each thruster, a range is given, dependent on inlet pressure. As per design specification # 2, the delivered thrust of each thruster shall lie between 100 mN and 1000 mN. For scoring, the higher end of the thrust range is considered. Values between 100 mN and 250 mN are assigned the score "poor", 251 mN and 500 mN "good", 501 mN and 1000 mN "excellent", values of 1001 mN and higher are scored "poor" as this may indicate that the thruster may not perform optimal for the required thrust range.
- $p_{t,in}$ (thruster inlet pressure): lower inlet pressure requires less high upstream pressure, resulting in lighter tanks, lines and other feed system components such as valves and filters. The higher end of the pressure range is considered for scoring. A range of pressure values between 4.5 bar and 37.9 bar is observed. Values between 4.5 bar and 10 bar are assigned the score "excellent", 10 bar and 20 bar "good", 21 bar to 50 bar "poor" and 51 bar and above "unacceptable" (design specification # 10 limiting the maximum allowable pressure of all components to 50 bar due to launch safety constraints).
- $P_{el,pre}$ (thruster pre-heating power): lower pre-heating power required translates to higher reserves for other systems. According to design specification # 8, the maximum allowable value for the entire MPS is 25 W, translating to 12.5 W per thruster considering two thrusters firing simultaneously; values in the range from 0 to 5 W are assigned the score "excellent", 6 W to 10 W "good", 11 W and 12.5 W "poor", values above 12.5 W "unacceptable".
- TRL: A higher TRL indicates less risk associated. TRL between 5 and 8 are assigned the score "poor", TRL 8 is assigned "good" and TRL 9 is assigned "excellent".

Table 3.2: Main Propulsion System thruster trade-off table.

Thruster	I_{sp}	F_T	$p_{t,in}$	$P_{el,pre}$	TRL
HPGP 100 mN	Yellow	Yellow	Blue	Green	Yellow
HPGP 1 N	Blue	Blue	Yellow	Green	Blue
GR-1	Blue	Yellow	Grey	Grey	Grey
BGT-X1	Green	Yellow	Grey	Blue	Grey
BGT-X5	Blue	Green	Yellow	Red	Yellow

Legend	Unacceptable	Poor	Good	Excellent	No data
	Red	Yellow	Green	Blue	Grey

Sensitivity Analysis

Due to the fact that the HPGP 1 N thruster scores "excellent" in three criteria and other thrusters were assigned the score "excellent" in a maximum of one criterion, the HPGP 1 N is far ahead of the other thrusters: omitting only one criterion from the trade-off does not change the outcome. Attempting to simultaneously omit two criteria from the trade-off also does not change the outcome.

Changing the numerical boundaries of the criteria is considered for the criteria in which the winning candidate (HPGP 1 N) scores excellent, to see whether the next best scoring candidates in that criterion are able to come close to the winning candidate. This is done varying only one criterion at a time while keeping all other criteria constant. For I_{sp} , the closest non-excellent other candidate is the BGT-X1 by Busek, with 215 s as opposed to 231 s for the HPGP 1 N. This difference of 16 s is a significant part of the total range of 200 s to 231 s. Changing the boundary may make the Busek BGT-X1 more favourable, however this candidate has no data available for two other criteria and is therefore not more likely to be considered. For the criterion F_T , the next best candidate is the BGT-X5 thruster, with the higher end of the range being 500 mN. Changing this boundary slightly downwards by 1 s will make this candidate score "excellent", however it is still an unfavourable candidate due to its unacceptably high pre-heat power consumption of 20 W. The third and final criterion in which the winning candidate scores "excellent" is TRL, with a TRL of 9. All other candidates for which TRL data is available are characterised by TRL 5, the difference from TRL 9 to TRL 5 is significant. Changing the lower boundary for the score "good" in this criterion to TRL 5 will make the BGT-X5 and 100 mN thrusters score "good", however still the BGT-X5 will not be selected due to its unacceptable high power consumption and scoring "excellent" only in 1 criterion. The 100 mN thruster will also not be close to the HPGP 1 N thruster due to only scoring "excellent" in 1 criterion.

Due to omission of two criteria simultaneously or changing of numerical boundaries of one criterion at a time not significantly influencing the outcome, it is concluded that sufficient margin between the winning candidate and other candidates is present. Therefore, the trade-off is decided to have been performed satisfactory.

3.2.2. Reaction Control System Thrusters

Trade-Off

The relevant properties of the candidates are presented in Table 2.13. The trade-off is presented in Table 3.3. Here it can be seen, that both CGT thrusters perform "unacceptable" in the criterion volumetric specific impulse (ρI_{sp}), causing an unacceptably high storage volume. This can furthermore be observed from Table 2.5, where a spherical tank diameter of an order of magnitude of 19 cm can be expected which would by far exceed the volume requirement. Clearly, the ARO thruster by Aurora is the only feasible thruster for the RCS. The ARO is furthermore a favourable candidate because of its low required inlet pressure, however it is heavier than the 58X125A thruster and requires more power to operate. The criteria for the trade-off are presented below:

- ρI_{sp} (volumetric specific impulse): a higher ρ value for this criterion means a lower required storage volume. For the cold gas thrusters which use gaseous nitrogen, this value is very low - around the order of magnitude of 4 g-s-cc⁻¹ (Table 2.5). For liquid water, this value is around the order of magnitude of 139 g-s-cc⁻¹ (Table 2.4).
- F_T (thrust force): higher thrust force translates to shorter firing times for achieving the same delivered impulse. Shorter firing times may be desirable for lower required energy for operating the RCS. A higher value is favourable and will receive a higher score.
- $p_{t,in}$ (thruster inlet pressure): lower feed pressure translates to lower tank mass and possibly a simpler pressurising/feed system. Here, a lower value is favourable over higher values and will receive a higher score.
- $P_{el,fire}$ (thruster firing power): lower firing power may translate to more power reserves present for other systems and may cause less heating of adjacent components. A lower value is favourable and will receive a higher score.

- Mass: A lower mass translates to more design freedom for other RCS components and will thus receive a higher score.

Table 3.3: Reaction Control System thruster trade-off table.

Thruster	ρI_{sp}	F_T	$p_{t,in}$	$P_{el,fire}$	Mass
58X125A					
58E143					
ARO					

Legend	Unacceptable	Poor	Good	Excellent

Sensitivity Analysis

Similar to the sensitivity analysis for the MPS thruster trade-off, first, omission of one criterion at a time is considered. Subsequently, changing the numerical boundaries for one criterion at a time is considered. Omitting the criterion of volumetric specific impulse may make the 58X125A thruster worth considering due to the higher mass and power required for the ARO. Omitting any other criterion does not change the outcome of the trade-off due to the unacceptable score for the volumetric specific impulse criterion. If however the criteria ρI_{sp} and $p_{t,in}$ were omitted simultaneously, the winning candidate would be the 58X125A.

The ARO thruster scores "excellent" in the criteria ρI_{sp} and $p_{t,in}$. For these criteria, changing of the numerical boundaries will be considered. If the lower boundary for ρI_{sp} were to be changed such that the higher required storage volume for the CGT candidates 58X125A and 58E143 were acceptable, still a significant difference between this criterion would exist between these candidates and the ARO thruster. Additionally, the ARO thruster scores "excellent" in the criterion for inlet pressure $p_{t,in}$, therefore still the ARO would be the winning candidate. Vice versa, changing the boundaries for the $p_{t,in}$ criterion would not change the outcome due to scoring "unacceptable" in the ρI_{sp} criterion.

Since omitting or changing numerical boundaries of one criterion at a time does not change the outcome, the trade-off is considered performed satisfactory.

3.2.3. Discussion of Chosen Thrusters

Figure 2.28b shows the selected MPS thruster, the High Performance Green Propellant (HPGP) 1 N thruster as offered by Bradford ECAPS, SE. As the only thruster considered with TRL 9, it has extensive flight heritage already with 46 thrusters currently on orbit. It utilises the "green" chemical monopropellant LMP-103s as developed by ECAPS in co-operation with the Swedish Defence Agency, further discussed in Section 3.3. A dual-seat solenoid thruster valve with PTFE seats is already integrated into the thruster, therefore no separate thruster valve is required. The thruster is furthermore equipped with a 25 μm inlet filter.

Figure 2.30a shows the selected RCS thruster, the Aurora Resistojet One by Aurora which was selected due to its superior ρI_{sp} performance as compared to the CGT thruster options. In the presented ARO thruster, a propellant tank is included as well, however it is assumed that only the thruster with valve and electronics are used. Still, the dry mass of 29 gram for the smallest version with propellant tank is used as this tank mass is considered negligible for 1 g of water-based propellant stored at below 1 bar. Since a propellant storage pressure of "below 100 kPa" (< 1 bar) is noted, for this thruster it is simply assumed that the inlet pressure is 1 bar. This thruster was announced at the end of 2020 and has no reported flight heritage. For this thruster, the thruster valve is included however without information about presence of a filter. Therefore, for this thruster too, a filter should be considered.

For the MPS, 2 thrusters are required as per requirement PROP.051; for the RCS, according to requirement RCS.051, no less than 4 thrusters shall be used however 6 or more are preferred. Due to the high power consumption of the ARO thruster, the minimum amount of thrusters is chosen for the first mass estimate, namely 4 thrusters. All thruster data relevant for concept generation is presented in Table 3.4. For the ARO thruster, the highest % of propulsion system wet mass is observed.

Table 3.4: Relevant thruster data for concept generation [40, 41, 90].

Quantity	ECAPS HPGP 1 N	Aurora ARO
F_T range	0.25 N - 1.00 N	0.6 mN - 4 mN
$p_{t,in}$ range	5.5 bar - 22.0 bar	n/a, nominal value 1 bar
I_{sp}	231 s	100 s
Propellant	LMP-103s	Water-based
Pre-heat power	8 - 10 W	n/a
Firing power	n/a	2 - 20 W
Valve actuating power ¹	5.389 W per coil	n/a
Valve holding power ¹	0.64 W per coil	n/a
T_{ch}	1,873.15 K	n/a
Mass	380 g	29 g
Length	n/a	20 mm
Width	n/a	20 mm
Height	n/a	20 mm
Total mass	760 g (2 thrusters)	116 g (4 thrusters)
Thruster mass fraction ²	12.67%	11.60%
Max. firing time	45 minutes	n/a
Max. firing sequences	1,500	n/a

¹Calculated from web-sourced data from [40]: 190 Ω coil resistance, worst case voltage of 28 \pm 4 V for actuation and 10 \pm 1 V for holding. Number of coils unknown.

²Total thruster mass % of max. propulsion system wet mass: 6 kg for the MPS (PROP.110, Appendix A.1), 1 kg for the RCS (RCS.110, Appendix A.2).

3.3. Thruster Data, Propellants and Pressurants

This section serves to present additional assumptions on the thrusters and to further describe the chosen propellants and pressurants for each concept.

3.3.1. Bradford-ECAPS HPGP 1 N Thruster: Propellant LMP-103s

The propellant specified for use in the chosen MPS thruster is LMP-103s, an ADN-based "green" chemical mono-propellant, discussed in Section 2.3.1. Consisting of a mixture of ADN, methanol, water and ammonia, this propellant is characterised by lower toxicity, lower vapour pressure and higher volumetric specific impulse performance, however higher required pre-heating power, all as compared to hydrazine, as discussed by Persson et al. in 2019 [23]. The properties of LMP-103s relevant for generating the storage and feed system concepts are presented in Table 3.5.

Table 3.5: Properties of propellant LMP-103s, interpolated for conditions at 300 K; gas properties for assumed decomposition temperature of 1873.15 K [23, 115].

Quantity	Value
Density $\rho_{p,MPS}$	1,236.520 kg-m ⁻³
Dynamic viscosity $\nu_{p,MPS,dyn}$	2.896 E-3 Pa-s
Speed of sound $a_{p,MPS}$	1,626.930 m-s ⁻¹
Vapour pressure	0.148 bar
Material compatibility	Ti-6Al-4V, Stainless Steels, PTFE (for valve seats)
Molar mass	19.65 g-mol ⁻¹
$c_{p,g}$	4,498.30 J-kg ⁻¹ -K ⁻¹
R_g	423.03 J-kg ⁻¹ -K ⁻¹
$c_{v,g}$	4,075.26 J-kg ⁻¹ -K ⁻¹
γ	1.10

3.3.2. Aurora ARO Thruster: Water Propellant

For the Aurora ARO, "water-based" propellant is specified without further details and therefore, water is chosen as propellant. In Section 2.3.2 it is shown that water propellant performs comparably well to other resistojet propellants, mainly due to its low molar mass of 18.02 g-mol⁻¹ and enabling storage in the liquid phase between 273.15 K and 373.15 K at 1 bar. One disadvantage of this propellant however is the high latent heat of vaporisation, which is more than double that of Ammonia. This results in high required heating power and therefore, the thruster may require operation at a low power level for use in the RCS. The properties of water relevant for generating the storage and feed system concepts are presented in Table 3.6.

Table 3.6: Properties of water at 300 K and 1 bar, gas properties at 729 K and 1 bar [49].

Quantity	Value
$\rho_{p,RCS}$	996.56 kg-m ⁻³
$\nu_{p,RCS,dyn}$	8.538 E-4 Pa-s
$a_{p,RCS}$	1,501.500 m-s ⁻¹
p_{vap}	0.035 bar
Material compatibility	Ti-6Al-4V, Stainless Steels
L_{vap}	2,437,300 J-kg ⁻¹
M_{mo}	18.02 g-mol ⁻¹
$c_{p,l}$	4,181.52 J-kg ⁻¹ -K ⁻¹
$c_{p,g}$	1,930.45 J-kg ⁻¹ -K ⁻¹
R_g	461.40 J-kg ⁻¹ -K ⁻¹
$c_{v,g}$	1,427.93 J-kg ⁻¹ -K ⁻¹
γ	1.323

3.3.3. Additional Assumptions on the ARO Thruster

For the selected RCS thruster, the Aurora ARO, no data on chamber pressure and chamber temperature is present and therefore, the critical mass flow relation cannot be used. Using Equation 2.10, the nozzle throat area is calculated for nominal conditions (Table 3.7), assuming a chamber pressure of 1 bar and a chamber temperature of 729 K: Figure 3.1 shows required heating power and resulting specific impulse for a chamber temperature ratio ranging from 400 K to 1,500 K, ideal conditions. It can be seen that between 400 K and 1,078 K, required heating power actually reduces. This effect can be ascribed to the high latent heat of vapourisation of water as compared with other resistojet propellants as presented in Table 2.4, causing the required heating power to be mostly dependent on mass flow and not so much on chamber temperature. Here, the mass flow required decreases for increasing chamber temperature, proportional to the inverse of the square root of chamber temperature and therefore a minimum is expected. Specific impulse ranges from 114 s to 221 s.

In order to choose an operating chamber temperature, it is considered that high chamber temperatures are undesirable from a thermal management and materials perspective. A resistojet microthruster using MEMS technology theoretically developing 1.48 mN - 1.52 mN of thrust was developed at TU Delft, with chamber temperatures of 550 K and 773 K at a chamber pressure of 5 bar as discussed by Cervone et al. in 2017 [116]. A microresistojet developed at the University of Tokyo developing roughly 4 mN of thrust (determined experimentally) using a chamber temperature of approximately 333 K without specifying thrust chamber pressure. The latter system achieved a specific impulse efficiency of 0.65, as discussed by Nishii et al. in 2020 [117]. Using this information, an assumed specific impulse efficiency of 0.65 is chosen due to similarity in thrust level, which using the specific impulse provided by the manufacturer of 100 s results in a required 153.85 s of theoretical specific impulse. This corresponds to a chamber temperature of 729 K at 9.05 W of heating power for the theoretical model, this temperature seems to be within the order of magnitude of the aforementioned systems in literature.

The accuracy of this model is not perfect, due to a number of reasons. Firstly, the only known parameters are thrust force and specific impulse as provided by the manufacturer. The chamber pressure is unknown, here the storage pressure of 1 bar is assumed as noted in the datasheet [90]. In reality, this pressure may be lower due to pressure losses, however also there is a possibility that the chamber pressure is chosen significantly lower than storage pressure to decrease the boiling point of the propellant. Secondly, due to no chamber temperature being known, a value is calculated using an assumed chamber pressure and specific impulse efficiency. Finally, the nozzle geometry is unknown and an expansion ratio of 25 is assumed, introducing further uncertainties in the results. For the generation of concepts however, it is assumed that the thruster data is sufficiently accurate to allow comparison between propellant feed & storage concepts.

Due to the maximum allowable power consumption of 25 W while firing (req. RCS.120, Appendix A), the thrusters need to be throttled to a lower thrust setting, shown in Table 3.8. Here, 24 W of electrical power is used for heating so that 1 W of power reserves are present for other components such as electronics. Furthermore, it must be noted that in the subsequent subsections, the real I_{sp} value of 100 s was used for calculating required propellant mass, however the calculated chamber temperature results from using an efficiency factor with the real specific impulse value.

Table 3.7: Aurora ARO Thruster properties at nominal conditions.

Nominal thrust force F_T	4E-3 N	Real specific impulse required	100 s
Specific heat ratio γ	1.323	Assumed specific impulse efficiency	0.650
Expansion ratio	25	Theoretical specific impulse required	153.85 s
Pressure ratio	2.470 E-3	Resulting chamber temperature	729 K
Throat area	2.290 E-8 m ²	Theoretical heating power required	9.05 W
Throat diameter	0.17 mm	Real heating power	20 W
Exit area	5.725E-7 m ²	Resulting heating efficiency	0.453
Exit diameter	0.85 mm		

Table 3.8: Aurora ARO Thruster properties at throttled conditions.

Quantity	Value
Number of thrusters firing simultaneously	2
Assumed total power while firing	24 W
Power per thruster	12 W
Resulting mass flow per thruster	1.590 E-6 kg-s ⁻¹
Resulting inlet pressure	0.600 bar
Thrust level	2.400 mN

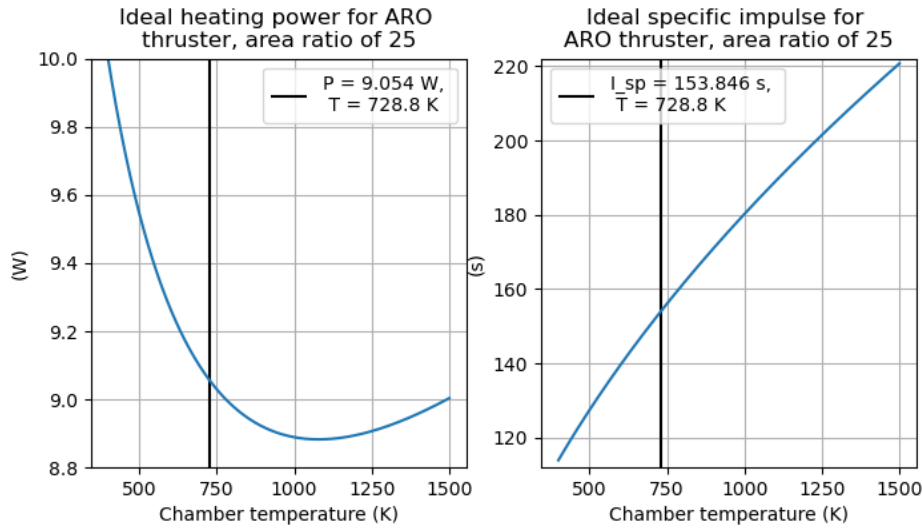


Figure 3.1: Ideal required heating power (l) and specific impulse (r) for the Aurora ARO at an expansion ratio of 25, thrust force of 4 mN, Python/Matplotlib.

3.3.4. Selected Pressurant Gas for Concepts: Nitrogen

As discussed in Section 2.5.1, the most common pressurant gases are Nitrogen and Helium. In Equation 2.14 it is observed, that pressurant gas mass is proportional to molar mass, therefore Helium pressurant results in lower pressurant mass for the same pressure, volume and temperature. This mass is however considered insignificant (approximately 0.34 g for Helium and 2.35 g for Nitrogen) as compared to the propulsion system wet mass of 1 kg for the RCS and 6 kg for the MPS, as demonstrated in Table 3.9 below. Based on this, the selection of pressurant gas mass is based solely on their likelihood of causing leakage problems, which is inversely proportional to molar mass as described by Michael Micci and Andrew Ketsdever in 2000 [118], making Nitrogen the more desirable option. Therefore, the chosen pressurant gas for the concept design stage is Nitrogen. If mass savings are required in the detailed design phase, Helium can be considered. The properties of gaseous Nitrogen at 300 K are presented in Table 2.6.

Table 3.9: Example pressurant gas mass calculation for Helium and Nitrogen gas.

Quantity	Helium	Nitrogen
Tank pressure, final	1.000 E+5 Pa	1.000 E+5 Pa
Tank radius	0.05 m	0.05 m
Tank total length	0.03 m	0.03 m
Tank volume	2.094 E-3 m ³	2.094 E-3 m ³
Temperature	300 K	300 K
R_g	2,077.264 J·kg ⁻¹ ·K ⁻¹	296.803 J·kg ⁻¹ ·K ⁻¹
Gas mass	3.361 E-4 kg	2.352 E-3 kg

3.4. Main Propulsion System Propellant Storage & Feed Concepts

The three concepts generated here are pressure regulated, blow-down and pump-fed types.

3.4.1. Pressure Regulated Concept

Two different designs are considered for the regulated type system. First, initial and final pressurant tank pressure values are taken as 50 bar and 22 bar, given that the thruster nominal pressure is 22 bar. Subsequently, a system is considered with 50 bar and 5.5 bar as initial and final pressure inside the pressurant tank, respectively. This still suits the thruster, with its minimum operating pressure of 5.5 bar, resulting in a lighter system however significantly lower thrust values over the entire mission increasing manoeuvre times. Table 3.10 shows the concept parameters. A cylindrical tank holds the propellant, and fits inside a 3U volume. It is observed that the high pressure version with a constant thruster pressure of 22 bar results in a large pressurant tank, which even in cylindrical configuration does not fit inside a 2 U volume. Therefore, the concept with low thruster pressure of 5.5 bar is considered in the trade-off. Furthermore it is observed that a very thin wall thickness is required for both pressure vessels, this has been scaled up to 1 mm to enable easier manufacturing. Finally, it is important to consider that no regulator valve is chosen yet, however it has to be realised that the mass of such a component may be significant.

Table 3.10: Pressure regulated concept for high and low regulated pressure for the Main Propulsion System.

Quantity	High Pressure	Low Pressure
Specific impulse I_{sp}	231 s	231 s
Required Δv delivered	203 m-s ⁻¹	203 m-s ⁻¹
Propellant volume	1.802 E-3 m ³	1.802 E-3 m ³
Ullage volume	5%	5%
Propellant tank volume	1.897E-3 m ³	1.897E-3 m ³
Chosen propellant tank radius	4.800 E-2 m	4.800 E-2 m
Total propellant tank length	2.941 E-1 m	2.941 E-1 m
Initial pressure pressurant tank	50 bar	50 bar
Final pressure pressurant tank	22 bar	5.5 bar
Constant pressure in propellant tank	22 bar	5.5 bar
Thrust level	1.00 N	0.25 N
Initial density pressurant gas in pressurant tank	56.160 kg-m ⁻³	56.160 kg-m ⁻³
Final density pressurant gas in pressurant tank	24.708 kg-m ⁻³	6.177 kg-m ⁻³
Pressurant tank volume	1.491 E-3 m ³	2.345 E-4 m ³
Required radius of spherical pressurant tank	7.086 E-2 m	3.825 E-2 m
Chosen radius of spherical pressurant tank	4.800 E-2 m	3.825 E-2 m
Total length of pressurant tank	2.380 E-1 m	-
Required wall thickness pressurant tank	7.896 E-4 m	3.146 E-4 m
Chosen wall thickness pressurant tank	1.000 E-3 m	1.000 E-3 m
Required wall thickness propellant tank	3.474 E-4 m	2.768 E-4 m
Chosen wall thickness propellant tank	1.000 E-3 m	1.000 E-3 m
Mass		
2 thrusters	0.760 kg	0.760 kg
Propellant	2.229 kg	2.229 kg
Pressurant gas	8.370 E-2 kg	1.317 E-2 kg
Propellant tank	0.398 kg	0.398 kg
Pressurant tank	0.323 kg	0.084 kg
Regulator valve	n/a	n/a
Total	3.793 kg	3.484 kg
Volume		
2 thrusters	TBD	TBD
Propellant tank	3 U	3 U
Pressurant tank	2.4 U	0.8 U
Total	5.4 U	3.8 U

3.4.2. Blow-down Type Concept

Table 3.11 shows the concepts for the blow-down type system concept. Due to the already long propellant tanks in the regulated concept, it is expected that tanks for the blow-down type concepts are too large (due to larger required gas ullage volume) and therefore two separate, identical tanks are considered: each configured for blow-down type operation, each containing both propellant and pressurant. The length of each tank of 19.80 cm confirms this expectation. In this concept, an initial pressure of 22 bar was chosen, to eliminate the requirement for a pressure regulator valve or passive flow control device between the propellant tank and the thruster.

Table 3.11: Properties of blow-down type concepts, for each tank (low duty cycle, isothermal expansion at 300 K).

Quantity	Value
Specific impulse I_{sp}	231 s
Required Δv delivered	203 m-s ⁻¹
Propellant volume	1.802 E-3 m ³
Initial tank pressure p_i	22.0 bar
Final tank pressure p_f	5.5 bar
Fill ratio Φ_0	0.750
Tank volume (each)	1.202 E-3 m ³
Total pressurant volume	6.008 E-4 m ³
Initial gas density $\rho_{pres,i}$	24.708 kg-m ⁻³
Required wall thickness cylindrical part	3.474 E-4 m
Required wall thickness spherical part	1.737 E-4 m
Chosen constant wall thickness	1.000 E-3 m
Tank length (each)	1.980-1 m
Mass	
2 thrusters	0.760 kg
Propellant	2.229 kg
Pressurant gas	1.484 E-2 kg
2 tanks	0.537 kg
Total	3.541 kg
Volume	
2 thrusters	TBD
2 tanks	4.0 U
Total	4.0 U

3.4.3. Pump-Fed Concept

The most suitable pump is selected using the selection criteria presented in Table 3.12, where the volumetric flow rate follows from 2 thrusters firing at maximum thrust, and for the pressure differential it is decided that a pressure differential range equal to that of the thruster inlet conditions is desirable. Finally, the power consumption may not exceed 10 W, as the firing power for the MPS is limited to 10 W (requirement PROP.120, Appendix A.1). The pump is selected from 42 listed models presented in Appendix C, where for each pump the characteristic curve was recorded for the line closest to pump requirements [56]. The 2212-M04C49 (Figure 3.2a) model was selected, due to being able to provide the highest pressure differential of all M-series pump models. A high pressure differential is chosen as desirable here to achieve the highest thrust level possible, as the pressure regulated and blow-down concepts also provide the maximum possible thruster inlet pressure at BOL. The pump concept may then illustrate how to maintain a high thrust level from BOL to EOL. A detailed investigation into the most suitable pump model for such a feed system is not considered in the concept phase.

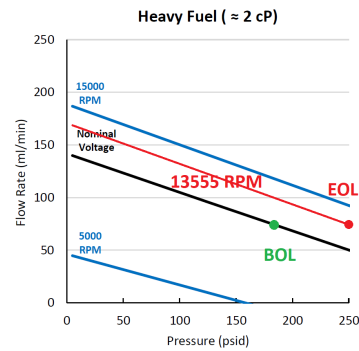
Data for this pump is presented in Table 3.13, where the differential pressure-mass flow and rotational velocity relations were determined graphically from the supplier-generated plots presented in Figure 3.2b, where furthermore the BOL and EOL conditions for this concept are indicated. In the pump datasheets, the pump characteristic diagrams are presented for fluids with different values of dynamic viscosity. The characteristics closest to LMP-103s are chosen, which has a dynamic viscosity of approximately 3 E-3 Pa-s , assumed valid for the use of LMP-103s [115]. This results in using the characteristic for heavy fuel with a dynamic viscosity of approximately 2 E-3 Pa-s . For this concept, the volumetric flow rate as function of pressure differential for each rotational velocity line was linearly interpolated to arrive at a simple concept, in contrast to the second order polynomial method handled during the detailed design phase.

Table 3.14 shows the chosen parameters of the concept. A very low ullage volume is chosen so that the propellant tank, which holds both propellant and pressurant gas, fits inside a volume of 3U in length. This low ullage fraction furthermore indicates a high ratio of BOL/EOL pressurant gas pressure. A simple PFCF design is considered, with 10 cm of orifice length and an orifice diameter of 265 micron. At these small pipe diameters, capillary effects may occur, this is however left out of scope for this stage and the PFCF performance is assumed satisfactory for this design.

Table 3.15 shows the calculation steps inside the PFCF for both the BOL and EOL condition. These are performed using the relations in Section 2.5.2 and Section 2.6. As mentioned before, the low ullage fraction results in a very high BOL/EOL pressurant gas pressure ratio, where the EOL pressure is 0.635 bar. At low pressures, pump cavitation may occur due to low pressure areas forming at the pump inlet. This is however left out of scope for this stage. Finally, a conservative estimate is made of the pump efficiency, namely a value of 0.5 (constant). This results in an electric power required of 3.165 W at BOL and 4.301 W at EOL, where at EOL a higher pressure differential and higher flow rate is provided. These values are well within the 10 W limit for MPS firing power.

Table 3.12: Pump selection criteria for the Main Propulsion System concept.

Criterion	Requirement
Volumetric flow capacity (2 thrusters max. thrust)	$42.84 \text{ ml-min}^{-1}$
Pressure differential	5.5 bar - 22.0 bar
Max. Power consumption	10 W



(a) Model 2212-M04C49, cropped from [119].(b) Pump characteristic with BOL and EOL working points indicated, edited from [119].

Figure 3.2: Selected Flightworks, inc. magnetically coupled micro-gear pump model 2212-M04C49 for the Main Propulsion System concept.

Table 3.13: Pump characteristics of selected Flightworks, inc. micro-gear pump. Pressure, mass flow and rotational velocity relations were determined graphically from pump characteristic diagram [119].

Quantity	Value
Mass	175 g
Nominal voltage	12 V
Speed constant	981 RPM-V ⁻¹
Port diameter	3 mm
Length	96.5 mm
Diameter	22 mm
Assumed efficiency	0.5
$\Delta p(m)$	$-8.922 \cdot 10^8 \cdot m + 2.643 \cdot 10^6$ [Pa]
$m(\Delta p)$ (nominal line)	$-1.121 \cdot 10^{-9} \cdot \Delta p + 2.962 \cdot 10^{-3}$ [kg - s ⁻¹]
Pressure range (low-high)	$6.895 \cdot 10^4 - 1.724 \cdot 10^6$ Pa
Mass flow range (high-low)	$2.885 \cdot 10^{-3} - 1.030 \cdot 10^{-3}$ kg - s ⁻¹
$\omega(m, \Delta p)$	$1.177E + 4 + 3.481E + 6 \cdot (m - \Delta p \cdot (-1.121E - 9) - 2.962E - 3)$ [min ⁻¹]

Table 3.14: Pump-fed concept for the Main Propulsion System.

Quantity	Value
Total Δv required	203 m-s ⁻¹
I_{sp}	231 s
Propellant volume	1.802 E-3 m ³
Ullage volume	7 %
Tank volume	1.938 E-3 m ³
Tank diameter	9.600 E-2 m
Tank length	3.000 E-1 m
Chosen tank wall thickness	1.000 E-3 m
Tank shell mass	0.406 kg
Ullage volume	1.357 E-4 m ³
PFCD	
Length of constriction	1.000 E-1 m
Pipe diameter large	3.000 E-3 m
Area large	7.069 E-6 m ²
Area ratio	128.037
Area small	5.521 E-8 m ²
Pipe diameter small	2.651 E-4 m
Outside width	5.000 E-3 m
Outside height	5.000 E-3 m
Port length	1.000 E-2 m
Outside length	12.000 E-2 m
Mass	
2 thrusters	0.760 kg
Propellant	2.229 kg
Pressurant	1.382 E-3 kg
Tank shell	0.406 kg
Pump	0.175 kg
PFCD	0.008 kg
Total	3.579 kg
Volume	
2 thrusters	TBD
Tank	3 U
Pump + PFCD	0.25 U ¹
Total	3.25 U

¹Based on a rectangular block containing the pump (diameter of 22 mm) and PFCD (length of 120 mm)

Table 3.15: MPS pump-fed concept calculation steps in PFCD.

Property	BOL	EOL
Thruster inlet pressure	22.000 bar	17.872 bar
Ullage pressure	9.072 bar	0.635 bar
Pressurant gas mass	1.382 E-3 kg	1.302 E-5 kg
Pump Δp	12.928 bar	17.237 bar
Pump mass flow	1.513 E-4 kg-s ⁻¹	1.543 E-4 kg-s ⁻¹
Pump rotational velocity	11772 min ⁻¹	13555 min ⁻¹
Total thruster mass flow	8.829 E-4 kg-s ⁻¹	7.172 E-4 kg-s ⁻¹
Loop mass flow	6.306 E-4 kg-s ⁻¹	8.253 E-4 kg-s ⁻¹
Flow velocity wide pipe	0.072 m-s ⁻¹	0.094 m-s ⁻¹
Flow velocity thin pipe	9.237 m-s ⁻¹	12.090 m-s ⁻¹
Pressure station 0	2.200 E+6 Pa	1.787 E+6 Pa
Pressure station 1	2.147 E+6 Pa	1.697 E+6 Pa
K_{con}	0.500	0.500
Δp contraction	2.638 E+4 Pa	4.519 E+4 Pa
Pressure station 2	2.121 E+6 Pa	1.652 E+6 Pa
Reynolds number stations 2, 3	1049	1372
Friction factor stations 2, 3	6.104 E-2	4.663 E-2
Δp friction	1.214 E+6 Pa	1.590 E+6 Pa
Pressure station 3	9.064 E+5 Pa	6.211 E+4 Pa
Pressure station 4	9.592 E+5 Pa	1.525 E+5 Pa
K_{exp}	9.844 E-1	9.844 E-1
Δp expansion	5.193 E+4 Pa	8.897 E+4 Pa
Pressure station 5	9.072 E+5 Pa	6.351 E+4 Pa
Δp loop	1.293 E+6 Pa	1.724 E+6 Pa
Pump hydraulic power required	1.582 W	2.150 W
Pump electric power	3.165 W	4.301 W

3.5. Reaction Control System Propellant Feed & Storage System Concepts

Similar to the MPS concept generation procedure, three concepts generated here are generated: pressure regulated, blow-down and pump-fed types.

3.5.1. Pressure Regulated Concept

Table 3.16 shows the calculations for the pressure regulated concept. Two different options are considered here: storage of pressurant gas and propellant in separate tanks, and an option where both are stored inside the same tank. It can be seen, that the total mass for both concepts is similar, however that the required storage volume for the "same tank" option is significantly lower. It must be noted, that for these concepts, a regulator valve is present, for the "separate tank" option this component is placed between the pressurant tank and propellant tank, for the "same tank" option, this component is placed between tank and thrusters. In this concept, a constant thruster pressure of 0.6 bar is used to arrive at a thrust level of 2.400 mN, corresponding to a total power consumption of 24 W for both thrusters firing simultaneously. Finally, the same BOL pressurant pressure is selected to allow for more direct comparison between both options.

Table 3.16: Pressure regulated concept for the Reaction Control System.

Quantity	Separate tanks	Same tank
Total impulse I_t required	170 N-s	170 N-s
I_{sp}	100 s	100 s
Propellant volume	1.740 E-4 m ³	1.740 E-4 m ³
Ullage volume	5.000 %	7.500 %
Propellant tank volume	1.831 E-4 m ³	1.881 E-4 m ³
Spherical propellant tank diameter	7.045 cm	7.108 cm
Chosen wall thickness	1.000 E-3 m	1.000 E-3 m
Pressurant pressure initial	8 bar	8 bar
Pressurant pressure final	0.6 bar	0.6 bar
Storage temperature (constant)	300 K	300 K
Density pressurant gas in pressurant tank initial	8.985 kg-m ⁻³	8.985 kg-m ⁻³
Density pressurant gas in pressurant tank final	6.738 E-1 kg-m ⁻³	6.738 E-1 kg-m ⁻³
Density pressurant gas in propellant tank	6.738 E-1 kg-m ⁻³	same as above ¹
Spherical pressurant tank diameter	3.049 E-2 m	0
Thruster inlet pressure (constant)	0.6 bar	0.6 bar
Thruster thrust	2.400 mN	2.400 mN
Power required per thruster (constant)	12 W	12 W
Mass		
4 thrusters	0.116 kg	0.116 kg
Propellant	0.173 kg	0.173 kg
Pressurant	1.334 E-4 kg	1.267 E-4 kg
Propellant tank	0.071 kg	0.072 kg
Pressurant tank	0.014 kg	0
Regulator valve	n/a	n/a
Total	0.374 kg	0.362 kg
Volume		
4 thrusters	TBD	TBD
Propellant tank	0.7 U	0.7U
Pressurant tank	0.3 U	0
Total	1.0 U ²	0.7U ²

¹For BOL, the "density pressurant gas in pressurant tank initial" value is taken, for EOL the "density pressurant gas in pressurant tank final" is taken.

²The volume of a regulator valve is still required to be added.

3.5.2. Blow-Down Concept

The maximum allowed pressure inside LUMIO's propulsion system is 50 bar, as per requirement RCS.160 (Appendix A). A high initial tank pressure is desirable to decrease the required tank volume, however it must be considered that the ARO thruster operates at an assumed 1 bar. In order to prevent the need for a regulator valve, a concept is generated where the pressure decreases from 0.6 bar to 0.25 bar in order to comply with the max. power consumption requirement and the minimum thrust requirement. This however results in a low fill ratio and thus a large propellant tank. In the detailed design, a higher fill ratio using a higher initial pressure in combination with a PFCD for pressure regulation can be investigated.

Table 3.17: Blow-down concept for the Reaction Control System.

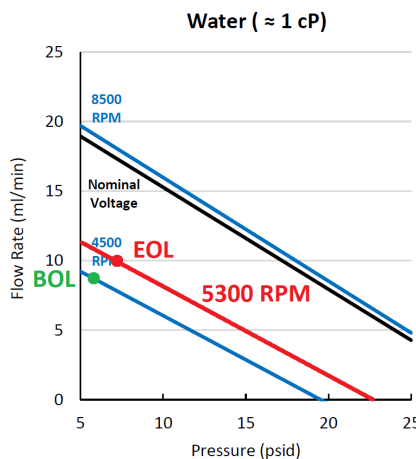
Quantity	Value
Total impulse I_t required	170 N-s
I_{sp}	100 s
Propellant volume	1.740 E-4 m ³
Ullage pressure initial	0.60 bar
Ullage pressure final	0.25 bar
Fill ratio	0.583
Tank volume	2.982 E-4 m ³
Spherical tank diameter	8.289 E-2 m
Chosen wall thickness	1 mm
Pressurant gas density initial	6.738 E-1 kg-m ⁻³
Thrust initial	2.400 mN
Thrust final	1.000 mN
Power required per thruster initial	12 W
Power required per thruster final	5 W
Mass	
4 thrusters	0.116 kg
Propellant	0.173 kg
Pressurant	8.373 E-5 kg
Tank	0.098 kg
Total	0.387 kg
Volume	
4 thrusters	TBD
Tank	0.8 U
Total	0.8 U

3.5.3. Pump-Fed Concept

Table 3.18 shows the pump selection criteria for the RCS. The Flightworks, inc. 2204-M03C01 pump (Figure 3.3a) is the smallest of the M-series and is of interest for the RCS due to its very low minimum pressure differential of 0.345 bar, however a significantly higher flow rate than required as taken from the datasheet supplied by the manufacturer [120]. The BOL and EOL conditions on the characteristic diagram of the pump are indicated in Figure 3.3b. Due to the restriction on thruster power level and an assumed 5 W of power reserve for the pump, only 10 W per thruster is allocated, resulting in a thrust level of 2 mN and inlet pressure of 0.5 bar. Factors that may challenge the feasibility of this concept are the low thruster inlet pressure of 0.5 bar (resulting from the low available heating power), minimum pressure differential of the pump of 0.345 bar and the vapour pressure of water of 0.035 bar as taken from NIST webbook [49]. The ullage pressure in this concept is set at 0.1 bar, resulting in a required pump pressure differential of 0.4 bar. At EOL, the ullage pressure may not go below the vapour pressure of 0.035 bar and therefore a final ullage pressure of 0.04 bar is chosen, resulting in a large required ullage volume of 40%. It is very important to note, that in reality such low EOL tank pressure may result in cavitation problems inside the pump. The resulting tank diameter of 8.2 cm does not exceed the volume requirement. It is also possible to choose a different pump rotational velocity at EOL with a lower pressure differential, in this case, a smaller tank can be used. Table 3.19 shows the pump characteristic functions for linking pressure differential and mass flow, including the relation for finding the required rotational velocity for an arbitrary working point. Similar to the pump concept for the MPS, linear interpolation is used. Table 3.20 shows the selected parameters for the concept, Table 3.21 shows the calculation steps for the PFCD.

Table 3.18: Pump selection criteria for the Reaction Control System concept.

Criterion	Requirement
Volumetric flow capacity (2 thrusters at low power)	0.160 ml/min
Pressure differential	< 1 bar
Max. Power consumption	5 W



(a) Model 2212-M03C01, cropped from [120]. (b) Pump characteristic with BOL and EOL working points indicated, edited from [120].

Figure 3.3: Selected Flightworks, inc. magnetically coupled micro-gear pump model 2212-M03C01 for the Reaction Control System concept.

Table 3.19: 2212M03C01 pump data.

Quantity	Value
Pump mass	0.065 kg
Pump diameter	22 mm
Pump length	66.3 mm
Port diameter	3 mm
Nominal voltage	6 V
Speed constant	1,380 RPM-V ⁻¹
Assumed efficiency	0.5
$m(\Delta p)$ 4500 RPM line	$2.130E - 4 - 1.626E - 9 \cdot \Delta p$ [kg - s ⁻¹]
$\omega(m, \Delta p)$	$8280 + 2.649E + 7 \cdot (m - \Delta p \cdot -1.626E - 9 - 3.550E - 4)$ [min ⁻¹]

Table 3.20: Pump-fed concept for the Reaction Control System.

Quantity	Value
Total impulse I_t required	170 N-s
I_{sp}	100 s
Propellant mass	0.173 kg
Propellant volume	1.740 E-4 m ³
Ullage volume	40 %
Tank volume	2.899 E-4 m ³
Spherical tank diameter	8.212 E-2 m
Chosen tank wall thickness	1.000 E-3 m
Tank shell mass	0.096 kg
Ullage volume	1.160 E-4 m ³
Thruster pressure (constant)	0.5 bar
Thrust force (constant)	2 mN
Thruster power (per thruster)	10 W
PFCD	
Length of constriction	5.000 E-2 m
Pipe diameter large	3.000 E-3 m
Area large	7.069 E-6 m ²
Area ratio	107.72
Area small	6.562 E-8 m ²
Pipe diameter small	2.890 E-4 m
Outside width	5.000 E-3 m
Outside height	5.000 E-3 m
Port length	1.000 E-2 m
Outside length	7.000 E-2 m
Mass	
4 thrusters	0.116 kg
Propellant	0.173 kg
Pressurant	1.302 E-5 kg
Tank shell	0.096 kg
Pump	0.065 kg
PFCD	0.005 kg
Total	0.455 kg
Volume	
4 thrusters	TBD
Tank	0.8 U
Pump + PFCD	0.1 U
Total	0.9 U

Table 3.21: RCS pump-fed concept calculation steps in PFCD.

Property	BOL	EOL
Thruster inlet pressure	0.5 bar	0.5 bar
Ullage pressure	0.1 bar	0.04 bar
Pressurant gas mass	1.302 E-5 kg	1.302 E-5 kg
Pump Δp	0.4 bar	0.46 bar
Pump mass flow	1.480 E-4 kg-s ⁻¹	1.678 E-4 kg-s ⁻¹
Pump rotational velocity	4500 min ⁻¹	5300 min ⁻¹
Total thruster mass flow	2.650 E-6 kg-s ⁻¹	2.650 E-6 kg-s ⁻¹
Loop mass flow	1.453 E-4 kg-s ⁻¹	1.651 E-4 kg-s ⁻¹
Flow velocity wide pipe	0.021 m-s ⁻¹	0.023 m-s ⁻¹
Flow velocity thin pipe	2.223 m-s ⁻¹	2.525 m-s ⁻¹
Pressure station 0	5.000 E+4 Pa	5.000 E+4 Pa
Pressure station 1	4.753 E+4 Pa	4.681 E+4 Pa
K_{con}	0.500	0.500
Δp contraction	1.231 E+3 Pa	1.588 E+3 Pa
Pressure station 2	4.630 E+4 Pa	4.522 E+4 Pa
Reynolds number stations 2, 3	750	852
Friction factor stations 2, 3	8.535 E-2	7.514 E-2
Δp friction	3.634 E+4 Pa	4.128 E+4 Pa
Pressure station 3	9.955 E+3 Pa	3.942 E+3 Pa
Pressure station 4	1.242 E+4 Pa	7.118 E+3 Pa
K_{exp}	9.815 E-1	9.815 E-1
Δp expansion	2.416 E+3 Pa	3.118 E+3 Pa
Pressure station 5	1.000 E+4 Pa	4.000 E+3 Pa
Δp loop	4.000 E+4 Pa	4.600 E+4 Pa
Pump hydraulic power required	5.938 E-3 W	7.741 E-3 W
Pump electric power required	0.012 W	0.02 W

3.6. Concept Selection

The most feasible concepts for LUMIO's MPS and RCS are selected using a trade-off. In contrast to the trade-off process used for the thruster selection, the process here is qualitative as no numerical boundaries are set for each criterion. The motivation for each assigned score is described for each criterion.

3.6.1. Selection of MPS Concept

Table 3.22 summarises the MPS concept data relevant for the trade-off.

Table 3.22: Relevant data for MPS trade-off.

Quantity	Regulated	Blow-down	Pump-fed
Total mass	3.484 kg (excl. regulator)	3.541 kg	3.579 kg
Mass of components	2 thrusters: 0.760 kg Propellant: 2.229 kg Pressurant: 0.081 kg Propellant tank: 0.398 kg Pressurant tank: 0.084 kg Regulator valve: n/a	2 thrusters: 0.760 kg Propellant: 2.229 kg Pressurant: 0.015 kg 2 propellant tanks: 0.537 kg	2 thrusters: 0.760 kg Propellant: 2.229 kg Pressurant: 0.001 kg Propellant tank: 0.406 kg Pump: 0.175 kg PFCD: 0.008 kg
Total volume	3.8 U + regulator	4.0 U	3.25 U
Volume of components	2 thrusters: TBD Propellant tank: 3 U Pressurant tank: 0.7 U	2 thrusters: TBD 2 tanks: 4.0 U	2 thrusters: TBD Tank: 3.0 U Pump + PFCD: 0.25 U
Power consumption	Pre-heating 20 W Firing n/a	Pre-heating 20 W Firing n/a	Pre-heating 20 W Firing: < 4.30 W (pump)
Power consumption of components	Thruster pre-heating: 20 W	Thruster pre-heating: 20 W	Thruster pre-heating: 20 W Pump: 4.30 W (EOL)
Thrust range	0.25 N (constant)	1.00 N (BOL) - 0.25 N (EOL)	1.00 N (BOL) - 0.81 N (EOL)
Pressurant pressure	50 bar (BOL) - 5.5 bar (EOL)	22 bar (BOL) - 5.5 bar (EOL)	9.07 bar (BOL) - 0.64 bar (EOL)
Propellant tank pressure	5.5 bar	22 bar (BOL) - 5.5 bar (EOL)	9.07 bar (BOL) - 0.64 bar (EOL)
Thruster chamber pressure	5.5 bar	22 bar (BOL) - 5.5 bar (EOL)	22 bar (BOL) - 17.87 bar (EOL)

Scoring criteria are all weighted equally, and are scored using the scores "unacceptable", "poor", "good" and "excellent". The trade-off is presented in Table 3.23, here it can be seen that the pump-fed concept scores best due to receiving the score "excellent" in the criteria of volume and propellant tank pressure. The selection criteria and scoring for the most feasible MPS propellant storage and feed system is described below:

- **Mass:** Lower mass means a lighter spacecraft, and less propellant required in case the wet mass of the spacecraft decreases. The mass for all three concepts is similar, however for the pressure regulated concept, a regulator valve needs to be included which may have significant mass as observed in Table 2.14, therefore this concept scores "poor". The blow-down and pump-fed concepts receive the score "good" due to being significantly below the wet mass limit of 6 kg (PROP.110, Appendix A).
- **Volume:** A lower volume means higher reserves for other spacecraft systems, and possibly propulsion system components being less in the proximity of other spacecraft systems, allowing more freedom for choosing placement of components. Similar to the mass criterion, the regulated system requires an additional regulator valve, increasing the volume of this concept and therefore the regulated concept scores "poor". The blow-down concept scores "good" due to being

well below the volume limitation of 5 U (PROP.100, Appendix A), the pump-fed concept scores "excellent" due to its significantly lower volume as compared to the blow-down and regulated concepts.

- **Power consumption:** Less power consumed by the propulsion system translates to more power reserves for other spacecraft systems. All systems are well within the power limits of 10 W for firing and 25 W for pre-heating (PROP.120 Appendix A), therefore all systems receive the score "good".
- **Thrust force:** A higher thrust force indicates shorter manoeuvre times. The pressure regulated concept has the lowest thrust force for the same volume as the other systems. This results from the low pressurant mass linked to a low final pressure in the pressurant tank, however this can be increased at a significant volume penalty. The blow-down system thrust varies over time, towards the minimum thrust value of 0.25 N per thruster. Therefore, both the regulated and blow-down concept receive the score "poor". The pump-fed system has the highest thrust at EOL, this however can be increased to the same thrust as at BOL at a volume penalty, allowing for more pressurant gas to be taken along.
- **Propellant tank pressure:** Lower propellant tank pressure indicates the possibility of using tank shapes that are more efficient in volume utilisation than spherical or cylindrical tanks, very low tank pressures enable the possibility of additively manufacturing the tank and achieving a higher level of integration of components. The regulated concept has the lowest propellant tank pressure, due to the selected thrust level. This increases however for a higher thrust level. The blow-down system has in this case the highest propellant tank pressure in order to achieve a similar system volume as the regulated concept and eliminating the need for a regulator valve. Finally, it is decided to score the pump-fed concept "excellent" since the pump provides a high pressure differential to the thruster, and a propellant tank pressure lower than that of the regulated concept can be selected if desired. The regulated and blow-down concept receive the score "poor" due to significantly higher propellant tank pressure than the pump-fed concept, here it must be noted that for the regulated concept, the propellant tank pressure would be significantly higher for the same thrust value as the pump-fed concept.

Table 3.23: Trade-off for selecting the most feasible Main Propulsion System concept.

Concept	Mass	Volume	Power consumption	Thrust force	Propellant tank pressure
Regulated					
Blow-down					
Pump-fed					

Legend	Unacceptable	Poor	Good	Excellent

Sensitivity Analysis

In Table 3.23 it is seen that the pump-fed concept scores at least "good" for every criterion and "excellent" for two criteria. Other concepts score at most "good" for all criteria and "poor" for at least two criteria, therefore in order for the result to be affected, more than two criteria are required to be omitted simultaneously. Therefore it is concluded that the trade-off was performed satisfactory.

3.6.2. Selection of RCS Concept

The summarised properties of the RCS concepts relevant for the trade-off are presented in Table 3.24. The "same tank" option is considered for the regulated option as the difference in volume is significant with respect to the "separate tanks" option, while all other properties are similar.

Table 3.24: Relevant data for RCS trade-off.

Quantity	Regulated "same tank"	Blow-Down	Pump-fed
Total mass	0.362 kg ¹	0.387 kg	0.455 kg
Mass of components	4 thrusters: 0.116 kg Propellant: 0.173 kg Pressurant: 1.267 E-4 kg Tank: 0.072 kg Regulator valve: TBD	4 thrusters: 0.116 kg Propellant: 0.173 kg Pressurant: 8.373 E-5 kg Tank: 0.098 kg	4 thrusters: 0.116 kg Propellant: 0.173 kg Pressurant: 1.302 E-5 kg Tank: 0.096 kg Pump: 0.065 kg PFCD: 0.005 kg
Total volume	0.7 U ¹	0.8 U	0.9 U
Volume of components	4 thrusters: TBD Tank: 0.7 U	4 thrusters: TBD Tank: 0.8 U	4 thrusters: TBD Tank: 0.8 U Pump + PFCD: 0.1 U
Power consumption	24 W	24 W (BOL), 10 W (EOL)	20 W
Power consumption of components	Thrusters: 24 W	Thrusters: 24 W	Thrusters: 20 W Pump: 0.020 W
Thrust force	2.400 mN	2.400 mN (BOL) - 1.000 mN (EOL)	2.000 mN
Pressurant pressure	8 bar (BOL) - 0.6 bar (EOL)	0.6 bar (BOL) - 0.25 bar (EOL)	0.1 bar (BOL) - 0.04 bar (EOL)
Propellant tank pressure	8 bar (BOL) - 0.6 bar (EOL)	0.6 bar (BOL) - 0.25 bar (EOL)	0.1 bar (BOL) - 0.04 bar (EOL)
Thruster chamber pressure	0.6 bar	0.6 bar (BOL) - 0.25 bar (EOL)	0.5 bar

The trade-off is presented in Table 3.25. Here it is observed, that the blow-down concept scores best due to receiving the score "good" in all metrics except propellant tank pressure where it scores "excellent", while other systems received the score "poor" in some metrics. This system is especially interesting due to its very low tank pressure with still sufficient margin above the vapour pressure of the propellant, furthermore for all other criteria it is within margins. Similar to the selection process for the most feasible MPS concept, scoring criteria are all weighted equally and scores are "unacceptable", "poor", "good" and "excellent". The criteria with explanation of scoring are as follows:

- **Mass:** Lower mass translates to lower spacecraft mass and lower required propellant mass in case the total wet mass decreases. Furthermore, more thrusters may be used when a concept has a sufficiently low mass. Due to all concepts weighing below the maximum allowed 1 kg (RCS.110, Appendix A.2), none score "unacceptable". Similar to the regulated concept for the MPS, the RCS regulated concept also excludes a regulator valve in the final mass. From Table 2.14 it is seen that such valves can have significant mass, and that no suitable option exists. Devising a custom solution however is expected to result in a design closer to the MEMS variant however, with not a significant amount of mass being added such that it exceeds the mass requirements. Therefore the regulated option scores "good". Similarly, the blow-down option scores "good" due to the mass being well within the maximum allowable value. Finally, the pump-fed option scores "poor" as its mass is significantly higher than that of the other concepts, even though it is still well within margins.
- **Volume:** Lower volume translates to more volume reserves being present for the spacecraft and allowing more freedom in integrating components. The blow-down concept is not significantly below the maximum allowable volume of 1 U (RCS.100, Appendix A.2) therefore it receives only the score "good". The volume of the regulated concept is lower than that of the other concepts, however a regulator valve must still be added. As seen in Table 2.14, no suitable option exists and therefore a custom option may need to be devised. It is expected however, that the volume

¹The mass and volume of a regulator valve is still required to be added.

of this component will be closer to the MEMS option than to the other, larger variants, therefore the concept still scores "good". The pump-fed option receives the score "poor" due to being very close to the maximum allowed volume of 1 U, leaving little reserves.

- Power consumption:** A low power consumption means more power reserves for other systems and less heat generated which may be transmitted to surrounding structures. All systems are compliant with the maximum firing power of 25 W (RCS.120, Appendix A.2). However, the power consumption for the regulated concept is expected to stay near this maximum allowable value over its entire lifetime, therefore it receives the score "poor". Comparably, the blow-down and pump-fed perform compare better: the blow-down concept power consumption decreases towards 10 W at EOL, therefore receives "good", the pump-fed concept power consumption stays at 20 W over the lifetime, leaving more margin as compared to the regulated concept, and therefore also receives the score "good".
- Thrust force:** A higher thrust force translates to a shorter manoeuvre time. The thrust force of all concepts are similar, with the exception of the blow-down concept, which is below all other thrust values at EOL. All concepts are within the required 1-10 mN thrust range (RCS.050, Appendix A.2) however on the lower end of the range and therefore all will receive the score "good".
- Propellant tank pressure:** Lower tank pressure translates to a lighter tank and may enable production of the tank using AM which may result in a higher level of component integration. The regulated pressure concept and blow-down system have the highest tank pressure, however comparably low as compared to propellant tank pressure values in the MPS blow-down concept (Table 3.22). The regulated concept receives the score "poor" here due to the selected high propellant tank pressure. It must be noted however, that this pressure value has been selected such to limit the volume of the propellant tank, while enabling a constant thrust force of 2.400 mN. The blow-down system thrust force varies from 2.400 mN at BOL to 1.000 mN at EOL, and to achieve this, a low pressure ratio was chosen which in turn related in a higher volume. This is by a large margin a lower tank pressure compared to the regulated concept, therefore the score "excellent" was assigned. Finally, the pump-fed concept has very low tank pressure due to the pump providing the largest part of the required chamber pressure, however at EOL a very low tank pressure results which is close to the vapour pressure of the propellant. This low final tank pressure is required to achieve a pressure ratio required to limit the required ullage volume of the tank. The pressure ratio cannot be further increased in another way due to the assumed low thruster chamber pressure in combination with the minimum differential pressure provided by the pump. The pump-fed concept therefore scores "poor" on this criterion.

Table 3.25: Trade-off for selecting the most feasible Reaction Control System concept.

Concept	Mass	Volume	Power consumption	Thrust force	Propellant tank pressure
Regulated					
Blow-down					
Pump-fed					

Legend	Unacceptable	Poor	Good	Excellent

Sensitivity Analysis

Table 3.25 shows the blow-down system as the clear best-scoring concept of all three, scoring "good" in 4 criteria and "excellent" for propellant tank pressure. Omission of propellant tank pressure will still result in the blow-down concept winning due to the regulated concept having higher power consumption over its lifetime. Omitting power consumption will not change the outcome either, as the propellant tank pressure of the blow-down system is lower than that of the regulated system. Due to the omission of a single criterion not resulting in a different outcome of the trade-off, it is concluded that the trade-off was performed satisfactory.

3.7. Discussion of Selected Concepts

Early in the concept design phase, the CGT technology was eliminated due to the available thrusters being specified for Nitrogen gas. Nitrogen gas at the maximum allowed storage pressure of 50 bar (RCS.160, Appendix A) resulted in an excessively large storage volume, making the CGT infeasible. It was seen however that also Ammonia or Butane propellants could be used for CGT, stored in the liquid phase. However, it was chosen not to pursue this due to firstly the higher specific impulse performance of resistojet technology and secondly the available cold gas thrusters only being specified to work with gaseous Nitrogen.

Selection of the most feasible propulsion system concepts for the MPS and RCS using the qualitative trade-off method has resulted in the choice of a pump-fed concept for the MPS and a blow-down concept for the RCS. The choice for a pump-fed system for the MPS is not a novel concept for CubeSat, the LFPM utilises a Flightworks, inc. micro-gear pump as discussed by Andrews et al. in 2020 [7] and some variants of the Aerojet Rocketdyne CHAMPS-series propulsion systems are pump-fed as presented in the datasheet of the CHAMPS MPS-13X-series propulsion systems (larger version of Figure 2.38a) [22]. For the RCS concept selection, the pump-fed concept scored worst of all, scoring "poor" in three criteria and "good" in two. The regulated concept scored "poor" on basis of power consumption and propellant tank pressure, however here it must be noted that the performance of this concept is a direct consequence of the choice of the maximum constant thrust level of both thrusters firing (2.400 mN) - additionally, a high propellant tank pressure was chosen to limit the volume of this concept. The blow-down concept won this trade-off due to the power consumption lowering over its lifetime, and having lower propellant tank pressure as compared to the regulated concept while having more margin above the propellant vapour pressure as compared to the pump-fed concept. In case the regulated concept were to have been designed with the same tank pressure values as the blow-down concept at BOL and EOL, effectively having the same tank conditions as the blow-down concept, the outcome of this trade-off would have been the same. In this case, the constant thrust level has to be set at the lowest possible thrust level, namely 1.000 mN, having lower power consumption over the lifetime. However, with the addition of the regulator valve, its total mass and volume would now be higher as that of the blow-down concept. Additionally, this regulator valve would have added more complexity to the system. A blow-down type system for the RCS effectively eliminates the need for a regulator valve and requires less components than a pressure regulated or pump-fed system.

It must be noted, that the selection of these concepts relies on a concept generation process using simplified theoretical methods and the results may therefore not be completely accurate and representative of real propulsion systems. In the generation of the concepts as described in Section 3.4 and Section 3.5, many assumptions were made: for the RCS concepts, thruster chamber temperature, chamber pressure and expansion ratio were assumed in order to enable use of the critical mass flow relation Equation 2.9. For the MPS, data on chamber pressure and temperature was available, enabling use of the critical mass flow relation. For the pump-fed concepts for both MPS and RCS, pump data was taken from datasheets which is unreliable. Subsequently, pressure, mass flow and rotational velocity relations were derived from data in graphs, introducing further inaccuracies. Moreover, the recirculation loop and PFCD design for the pump concepts ignored any pressure losses in low-flow velocity parts of the system and using pressure drop relations based on empirical relations. In reality, determining pressure losses in such a system and resulting pump performance must be evaluated using testing. Finally, the tank wall thickness in each concept was determined considering mechanical strength only, ignoring the possible deformations these tanks could experience under the pressure of the fluids within. The aforementioned methods all however do result in approximate thrust levels and pressure, mass, volume and power consumption values of the concepts, allowing comparison between the concepts and deciding which concepts to pursue in the detailed design phase.

4

Detailed Design

This chapter delineates the detailed design phase of the propulsion system design for the MPS and RCS. Chapter 3 contained the concept design phase, where a pump-fed type concept was chosen for the MPS and a blow-down type concept for the RCS. These concepts will be designed in more detail in this chapter. The system layouts are presented below with a cursory overview of what components will be designed in this chapter. The first section of this chapter discusses the design of the MPS and RCS propellant tanks, the second section discusses the pump selection, PFCD design and throttling for the MPS only. The third section contains the selection of COTS components and discusses the placement of all components inside the spacecraft bus, illustrated as a Digital Mockup (DMU), for both the MPS and RCS. The fourth section delineates the approximation of pressure loss over the feed paths of the MPS and RCS. The fifth section presents a summary of the final designs of the MPS and RCS and furthermore presents the compliance check of all requirements from Appendix A. Finally, the sixth section contains the comparison of the final custom designs to COTS options: first, representative COTS systems are selected and subsequently, the comparison is made.

Figure 4.1 shows the layout of the MPS. Two thrusters will be used, as per requirement PROP.051 Appendix A.1. These thrusters require a pressure regulator valve to comply with the throttling requirement PROP.052. As the chosen feed system type is a pump-fed concept, a pump and PFCD are included. In front of the pump, a latching valve is present to isolate the system before launch and in case of any leakage. A propellant tank is required to store the propellant and pressurant, and will be equipped with thermocouples and pressure transducer to monitor the temperature and pressure inside the propellant tank to comply with requirement PROP.190. As the length of the thrusters (178 mm, Table 2.12) is significant, it poses a challenge to using two separate tanks, leaving a length of only roughly 230 mm for the tanks (refer to Appendix D for the dimensions of the 12U CubeSat bus). Furthermore, using a single tank greatly improves the simplicity of the design as less feed lines, sensors, fill/drain valves and latch valves are required, of which the latter two are additionally characterised by significant mass (Table 2.17, Table 2.18). Therefore, one single tank is chosen.

The RCS (Figure 4.2) has a similar layout to that of the MPS, however lacking a pump and PFCD due to a blow-down type feed system being chosen during the concept design phase. Furthermore, a regulator valve in front of the thrusters is not required due to lack of a throttling requirement (Appendix A.2). Just as in the concept, four thrusters are chosen as this enables rotation around all three spacecraft body axes and is the minimum acceptable amount of thrusters as per requirement RCS.051 (Appendix A.2). It is important to note that the available mounting area for the RCS is in one of four corners of the spacecraft rear (Appendix D.2) as the others are occupied by the optical payload and the MPS thrusters. This mounting position of the system has the disadvantage of causing cross-coupling between rotational motions, however this is left out of scope for the thesis.

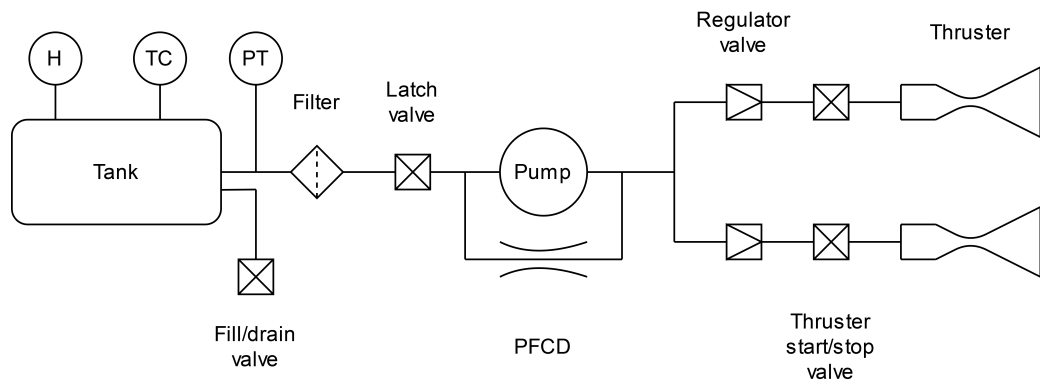


Figure 4.1: Hydraulic diagram for the Main Propulsion System, draw.io.

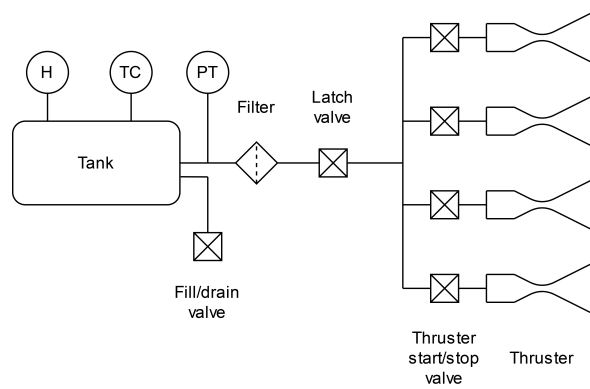


Figure 4.2: Hydraulic diagram for the Reaction Control System, draw.io.

4.1. Propellant Tank

This Section delineates the tank design for both the MPS and the RCS. First, the PMD design is discussed for both the MPS and RCS. A selection is made and the design is presented. Subsequently, the MPS propellant tank is designed. Finally, the RCS tank is designed.

4.1.1. Propellant Management Devices

As discussed in Section 2.8.4, the liquid-vapour interface of propellant and pressurant in a microgravity environment is mostly dictated by surface tension forces, i.e. the propellant tends to stick to the walls. With a gas bubble in the centre of the tank, during adverse accelerations (translational or rotational), gas may travel towards the outlet port with the risk of feeding gas to components downstream, damaging those components. In order to provide gas-free expulsion at all times and better control the centre of gravity of liquids inside tanks, one or more PMDs are required.

Selection of Propellant Management Device Types

A summary of PMDs of interest is presented in Table 2.11. As discussed by Collicott et al. in 2019 [79], for conformal tanks, typically capillary type devices are used. Considering that for the capillary devices, the vane-type device is much more simple as compared to the gallery-type device, a vane-type device is selected. Since it is difficult to design PMD and the resulting feed rate of the vanes requires extensive analysis (decided out of scope), a sponge-type PMD is conservatively chosen to be added to provide a fixed amount of propellant on-demand. This choice is underlined by the combination of sponge- and vane-type devices in the Lunar Flashlight Propulsion Module as discussed by Andrews in 2020 [7] and Huggins in 2021 [8]. As previously mentioned, the design of such devices is complicated and difficult to verify, the detailed design of these devices is left out of scope and a simple volume and mass estimate of such devices is made using design steps discussed by Jaekle in 1991 and 1993 [80, 81]. Additionally, the tanks for both MPS and RCS will be designed with a fillet radius of 10 mm to prevent sharp edges trapping fluids and furthermore to reduce stress concentrations along tank wall edges. The fillets are considered PMD and the material of all PMDs is chosen identical to that of the tank for material compatibility.

Sponge Design

In order to design the sponge, it is assumed that the sponge should hold all the propellant required to perform a worst-case manoeuvre. For the MPS, this is chosen as 60 s of continuous firing of both thrusters at their maximum thrust level of 1 N. For the RCS, this is the de-saturation manoeuvre, where all four reaction wheels carrying 30 mN-m-s of angular momentum are fully de-saturated using one thruster at a time at a maximum thrust level of 4 mN. Here it is assumed that during RCS thruster firing, the torque only works over one axis. In reality, an attitude control strategy is required to be made accounting for the thruster position on the spacecraft. The required hold volume of the sponge is calculated using the propellant mass resulting from the aforementioned firing times, including a safety factor of 2 to be conservative. A circular sponge design is chosen and the diameter is calculated using 1 inch of spacing from the nearest wall to prevent leakage, according to the method of Jaekle presented in 1993 [80]. The porous centre tube of the sponge has an inner diameter of 3 mm, equal to that of the pump ports for the MPS; a wall thickness of 1 mm for the tube is assumed. For the RCS, the same centre tube inner and outer diameters are taken preliminarily. The number of plates is chosen as 20, this results in a plate gap of 6.864 mm at the outer radius of the sponge. It is unknown if this allows for holding fluid using surface tension, however this dimensioning process shows a mass estimate. Performance of the sponge may be improved by increasing the number of plates or using porous plates. It is important to note, that RCS calculations are with respect to BOL thrust, in order to make a conservative estimate.

Vane Design

In this design, the purpose of the vanes is to collect propellant from the walls of the tank and subsequently refill the sponge, which may start leaking some propellant during adverse accelerations resulting from manoeuvring and which will slowly deplete during thruster operation. Jaekle has proposed several design methods for vanes in 1991 [81], however most require very in-depth analysis with still many assumptions and uncertainties. In order to arrive at a mass and volume estimate of the vanes, a simple ribbon-type (parallel to the tank wall surface) with 10 mm of width, 1 mm of thickness and 10

mm of stand-off distance from the tank walls is chosen. For the MPS, six vanes are chosen (two on top/bottom, four on the side panels) and for the RCS, four vanes are chosen (two on front/rear, two on the side panels). All vanes connect at the outlet port of the tank and at the opposite end of the tank. As the tank dimensions are not known yet for both the MPS and RCS, no estimate of mass and volume is given yet for volume and mass for these devices.

According to Jaekle, a possible upper limit on the flow rate inside the vanes is the choking velocity or wave propagation speed, as discussed in Section 2.8.4. This will be used to calculate the sponge refill time and thereby provide a check on the usefulness of the vanes. For this calculation, the absolute surface tension of the propellant is required. For LMP-103s, this value could not be found and therefore the value for FLP-106 will be used, which is a propellant with similar properties as LMP-103s; LMP-103s consists of 63 % ADN, 18.4% methanol, 14% water and 4.6% ammonia - FLP-106 consists of 64.6% ADN, 23.9% water, 11.5% "low volatile hydrocarbon fuel" as discussed by Persson, et al. in 2019 [23] and Wurdak, et al in 2012 [121]. The surface tension value is assumed to be valid for these calculations, and should give an order of magnitude for the sponge re-fill rate. The flow area around a vane is conservatively estimated to be simply the area between the vane and the wall (vane width times vane stand-off distance), ignoring the propellant forming the fillets around this area. The vane fillet radius is chosen to be equal to the stand-off distance. It can be seen that at choking velocity, the MPS sponge is refilled within roughly 3 seconds, for the RCS this is roughly 0.5 s. Table 4.1 shows these calculations. The mass flow along the vanes for these calculations is shown to be sufficient for thruster operation, theoretically eliminating the need for a sponge. However, being conservative, both PMD are still decided to be used: in reality, during adverse accelerations, vanes may start leaking or the flow velocity along the vanes may be lower than the choking velocity calculated here. Furthermore, the flow area is only assumed.

Table 4.1: Vane-type Propellant Management Device design. Surface tension values taken at 25 deg. C, closest available to 300 K.

Parameter	MPS	RCS
Number of vanes	6	4
Vane width	10 mm	10 mm
Stand-off distance	10 mm	10 mm
Vane flow area	1.000 E-4 m ²	1.000 E-4 m ²
Propellant density	1,236.520 kg-m ⁻³	996.560 kg-m ⁻³
Propellant surface tension (abs.) ζ_{st}	54.900 mN-m ⁻¹ [121]	72.015 mN-m ⁻¹ [122]
Wave celerity	0.047 m-s ⁻¹	0.060 m-s ⁻¹
Total flow rate	2.827 E-5 m ³ -s ⁻¹	2.404 E-5 m ³ -s ⁻¹
Sponge refill time	3.031 s	0.535 s
Vane mass flow	0.035 kg-s ⁻¹	0.024 kg-s ⁻¹

Table 4.2: Sponge-type Propellant Management Device design for worst-case scenario.

Parameter	MPS	Parameter	RCS
Thrust force	1 N	Thrust force	4 mN
Specific impulse	231 s	Specific impulse	100 s
Propellant mass flow (total)	8.883 E-4 kg-s ⁻¹	Propellant mass flow (total)	4.079 E-6 kg-s ⁻¹
		Total angular momentum	120 mN-m-s
		Angular momentum per axis	40 mN-m-s
		Roll axis arm	0.113 m
		Pitch/yaw axis arm	0.177 m
		Impulse required roll axis	0.354 N-s
		Impulse required pitch/yaw axis	0.227 N-s
		Burn time roll axis	88.496 s
		Burn time pitch/yaw axis	56.657 s
Burn time	60 s	Burn time total	201.810 s
Propellant mass total	0.053 kg	Propellant mass total	0.823 g
Safety factor hold mass	2	Safety factor hold mass	2
Propellant hold mass	0.106 kg	Propellant hold mass	1.646 g
Propellant density	1,236.520 kg-m ⁻³	Propellant density	996.560 kg-m ⁻³
Propellant hold volume	8.568 E-5 m ³	Propellant hold volume	1.652 E-6 m ³
Shortest tank width	94.500 mm	Shortest tank width	94.500 mm
Sponge diameter	43.700 mm	Sponge diameter	43.700 mm
Number of plates	20	Number of plates	20
Plate thickness	0.5 mm	Plate thickness	0.5 mm
Edge gap	6.864 mm	Edge gap	6.684 mm
Centre tube inner diameter	3 mm	Centre tube inner diameter	3 mm
Centre tube wall thickness	1 mm	Centre tube wall thickness	1 mm
Fluid hold area	1.287 E-3 m ²	Hold area	1.287 E-3 m ²
Required sponge height	66.587 mm	Required sponge height	1.284 mm
Chosen sponge height	66.587 mm	Chosen sponge height	10 mm
Propellant hold mass	0.106 kg	Propellant hold mass	12.823 g
Burn time (excluding safety factor) ¹	60 s	Burn time (excluding safety factor)	1,571.890 s
Sponge structure volume	1.378 E-5 m ³	Sponge structure volume	1.966 E-6 m ³
Sponge structure mass	61.064 g	Sponge structure mass	8.711 g

¹The burn time here is related to the total propellant hold mass before the hold mass safety factor is applied (conservative).

4.1.2. Main Propulsion System Propellant Tank

The design of the MPS propellant tank is parametric. A conformal tank design using a cuboid shape is chosen to maximise the volumetric efficiency of the propellant storage. Using a cylindrical shape in contrast is not effective as seen in Table 3.14, which would require the entire spacecraft bus length, providing only 7% ullage volume. Furthermore, no space would be available for the thrusters of the MPS and the RCS and therefore the tank volume would require to be split into two tanks. This could, as mentioned at the beginning of this chapter, cause the need for extra feed lines, latch valves and fill/drain valves, increasing complexity and mass of the system. Using a single cuboid tank therefore is the more suitable option. It must be noted, that the choice of one single tank of a different shape is different from what was devised in the concept generation stage of the project. This is however not expected to change the validity of the trade-off between different propulsion system concepts, due to both the blow-down and regulated pressure in any case requiring a higher total tank volume, and the higher pressure in the blow-down concept is expected to still result in higher tank mass, all as compared to the pump-fed concept, still resulting in a pump-fed concept being the most feasible solution.

Table 4.3 shows the selected input parameters for the tank design. The available interior volume of the spacecraft bus in which the propellant tank of the MPS can be placed is calculated using an assumed worst-case wall thickness of 5 mm. The outer height of this volume results from subtracting the width of two structural rails from the outside height; the outer width results from taking half that value, considering the presence of the payload inside the spacecraft bus. Figure D.1 shows the aforementioned dimensions. It is decided to utilise the full available interior width and height of the propellant tank, leaving the tank length as the sole free variable for the tank dimensioning process. This maximises the space available between the propellant tank and other systems, namely the MPS thrusters and the complete RCS. The interior volume of the tank is used for dimensioning to simplify the dimensioning process so that the tank interior width and height can be kept constant and do not have to change to accommodate for different required wall thickness values.

Selected Tank Material

The selected tank material is Ti-6Al-4V due to its compatibility with selected MPS propellant LMP-103s and its superior specific strength and similar specific stiffness as compared to stainless steels 301 and 304L, properties presented in Table 2.10. The applied load factors to the analysis are the ultimate load factor $j_u = 1.25$ and burst load factor $j_b = 2.50$ in order to calculate the maximum allowable stresses, resulting in a value of 374.40 MPa for ultimate tensile stress.

Table 4.3: Input parameters for the Main Propulsion System tank detail design.

Parameter	Value	Parameter	Value
Worst-case wall thickness	5 mm	EE	0.9
Outer width available	104.5 mm	M_p ¹	2.476 kg
Inner width available	94.5 mm	V_p	2.002 E-3 m ³
Outer height available	209 mm	Assumed Δp margin	0.024 bar
Inner height available	199 mm	Selected EOL tank pressure	0.741 bar
Minimum inlet pressure pump	0.717 bar		

Optimisation Process

Assuming incompressible propellant, low duty cycle operation and thus isothermal expansion of the pressurant gas, varying the tank length results in a changing BOL/EOL pressure ratio. In order to achieve minimum tank mass, the lowest allowable tank pressure is selected, which is set by the cavitation requirements of the pump (Table 2.8). This was, including a pressure drop margin of 0.024 bar and rounding up, determined to be 0.741 bar. The vapour pressure of the propellant LMP-103s is 0.148 bar at 300 K Table 3.5, considering the pump tests performed by Flightworks, Inc. as discussed in Section 2.5.2 the selected EOL pressure is assumed sufficient to provide sufficient NPSH. The value

¹Calculated using a spacecraft wet mass of 26 kg, I_{sp} of 231 s and EE of 0.9

for pressure drop margin is taken as representative for micropropulsion systems in CubeSats as discussed by Berg and Rovey in 2017 [123]. PMD are included in the tank volume and mass, according to the calculations in Section 4.1.1 and methods in Section 2.8.4.

The effect of variation of tank length on BOL tank pressure, ullage fraction and pressurant gas mass is shown in Figure 4.3. With varying tank length and therefore varying BOL pressure, each tank wall requires a minimum thickness. For this, out-of-plane displacements and von Mises stresses are considered, calculated according to thin plate theory assuming simply supported edges as discussed by T.H.G. Megson in 2013 [71], methods presented in Section 2.8.2. In reality, the edge support conditions are somewhere between simply supported and clamped, however the simply supported situation is considered for a preliminary estimate, to later be verified by FE analysis. The maximum allowable von Mises stress at the centre of each wall is 374.4 MPa, resulting from the tensile ultimate stress 1170 MPa of the material, dividing by the burst safety factor of 2.5 and ultimate load factor of 1.25. The maximum allowable out-of-plane displacement of each tank wall centre is set conservatively at 1 mm, so that the tank walls even under pressure will not expand such that they touch the outer wall of the spacecraft bus. As seen in Table 4.3, a worst-case wall thickness of 5 mm is used. As seen in Figure D.1, the guide rails inside the spacecraft reach 6.5 mm into the spacecraft bus, measured from the outer walls sides. Therefore, at worst-case wall thickness and wall displacement, still 5.5 mm will be left until the outer edge of the bus volume is reached. This distance of 5.5 mm is taken as sufficient to allow for the bus walls to take place, and additionally some margin for insulation and mounting materials. The von Mises stresses at the centre of the tank walls are shown in Figure 4.4 for tank wall thickness values of 1, 3 and 5 mm. The stiffness requirement to achieve a maximum displacement at the plate centre of either 1, 0.1 or 0.01 mm is shown in Figure 4.5.

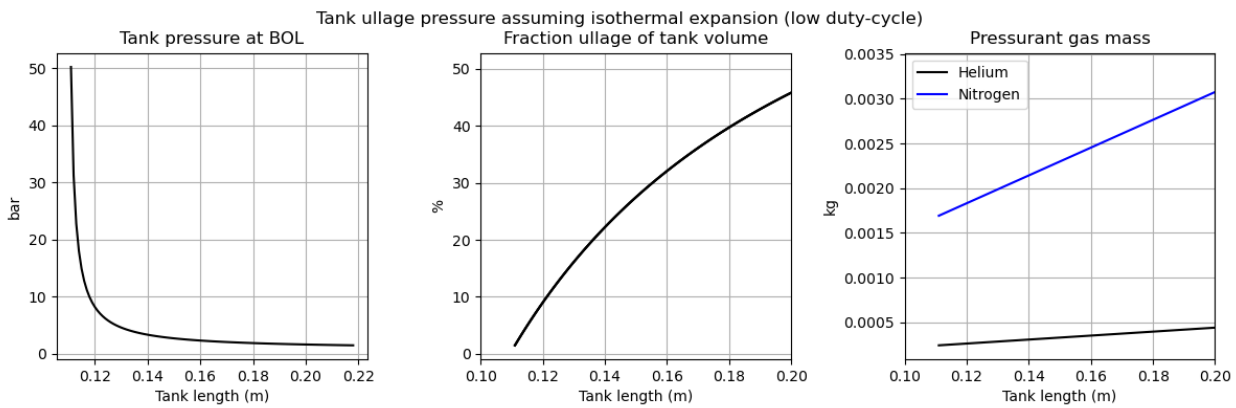


Figure 4.3: BOL tank pressure, ullage fraction and pressurant gas mass as function of tank length, Python/Matplotlib.

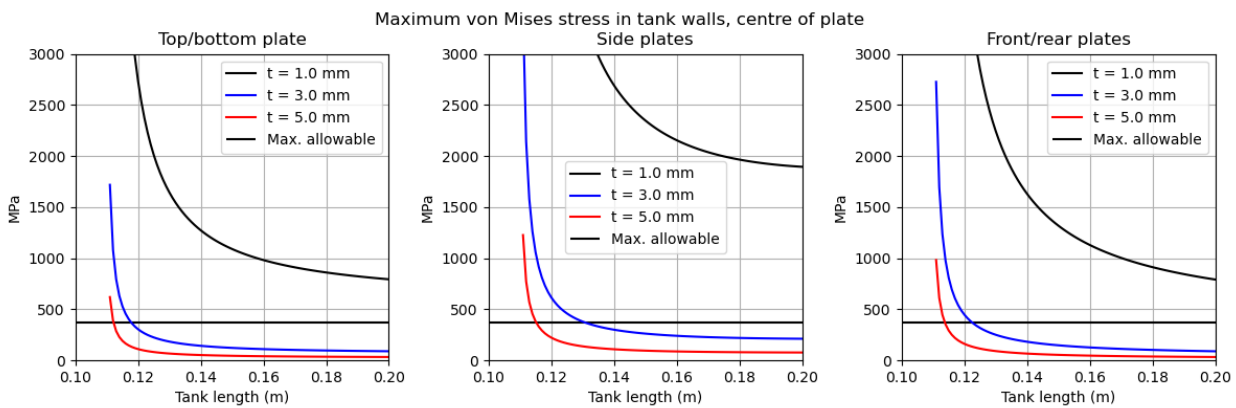


Figure 4.4: Von Mises stresses in tank walls at centre of plate as function of tank length, Python/Matplotlib.

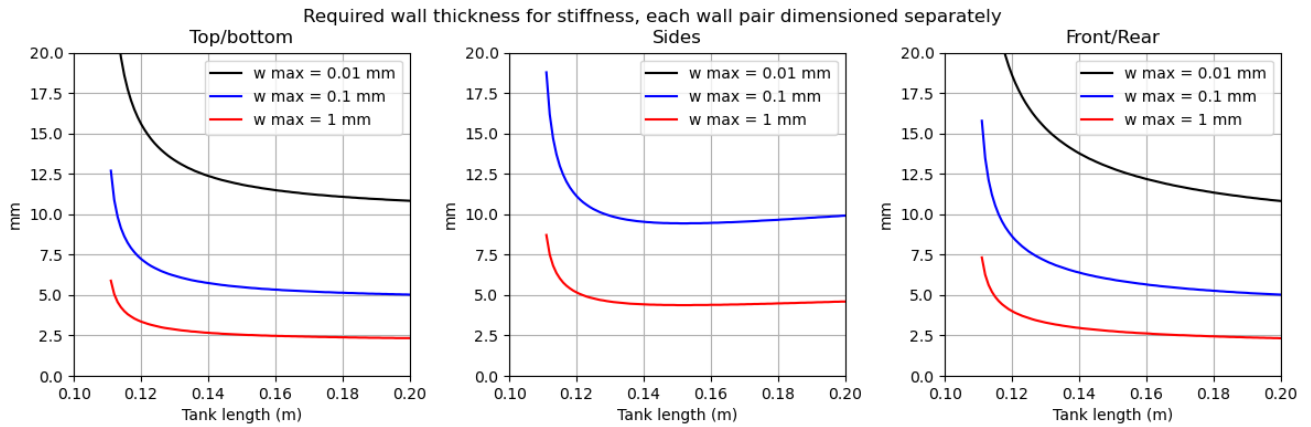


Figure 4.5: Required tank wall thickness for maximum displacement, Python/Matplotlib.

Final results

The results for maximum displacements are shown in Figure 4.5 and Table 4.4. Given that the value for maximum allowable displacement is selected driven by spacecraft bus volume available and not by any specific stiffness requirements, caution must be made with selection of the wall thickness. However, it is observed in the aforementioned figure that the optima for tank length for different displacement allowables are close together, therefore the choice with regard for tank length is deemed satisfactory. As the calculations performed here are treated as preliminary, the lightest solution is verified using FE-analysis in Ansys Workbench in the next paragraph. Finally, it is observed that the PMDs add significant mass to the tank. The volume these devices occupy as compared to the tank dry volume is small, however not insignificant - the volume of the PMD is on the order of magnitude of $E-5 \text{ m}^3$ as compared to $E-3 \text{ m}^3$ for tank volume - i.e. the PMD volume occupies a volume in the order of 1-2% of the tank interior volume. The tank dry volume denotes the volume usable for propellant and pressurant gas storage. The tank dry mass is a significant fraction of the allowable propulsion system wet mass of 6 kg, namely 2.246 kg.

It is important to note here, that these results stem from analysis using thin plate theory. In the FE-analysis, the stresses and displacements will be checked and in case sufficient margin exists on these, an iteration will be made to the tank where the wall thickness is reduced.

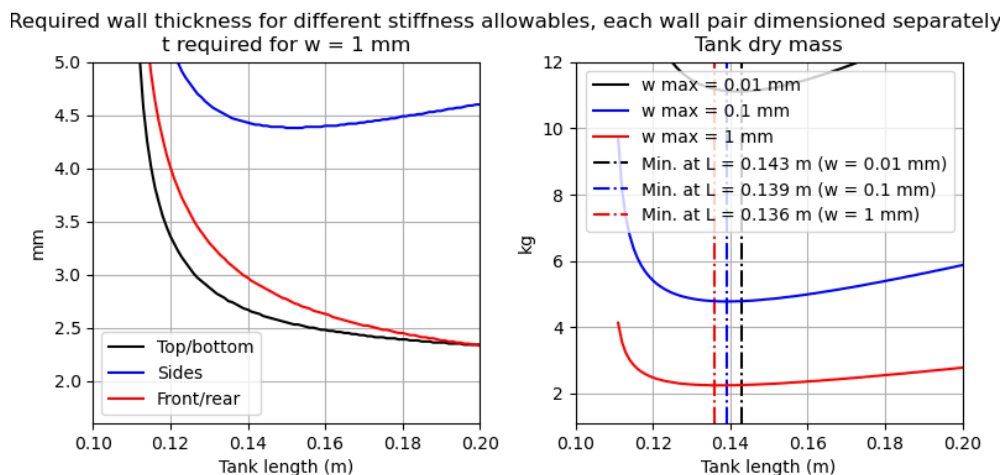


Figure 4.6: Final required wall thickness considering maximum displacements, Python/Matplotlib.

Table 4.4: Optimisation results for MPS propellant tank dimensioning using thin plate theory.

Parameter	Value
Tank length	136 mm
Inner dimensions	94.5 x 199 x 136 mm
Required wall thickness top/bottom walls	2.74 mm
Required wall thickness side walls	4.47 mm
Required wall thickness front/rear walls	3.08 mm
Fillet radius	10 mm
Tank dry volume	2.500 E-3 m ³
Ullage fraction BOL	21.701 %
Helium pressurant mass	0.297 g
Nitrogen pressurant mass	2.080 g
BOL pressure	3.725 bar
EOL pressure	0.741 bar
Tank dry mass (total)	2.246 kg
Vane mass	31.785 g
Sponge mass	60.786 g
Fillet mass	163.328 g
Total PMD mass	255.899 g
Vane volume	7.175 E-6 m ³
Sponge volume	1.372 E-5 m ³
Fillet volume	3.687 E-5 m ³
Total PMD volume	5.776 E-5 m ³
Max. von Mises stress top/bottom wall pair	184.651 MPa
Max. von Mises stress side wall pair	145.787 MPa
Max. von Mises stress front/rear wall pair	192.050 MPa
Margin of safety von Mises stress top/bottom wall pair	1.028
Margin of safety von Mises stress side wall pair	1.568
Margin of safety von Mises stress front/rear wall pair	0.949
Out-of-plane wall displacement all walls	1 mm

Finite Element Analysis

The tank excluding PMD and the outlet port, is modeled in Autodesk Inventor 2022 and subsequently imported into ANSYS Mechanical 2019 R3. The load applied is the pressure at BOL (3.725 bar, Table 4.4). Tetrahedron elements are selected as they better fit the rounded fillets in the design as compared to e.g. triangle-shaped elements. Maximum element size for the mesh is set at 2.00 mm due to numerical limits to the academic license. In thickness direction however, always at least two elements are used as the lowest thickness here is 2.74 mm of the top/bottom walls. For analysis, the tank is cut in half three times, over each half-plane: an eighth of the tank results. Normal to each cutting plane, a symmetry condition and a displacement constraint is placed.

The von Mises stress solution is shown in Figure E.1, where it is seen that the maximum occurring von Mises stress occurs close to the edge of the side and bottom walls, and side and front walls. This location of maximum stresses indicates a boundary condition tending more towards fixed edges instead of pinned edges, as assumed for the hand calculations: this makes sense due to the fillets applied, increasing the stiffness at the edge of the walls. Figure E.2 shows the deformation, with the maximum deformation occurring at the centre of the side plates.

It is concluded, that the tank as dimensioned using the aforementioned thin plate theory optimisation process has sufficient wall thickness for the load case of 3.725 bar at BOL. The maximum stress of 153.460 MPa is far below the maximum allowable value of 374.40 MPa and the maximum occurring deformation of 0.407 mm is far below the allowable value of 1 mm. These allowables are defined and discussed at the start of the optimisation process section. There is a possibility however that

the optimum found using the methods in the previous paragraph is not the real optimum. This is due to the inaccuracy between reality and the results obtained from thin plate theory equations. In order to investigate whether a true optimum is achieved, a more thorough analysis of the wall stress and displacements using a plate support somewhere in between pinned and fixed conditions would be required. This is however decided out of scope due to the time limitations on the MSc thesis. The tank design for the MPS is therefore decided as satisfactory.

Design Iteration: Reducing Each Wall Thickness by 1 mm

As the tank mass is a significant part of the total wet mass, an iteration is made where each wall thickness is reduced by 1 mm. The relevant changes are presented in Table 4.5, a lower tank dry mass (including PMD - as for the original tank dry mass) is observed - 25.253% lower as compared to the value in the initial design. The FE-analysis is repeated, von Mises stresses shown in Figure E.3, deformations in Figure E.4. Significantly higher stresses (max. 349.540 MPa) and displacements (max. 0.883 mm) are observed - however, displacements and von Mises stresses are still below their allowable values. Given the achieved mass savings and the acceptable stresses and deformations, the dimensions resulting from this iteration are taken as final.

Table 4.5: Design iteration: reducing wall thickness of the MPS propellant tank: relevant changes.

Parameter	Value
Wall thickness top/bottom plates	1.74 mm
Wall thickness side plates	3.47 mm
Wall thickness front/rear plates	2.08 mm
Propellant tank dry mass	1.679 kg
Mass savings	25.253 %

Sensitivity Analysis

In order to show that the FE-analysis has presented acceptable results, the element size is increased from the original element size of 2 mm. A solution is considered for element sizes of 3 mm, 5 mm and 10 mm. The results are presented in Appendix E.1.2 and summarised in Table 4.6. Here it can be seen, that for increasing element size, the magnitudes of stress and deformation decrease. A trend for decreasing element size with regards to especially maximum von Mises stress is observed. From this it can be concluded, that a more detailed FE-analysis using a smaller element size may result in higher stresses, however the trend does not indicate that the maximum allowable stress of 374.40 MPa and maximum deformation of 1 mm will be exceeded.

The sensitivity analysis is repeated for the wall thickness iteration, results shown in Appendix E.1.2 and summarised in Table 4.7. The same trends are observed, however the stress increase with decreasing mesh size is not significant from an element size of 3 mm to 2 mm. What can be observed clearly here, is the extreme difference in von Mises stress at an element size of 10 mm - the von Mises stress here is only roughly half of that of the other samples. For this analysis it is also expected that using a smaller element size will result in higher stresses, although it is not expected that it will exceed the maximum allowable stress of 374.40 MPa and maximum deformation of 1 mm will be exceeded. Therefore, the result of the FE-analysis is deemed accurate enough for verification of the thin plate theory results. Due to license constraints, a FE-analysis with smaller elements is not further pursued.

Table 4.6: Sensitivity analysis on the FE-analysis of the Main Propulsion System tank.

Element size	Stress Max.	Stress Min.	Deformation Max.	Deformation Min.
2 mm	153.460 MPa	0.344 MPa	0.407 mm	8.769 E-5 mm
3 mm	146.360 MPa	0.530 MPa	0.406 mm	6.339 E-5 mm
5 mm	138.410 MPa	0.855 MPa	0.404 mm	1.553 E-4 mm
10 mm	121.10 MPa	0.856 MPa	0.389 mm	1.685 E-4 mm

Table 4.7: Sensitivity analysis on the FE-analysis of the Main Propulsion System tank after the wall thickness reduction iteration.

Element size	Stress Max.	Stress Min.	Deformation Max.	Deformation Min.
2 mm	349.540 MPa	0.816 MPa	0.883 mm	1.469 E-4 mm
3 mm	346.110 MPa	1.057 MPa	0.881 mm	1.833 E-5 mm
5 mm	315.750 MPa	1.399 MPa	0.873 mm	3.722 E-4 mm
10 mm	167.770 MPa	1.782 MPa	0.812 mm	2.632 E-4 mm

4.1.3. Reaction Control System Propellant Tank

The propellant tank dimensions for the RCS are dictated by the selected BOL/EOL pressure, therefore the design is more straightforward as compared to the parametric design of the MPS propellant tank. A blow-down type feed system was selected in the concept phase, meaning that the tank pressure decreases from BOL to EOL, similarly to the MPS, however with no pump to provide a pressure differential to achieve constant thruster inlet conditions. As the vapour pressure of the water propellant is very low (roughly 0.035 bar at 300 K [49]), the EOL thruster pressure is dictated by the minimum thrust requirement: 1 mN at a thruster inlet pressure of 0.250 bar and a power consumption of 5W. For blow-down type systems, a high BOL/EOL tank pressure ratio is desirable in order to limit the required ullage volume, however in order to eliminate requiring a pressure regulator valve, a low BOL tank pressure is chosen, corresponding to the selected thrust level at BOL. The selected thrust levels at BOL and EOL for the thruster are shown in Table 4.8. A pressure drop margin is included, to prevent the thruster inlet pressure falling below the minimum pressure at EOL; at BOL, no margin is added in order to prevent excessive thruster inlet pressure in case the pressure drop is lower than the assumed margin. The magnitude of the aforementioned margin, which can be expected for CubeSat propulsion systems is 0.024 bar, as discussed by Berg and Rovey in 2017 [123].

The volume of the sponge is known, however the volume of the vanes and fillets is unknown as they are a function of tank length. The tank length is solved for, to compensate for the volume required by all PMD, and results in 32 mm of length. Table 4.9 shows the tank dimensioning results. As the length is fixed, the only variable left is the wall thickness, of which the influence on von Mises stress and displacements of the centre of the tank walls is presented in Figure 4.7. Here it can be seen, that stiffness is design-driving and a wall thickness of 0.495 mm is required for the side plates and 1.45 mm for the front/rear plates. For the front/rear plates, this thickness is taken as the actual thickness; for the side plates, a thickness of 1 mm is taken conservatively. The results of the dimensioning process are presented in Table 4.9.

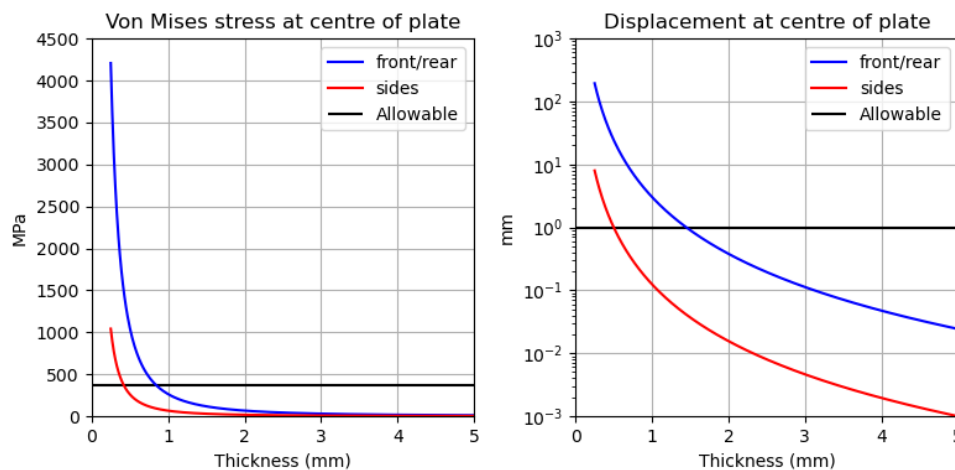


Figure 4.7: Von Mises stress and displacements for the RCS propellant tank, at the centre of the plates, Python/Matplotlib.

Table 4.8: Thruster and tank conditions (1 thruster firing).

Parameter	BOL	EOL
Thrust level	4.000 mN	1.000 mN
Inlet pressure	1.000 bar	0.250 bar
Power consumption	20.00 W	5.000 W
Pressure drop margin	0	0.024 bar
Tank pressure	1.000 bar	0.274 bar
Propellant mass ¹	0.193 kg	-
<i>EE</i>	0.9	-

Table 4.9: Dimensioning results for RCS propellant tank.

Parameter	Value
Tank length	32.344 mm
Required wall thickness sides	0.495 mm
Required wall thickness front/rear	1.450 mm
Chosen wall thickness sides	1.000 mm
Chosen wall thickness front/rear	1.450 mm
Fillet radius	10 mm
Tank dry volume	2.662 E-4 m ³
Ullage fraction BOL	27.400 %
Helium pressurant mass	0.012 g
Nitrogen pressurant mass	0.082 g
BOL pressure	1.000 bar
EOL pressure	0.274 bar
Tank dry mass (total)	250.480 g
Vane mass	7.296 g
sponge mass	8.850 g
Fillet mass	84.171 g
Total PMD mass	100.317 g
Vane volume	1.647 E-6 m ³
Sponge volume	1.998 E-6 m ³
Fillet volume	1.900 E-5 m ³
Total PMD volume	2.265 E-5 m ³
Max. von Mises stress top/bottom, side wall pairs	65.091 MPa
Max. von Mises stress front/rear wall pair	125.063 MPa
Margin of safety von Mises stress top/bottom, side wall pairs	4.752
Margin of safety von Mises stress front/rear wall pair	1.994

¹Using I_{sp} of 100 s, required I_t of 170 N-s and *EE* of 0.9

Finite Element Analysis

The same procedure as for the MPS is followed. For this tank however, due to the smaller size and lower thickness of the walls, the maximum element size is 0.5 mm, therefore this FE-analysis is expected to be more accurate as compared to that of the MPS. Figure E.17 shows a maximum von Mises stress of 56.557 MPa, barely visible however occurring at the edge of the front/rear plate, at half-tank width distance. Figure E.18 shows the deformations, with the maximum occurring at the centre of the front/rear plate pair and a magnitude of 0.267 mm. These values are acceptable, and are within the same order of magnitude as those in the analytical results (Table 4.9). The tank design is therefore decided sufficient. Due to the fact that the tank dry mass is only roughly 25% of the allowed propulsion system wet mass, a wall thickness reduction iteration is not performed.

Sensitivity Analysis

The same procedure as for the MPS is followed. The baseline maximum element size here however is 0.5 mm, the sensitivity analysis is performed on element sizes 1, 3 and 10 mm. The results are shown in Appendix E.2 and summarised in Table 4.10. Here it can be seen, that the results have only very small differences between element sizes 0.5 mm, 1 mm and 3 mm. However, considering a large element size of 10 mm, the results start to show lower stresses and deformations. Due to the small change in stresses and deformations for the three smallest element sizes, it is concluded that this FE-analysis is sufficiently accurate to verify the results of the thin plate theory results.

Table 4.10: Sensitivity analysis on the FE-analysis of the Reaction Control System tank.

Element size	Stress Max.	Stress Min.	Deformation Max.	Deformation Min.
0.5 mm	56.557MPa	0.081 MPa	0.267 mm	6.327 E-5 mm
1 mm	56.557 MPa	0.081 MPa	0.267 mm	6.327 E-5 mm
3 mm	56.188 MPa	0.579 MPa	0.263 mm	6.924 E-5 mm
10 mm	33.872 MPa	1.019 MPa	0.141 mm	2.050 E-4 mm

4.1.4. Radiative Heat Loss, Pressurant Gas Expansion and Heating

In reality, as the propellant tank is mechanically connected to surrounding structures, the temperature will find an equilibrium with the rest of the spacecraft structure. The propellant tanks of the MPS and RCS are expected to cool down due to radiative heat loss, the worst-case magnitude of this loss is checked here. For this estimate, it is assumed that the tank outer walls and the MLI remain at a constant temperature of 300 K, with uniform emissivity over the total surface area. The surface area of the MLI is assumed equal to the outer surface area tank. The heat radiated outward by the tank is assumed not to be reflected back to the tank by any other surfaces in order to assume a worst-case heat loss to be compensated for by electric heating. Furthermore due to expansion of the pressurant gas during thruster operation, a drop in pressurant gas temperature is expected. From this drop, a worst-case heating power is calculated assuming isentropic expansion of the pressurant gas over the total burn time of the system. The burn time to calculate the worst-case power required for this is calculated assuming both MPS thrusters firing at 1 N of thrust and 1 RCS thruster firing at 4 mN.

These calculations are made for both MPS and RCS and are presented in Table 4.11. Very low radiative heat loss (Order of E-2 W for MPS and RCS) and heating required due to pressurant gas expansion (order of E-1 W for the MPS and E-4 for the RCS) are observed, significantly smaller than the maximum allowed standby power consumption for the MPS of 1 W for the MPS (requirement MPS.120, Appendix A.1) and 0.5 W for the RCS (requirement RCS.120, Appendix A.2). For the RCS, the maximum thrust level was assumed as constant thrust in order to arrive at a conservative heating power required. Approximations made using relations presented in Section 2.8.5.

Table 4.11: Results for approximate heating required for MPS and RCS.

Parameter	MPS	RCS
Outer surface area tank	1.287 E-1 m ²	3.222 E-2 m ²
Outer wall temperature	300 K	300 K
MLI layers	40	40
Emissivity ε	0.001	0.001
Radiative heat loss	5.913 E-2 W	1.480 E-2 W
MLI mass	72.299 g	18.093 g
Constant tank temperature	300 K	300 K
BOL tank pressure	3.725 bar	1.000 bar
EOL tank pressure	1.293 bar	0.274 bar
Worst-case EOL pressurant gas temperature	189.124 K	207.242 K
Pressurant gas mass (Nitrogen)	2.080 E-3 kg	8.200 E-5 kg
Heating energy required	301.213 J	5.650 J
Thrust level	1.0 N	4 mN
Total mass flow	8.828 E-4 kg-s ⁻¹	4.079 E-6 kg-s ⁻¹
Total propellant mass	2.476 kg	0.193 kg
Burn time	2804.486 s	47,317.086 s
Heating power required	0.107 W	1.194 E-4 W

4.2. Pump-PFCD-Thruster-Regulator System for MPS

A micro-gear pump by Flightworks, Inc. is selected from the 43 models listed in Appendix C. In order to select the most feasible pump, two factors are of importance: first of all, the pump must be able to provide a sufficient pressure differential in order to achieve the desired thrust level. Secondly, the pump must be able to provide a sufficient flow rate in order to feed the thrusters and to achieve the desired pressure differential over the PFCD of a given length.

In the concept design stage, the pump model 2212-M04C49 was selected, due to being able to provide the highest pressure differential possible, and thereby able to achieve the maximum possible thrust level at BOL. At that stage, the flow rate (max. achievable flow rate at max. differential pressure: $95 \text{ ml}\cdot\text{min}^{-1}$) was considered sufficient as it was above the required thruster flow rate of $42.84 \text{ ml}\cdot\text{min}^{-1}$ for two thrusters firing at 1 N (Table 3.12). The flow rate requirement in order to generate sufficient pressure drop over the PFCD of a given length to achieve the desired pump pressure differential was not considered yet, and the PFCD design resulted in an orifice length of 100 mm and an orifice diameter of 0.265 mm (Table 3.14). As this orifice length is quite significant considering the dimensions of the spacecraft bus, this pump is not deemed feasible for the detailed design.

In this section, first, three thrust levels are considered: minimum, medium (exactly half way between minimum and maximum) and maximum are considered to present the required pump pressure differential and flow rates for the thrusters. Secondly, the attainable pressure drop over the PFCD is presented for various orifice lengths. Thirdly, the pump requirements are presented, a shortlist of pumps is assembled based on attainable pressure differential, infeasible pumps are eliminated using the pump requirements, and finally the lightest option of the remaining pumps is taken. Fourthly, the operating points of the selected pump are presented for BOL and EOL tank pressure, and for thruster valve position. Fifth and finally, a custom regulator valve design is presented in order to comply with the throttling requirement PROP.052 (Appendix A.1).

4.2.1. Thrust Level

As per requirement PROP.050 and PROP.053 (Appendix A.1), the thrust level of each of the two thrusters must be between 100 mN and 1000 mN. The thrust range of the selected MPS thruster, namely the ECAPS HPGP 1N, lies between 250 mN and 1000 mN and therefore its entire thrust range is compliant with the requirements. In order to select the thrust level, three values are presented: minimum, medium (halfway between minimum and maximum) and maximum, shown in Table 4.16, where the total flow rate required by the thrusters and the required pump pressure differential are additionally expressed in the units handled in the datasheets supplied by Flightworks, Inc., namely psid for pressure and $\text{ml}\cdot\text{min}^{-1}$ for volumetric flow rate. From Appendix C it is observed that pumps exist complying with the required inlet pressure and flow rate for each of these thrust levels.

Table 4.12: Thrust level options for the Main Propulsion System.

Parameter	Minimum	Medium	Maximum
Thrust level	0.250 N	0.625 N	1.000 N
Inlet pressure	5.500 bar	13.750 bar	22.000 bar
Required pump Δp	4.759 bar	13.009 bar	21.259 bar
Required pump Δp	69.023 psid	188.680 psid	308.336 psid
Mass flow 1 thruster	$1.104\text{E-}4 \text{ kg}\cdot\text{s}^{-1}$	$2.759\text{E-}4 \text{ kg}\cdot\text{s}^{-1}$	$4.414\text{E-}4 \text{ kg}\cdot\text{s}^{-1}$
Volumetric flow rate 2 thrusters	$10.710 \text{ ml}\cdot\text{min}^{-1}$	$26.775 \text{ ml}\cdot\text{min}^{-1}$	$42.840 \text{ ml}\cdot\text{min}^{-1}$

4.2.2. Passive Flow Control Device Dimensioning Considerations

In order to set the working point of the pump, a PFCD is used, which furthermore enables the pump to spool up close to its operating point without expelling any propellant at low and possibly insufficient thruster pressure. This is discussed in Section 2.7. The PFCD requires a flow rate to cause a pressure drop over its length, illustrated by Figure 4.8. Here, the volumetric flow rate through the PFCD is displayed on the x-axis and achievable pressure drop is displayed on the y-axis, for the three different thrust levels as presented in Table 4.16. Here, ideal flow is assumed with no losses outside the PFCD.

The first plot shows the pressure drop over the PFCD for a PFCD inlet pressure of 5.5 bar, here it is seen that for short orifice lengths a higher flow rate is required; a higher flow rate means a higher flow velocity which in turn increases the pressure drop. If at any point in the PFCD the pressure is below zero, no result is recorded. This may happen if the friction pressure loss is greater than the pressure after the contraction. A jump is seen in the data: this occurs at the point where the Reynolds number surpasses 2100 and the Blasius relation is used instead of the Hagen-Poiseuille relation. In reality, the transition that occurs around this Reynolds number is smooth, and not accounted for well by the equations. The jump shown here is merely a result of the mathematical relations used. The Reynolds number and Darcy-Weissbach friction factor are presented in Figure 4.9. The results corresponding to Reynolds numbers around 2100 should be treated with caution as some inaccuracies are present. An orifice diameter of 500 μm is preliminarily chosen. A large orifice length is observed to be required to limit the required flow rate. It is observed that for the minimum thrust level with thruster inlet pressure of 5.5 bar, the maximum achievable pressure drop for an orifice length of 100 mm is lower as compared to other orifice lengths. This is caused by a jump being present in the friction factor calculated for $Re > 2100$, and the resulting approximated pressure drop exceeding the thruster pressure. Subsequently, the static pressure (theoretically, ignoring vaporisation of the working fluid) reaches zero at some point inside the PFCD orifice, making the solution invalid. This is discussed further in Section 2.5.2. This jump is furthermore seen in Figure 4.9 at a volumetric flow rate of roughly $115 \text{ ml}\cdot\text{min}^{-1}$.

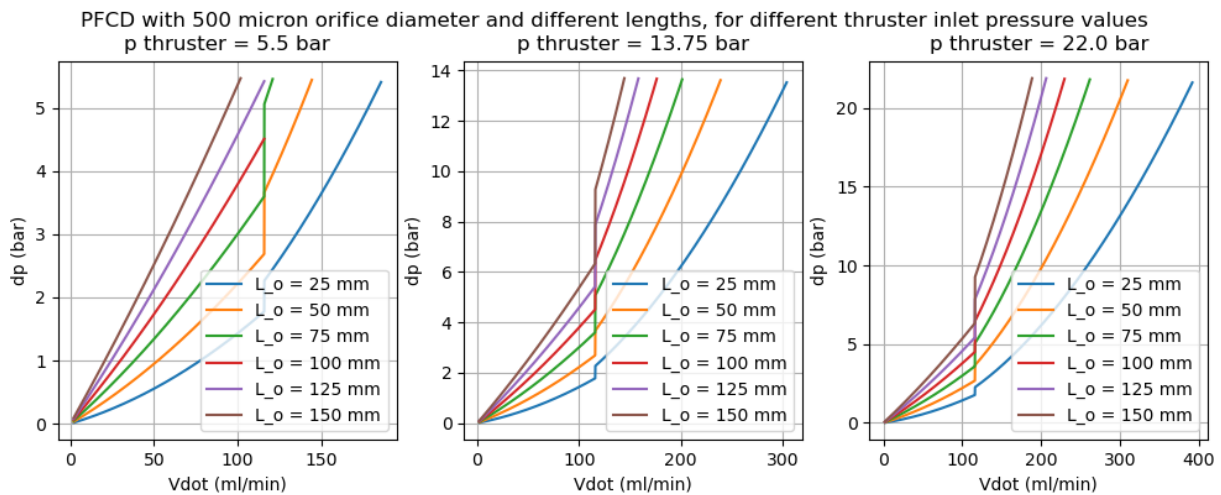


Figure 4.8: Recirculation loop pressure drop as function of volumetric flow rate for different thruster pressure values, Python/Matplotlib.

4.2.3. Pump Requirements and Final Selection

Due to the large amount of freedom in selecting parameters for the propulsion system, choices are made to continue with the design:

- The thrust level is set as constant.
- The thrust level is chosen as the maximum possible thrust achievable with the selected pump.
- The worst case required volumetric flow rate for the pump is estimated as $200 \text{ ml}\cdot\text{min}^{-1}$ for the aforementioned medium thrust level. The maximum thrust level is at an inlet pressure of 22 bar. This is not attainable due to the low tank pressure at EOL in combination with the highest attainable pressure differential from these pumps being 17.237 bar.
- The PFCD orifice length is chosen as 50 mm in order to limit the volume and mass of the component as compared to the PFCD used in the concept design stage, utilising an orifice length of 100 mm. Figure 4.8 shows an attainable pressure differential of roughly 10 bar for a flow rate of $200 \text{ ml}\cdot\text{min}^{-1}$. To illustrate the achievable thrust at this pressure differential and an example tank EOL pressure of 1 bar, a thruster inlet pressure of 11 bar corresponding to a thrust level of 0.5 N would be attainable.

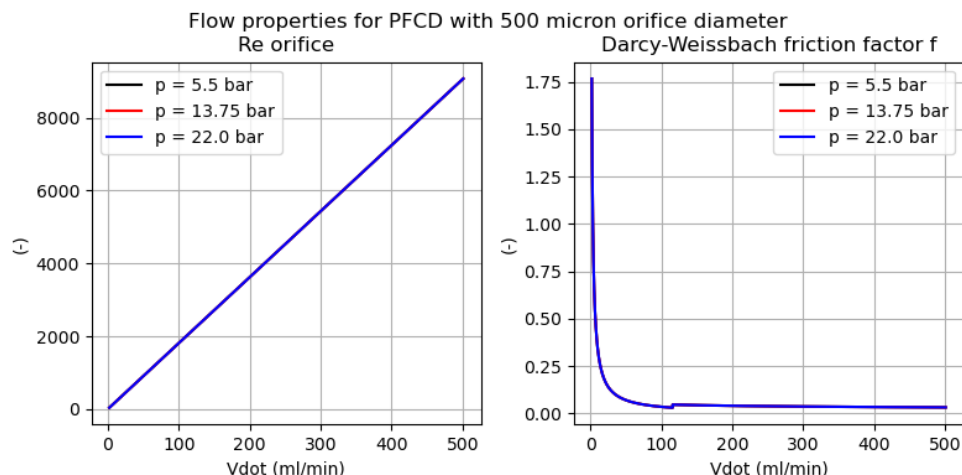


Figure 4.9: Recirculation loop Reynolds number and Darcy-Weissbach friction factor as function of volumetric flow rate for different thruster pressure values, Python/Matplotlib.

- The PFCD inlet diameter is chosen equal to the port diameter of the pump.
- The PFCD orifice diameter is preliminarily set at 500 μm . In reality, at a certain flow cross-sectional area, capillary action may occur, analysis of this is however left out of scope and it is not assumed to happen at this orifice diameter.
- Throttling of the thrusters occurs by keeping the total thruster mass flow constant, increasing the mass flow to one thruster and decreasing the mass flow to the other thruster. This facilitates the mitigation of torques caused by misalignment.

A shortlist of five pumps able to provide the highest pressure differential for flow rates below 500 ml/min is presented in Table 4.13. For increasing pressure differential, the flow rate decreases. The highest differential pressure at highest rotational velocity is chosen for reference. For these pumps a very similar mass is observed. Even for the lowest thrust level with thruster inlet pressure of 5.5 bar, still a volumetric flow rate of around 100-150 ml through the PFCD is required (Figure 4.8). Pump models 2212-M04C10.C12.C15, 2212-M04C49.C50.C51 and 2212-M04X05.X06.X07 are not considered due to a very low flow rate resulting in requiring a very large PFCD orifice length. Finally, the pump with model designation 2222-M04C58.C59.C60 is selected due to its mass being lower than that of model 2222-M04X10.X11, and having an acceptable flow rate. Its mass is furthermore not significantly higher than that of other shortlisted pumps (show also some pumps that comply with lowest thrust setting). During the concept phase, a much higher thrust level was achieved due to higher EOL tank pressure and a higher achievable PFCD pressure drop using an orifice diameter below 500 micron. The pumps listed in Appendix C include pumps with higher pressure differentials than those in Table 4.13, however they provide a much lower flow rate ($95 \text{ ml}\cdot\text{min}^{-1}$) at max. Δp , which would be insufficient for any of the proposed PFCD for the 13.8 bar and 22.0 bar thruster pressure plots presented in Figure 4.8.

Table 4.13: Shortlist of pumps, data for highest rotational velocity, highest pressure differential attainable. Selected pump marked in **bold**. Infeasible pumps marked in *italics*. From Appendix C.

Model	Max. Flow rate at max. Δp	Δp	Mass
<i>2212-M04C10.C12.C15</i>	<i>20 ml·min⁻¹</i>	<i>13.790 bar</i>	<i>140 g</i>
<i>2212-M04C49.C50.C51</i>	<i>95 ml·min⁻¹</i>	<i>17.237 bar</i>	<i>175 g</i>
<i>2212-M04X05.X06.X07</i>	<i>120 ml·min⁻¹</i>	<i>12.411 bar</i>	<i>160 g</i>
2222-M04C58.C59.C60	270 ml·min⁻¹	12.066 bar	150 g
2222-M04X10.X11	350 ml·min ⁻¹	12.066 bar	190 g

4.2.4. Pump-PFCD-Thruster Working Points

It has to be considered that during the TVC condition, the total mass flow being transported by the pump decreases, while the generated differential pressure increases. As the differential pressure the pump is able to supply is limited, some margin for nominal thrust is required. Furthermore, as requirement PROP.052 (Appendix A.1) states that each thruster shall be throttled by $\pm 10\%$ of nominal thrust, it is decided that the system provides a high-pressure end pressure corresponding to that of maximum thrust (110% of nominal thrust) plus some assumed pressure drop margin, to be regulated down by a pressure regulator valve to achieve nominal thrust. Ideally, this provides a fixed inlet pressure and therefore fixed mass flow in each thruster. For throttling to correct for misalignment effects by a given % of nominal thrust, the inlet pressure of one thruster is increased by half that percentage, for the other thruster it is decreased by half that percentage.

Given that the selected pump provides a maximum pressure differential of 12.066 bar (Table 4.13) and the tank EOL pressure is 0.741 bar (Table 4.4), a theoretical thruster inlet pressure of 12.807 bar results, ignoring any flow losses. This inlet pressure corresponds to a maximum thrust (nominal + 10%) of 0.582 N, or nominal thrust of 0.53 N. Subsequently it must be considered that for the TVC situation where the differential pressure at a fixed rotational velocity of the pump increases, and that pressure losses will occur in the feed system. Therefore, a nominal thrust level of **0.45 N** is selected, to provide sufficient margins for operation. The working points of the system are presented in Figure 4.10. Here it is observed, that a significantly higher differential pressure results inside the pump-PFCD system at TVC condition, therefore the margins are justified. The pressure at all PFCD stations is presented in Figure 4.11. The calculation data is presented in Table 4.14. Finally, it is observed that at BOL, a significantly higher cavitation constant results with the experimental result of 8.657 (Table 2.8). At EOL however, much lower $NPSH_a$ is observed at a higher rotational velocity, causing a comparably very low value of this constant. This indicates that at this condition, the pump operates closer to risk of cavitation as compared to the test. However, it must be noted that nothing with respect to cavitation was mentioned during the tests described by Besnard et al. in 2019 [55], therefore it cannot be concluded with certainty whether cavitation will occur. One other observation is that the $NPSH_a$ value at EOL calculated here is slightly higher to that of the larger pump during test 4. However, no rotational velocity was provided with that test, therefore no cavitation constant could be calculated for that situation. It is concluded, that cavitation may be expected for pump operation due to the comparatively low cavitation constant, therefore testing of the pumps is required in order to determine the cavitation characteristics in combination with propellant LMP-103s at the selected working points and tank pressure values.

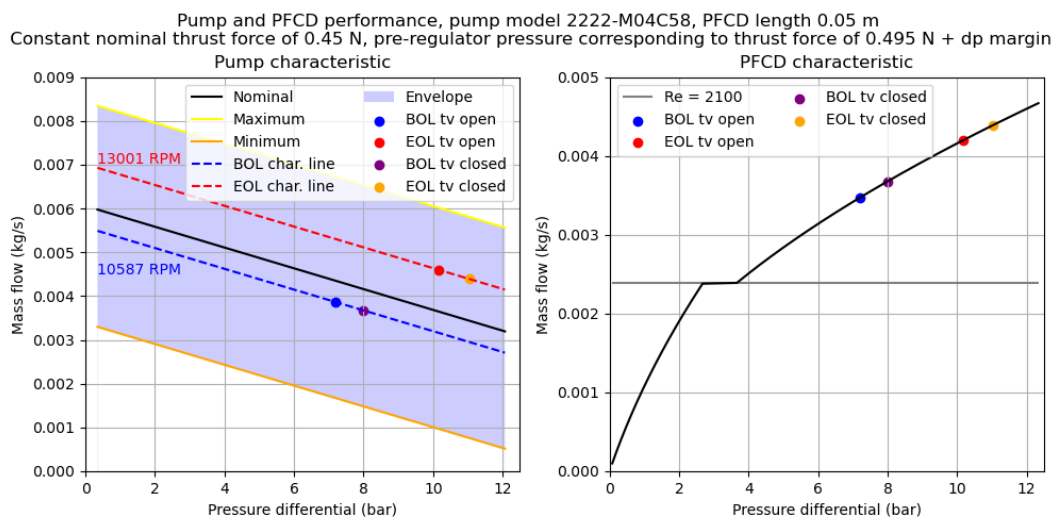


Figure 4.10: Pump-PFCD operating point for a constant thrust force of 0.5 N, Python/Matplotlib.

¹Total mass flow (for 2 thrusters)

²Numpy minimisation function in Python

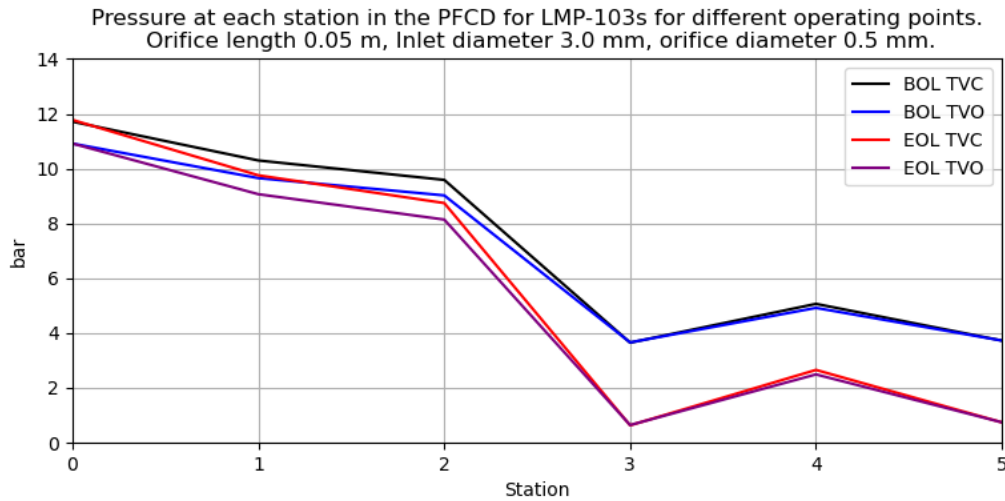


Figure 4.11: PFCD pressure at all stations for a constant thrust force of 0.5 N, Python/Matplotlib.

Table 4.14: Pump-PFCD-Thruster system at BOL, EOL conditions for TVC and TVO conditions.

Parameter	BOL TVO	BOL TVC	EOL TVO	EOL TVC
Nominal thrust level	0.450 N	0.000 N	0.450 N	0.000 N
Thruster pressure	9.900 bar	0.000 bar	9.900 bar	0.000 bar
Thruster mass flow ¹	3.973 E-4 kg·s ⁻¹	0.000 kg·s ⁻¹	3.973E-4 kg·s ⁻¹	0.000 kg·s ⁻¹
ω pump	10,587.209 min ⁻¹	10,589.209 min ⁻¹	13,001.382 min ⁻¹	13,001.382 min ⁻¹
Tank pressure	3.725 bar	3.725 bar	3.725 bar	3.725 bar
High pressure	10.914 bar	11.713 bar	10.914 bar	11.777 bar
Δp_{pump}	7.189 bar	7.988 bar	10.173 bar	11.036 bar
Δp_{PFCD}	7.189 bar	7.988 bar	10.173 bar	11.036 bar
m_{pump}	3.866 E-3 kg·s ⁻¹	3.676 E-3 kg·s ⁻¹	4.597 E-3 kg·s ⁻¹	4.392 E-3 kg·s ⁻¹
m_{PFCD}	3.467 E-3 kg·s ⁻¹	3.676 E-3 kg·s ⁻¹	4.200 E-3 kg·s ⁻¹	4.392 E-3 kg·s ⁻¹
Solver used	fmin ²	line search	fmin	line search
Solver mismatch	5.260 E-4 Pa	0.846 Pa	6.400 E-5 Pa	3.426 Pa
$P_{h,pump}$	2.375 W	2.247 W	3.920 W	3.782 W
$NPSH_a$	29.498 m	29.498 m	4.890 m	4.890 m
Cavitation constant C_{ca}	15.56	15.56	1.71	1.71

4.2.5. Throttling

As per requirement PROP.052 (Appendix A.1), the thrust of each thruster is required to be able to be throttled by +/-10% from nominal thrust. This can be achieved by the use of a regulator valve to regulate pressure, assuming specific impulse of the thruster stays constant and thrust force is proportional to thruster inlet mass flow. The inlet mass flow in turn is proportional to thruster chamber pressure as observed in Equation 2.9. Assuming that chamber pressure is proportional to inlet pressure (with unknown pressure drop over the catalyst bed and the inlet port), the thrust force is therefore assumed to be proportional to thruster inlet pressure. Furthermore, because changing the total thruster mass flow would mean a change in the operating point of the pump, and the rationale behind the throttling requirement is to compensate for misalignment of thrusters, it is decided to keep the total thruster mass flow constant by throttling one thruster up and the other thruster down by the same percentage.

As thruster mass flow is low (in the order of 2.200 E-4 kg·s⁻¹ per thruster assuming a thrust level of 0.5 N) and the found commercially available regulator valves such as the Valcor pressure regulator (Table 2.14) are dimensioned for much larger mass flows and higher pressures, and finally are characterised by high mass, it is decided to assume a custom designed valve can be used. This valve is modeled after the MEMS Pressure Regulator Module by GOMSpace/NanoSpace AB. It is realised that

this valve was designed for Xenon gas applications and for a very low MEOP of just 2 bar, however due to the lack of suitable options, these properties are left out of scope, to arrive at a mass and volume estimate of such a component. The maximum specified mass flow through the valve is $50 \mu\text{g}\cdot\text{s}^{-1}$ of Xenon gas.

As a larger mass flow rate through the valve must be accommodated for fluids with different densities, the mass flow equation $m = \rho v A$ is rearranged:

$$\frac{A_{new}}{A_{old}} = \frac{m_{new}\rho_{old}}{\rho_{new}m_{old}} \quad (4.1)$$

where the subscript *new* corresponds to the upscaled version and *old* to the original scale of the valve. Calculations are shown in Table 4.15, resulting in a required upscaling of the flow cross-sectional area by a factor of 30.650. To keep the valve design simple, two dimensions of the valve are simply scaled up by a factor equal to the square root of this area ratio, namely 5.536, then the final dimensions are rounded up. A final mass of 11.995 g results for the custom regulator valve. For this valve, it is assumed that it can withstand the maximum pressure observed in the system of 10.914 bar, and regulate the TVO pressure of 10.914 bar (pressure corresponding to nominal thrust +10%) down to 9.900 bar for nominal thrust and 8.910 bar for -10% thrust (Table 4.16).

Table 4.15: Custom regulator valve design.

Parameter	Value
Original regulator mass flow rate	5.000 E-8 kg·s ⁻¹
Required mass flow rate	2.200 E-4 kg·s ⁻¹
Density of Xenon (300 K, 2 bar) ³	10.527 kg·m ⁻³
Density of LMP-103s (300 K, assumed incompressible)	1,236.520 kg·m ⁻³
Flow area ratio	37.460
Scale factor for two outer dimensions	6.120
Original valve outer dimensions	20 x 7 x 1.2 mm
Upscaled valve outer dimensions	20 x 43 x 7 mm
Material volume upscaled	6.293 E-6 m ³
Assumed material density ⁴	2,329.600 kg·m ⁻³
Material mass upscaled	14.661 g

Table 4.16: Operating conditions for one thruster.

Thrust level	Thrust force	Pressure before regulator	Pressure after regulator
Nominal	0.450 N	10.914 bar	9.900 bar
+10%	0.495 N	10.914 bar	10.914 bar
-10%	0.450 N	10.914 bar	8.910 bar

³Calculated using the ideal gas law, using a molar mass for Xe of 131.293 g·mol⁻¹ [49]

⁴Taken for Silicon, from Pubchem/NLM [124]

4.3. COTS Component Selection, Integration and Digital Mockup

This Section serves to discuss the custom designed components and chosen COTS components. The components are first discussed for the MPS, subsequently for the RCS. For each component, a simple Digital Mockup (DMU) is created, to use in the final full system DMU. Not all dimensions may be presented for a component, therefore some dimensions may be assumed. The purpose of all DMUs presented here is to achieve a preliminary layout of the complete propulsion system and to determine the required line lengths, bends and T-junctions in order to approximate the pressure loss for this preliminary propulsion system layout. The spacecraft bus including a black box representation of the 3x1 U payload is presented in Figure 4.12. It is modeled after the CubeSat standard for a 12U bus, shown in Appendix D.

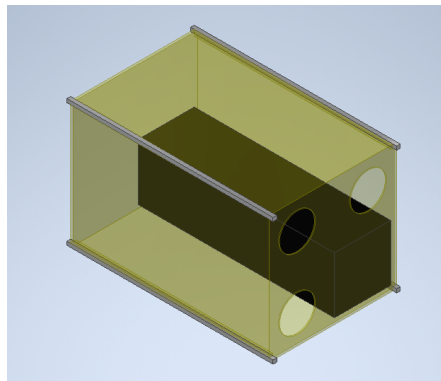


Figure 4.12: Spacecraft bus including "black box" payload, Inventor 2022.

4.3.1. Main Propulsion System Components

Fill/Drain Valve

As FDV, the Omnidea Hydrazine FDV is selected, as for the VACCO FDV, no material compatibility was found with LMP-103s due to the Tungsten Carbide ball used. Furthermore, the Arianespace FDV series require a separate valve for each filling/draining purpose. For this component, dimensions were not clearly indicated. The outer dimensions were taken as provided by Omnidea in the datasheet [105], all other dimensions were assumed. The DMU is shown in Figure 4.13a.

Pressure Transducer

The GP:50 Miniature Pressure transducer 7000 is selected due to its low mass. Due to requirement ECSS.140 (Appendix A.4), a solution for a redundant setup is needed. A simple block is created to connect the components to a flow tube with 3 mm inner diameter, measuring 20x20x10 mm, resulting in a material volume of 3.859 E-6 m^3 , using Ti-6Al-4V this results in a mass of 17 g. The DMU is shown in Figure 4.13b.

Thermocouple

The selected thermocouple is the RS Pro K-type thermocouple (Table 2.20). Its mass and dimensions are unknown, and integration in the DMU is left out of scope. Two small ports will be required to be made into the tank wall, one for each thermocouple, and the probes must be in contact with the fluid, e.g. connected to the sponge PMD.

Latch Valve

The 1/4" Low Pressure Miniature Latch Valve V1E10728-01 by VACCO was selected due to being the lightest suitable option. This component includes a 40 μm etched disk filter at the inlet, eliminating the need for a separate filter. For this component, no dimensions are assumed as all are provided in the datasheet published by VACCO [103]. The DMU is shown in Figure 4.13c.

Pump

As discussed in Section 4.2, the Flightworks, Inc. model 2222M04C58 pump was selected. Its dimensions are provided by Flightworks, Inc. [56] and are 79.9 mm length, 22 mm diameter and 3 mm inlet/outlet ports of 10 mm length. The DMU is shown in Figure 4.14a.

Passive Flow Control Device

As discussed in the Section 4.2, the chosen orifice length is 500 mm and the inlet diameter is equal to the pump port diameter of 3 mm. The orifice diameter is set as 500 μm . Using 5 mm of inlet and outlet port lengths, this results in a total length of 60 mm. The wall thickness is chosen as 7 mm, therefore the final dimensions of the PFCD are 60 x 7 x 7 mm. The material volume is 2.860 E-6 m^3 and the chosen material is Ti-6Al-4V for material compatibility, resulting in a mass of 13 g. The DMU is shown in Figure 4.14b.

Regulator Valve

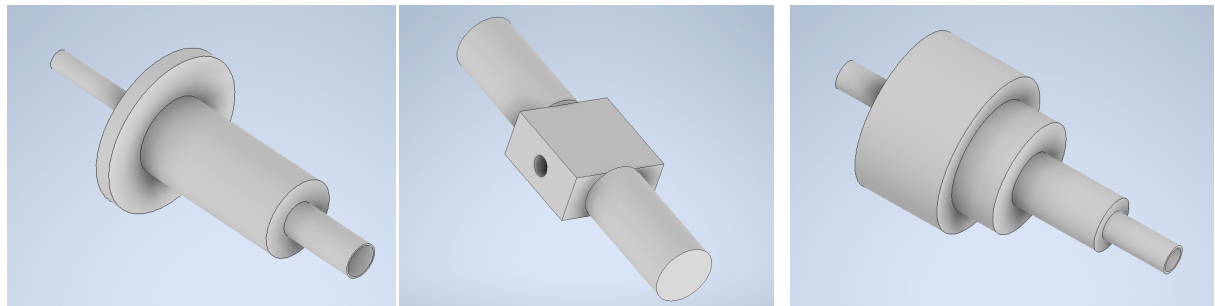
The regulator valve design is discussed in Section 4.2 and the DMU is shown in Figure 4.14c.

Thruster

The only provided thruster dimension is the length - 178 mm as presented by Persson et al. in 2012 [41]. All other dimensions are assumed. The DMU is shown in Figure 4.15a.

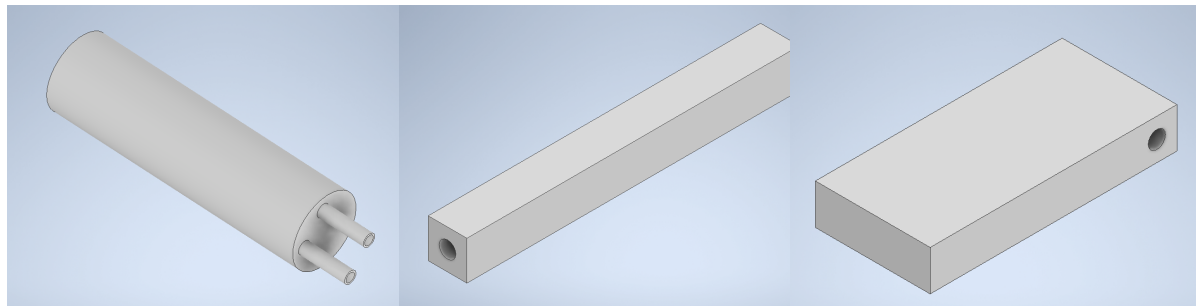
Tank and Propellant Management Devices

The design of the tank and PMDs is discussed in Section 4.1. The DMU is shown in Figure 4.15b. A separate view of the PMDs is provided in Figure 4.15c.



(a) Fill/Drain valve for the Main Propulsion System. (b) Two connected pressure Transducers for the Main Propulsion System. (c) Latch valve for the Main Propulsion System.

Figure 4.13: Digital Mockups of Main Propulsion System Components, 1, Inventor 2022.



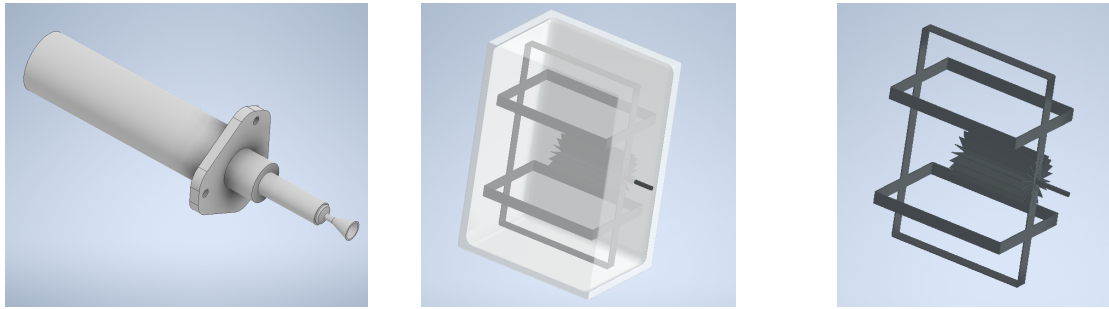
(a) Flightworks, Inc. 2222M04C58 pump for the Main Propulsion System. (b) Passive Flow Control Device for the Main Propulsion System. (c) Custom designed regulator valve for the Main Propulsion System.

Figure 4.14: Digital Mockups of Main Propulsion System Components, 2, Inventor 2022.

4.3.2. Reaction Control System Components

Fill/Drain Valve

The selected FDV is the VACCO Fill/Drain Valve Table 2.18, due to the lowest mass option and its material compatibility with water. The Arianespace valves require two separate valves for fill/drain operations, resulting in higher total mass and are therefore undesirable. The length of 103.759 mm and diameter of the triangular mounting plate of 47.498 mm are used, all other dimensions are assumed. The hind tube is shortened here in order to be able to fit the volume. The DMU is presented in Figure 4.16a.



(a) ECAPS HPGP 1N Thruster for the Main Propulsion System. (b) Tank for the Main Propulsion System. (c) Propellant Management Devices for the Main Propulsion System.

Figure 4.15: Digital Mockups of Main Propulsion System Components, 3, Inventor 2022.

Filter

The selected filter is based on the VACCO model F1D10807-02 filter (Table 2.19), customised for use in the RCS. Due to the very low flow rate in the RCS with only one thruster firing (max. $4.079 \text{ E-6 kg-s}^{-1}$), the model by VACCO is too large. Due to lack of smaller options, a custom model is made, shown in Figure 4.16b with protruding inlet and outlet ports. An inlet diameter of 1 mm is chosen, using the area ratio from the original filter with an inlet diameter of 6.35 mm and a maximum diameter of 14 mm, the maximum diameter results in 4.86 mm, rounded up to 5 mm. The length is arbitrarily set at twice the maximum diameter, namely 10 mm. Assuming a wall thickness of 1 mm throughout for the cylindrical centre part, the mass of the cylindrical part is 0.870 g, rounded up to 1 g.

Pressure Transducer

This component is identical to the one used in the MPS, however with TBD inner diameter. The DMU is presented in Figure 4.17a.

Thermocouple

The selected thermocouple is the RS Pro K-type thermocouple (Table 2.20). Its mass and dimensions are unknown, and integration in the DMU is left out of scope. Two small ports will be required to be made into the tank wall, one for each thermocouple, and the probes must be in contact with the fluid, e.g. connected to the sponge PMD.

Latch Valve

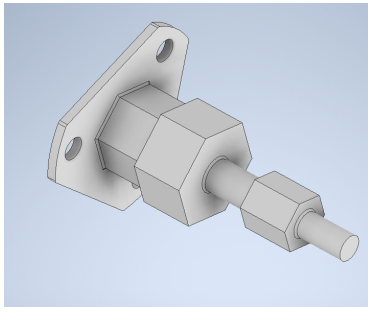
The selected latch valve is the Moog Latching Valve (Table 2.17), it is important to note that no compatibility with water was noted, however it is assumed that this component is indicative of the mass and volume required for fulfilling latch valve functionality for the RCS. The dimensions are 10 x 10 x 10 mm. The DMU is presented in Figure 4.17b.

Thrusters

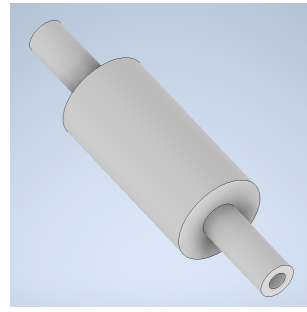
The selected thrusters are the Aurora ARO thrusters, which according to the datasheet measure 20 x 20 x 20 mm in their smallest configuration [90]. The DMU is shown in Figure 4.18a.

Tank and Propellant Management Devices

The tank and PMD design is presented in Section 4.1. The DMU is presented in Figure 4.18b. A separate view of the PMDs is presented in Figure 4.18c.

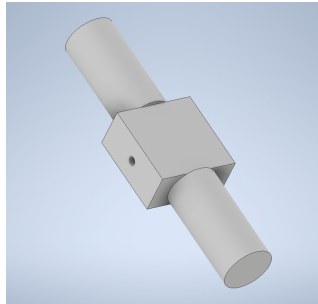


(a) Fill/drain valve for the Reaction Control System.

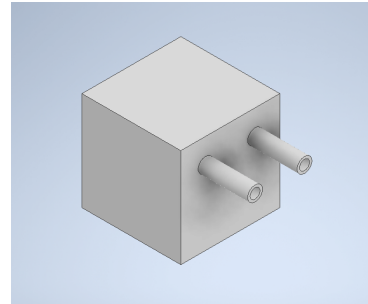


(b) Filter for the Reaction Control System

Figure 4.16: Digital Mockups of Reaction Control System Components, 1, Inventor 2022.

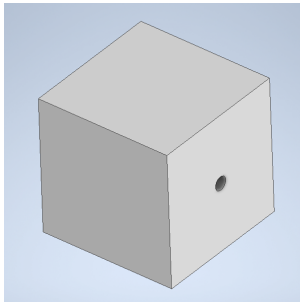


(a) Two connected pressure transducers for the Reaction Control System.

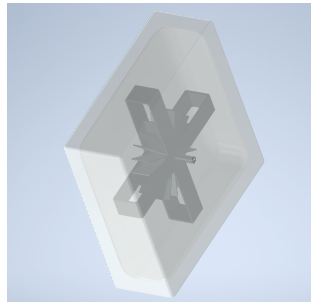


(b) Latch valve for the Reaction Control System.

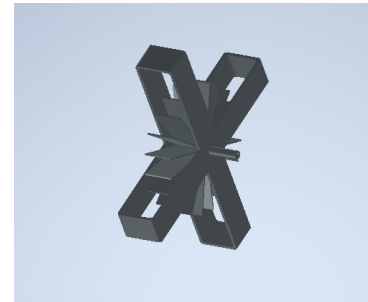
Figure 4.17: Digital Mockups of Reaction Control System Components, 2, Inventor 2022.



(a) Aurora ARO thruster for the Reaction Control System.



(b) Tank including Propellant Management Devices for the Reaction Control System.



(c) Propellant Management Devices for the Reaction Control System

Figure 4.18: Digital Mockups of Reaction Control System Components, 3, Inventor 2022.

4.3.3. Integration into Spacecraft Bus

The complete system is integrated into the spacecraft bus and interconnected using feed lines. The feed line diameter for the RCS here is purely for illustration, the inner diameter is TBD. The DMU of the complete integrated system is presented in Figure 4.19. The MPS alone is presented in Figure 4.20a and Figure 4.20b, the RCS alone is presented in Figure 4.21a and Figure 4.21b.

In this layout, the MPS thrusters have been placed in two of the three available mounting volumes at the rear end of the spacecraft, diagonally opposed as to not cause a torque over the pitch or yaw axes of the spacecraft. The MPS thrusters occupy the full available length of the additional "tuna can" volume. The free corner is occupied by the RCS, here the thrusters are placed at the far end of the tuna can volume. Some implications of this layout must be addressed: first of all, the MPS propellant tank and MPS thrusters are very far apart, with a significant amount of space being occupied by feed lines and other components. Integration of other spacecraft subsystems may require a different feed line layout to accommodate for these subsystems.

For the integration, three important notes must be made. The first is, that all components have been placed such that as little space in the bus-length direction is occupied as possible, while getting as little feed line bends as possible. The second note is that all mounting means are left out of scope. Therefore, no brackets are shown in the DMUs. The third note is that the MLI blankets, heaters and thermocouples have been left out of the integration as the placement of these components may be driven by thermal considerations, which can only be made when the integration of all other components of the spacecraft is considered. The power and mass considerations for these components is considered however, at the end of this Chapter in the system summary.

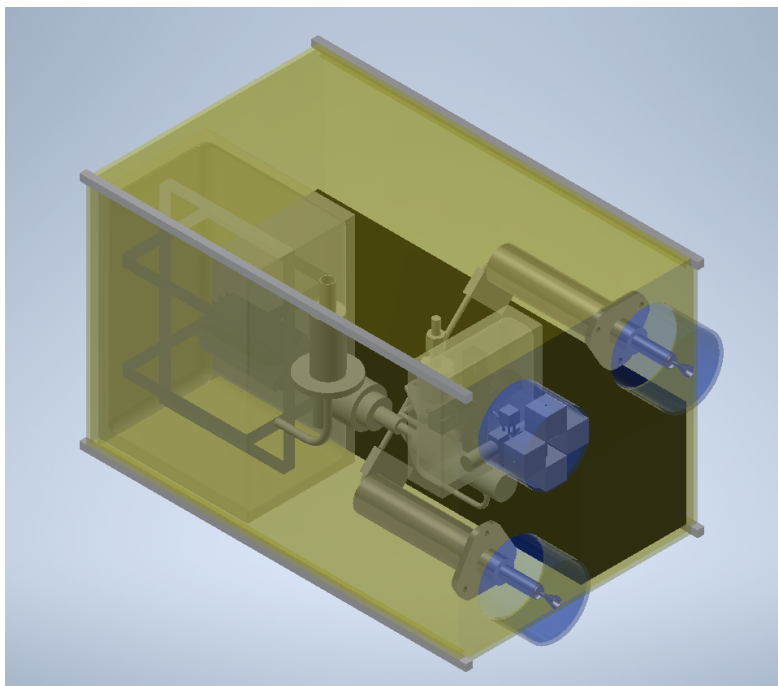
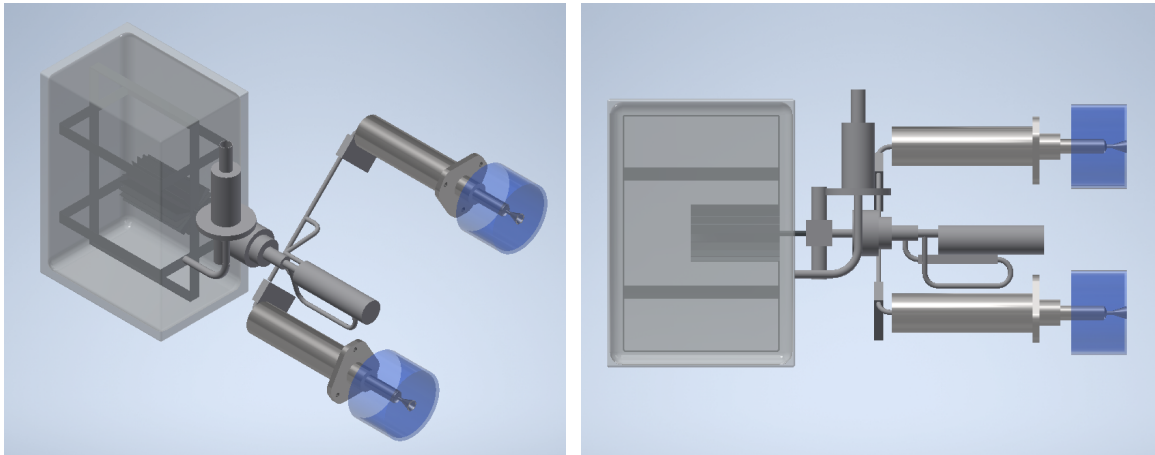


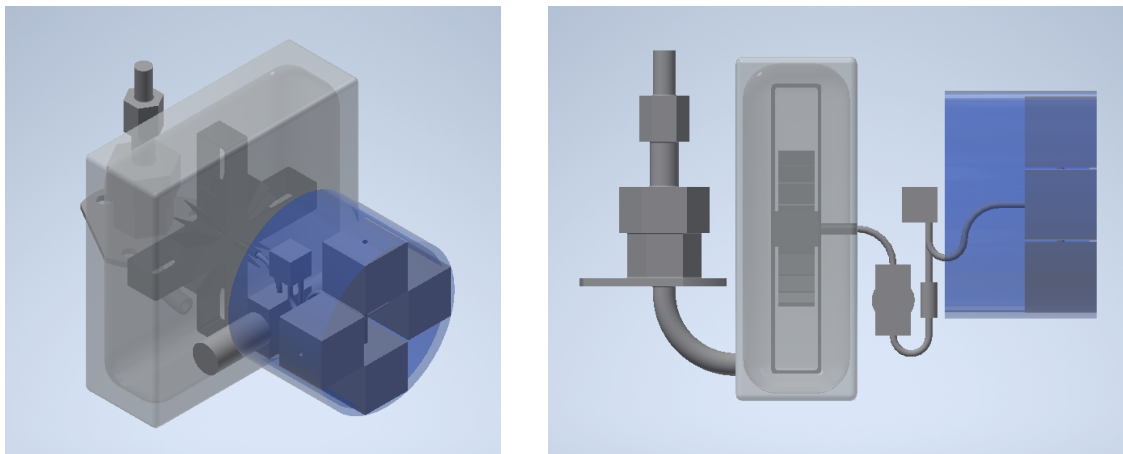
Figure 4.19: Complete propulsion system integrated into the 12U spacecraft bus, Inventor 2022.



(a) Main Propulsion System, isometric perspective.

(b) Main propulsion System, side perspective.

Figure 4.20: Main Propulsion System DMU, two views, Inventor 2022.



(a) Reaction Control System, isometric perspective.

(b) Reaction Control System, side perspective.

Figure 4.21: Reaction Control System DMU, two views, Inventor 2022.

4.4. Pressure Drop and Fluid Hammer

This section delineates the approximation of pressure drop over the feed system of the MPS and RCS, additionally the worst-case fluid hammer magnitude is approximated. The theory for this is presented in Section 2.6. In the previous section, the DMUs for the MPS and RCS were discussed, from these, the line lengths were measured in Inventor and used here to approximate the pressure loss. For the MPS, a bend radius of 10 mm was chosen, for the RCS, a bend radius of 5 mm was chosen. If "-" is noted for length, this means that the components are directly interconnected. For the T-junctions, a bend radius of 3 mm was selected for the MPS, a bend radius of 1 mm was selected for the RCS. It is assumed that no coiling effects occur during bends, i.e. all bend flow flows through the plane of the bend.

4.4.1. Main Propulsion System

The hydraulic diagram as used in the DMU including all bends and T-junctions is shown in Figure 4.22 including station numbering. The segments are described with their section length, diameter, flow velocity and resulting approximated pressure drop in Table 4.18. All calculations are made for the steady-state TVO situation at EOL at the selected constant nominal thrust level of 0.45 N with the highest PFCD mass flow as seen from Table 4.14. A graphical representation is shown in Figure 4.23.

Note that the T-junction at station 6 coincides with the pump inlet as seen in Figure 4.20b, and the flow from 5-7 flows straight through, this pressure loss is approximated using a straight segment. It is important to note, that only one thruster branch is considered here. For the flow from from tank to thruster, a constant velocity is taken, this is achieved by halving the pipe cross-sectional area after station 13. The flow exiting the PFCD is routed to the pump inlet using the T-junction at station 6. For approximating the pressure drop over the LV, Equation 2.26 is used in combination with manufacturer data as published by VACCO [103], where the lowest presented pressure drop of 0.6 psid at 0.03 GPM and the highest presented pressure drop of 4.25 psid at 0.10 GPM is used considering water propellant. Converted to metric units, this corresponds to a friction loss factor K of 2324.373 for the minimum flow rate and K of 1481.786 for the maximum flow rate. In order to arrive at a simple estimate, the average of these values is used, namely 1903.080.

A pressure mismatch at station 6 for the tank-pump flow and station 27 for the recirculation loop-pump outflow is observed: the pressure at the exit of the recirculation loop is 0.725 bar, the pressure coming from the tank side towards the pump inlet is 0.739 bar - an error of approximately 1.894%. In reality, this is not likely to cause problems for the system functionality, as the pump-PFCD system will adjust for this slight mismatch and the pump-PFCD working point will change by a small amount.

Table 4.17: Required input data for pressure drop approximation for the Main Propulsion System, steady state TVO situation at EOL.

Property	Value
Thrust level	0.450 N
Mass flow 2 thrusters	3.973 E-4 kg-s ⁻¹
Pump mass flow m_{pump}	4.597 E-3 kg-s ⁻¹
PFCD mass flow m_{PFCD}	4.200 E-3 kg-s ⁻¹
Tank pressure	0.741 bar
Pump differential pressure Δp_{pump}	10.173 bar
Bend radius	10 mm
T-junction bend radius	3 mm
Pipe baseline diameter	3 mm

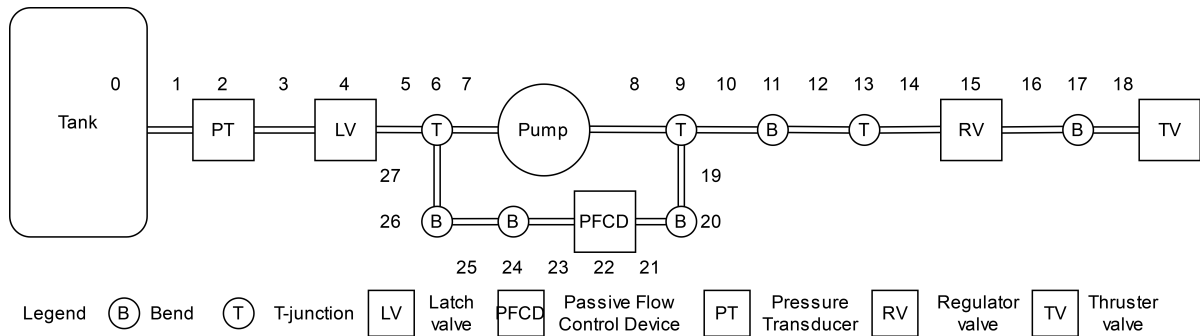


Figure 4.22: Line segments and components of the Main Propulsion System for approximating pressure drop, draw.io.

Table 4.18: Feed line segments and their pressure drop for the Main Propulsion System. Each station refers to the downstream end of the component.

Station	Description	Length	Diameter	Velocity	Pressure drop	Pressure
0	Tank	-	-	0	-	1.293 bar
1	Straight	8.610 mm	3.00 mm	0.045 m·s ⁻¹	4.030 Pa	0.741 bar
2	PT block	20 mm	3.00 mm	0.045 m·s ⁻¹	9.362 Pa	0.741 bar
3	Straight	0	3.00 mm	0.045 m·s ⁻¹	0	0.741 bar
4	Latch valve	n/a	6.35 mm	0.010 m·s ⁻¹	121.107 Pa	0.740 bar
5	Straight	0 mm	3.00 mm	0.045 m·s ⁻¹	0	0.740 bar
6	T-junction	10 mm	3.00 mm	0.548 m·s ⁻¹	56.164 Pa	0.739 bar
7	Pump inlet	0	3.00 mm	0.548 m·s ⁻¹	0	0.739 bar
				(Sub) total	190.663 Pa	-
8	Straight	25 mm	3.00 mm	0.548 m·s ⁻¹	135.409 Pa	10.911 bar
9	T-junction	4.712 mm	3.00 mm	0.045 m·s ⁻¹	2.616 Pa	10.911 bar
10	Straight	33.968 mm	3.00 mm	0.045 m·s ⁻¹	15.901 Pa	10.911 bar
11	Bend 90°	15.708 mm	3.00 mm	0.045 m·s ⁻¹	8.721 Pa	10.910 bar
12	Straight	10.000 mm	3.00 mm	0.045 m·s ⁻¹	4.681 Pa	10.910 bar
13	T-junction	4.712 mm	2.12 mm	0.045 m·s ⁻¹	4.701 Pa	10.910 bar
14	Straight	57.774 mm	2.12 mm	0.045 m·s ⁻¹	54.088 Pa	10.910 bar
15	Regulator	20.000 mm	2.12 mm	0.045 m·s ⁻¹	100,985.22	9.900 bar
16	Straight	0	2.12 mm	0.045 m·s ⁻¹	0	9.900 bar
17	Bend 90°	15.708 mm	2.12 mm	0.045 m·s ⁻¹	15.672 Pa	9.900 bar
18	Straight	0	2.12 mm	0.045 m·s ⁻¹	0	9.900 bar
				(Sub) total	101,227.009 Pa	-
9	T-junction	4.712 mm	3.00 mm	0.480 m·s ⁻¹	202.580 Pa	10.910 bar
19	Straight	10.000 mm	3.00 mm	0.480 m·s ⁻¹	49.482 Pa	10.910 bar
20	Bend 90°	15.708 mm	3.00 mm	0.480 m·s ⁻¹	161.056 Pa	10.910 bar
21	Straight	0	3.00 mm	0.480 m·s ⁻¹	0	10.910 bar
22	PFCD inlet	5.000 mm	3.00 mm	0.480 m·s ⁻¹	24.741 Pa	10.910 bar
22	PFCD orifice	50.000 mm	0.50 mm	17.298 m·s ⁻¹	1,017,259.968 Pa	0.735 bar
22	PFCD outlet	5.000 mm	3.00 mm	0.480 m·s ⁻¹	24.741 Pa	0.735 bar
23	Straight	0	3.00 mm	0.480 m·s ⁻¹	0	0.735 bar
24	Bend 180°	31.416 mm	3.00 mm	0.480 m·s ⁻¹	322.112 Pa	0.732 bar
25	Straight	45.000 mm	3.00 mm	0.480 m·s ⁻¹	222.671 Pa	0.729 bar
26	Bend 90°	15.708 mm	3.00 mm	0.480 m·s ⁻¹	322.112 Pa	0.726 bar
27	Straight	30.000 mm	3.00 mm	0.480 m·s ⁻¹	148.447 Pa	0.725 bar
6	T-junction	4.712 mm	3.00 mm	0.526 m·s ⁻¹	57.886 Pa	0.724 bar
				(Sub) total	1,018,795.796 Pa	-

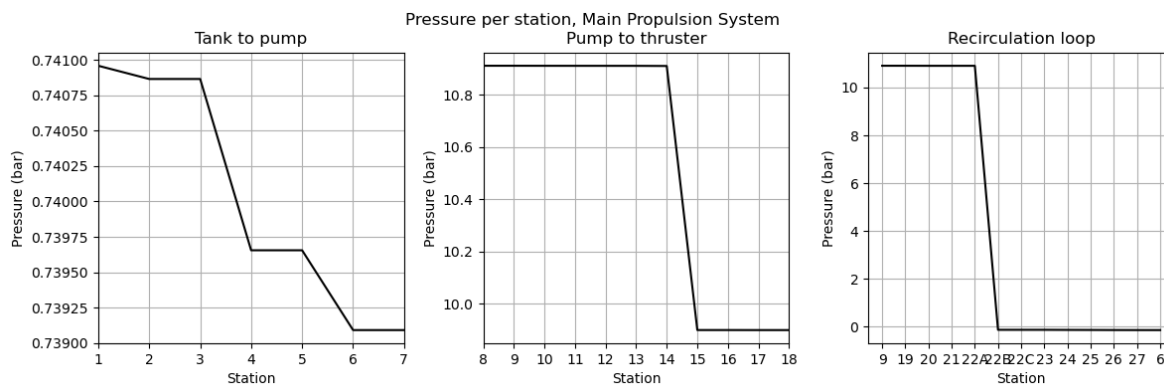


Figure 4.23: Approximated pressure per station for the Main Propulsion System, Python/Matplotlib.

Reaction Control System

A visual representation of the line segments and components in the RCS is shown in Figure 4.24. The calculations from the previous section are repeated for this case, presented in Table 4.20. The input data for these calculations are presented in Table 4.19. This data corresponds to the BOL situation, as the RCS operates in blow-down mode and at BOL the thruster pressure and therefore mass flow are at their highest. For the bend at stations 2 and 14, a radius of 10 mm is used instead of 5 mm as used everywhere else. This was a necessary choice in the DMU to allow placements of the components and leaving some space between them. Using the single datapoint for pressure drop provided by VACCO for filter model F1D10807-02 [108] (10342.1 Pa for $0.024 \text{ kg}\cdot\text{s}^{-1}$ of Hydrazine), a factor K is determined as 36.038, assumed to be valid for a preliminary approximation of pressure drop through the customised variant. For the Moog Latching Valve, the same value is assumed due to lack of information. Figure 4.25 shows the approximated pressure per station for the RCS at BOL. Due to the very low flow velocity, a very low Reynolds number results of 6.08. Taking the pipe diameter of 1 mm, in order to achieve a Dean number De of 11, a bend radius of 0.153 mm would be required, which does not occur here. Assuming that below this value of De , no helical vortices form, all bends here are simply assumed as straight flows. The total

Table 4.19: Required input data for pressure drop approximation for the Reaction Control System, steady state thruster firing at BOL.

Property	Value
Thrust level	4.000 mN
Mass flow 1 thruster	$4.079 \text{ E-6 kg}\cdot\text{s}^{-1}$
Tank pressure	1.000 bar
Pipe diameter	1.000 mm
Bend radius	5.000 mm
T-junction bend radius	1.000 mm

4.4.2. Conclusion Pressure Loss

For the MPS, in Table 4.18 the thruster valve inlet pressure is observed to be 9.900 bar (stations 17 and 18). The pressure before the regulator is 10.910 bar (at least 10.890 bar required for nominal thrust level + 10%), which has some margin above the aforementioned required 10% above 9.900 bar inlet pressure. Therefore, the pressure drop in the feed system of the MPS is considered acceptable and the pipe diameter is taken as acceptable as well. However, it was seen that a small pressure mismatch was present at station 6, namely between the branches coming from the tank and from the recirculation loop. This is as mentioned not expected to be a problem due to in reality, the pump-PFCD system adjusting its working point slightly for such situations.

For the RCS, due to very low flow velocity at the chosen pipe diameter of 1 mm, a very small pressure loss of 20.711 Pa is observed, which is negligible compared to the feed pressure of 1 bar. It must be

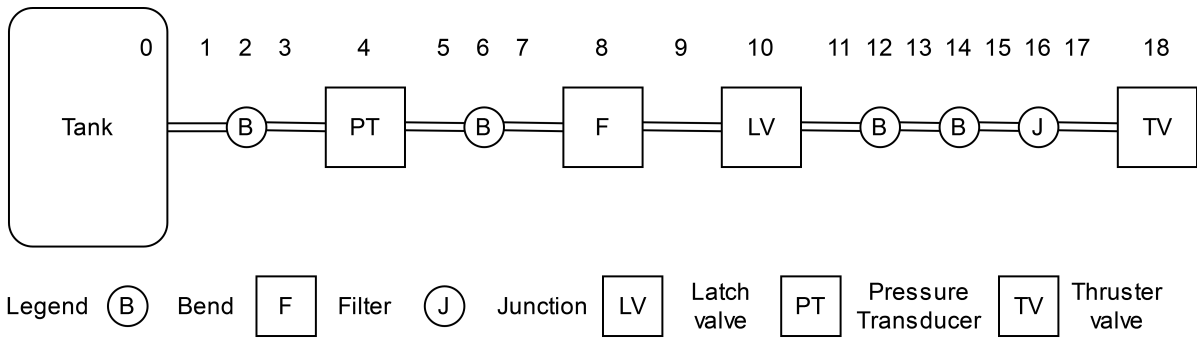


Figure 4.24: Line segments and components of the Reaction Control System for approximating pressure drop, draw.io.

Table 4.20: Feed line segments and their pressure drop for the Reaction Control System. Each station refers to the downstream end of the component.

Station	Description	Length	Diameter	Velocity	Pressure drop	Pressure
0	Tank	-	-	0	-	1.000 bar
1	Straight	0	1.000 mm	5.211 E-3 m-s ⁻¹	0	1.000 bar
2	Bend 90°	15.708 mm	1.000 mm	5.211 E-3 m-s ⁻¹	2.237 Pa	1.000 bar
3	Straight	0	1.000 mm	5.211 E-3 m-s ⁻¹	0	1.000 bar
4	PT block	20 mm	1.000 mm	5.211 E-3 m-s ⁻¹	2.848 Pa	1.000 bar
5	Straight	0	1.000 mm	5.211 E-3 m-s ⁻¹	0	1.000 bar
6	Bend 180°	15.708 mm	1.000 mm	5.211 E-3 m-s ⁻¹	2.237 Pa	1.000 bar
7	Straight	5.000 mm	1.000 mm	5.211 E-3 m-s ⁻¹	0.712 Pa	1.000 bar
8	Filter	0	1.000 mm	5.211 E-3 m-s ⁻¹	0.488 Pa	1.000 bar
9	Straight	16.750 mm	1.000 mm	5.211 E-3 m-s ⁻¹	2.385 Pa	1.000 bar
10	Latch valve	0	1.000 mm	5.211 E-3 m-s ⁻¹	0.488 Pa	1.000 bar
11	Straight	5.000 mm	1.000 mm	5.211 E-3 m-s ⁻¹	0.712 Pa	1.000 bar
12	Bend 180°	15.708 mm	1.000 mm	5.211 E-3 m-s ⁻¹	2.237 Pa	1.000 bar
13	Straight	0	1.000 mm	5.211 E-3 m-s ⁻¹	0	1.000 bar
14	Bend 90°	15.708 mm	1.000 mm	5.211 E-3 m-s ⁻¹	2.237 Pa	1.000 bar
15	Straight	17.054 mm	1.000 mm	5.211 E-3 m-s ⁻¹	2.428 Pa	1.000 bar
16	4-way junction	1.571 mm	1.000 mm	5.211 E-3 m-s ⁻¹	0.224 Pa	1.000 bar
17	Straight	10.397 mm	1.000 mm	5.211 E-3 m-s ⁻¹	1.480 Pa	1.000 bar
18	Thruster valve	0	1.000 mm	5.211 E-3 m-s ⁻¹	0	1.000 bar
				Total	20.711 Pa	-

noted however, that this pipe diameter was chosen preliminarily and was not driven by any component constraints such as for the MPS, where the pipe diameter was driven by the pump inlet and outlet port inner diameters.

4.4.3. Feed Line Mass Estimate

For creating the feed line mass estimate, all section lengths are added, for the MPS this is from Table 4.18, for the RCS, the values from Table 4.20 are taken. The mass of the junctions are simply estimated using the flow path length through them. A wall thickness of 1 mm is assumed for the MPS, for the RCS, a wall thickness of 0.5 mm is assumed. Using Ti-6Al-4V as material with an ultimate tensile strength of 1170 MPa and a material density of 4430 kg-m⁻³ (Table 2.10), a mass of 0.020 kg results for the MPS and 0.001 kg for the RCS. A maximum pressure of 11.777 bar will occur using operation for the MPS (at EOL TVC condition Table 4.14) and 1.000 bar for the RCS (Table 4.9).

4.4.4. Fluid Hammer

This subsection contains a check for the worst-case magnitude of a fluid hammer pressure surge upon valve closing using the Joukowski equation (Equation 2.34). For the MPS, the flow velocity at maxi-

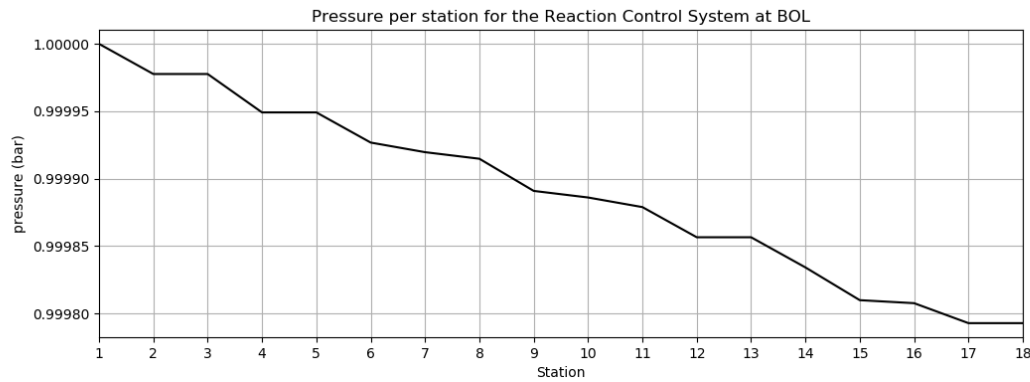


Figure 4.25: Approximated pressure per station for the Reaction Control System, Python/Matplotlib.

Table 4.21: Feed line mass estimate for the Main Propulsion System and the Reaction Control System.

Property	MPS	RCS
Total feed line length	363.448 mm	118.604
Line inner diameter	3.0 mm	1.0 mm
Line wall thickness	1.0 mm	0.5 mm
Line mass	0.020 kg	0.001 kg
Max. pressure	11.777 bar	1.000 bar
Hoop stress	1.767 MPa	0.100 MPa
Burst load factor j_{bu}	2.5	2.5
Ultimate load factor j_u	1.25	1.25
Hoop stress including load factors	5.520 MPa	0.313 MPa

imum nominal thrust is used, assuming a constant flow velocity from tank to thruster valve. Propellant properties are taken from Table 3.5 for LMP-103s for the MPS and Table 3.6 for the water propellant used in the RCS. As seen in Table 4.22, the magnitudes observed of 1.026 bar for the MPS and 0.078 bar for the RCS are insignificant compared to the static steady-state pressure values in either system.

Table 4.22: Fluid hammer calculations.

Property	MPS	RCS
Density	1,236.520 kg-m ⁻³	996.560 kg-m ⁻³
Wave celerity	1,626.930 m-s ⁻¹	1,501.500 m-s ⁻¹
Flow velocity	0.045 m-s ⁻¹	5.211 E-3 m-s ⁻¹
Surge magnitude	1.026 bar	0.078 bar

4.5. Summary of Final Designs and Requirements Compliance

The most important properties of the MPS and RCS are summarised in Table 4.23. The mass budget for the MPS is presented in Table 4.24, the mass budget for the RCS is presented in Table 4.25. The power budgets are presented in Table 4.26 and Table 4.27 for the MPS and RCS, respectively.

The requirements compliance table for the MPS is presented in the first subsection, the second subsection contains the RCS requirements compliance table.

Table 4.23: Summary of specifications of the Main Propulsion System and the Reaction Control System.

Parameter	MPS	Ref.	RCS	Ref.
Wet mass	5.563 kg	Table 4.24	0.822 kg	Table 4.25
Volume	TBD	n/a	1 U + T	n/a
Thrust level	0.450 N	Section 4.2.4	1 mN - 4 mN	Table 4.8
Number of thrusters	2	Table 4.24	4	Table 4.25
Propellant mass	2.476 kg	Table 4.24	0.193 kg	Table 4.25
Usable propellant mass	2.228 kg	EE of 0.9	0.174 kg	EE of 0.9
Δv achievable ¹	203 m-s ⁻¹	Table 4.3	n/a	n/a
I_t achievable ¹	-	-	170 N-s	Table 4.8
Thruster pre-heat power	20 W	Table 2.12	n/a	-
Thruster firing power	n/a	-	20 W	Table 4.8
Temperature (constant)	300 K	-	300 K	-
Tank heating power Valve power	0.5 W 10.779 W (opening), 1.274 W (holding)	Table 4.11 Per coil, Table 4.26.	0.012 W n/a	Table 4.11 [90]

Table 4.24: Mass budget for the Main Propulsion System.

Component	Mass	Ref.
Tank (dry) including PMDs	1.679 kg	Table 4.5
Propellant	2.476 kg	Table 4.3
Pressurant	0.004 kg	Table 4.4
Multi-layer insulation	0.073 kg	Table 4.11
Thermocouples (2)	n/a	Table 2.20
Pressure transducers (2)	0.024 kg	Table 2.20
Pressure transducer block	0.017 kg	Section 4.3.1
Fill/drain valve	0.150 kg	Table 2.18
Latch valve	0.168 kg	Table 2.17
Pump	0.150 kg	Table 4.13
PFCD	0.013 kg	Section 4.3.1
Regulator valves (2)	0.029 kg	Table 4.15
Thrusters (2)	0.760 kg	Table 2.12
Feed lines	0.020 kg	Table 4.21
Total	5.563 kg	

¹Required propellant mass calculated backwards from required Δv and I_t .

Table 4.25: Mass budget for the Reaction Control System.

Component	Mass	Ref.
Tank (dry) including PMDs	0.250 kg	Table 4.9
Propellant	0.193 kg	Table 4.8
Pressurant	0.082 kg	Table 4.9
Multi-layer insulation	0.018 kg	Table 4.11
Thermocouples (2)	n/a	Table 2.20
Pressure transducers (2)	0.024 kg	Table 2.20
Pressure transducer block	0.017 kg	Section 4.3.1
Fill/drain valve	0.113 kg	Table 2.18
Filter	0.001 kg	subsection 4.3.2
Latch valve	0.007 kg	Table 2.17
Thrusters (4)	0.116 kg	Table 2.13
Feed lines	0.001 kg	Table 4.21
Total	0.822 kg	

Table 4.26: Power budget for the Main Propulsion System.

Property	Value	Ref.
Thruster valve actuation (2 thrusters)	10.779 W (per coil)	Table 3.4
Thruster valve holding	1.274 W (per coil)	Table 3.4
Worst case pump power assuming η of 0.5	8.702 W	Table 4.14
Latch valve	n/a	[103]
Worst case tank heating	0.5 W	Table 4.23
Worst case pre-heating	20 W	Table 2.12

Table 4.27: Power budget for the Reaction Control System.

Property	Value	Ref.
Thruster valve actuation	n/a	[90]
Thruster valve holding	n/a	[90]
Latch valve actuation	n/a	[102]
Firing power	5 - 20 W	Table 4.8
Worst case tank heating	0.012 W	Table 4.23

4.5.1. Requirements Compliance of the Main Propulsion System

The tables containing the requirements for the MPS are Table 4.28, Table 4.29 and Table 4.30, additional verification required is described by "A" = Analysis, "I" = Inspection and/or "T" = Testing.

Table 4.28: Requirements compliance check for the MPS. Y = Yes, N = No, TBD = To Be Determined. Requirements PROP.010 - PROP.080.

ID	Text	Compliance	Remarks	Verification
PROP.010	The propulsion system shall provide a minimum Δv of 200 m·s ⁻¹ for stationkeeping and orbital transfer.	Y	Propellant mass calculated backwards from this requirement and PROP.020, Table 4.23.	A - Expulsion efficiency must be analysed.
PROP.020	The propulsion system shall allow for a minimum Δv of 3 m·s ⁻¹ to remain available at the end of the mission for EOL manoeuvres.	Y	Included in Δv budget, refer to PROP.010 and Table 4.23.	A - Expulsion efficiency must be analysed.
PROP.050	The thrust delivered by each thruster shall be no more than 1000 mN	Y	Nominal thrust level constant 0.450 N, Table 4.23.	T
PROP.051	The number of main thrusters shall be 2, placed symmetrically with respect to the spacecraft principal axis of inertia	TBD	2 thrusters used (Table 4.23), however position with respect to principal axis of inertia not considered.	A, I - P. axis of inertia must be determined.
PROP.052	Each thruster shall be throttleable within a range of no less than $\pm 10\%$ of the nominal thrust.	Y	Custom regulator valves included, Section 4.2.	T - Testing of regulator valve performance.
PROP.053	The thrust delivered by each thruster shall be more than 100 mN.	Y	Nominal thrust level constant 0.450 N, Table 4.23	T
PROP.060	The propulsion system shall have a maximum thrusting time of 60 min per manoeuvre. Maximum manoeuvre time is needed for the Stable Manifold Injection Manoeuvre (SMIM) with a Δv of 73 m·s ⁻¹ .	Y	Thruster specifications state 45 min of max. continuous firing time (Table 3.4), however at thrust level of 0.45 N each thruster, the SMIM manoeuvre takes only 35.15 min. PMD feed rate is higher than thruster mass flow rate at nominal thrust, Table 2.11, Table 4.1.	T - Testing of system performance for 60 min thrust time.
PROP.070	The propulsion system shall have an operational life in space of at least 1.5 years.	TBD	TBD	A
PROP.080	The propulsion system shall be able to operate in a vacuum external environment.	TBD	TBD	T

Table 4.29: Requirements compliance check for the MPS. Y = Yes, N = No, TBD = To Be Determined. Requirements PROP.090 - PROP.180

ID	Text	Compliance	Remarks	Verification
PROP. 090	The propulsion system shall be operational in the temperature range between 278 K and 323 K.	TBD	Constant temperature of 300 K considered for all calculations. Heating power within power budget, Table 4.23.	T - Performance of system over this range must be tested.
PROP. 091	The propulsion system shall withstand a non-operational temperature in the range between 273 K and 313 K.	TBD	See PROP.090	T - Performance of system over this range must be tested.
PROP. 100	The propulsion system shall have a maximum volume of 5U (CubeSat form factor)	TBD	TBD	A - Precisely analyse occupied volume.
PROP. 110	The propulsion system shall have a wet mass of no more than 6 kg.	Y	Propulsion system wet mass 5.563 kg, Table 4.23.	I - Weighing of system components.
PROP. 120	The propulsion system shall require a total power of no more than 10 W during firing, 25 W for pre-heating, and 1 W during standby.	Y	Pre-heat power, pump power and valve power within bounds, Table 4.26.	T - Measure power consumption for every component from BOL to EOL.
PROP. 124	The propulsion system shall operate at a voltage of no more than 32 V, and allow for switching to lower voltage to keep the thrust valve open (when needed).	Y	Pump voltage 6 V [56], latch valve 11 V [103], thruster valve hold voltage 11 V [40].	n/a
PROP. 130	The propulsion system shall reach steady state conditions in less than 2 s after the thrust valve opening command is sent.	TBD	Thruster characteristics w.r.t this requirement are not found.	T - Hot-fire tests required.
PROP. 150	The propulsion system shall be able to be restarted for a minimum of 500 times.	TBD	Thruster 1500 firings Table 3.4. No specifications for other components found.	T
PROP. 160	The pressure in all components of the propulsion system shall be no more than 50 bar.	Y	Highest system pressure at EOL TVC condition, Table 4.14.	A
PROP. 161	The pressure drop between propellant tank and thruster shall be less than 0.1 bar.	Y	Approximated pressure drop tank - pump 221 Pa, pump - regulator 242 Pa, regulator - thruster 18 Pa, Table 4.18.	T
PROP. 162	All propulsion system components shall be designed on a burst factor of at least 2.5.	Y	Tank design uses $j_b = 2.5$, Section 4.1.2.	A - Must be checked for all components.
PROP. 170	The propulsion system shall allow for spacecraft passivation, by releasing all remaining propellant.	TBD	TBD	A
PROP. 180	The propulsion system shall include sensors to continuously monitor the pressure and temperature in the propellant tank.	Y	Pressure transducers and thermocouples included in DMU, Section 4.3.1.	n/a

Table 4.30: Requirements compliance check for the MPS. Y = Yes, N = No, TBD = To Be Determined. Requirements PROP.190 - PROP.200

ID	Text	Compliance	Remarks	Verification
PROP. 190	The propellants shall not include any substance that is classified as toxic according to the REACH regulations.	Y	Only fluids are LMP-103s, Nitrogen.	n/a
PROP. 191	All propulsion system components shall be compatible to the propellants used by the system.	Y	All component materials Ti-6Al-4V or stainless steels. Latch valve PTFE seats are compatible with LMP-103s [109].	n/a
PROP. 200	Payload reserved volume not to be used by any propulsion system components: 3U in length (one quarter of the bus)	Y	Used as design input. Seen in Figure 4.20a.	I

4.5.2. Requirements Compliance of the Reaction Control System

The tables presenting the requirements compliance of the RCS are Table 4.31, Table 4.32 and Table 4.33, additional verification required is described by "A" = Analysis, "I" = Inspection and/or "T" = Testing.

Table 4.31: Requirements compliance check for the RCS. Y = Yes, N = No, TBD = To Be Determined. Requirements RCS.030 - RCS.070.

ID	Text	Compliance	Remarks	Verification
RCS. 030	The RCS propulsion system shall provide a minimum Total Impulse for all RCS tasks of 110 N-s (if the Aurora ARM-A system is used), or 170 N-s (if the GomSpace 6DOF system is used). The custom system shall provide a worst-case total impulse of 170 N-s.	Y	Propellant mass calculated backwards from this requirement, Table 4.8.	A - Expulsion efficiency must be analysed.
RCS. 050	The thrust delivered by each RCS thruster shall be in the range 1-10 mN.	Y	Thrust levels are 4 mN (BOL) - 1 mN (EOL) Table 4.8	T
RCS. 051	The number of RCS thrusters shall be no less than 4.	Y	Figure 4.21a, Table 4.25.	n/a
RCS. 070	The RCS propulsion system shall have an operational life in space of at least 1.5 years.	TBD	TBD	A

Table 4.32: Requirements compliance check for the RCS. Y = Yes, N = No, TBD = To Be Determined. Requirements RCS.080 - RCS.170.

ID	Text	Compliance	Remarks	Verification
RCS.080	The RCS propulsion system shall be able to operate in a vacuum external environment.	TBD	TBD	T
RCS.090	The RCS propulsion system shall be operational in the temperature range between 278 K and 308 K.	TBD	Constant system temperature of 300 K used in all calculations. Heating power within bounds, Table 4.27.	T - Performance of system over this range must be tested.
RCS.091	The RCS propulsion system shall withstand a non-operational temperature in the range between 273 K and 313 K, eventually using its own thermal control if the spacecraft thermal control is not sufficient.	TBD	See PROP.090	T - Performance of system over this range must be tested.
RCS.100	The RCS propulsion system shall have a maximum volume of 1U (CubeSat form factor).	Y	Figure 4.21a	I
RCS.110	The RCS propulsion system shall have a wet mass of no more than 1 kg.	Y	Total system wet mass is 0.822 kg, Table 4.25.	T - Weighing of system components.
RCS.120	The RCS propulsion system shall require a power of no more than 25 W during operation, and no more than 0.5 W during standby.	Y	Thruster firing power of 20 W at BOL, lower at EOL, heating power within bounds, Table 4.27.	T - Measure power consumption for every component from BOL to EOL.
RCS.124	The RCS propulsion system shall operate at a voltage between 3.3V and 16V.	TBD	No data published for LV and thruster operating voltage [90], [102].	n/a
RCS.140	The RCS propulsion system shall be able to provide a minimum impulse bit of 2 mN-s.	TBD	No data w.r.t. minimum impulse bit published [90].	T - Hot fire tests required.
RCS.150	The RCS propulsion system shall be able to be restarted for a minimum of 2000 times.	TBD	No data w.r.t. lifetime of LV and thruster published [102], [90].	T - Hot fire tests required.
RCS.160	The pressure in all components of the RCS propulsion system shall be no more than 50 bar.	Y	BOL tank pressure of 1.000 bar Table 4.8.	A
RCS.161	The pressure drop between propellant tank and thruster shall be less than 0.1 bar.	Y	Total pressure drop approximated as 21 Pa, Table 4.20.	T
RCS.162	All RCS propulsion system components shall be designed based on a burst factor of at least 2.5.	Y	Tank designed using burst factor $j_b = 2.5$, Section 4.1.3.	A - Must be checked for all components.
RCS.170	The RCS propulsion system shall allow for spacecraft passivation, by releasing all remaining propellant.	TBD	TBD	A

Table 4.33: Requirements compliance check for the RCS. Y = Yes, N = No, TBD = To Be Determined. Requirements RCS.180 - RCS.200.

ID	Text	Compliance	Remarks	Verification
RCS.180	The RCS propulsion system shall include sensors to continuously monitor the pressure and temperature in the propellant tank.	Y	Two thermocouples and two pressure transducers included, Section 4.3.2.	n/a
RCS.190	The propellant shall not include any substance that is classified as toxic according to the REACH regulations.	Y	Only fluids are LMP-103s, Nitrogen.	n/a
RCS.191	All RCS propulsion system components shall be compatible to the propellants used by the system.	TBD	Tank and line material is Ti-6Al-4V, LV unknown, thruster designed for water-based propellants.	n/a
RCS.200	Payload reserved volume not to be used by any propulsion system components: 3U in length (one quarter of the bus).	Y	Not conflicting with payload space, Figure 4.21a.	I

4.5.3. ECSS and Miscellaneous Requirements

The requirements compliance for ECSS and miscellaneous requirements is shown in Table 4.34, Table 4.35 and Table 4.36, additional verification required is described by "A" = Analysis, "I" = Inspection and/or "T" = Testing.

Table 4.34: Requirements compliance check for the MPS and RCS. Y = Yes, N = No, TBD = To Be Determined. Requirements ECSS.020 until ECSS.080.

ID	Text	Compliance	Remarks	Verification
ECSS.020	Evaluation shall be performed to confirm no water hammer issues ensure proper propulsion system functioning. This shall include assessment of worst case pressure transients.	Y	Worst case surge magnitude 1.026 bar for MPS, 0.078 bar for RCS. Section 4.4.4	T
ECSS.060	If the flight version of the system is divided into independent blocks, they should be separated by safety barriers such as pyrovalves, latch valves or burst membranes.	Y	LV present in both MPS and RCS Figure 4.1, Figure 4.2.	n/a
ECSS.080	The system design shall allow for on-ground draining.	Y	FDV present in both MPS and RCS Figure 4.1, Figure 4.2.	n/a

Table 4.35: Requirements compliance check for the MPS and RCS. Y = Yes, N = No, TBD = To Be Determined. Requirements ECSS.090 until ECSS.140.

ID	Text	Compliance	Remarks	Verification
ECSS.090	The location of fill-and-drain valves and piping layout shall prevent contact between dissimilar fluids.	Y	Pressurant and propellant not separable. No other fluids in system.	n/a
ECSS.100	All filters used at system or component level shall be designed and positioned according to the result of contaminant control and reliability studies.	TBD	TBD	A
ECSS.110	Filters shall be installed immediately downstream of potential particle generating components and, depending on the result of the failure risk analysis, directly upstream of components sensitive to pollution or contamination.	Y	MPS LV and thrusters include filter [41], [103]. RCS includes filter (Figure 4.2).	T - Particle generation of all components must be investigated.
ECSS.120	To avoid propellant freezing and control propellant tank pressures, the tank and line temperatures shall be controlled during the whole mission.	TBD	Tank heating power preliminarily calculated Table 4.23.	n/a
ECSS.130	For propulsion systems working in blow-down mode, the ratio of pressurant volume shall be consistent with thruster specifications.	TBD	Thruster specifications in this design assumed dependent only on thruster inlet pressure.	A - Thruster specifications required.
ECSS.140	Redundant functional transducers shall be installed.	Y	Two pressure transducers and thermocouples for each system, Section 4.3.1, Section 4.3.2.	n/a

Table 4.36: Requirements compliance check for the MPS and RCS. Y = Yes, N = No, TBD = To Be Determined. Requirements PLD.150 and SYS.040 until SYS.060.

ID	Text	Compliance	Remarks	Verification
PLD.150	The maximum size of the payload shall be 98 mm x 98 mm x 290 mm.	Y	Used as input for design.	n/a
SYS.040	The system shall be free of components as described in ITAR regulations.	TBD	TBD	n/a
SYS.050	The integrated system shall have a mass of ≤ 26 [kg] (TBC).	Y	MPS and RCS within mass constraints (Table 4.24, Table 4.25). Wet mass used to calculate required Δv .	T - Weighing of the complete system.
SYS.060	In the launch configuration, the satellite shall comply with the 12U standard.	Y	Used as input for design.	n/a

4.5.4. Requirements Compliance Discussion

Compliance with requirements of both systems is discussed here.

Main Propulsion System

The requirements for which compliance is set at TBD are PROP.051, 070, 080, 090, 100, 130, 150 and 170. Placement of the MPS thrusters according to PROP.051 requires knowledge of the location of the principal axes of inertia, which is currently unknown. PROP.070 refers to the operational lifespan of 1.5 years in space, which cannot be determined due to lack of information published on all components. Compliance with PROP.080 cannot be determined before custom components are tested in a vacuum environment. PROP.090 and PROP.091 refer to operational and non-operational temperature ranges for the propulsion system, however all calculations refer to the nominal temperature of 300 K. Compliance with PROP.100 is still TBD as the MPS components are spread out over more than 5U, it is TBD whether this is acceptable. For PROP.130, thruster data is lacking. For PROP.150, specifications for all components other than the thruster is lacking. Finally, PROP.170 may be complied with if the propulsion system is simply kept firing until EOL, however it is TBD whether all propellant will be expelled at that time.

Reaction Control System

For the RCS, requirement compliance for RCS.070, 080, 090, 091, 124, 140, 150, 170, 191 is TBD. For RCS.070, 080, 090, 091, the same reasons as provided for the MPS apply. For RCS.124, 140 and 150, data on the thruster is lacking. For RCS.170, the same reasons as for the MPS apply. RCS.191 is TBD due to no data being known on the LV.

ECSS and Miscellaneous Requirements

For compliance, ECSS.100, 120, 130 and SYS.040 have been marked TBD. ECSS.100 cannot be complied with until contaminant control and reliability studies have been performed. ECSS.120 requires heating of propellant lines, this has not been considered. Determining compliance with ECSS.130 requires information on the thruster, thruster inlet pressure was assumed linear with thrust level and power consumption. Finally, SYS.040 is left at TBD because for none of the components used, specifics w.r.t ITAR were published.

4.6. Comparison of Designs to Commercial-off-the-Shelf Systems

Through comparing the final custom designs to COTS systems, an additional step of preliminary verification of the designs is achieved. First, the metrics on which the comparison is made are presented:

1. Wet mass
2. Volume
3. Power consumption
4. Thrust level

Low wet mass for a given required Δv is desirable, as it decreases the spacecraft wet mass. Low system volume is desirable, as it enables a higher volume margin for other spacecraft components. Low power consumption is desirable, as it enables higher power margins for other spacecraft components. Finally, a high thrust level is desirable as it decreases manoeuvre time.

4.6.1. Commercial-off-the-Shelf System Selection

Main Propulsion System

The options considered are listed in Table 2.21: Aerojet Rocketdyne MPS-135, Busek AMAC and NanoAvionics EPSS. Of these systems, the Busek AMAC is not considered due to lack of information on dry mass and propellant mass. Between the systems EPSS and MPS-135, the system by MPS-135 is characterised by higher I_{sp} , and the larger version of the MPS-135 furthermore shows a higher value of ϕ , namely 0.507 as compared to 0.308 for the EPSS. Due to lack of more datapoints for the NanoAvionics EPSS, and due to the excessive wet mass resulting from scaling up the EPSS system to accommodate a Δv of 203 m-s⁻¹, the MPS-135 is chosen to serve as baseline for the comparison for the MPS.

Reaction Control System

The options considered are listed in Table 2.22: Aurora ARM-A, GOMSpace/Nanoprop 6DOF, VACCO MiPS CGT. Here, the Aurora ARM-A is chosen as the most suitable candidate due to its highest specific impulse and propellant wet mass fraction ϕ .

4.6.2. Comparing Custom Designs to COTS Systems

In this subsection, the comparison is made.

Main Propulsion System

Table 4.37 shows the comparison. For the COTS, two systems are chosen, placed in the same location as the thrusters are placed in the custom design. The wet mass results from the propellant wet mass fraction ϕ and the required propellant mass considering a spacecraft wet mass of 26 kg and the highest reported I_{sp} of the system. For volume, the 2U version of the MPS-135 is considered, as it is unknown whether or not the length of the system changes to account for varying propellant mass. For power consumption, the pre-heat power is considered as it is observed to be the most critical (> 25 W for the COTS version). Mass data for the custom design from Table 4.24, power data for the custom design from Table 4.26. Specifications for the COTS from Table 2.21.

On the first metric, the custom version performs much worse than the COTS version, with an observed significant difference in wet mass. Similarly, the COTS version requires only 4U in total, in CubeSat form factor. For the custom design, the total volume remains unclear however if the CubeSat form factor is considered it is at least above 4U, considering the tank alone is already occupying roughly 2x1.37 U (Table 4.4) and the thrusters each are occupying 1.78 U (thruster length from inlet to tip of the nozzle is 178 mm, Table 2.12). For the power consumption, the custom version performs much better, with only 20 W worst-case pre-heat power as compared to 56 W worst-case pre-heating power for the COTS version. Finally, the thrust level of the custom version is much lower as only two thrusters are used and a low constant nominal thrust level is chosen. The COTS version has eight thrusters each capable of generating 1.00 N of thrust, however it is unclear whether this system operates in blow-down mode. According to the Carpenter et al. in 2013 [78], it is piston tank fed by a separate pressurant tank

without regulator valve and therefore it is assumed that it operates in blow-down mode with significantly lower EOL thrust, possibly 0.25 N as noted in the datasheet as the lower end of the thrust force range [22]. Whether or not this is worse performance as compared to the custom design depends on the preference of the thrust level. If the system were to require constant thrust force, the custom design here were to perform better.

Table 4.37: Comparing the custom design to the commercial-off-the-shelf version. Main Propulsion System.

Parameter	Custom design	COTS
Wet mass	5.563 kg	4.324 kg
Volume	TBD	4U
Power consumption (pre-heating)	20 W	56 W
Thrust level	1.0 N	2.00 - 8.00 N

Reaction Control System

Table 4.38 shows the comparison. An important note here is that both the custom and the COTS system utilise the same thruster - the Aurora Resistojet One, using the same propellant and assuming the same I_{sp} of 100 s. The COTS system may be placed in the same location as the custom solution, namely in the free hind 1U space left behind by the payload and the two diagonally opposed thrusters. The propellant mass is identical to the custom solution, as the same total impulse requirement of 170 N-s is used. Using the value of ϕ from Table 2.22, the wet mass results. According to the datasheet, the form factors are 0.35 U, 1 U and 4 U, with options for intermediate steps [33]. Assuming a volume of 0.35 U required for a propellant mass of 0.070 kg, a conservative estimate proportional to these values results in a volume of 0.865 U for a propellant mass of 0.173 kg. Finally, the thrust level and power consumption are correlated. It is unclear whether or not the system operates in blow-down mode, if it would, it would perform similar to the custom solution.

On basis of the first metric, the COTS system performs better, less significantly than for the MPS. Comparison based on the second metric is difficult as the precise volume of the custom solution is not determined. The final two metrics result in the same performance, assuming blow-down operation from maximum thrust level to the acceptable minimum thrust level of 1 mN.

Table 4.38: Comparing the custom design to the commercial-off-the-shelf version. Reaction Control System.

Parameter	Custom design	COTS
Wet mass	0.822 kg	0.750 kg
Volume	<1U	0.865 U
Power consumption (firing)	5 - 20 W	5 - 20 W
Thrust level	1 mN - 4 mN	1 mN - 4 mN

4.6.3. Conclusions on the Comparisons

For both systems, the COTS version performs better than the custom solution. First and foremost it must be considered that the custom solution is a preliminary design generated by one person during a MSc thesis project, and the COTS solutions are finalised designs over presumably larger timeframes than the duration of a MSc thesis, designed by a team of engineers. Secondly, and more importantly, an important factor in the performance of the COTS systems is the significantly higher level of integration of all components. Due to the custom solution relying on a limited selection of commercially available components, suboptimal performance with respect to system volume and mass results. An important example of this is e.g. the FDV for both the MPS and RCS, which significantly contribute to system volume and mass. For the RCS COTS version no information is published on the feed network layout, however for the MPS-135 by Aerojet Rocketdyne, a high level of integration results from the use of AM methods, integration fluid flow paths and manifolds into the monolithic structure. The valves for both COTS systems are not mentioned anywhere, however possibly custom-created valves were used to suit the specific requirements of these systems, contributing to a lower volume and mass as compared to using COTS valves from online sources. Finally, it must be noted that the custom propulsion

system was specifically designed for the required Δv and I_t delivered. The COTS systems on the other hand were scaled up from a fixed design, assuming a linear propellant mass-total system wet mass relationship. This is not completely fair to the COTS systems due to the added tank mass in reality not scaling linearly with the propellant mass - where it is expected that the step addition of dry mass decreases for every step of propellant mass added.

5

Conclusions and Recommendations

First, the conclusions are presented through answering the research questions. Subsequently, the recommendations are presented. A note added to this project is that parts of this work are included in a paper to be presented at the International Astronautical Congress of 2021 in Dubai, United Arab Emirates: "Propellant Line Dimensioning for 'Green' CubeSat Mono-Propellant Propulsion Systems".

5.1. Conclusions

In order to present the conclusions of this project, the research questions are answered in order:

1. *What are the most relevant performance and design metrics for the LUMIO propulsion system?*

The most relevant metrics to describe the propulsion system performance are wet mass, volume, power consumption and thrust level, as used for the comparison between the custom solution and the COTS solution. These metrics have been chosen as they are dictated by the requirements and are the most critical, due to the following reasons. The wet mass of both the MPS and the RCS is close to the maximum allowable value: 5.563 kg for the MPS as compared to the 6.000 kg limit as stated by requirement PROP.110, and 0.822 kg for the RCS as compared to the 1.000 kg limit as stated by requirement RCS.110. The system volume of both MPS and RCS are difficult to determine, however the MPS occupies a significant amount of space inside the spacecraft bus, mainly due to the length of the COTS thrusters. The RCS is observed to occupy close to 1 U of volume inside the spacecraft bus, as compared to the limit of 1 U as stated by requirement RCS.100. Power consumption for both systems is critical due to the high pre-heating power of both MPS thrusters of 20 W (worst case), close to the allowable maximum of 25 W as per requirement PROP.120, an. For the RCS, this metric is even more critical, as water resistojets require a high amount of power for firing due to the high latent heat of vaporisation of water. This is reflected in the firing power of one single thruster at a BOL thrust level of 4 mN corresponding to 20 W of electrical power needed, as compared to the allowable 25 W (RCS.120). Finally, the thrust level of the MPS influences the transfer time of a manoeuvre. There is no specific requirement dictating the maximum manoeuvre time for any given manoeuvre, only a requirement on the thrust levels themselves which are complied with. Furthermore, in reality, some manoeuvres can be split into multiple burns. However, this may be time-consuming and may significantly limit the operational envelope of the mission.

(a) *If these metrics have an order of importance, what is the order?* The order of the metrics is selected as the following, based on the criticality of the requirements. First, wet mass and volume, as they are critically close to the maximum as compared to the requirements, especially for the MPS. Secondly, power consumption, as this limits the number of RCS thrusters firing. Finally, thrust level is the least critical metric as some manoeuvres can be split into multiple burns as mentioned before.

2. *What are feasible concepts for the propulsion system of LUMIO?* Three concepts were generated for both the MPS and RCS, namely a pressure regulated concept, a blow-down type concept and

a pump-fed concept. These concepts were very simple designs, much less in-depth than the detailed design phase, only to determine the most feasible feed system option for the propulsion systems. For the MPS, all three concepts were feasible as none exceeded the metrics of mass, volume, power consumption, thrust force and propellant tank pressure. For the RCS, all three concepts were feasible as well, on the basis that none of the aforementioned metrics were exceeded.

- (a) *What are feasible COTS systems for the propulsion system of LUMIO and what are their characteristics?* The only feasible COTS system for the MPS from the options considered is the Aerojet Rocketdyne MPS-135, as the other systems would result in excessive propulsion system wet mass due to their low propellant wet mass fraction ϕ . For the RCS, the only feasible COTS system of the systems considered is the Aurora ARM, the other systems are deemed infeasible due to their excessive wet mass resulting from low I_{sp} and low propellant wet mass fraction ϕ .
 - (b) *What COTS systems are chosen as the baseline to compare the in-house designed system to and what are their characteristics?* The baseline systems for comparison to COTS systems are the Aerojet Rocketdyne MPS-135 for the MPS and the Aurora ARM for the RCS due to the other options being deemed infeasible.
 - (c) *What are the most feasible propulsion system concepts for the in-house design of LUMIO and what are their characteristics?* The most feasible propulsion system concepts for LUMIO based on the concept generation and selection process are the pump-fed concept for the MPS and the blow-down type concept for the RCS. The pump-fed concept for the MPS was chosen due to its comparatively excellent performance with regards to volume and propellant tank pressure, furthermore it enables constant thrust force over the lifetime of the spacecraft. The low propellant tank pressure results in lower propellant tank mass due to the pump providing significant pressure differential between the tank pressure and the thruster inlet pressure, and as a result additionally requires a lower pressurant gas volume as compared to the regulated type and blow-down type concepts. The blow-down type concept for the RCS was selected due to the pressure regulated concept performing poorly based on propellant tank pressure, due to the high required storage pressure in order to enable constant maximum thrust. As noted however, the BOL and EOL tank pressure values here can be chosen as identical to those of the blow-down system, enabling constant minimum thrust. In this case however, the regulated concept would still not win the trade-off due to the required extra mass and volume for the integration of a regulator valve while tank mass and dimensions are identical as compared to the blow-down concept. The pump-fed concept performed worse as compared to the blow-down concept due to the pump taking up significant volume inside the limited volume of 1U. Furthermore, the pump-fed system would operate at a very low differential pressure due to the very low inlet pressure of the selected thruster. Additionally, a very low EOL tank pressure is used in the pump-fed concept which is close to the vapour pressure of the propellant.
3. *What is the detailed design for the propulsion system of LUMIO?* The detailed design for LUMIO's MPS consists of a custom, cuboid tank with custom PMDs, COTS FDV, LV, pump, PFCD and thrusters. The detailed design of the RCS consists of a custom, cuboid tank including custom PMDs as well, and COTS FDV, filter, LV and thrusters.
- (a) *What are the characteristics of this design?* The MPS is first of all characterised by its wet mass of 5.563 kg and constant thrust level of 0.450 N. The propellant tanks are cuboid due to higher volumetric efficiency as compared to cylindrical tanks. This tank includes a custom vane-type PMD combined with a sponge PMD, designed conservatively to ensure on-demand gas free propellant expulsion with a vane mass flow rate higher than the required thruster mass flow. A conservative EE of 90% was assumed, meaning that at EOL, 10% of propellant mass may be left behind inside the propellant tank. Pressurant gas is Nitrogen, selected due to its higher molar mass than Helium and expected lower leak rates, at only an insignificant mass increase. The tank is covered in MLI, specifically 40 aluminised Mylar sheets to reduce the emissivity of the propellant tank. The thrusters used are two Bradford/ECAPS HPGP 1N thrusters using propellant LMP-103s stored at 300 K, fed by a Flight-

works, Inc. 2222-M04C58 micro-gear pump passively controlled by the custom designed PFCD. The RCS is first of all characterised by its wet mass of 0.822 kg and a decreasing thrust level of 4 mN - 1 mN from BOL to EOL. The propellant tanks are similar to the MPS, in being of cuboid shape and featuring custom designed PMDs: a vane-type PMD in combination with a sponge-type PMD is used here as well. The same EE was assumed here, and the same pressurant gas and MLI is used. The thrusters used are four Aurora ARO thrusters at an assumed I_{sp} of 100 s using water propellant stored at 300 K.

- (b) *How will this system be integrated into the spacecraft?* The tanks and feed lines were designed such that they would in any case not interfere with the payload reserved volume. All thrusters are integrated at the rear end of the spacecraft bus, fully utilising the three "tuna can" volumes. Preliminary placement of components is performed in a DMU, in which the feed line lengths are measured and these lengths are used to determine the feed system pressure drop and fluid hammer characteristics for both the MPS and RCS.
- (c) *How will the system performance and health be monitored on-orbit?* As per requirements PROP.180 and RCS.180, the propellant tank temperature and pressure shall be continuously monitored. As per requirement ECSS.140, all transducers shall be redundant. Therefore, both MPS and RCS are equipped with each two pressure transducers and two thermocouples. The pressure transducers are installed at the outlet port of the propellant tank to monitor tank pressure, the model is GP:50 miniature pressure transducer 7000 series. Thermocouples are considered in the preliminary design as well, and the RS Pro K-type thermocouple can be used. Its mass and dimensions are unknown and integration into the DMU is left out of scope. Integration of these components will require additional ports in the propellant tank with increased risk of leakage. Furthermore, the end of the thermocouple must be in contact with the propellant at all times, therefore it should be connected to a PMD, e.g. the sponge.
- (d) *How does this design compare to the COTS baseline systems?* Both systems are significantly heavier and occupy a higher volume inside the spacecraft bus as compared to the COTS versions. This is first of all attributed to the higher level of integration possible in the COTS versions, possibly using completely custom designed components such as valves, filters and thrusters and not relying on web-sourced commercial available components. Furthermore, the COTS version is produced using AM, integrating fluid passages into the monolithic system. For the MPS, higher power required is observed for the COTS version due to eight thrusters being used. Each MPS-135 is equipped with four thrusters, and due to the requirement of thrusters being mounted symmetrically around the principal axes of inertia, two systems are used therefore resulting in eight thrusters. The custom design only uses two thrusters and therefore is characterised by lower pre-heating power. This is however considering that all eight thrusters are fired simultaneously and therefore all eight must be pre-heated while in reality a lower number of thrusters could be used. The RCS custom and COTS designs both utilise the same thrusters, namely the Aurora ARO, and the power is dependent on the set thrust level. Due to the same thrust levels being used (4 mN maximum available and 1 mN minimum allowable), the power consumption is expected to be the same between these systems. Finally, the thrust level for the custom version of the MPS is able to be kept constant due to the use of the pump, and the COTS version is taken to be a blow-down type system, due to lack of a regulator valve between the pressurant tank and the piston-type tank pressurant cavity. For the RCS, the same thrust levels are possible as for the COTS, due to the aforementioned maximum available 4 mN of thrust and minimum allowable value of 1 mN.
- (e) *What are the most critical requirements for this design?* As seen by the wet mass of the MPS which is close to the maximum requirement, and the high volume occupied by the MPS inside the spacecraft bus, for the MPS, the most critical requirements are PROP.100 and PROP.110 for volume and mass, respectively. For the RCS, this is the power level requirement, namely RCS.120 - this requirement enables only the use of one thruster at full thrust simultaneously. The maximum available firing power is 25 W and the maximum firing power consumption of one Aurora ARO thruster is 20 W - four thrusters firing simultaneously would consume 80 W of electrical power.

5.2. Recommendations

In this thesis, the following challenges are identified. First of all, the high mass and volume of the custom MPS and RCS systems leaves room for improvement. This should be addressed by custom valve solutions, decreasing the size of the MPS thrusters with integrated thruster valves. Ideally, an AM solution should be considered to achieve a higher degree of integration. Secondly, a more efficient propellant tank design can be pursued, perhaps L-shaped or shaped such that it mostly takes place behind the RCS inside the spacecraft bus. Thirdly, a high power consumption of the RCS thrusters during firing is observed and the choice was made to utilise only a single thruster simultaneously. If the ACS strategy would require using two thrusters simultaneously, or in case any requirement were to dictate this, the feed pressure of the thrusters must be decreased. This can be achieved by either lowering the BOL tank pressure and roughly doubling the RCS propellant tank length to accommodate for this lower pressure without having to decrease the EOL pressure, or by integrating a pressure regulator valve to throttle the thruster inlet pressure. Fourthly, as observed from the pump working point calculations (Table 4.14), the dimensionless cavitation coefficient at EOL is significantly below the value obtained from the tests described in Table 2.8. As mentioned in the description of the working point calculations, this does not yet indicate whether the system is actually experiencing cavitation at that working point or not, only that it is in any case closer to cavitation as compared to the test situation. Therefore, qualification tests of the pump for the specified propellant tank pressures and working points are required. Fifthly and finally, the feed pressure losses inside the feed systems for both the MPS and RCS were determined only using empirical relations and were deemed insignificant compared to the thruster inlet conditions for both the MPS and RCS. However, no additional losses introduced by fittings were considered yet (e.g. burrs, even smaller bend radii or small changes in cross-sectional area), this should be included in further research. The pressure loss in a real system must additionally be validated by testing.

Bibliography

- [1] Cover image (edited) from "cubesats for hunting secrets in lunar darkness". http://www.esa.int/Enabling_Support/Space_Engineering_Technology/CubeSats_for_hunting_secrets_in_lunar_darkness, 2018. Accessed: 20-Nov-2020.
- [2] Armen Poghosyan and Alessandro Golkar. Cubesat evolution: Analyzing cubesat capabilities for conducting science missions. *Progress in Aerospace Sciences*, 88:59 – 83, 2017. ISSN 0376-0421. doi: <https://doi.org/10.1016/j.paerosci.2016.11.002>. URL <http://www.sciencedirect.com/science/article/pii/S0376042116300951>.
- [3] Thyrso Villela, Cesar A Costa, Alessandra M Brandão, Fernando T Bueno, and Rodrigo Leonardi. Towards the thousandth cubesat: A statistical overview. *International Journal of Aerospace Engineering*, 2019, 2019.
- [4] Stefano Speretta, Francesco Topputo, James Biggs, Pierluigi Di Lizia, Mauro Massari, Karthik Mani, Diogene Dei Tos, Simone Ceccherini, Vittorio Franzese, Angelo Cervone, et al. Lumio: achieving autonomous operations for lunar exploration with a cubesat. In *2018 SpaceOps Conference*, page 2599, 2018.
- [5] A. Cervone et al. Phase a design of the lumio spacecraft: a cubesat for observing and characterizing micro-meteoroid impacts on the lunar far side. *Proceedings of the 71st International Astronautical Congress (IAC) – The CyberSpace Edition*, 2020.
- [6] Sami W Asmar and Steven Matousek. Mars cube one (marco) shifting the paradigm in relay deep space operation. In *14th International Conference on Space Operations*, page 2483, 2016. doi: <https://doi.org/10.2514/6.2016-2483>.
- [7] Dawn Andrews, Grayson Huggins, E Glenn Lightsey, Nathan Cheek, Nathan Daniel Lee, Ali Talaksi, Sterling Peet, Lacey Littleton, Sahaj Patel, Logan Skidmore, et al. Design of a green monopropellant propulsion system for the lunar flashlight cubesat mission. In *Proceedings of the 34th Annual AIAA/USU Small Satellites Conference, Logan, UT*, 2020.
- [8] Grayson M Huggins, Ali Talaksi, Dawn Andrews, E Glenn Lightsey, Daniel Cavender, Don McQueen, Hunter Williams, Carlos Diaz, John Baker, and Matthew Kowalkowski. Development of a cubesat-scale green monopropellant propulsion system for nasa's lunar flashlight mission. In *AIAA Scitech 2021 Forum*, page 1976, 2021.
- [9] David Sternberg, John Essmiller, Cody Colley, Andrew Klesh, and Joel Krajewski. Attitude control system for the mars cube one spacecraft. In *2019 IEEE Aerospace Conference*, pages 1–10. IEEE, 2019. doi: 10.1109/AERO.2019.8741816.
- [10] Lunar flashlight propulsion system. <http://www.ssd1.gatech.edu/research/projects/lunar-flashlight-propulsion-system>. Accessed:18-01-2021.
- [11] George P. Sutton. *Rocket Propulsion Elements - An Introduction to the Engineering of Rockets (6th ed.)*. John Wiley and Sons, Chichester, United Kingdom, 1992. ISBN 0471529389.
- [12] Peter Fortescue and John Stark. *Spacecraft Systems Engineering*. John Wiley and Sons, Chichester, United Kingdom, 1992. ISBN 0471934518.
- [13] Kristina Lemmer. Propulsion for cubesats. *Acta Astronautica*, 134, 02 2017. doi: 10.1016/j.actaastro.2017.01.048.
- [14] Juergen Mueller, Richard Hofer, and John Ziemer. Survey of propulsion technologies applicable to cubesats. *NASA Publication*, 2010.

- [15] Khary I. Parker. State-of-the-art for small satellite propulsion systems. In *NASA Publication (Goddard Space Flight Centre, Greenbelt, MD, USA)*, 2016.
- [16] A.R. Tummala and A. Dutta. An overview of cube-satellite propulsion technologies and trends. *Aerospace*, 4(4):58, Dec 2017. ISSN 2226-4310. doi: 10.3390/aerospace4040058. URL <http://dx.doi.org/10.3390/aerospace4040058>.
- [17] Sasha Weston. *State of the Art - Small Spacecraft Technology*. National Aeronautics and Space Administration, Small Spacecraft Systems Virtual Institute, Ames Research Center, Moffett Field, California, Dec 2018. URL <https://www.nasa.gov/smallsat-institute/sst-soa>.
- [18] D. Krejci and P. Lozano. Space propulsion technology for small spacecraft. *Proceedings of the IEEE*, 106(3):362–378, 2018. doi: 10.1109/JPROC.2017.2778747.
- [19] GOMSpace nanoproprop 6dof. https://gomspace.com/UserFiles/Subsystems/flyer/Flyer_NanoProp_6DOF.pdf. Accessed: 2-Dec-2020.
- [20] Jpl marco - micro cubesat propulsion system. https://cubesat-propulsion.com/wp-content/uploads/2015/11/X14102000-01_2019update.pdf. Accessed: 10-01-2021.
- [21] Ronald A Spores. Gpim af-m315e propulsion system. In *51st AIAA/SAE/ASEE Joint Propulsion Conference*, page 3753, 2015. doi: 10.2514/6.2015-3753.
- [22] Aerojet Rocketdyne mps-130 innovative propulsion solutions for smallsats. <https://www.rocket.com/sites/default/files/documents/CubeSat/MPS-130%20data%20sheet%20crop.pdf>. Accessed: 30-Nov-2020.
- [23] Mathias Persson, Kjell Anflo, and Pete Friedhoff. Flight heritage of ammonium dinitramide (adn) based high performance green propulsion (hpgp) systems. *Propellants, Explosives, Pyrotechnics*, 44(9):1073–1079, 2019. doi: 10.1002/prop.201900248.
- [24] Aerojet Rocketdyne enabling high performance green propulsion for smallsats. <https://digitalcommons.usu.edu/cgi/viewcontent.cgi?filename=0&article=3240&context=smallsat&type=additional>. Accessed: 10-Dec-2020.
- [25] Michael Tsay, Charlie Feng, and Jurg Zwahlen. System-level demonstration of busek's 1u cube-sat green propulsion module "amac". In *53rd AIAA/SAE/ASEE Joint Propulsion Conference*, page 4946, 2017. doi: 10.2514/6.2017-4946.
- [26] Vacco argomoon propulsion system (x17025000-data-sheet-080217.pdf). <https://cubesat-propulsion.com/wp-content/uploads/2017/08/X17025000-data-sheet-080217.pdf>. Accessed: 1-Dec-2020.
- [27] NanoAvionics cubesat propulsion system epss | nanoavionics. <https://nanoavionics.com/cubesat-components/cubesat-propulsion-system-epss/>. Accessed: 1-Dec-2020.
- [28] Elizabeth T. Jens, Ashley C. Karp, Jason Rabinovitch, Antonietta Conte, Barry Nakazono, and David A. Vaughan. Design of Interplanetary Hybrid CubeSat and SmallSat Propulsion Systems. In *2018 Joint Propulsion Conference*, Cincinnati, Ohio, July 2018. American Institute of Aeronautics and Astronautics. ISBN 978-1-62410-570-8. doi: 10.2514/6.2018-4668. URL <https://arc.aiaa.org/doi/10.2514/6.2018-4668>.
- [29] Tyson K Smith, Zachary Lewis, Kurt Olsen, A Marc Bulcher, North Logan, and Stephen A Whitmore. A Miniaturized Green End-Burning Hybrid Propulsion System for CubeSats. In *Proceedings of the 34th Annual AIAA/USU Small Satellites Conference*, Logan, UT, page 12, 2020.
- [30] S. Powell, Tobias Knop, and S. Engelen. Experimental evaluation of a green bi-propellant thruster for small satellite applications. In *Proceedings of the 30th Annual AIAA/USU Small Satellites Conference*, Logan, UT, 2016.

- [31] Hyperion Technologiespm200. https://hyperiontechnologies.nl/wp-content/uploads/2019/11/HT_PM200.pdf. Accessed: 23-Dec-2020.
- [32] Vacco Space Productspropulsion unit for cubesats. https://www.vacco.com/images/uploads/pdfs/Propulsion_Unit_for_CubeSats_Rev_NC.pdf, . Accessed: 2-Dec-2020.
- [33] Aurora Propulsion Technologiesarm-a attitude control module. https://aurorapt.fi/2020site/wp-content/uploads/2020/08/Aurora_ARM-A_v4.pdf, . Accessed: 22-Dec-2020.
- [34] Valérie F Mistoco, Thomas A Trudel, Sven G Bilén, and Michael M Micci. Vacuum testing of the miniature radio-frequency ion thruster. In *The 29th International Electric Propulsion Conference, Princeton, NJ, 2005*.
- [35] H Takegahara, H Kuninaka, I Funaki, A Ando, K Komurasaki, H Koizumi, T Schoenherr, S Shinohara, T Tanikawa, M Nakano, et al. Overview of electric propulsion research activities in japan. In *30th Int. Symp. Space Technology Science, 34th Int. Electric Propulsion Conf., 6th Nano-Satellite Symp.*, 2015.
- [36] Halo hall-effect thruster. https://exoterracorp.com/wp-content/uploads/2020/08/NEWBrochureHaloThruster_Web-1.pdf. Accessed:02-01-2021.
- [37] Filip Rysanek, John Hartmann, Jochen Schein, and Robert Binder. Microvacuum arc thruster design for a cubesat class satellite. In *Proceedings of the 16th Annual AIAA/USU Conference on Small Satellites, Logan, UT, 2002*.
- [38] Amir S. Gohardani, Johann Stanojev, Alain Demairé, Kjell Anflo, Mathias Persson, Niklas Wingborg, and Christer Nilsson. Green space propulsion: Opportunities and prospects. *Progress in Aerospace Sciences*, 71:128 – 149, 2014. ISSN 0376-0421. doi: 10.1016/j.paerosci.2014.08.001.
- [39] Robert L Sackheim and Robert K Masse. Green propulsion advancement: challenging the maturity of monopropellant hydrazine. *Journal of Propulsion and Power*, 30(2):265–276, 2014. doi: 10.2514/1.B35086.
- [40] Bradford ECAPS bradford ecaps - products - 1n hpgp thruster. <https://www.ecaps.space/products-1n.php>, . Accessed: 1-Dec-2020.
- [41] Mathias Persson, Kjell Anflo, Aaron Dinardi, and J Bahu. A family of thrusters for adn-based monopropellant Imp-103s. In *48th AIAA/ASME/SAE/ASEE Joint Propulsion Conference & Exhibit*, page 3815, 2012.
- [42] Juergen Mueller. Thruster options for microspacecraft: a review and evaluation of state-of-the-art and emerging technologies. *Micropropulsion for Small Spacecraft*, 187:45–137, 2000.
- [43] Juergen Mueller. A review and applicability assessment of mems-based microvalve technologies for microspacecraft propulsion. In *35th Joint Propulsion Conference and Exhibit*, page 2725, 2000. doi: 10.2514/5.9781600866586.0449.0476.
- [44] B Ravi Kumar, Raghuvir Singh, Bhupeshwar Mahato, PK De, NR Bandyopadhyay, and DK Bhat-tacharya. Effect of texture on corrosion behavior of aisi 304l stainless steel. *Materials Characterization*, 54(2):141–147, 2005.
- [45] SE Ziemniak and M Hanson. Corrosion behavior of 304 stainless steel in high temperature, hydrogenated water. *Corrosion Science*, 44(10):2209–2230, 2002.
- [46] Satendra Kumar, TSN Sankara Narayanan, S Ganesh Sundara Raman, and SK Seshadri. Thermal oxidation of ti6al4v alloy: Microstructural and electrochemical characterization. *Materials Chemistry and Physics*, 119(1-2):337–346, 2010.

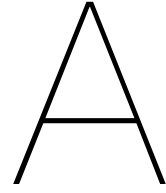
- [47] Harry A Conomos, Christopher G Alongi, Jeffrey Moore, Jackie Yager, Richard Goddard, Todd Salzler, James Fetes, and Keith Burch. Development of 10 inch diameter titanium rolling metal diaphragm tank for green propellant. In *53rd AIAA/SAE/ASEE Joint Propulsion Conference*, page 4915, 2017.
- [48] Yueting Liu, JMC Mol, and GCAM Janssen. Combined corrosion and wear of aluminium alloy 7075-t6. *Journal of Bio-and Tribo-Corrosion*, 2(2):9, 2016.
- [49] Welcome to the nist chemistry webbook. <https://webbook.nist.gov/>. Accessed:02-01-2021.
- [50] Derek Schmuland, Christian Carpenter, and Robert Masse. Mission applications of the mrs-142 cubesat high-impulse adaptable monopropellant propulsion system (champs). In *48th AIAA/ASME/SAE/ASEE Joint Propulsion Conference & Exhibit*, page 4269, 2012. doi: 10.2514/6.2012-4269.
- [51] NJCA Hejmanowski, RB Woodruff, RL Burton, DL Carroll, J Cardin, and C South El Monte. Cubesat high impulse propulsion system (chips). In *Proceedings of the 62nd JANNAF Propulsion Meeting (7th Spacecraft Propulsion)*, Nashville, TN, USA, pages 1–5, 2015.
- [52] NJ Hejmanowski, CA Woodruff, RL Burton, DL Carroll, AD Palla, JM Cardin, and CA South El Monte. Cubesat high impulse propulsion system (chips) design and performance. In *63rd JANNAF Propulsion Meeting (8th Spacecraft Propulsion)*, 2016.
- [53] Elliot Ring. *Rocket propellant and pressurization systems*. Prentice-Hall, 1964.
- [54] Flight works, inc., sbir.gov. <https://www.sbir.gov/sbc/flight-works-inc>. Accessed:16-03-2021.
- [55] Andrea Besnard, Sudathsi Tennakoon, Jose Torres, and Eric Besnard. Preliminary results of a micropump for mon-25/mmh propulsion and attitude control. In *AIAA Propulsion and Energy 2019 Forum*, page 4028, 2019. doi: 10.2514/6.2019-4028.
- [56] M-series - magnetic drive gear pumps. <http://products.flightworksincl.com/viewitems/micro-gear-pumps/m-series-magnetic-drive-gear-pumps>. Accessed:16-01-2021.
- [57] Pubchem - National Library of Medicine acetone. <https://pubchem.ncbi.nlm.nih.gov/compound/Acetone#section=Autoignition-Temperature>. Accessed: 25-08-2021.
- [58] Alfred C Wright. Usaf propellant handbooks. nitric acid/nitrogen tetroxide oxidizers. volume ii. Technical report, MARTIN MARIETTA AEROSPACE DENVER CO, 1977.
- [59] Ran Tao, Ruofu Xiao, Fujun Wang, and Weichao Liu. Cavitation behavior study in the pump mode of a reversible pump-turbine. *Renewable Energy*, 125:655–667, 2018.
- [60] KM Assefa and DR Kaushal. A comparative study of friction factor correlations for high concentrate slurry flow in smooth pipes. *Journal of Hydrology and Hydromechanics*, 63(1):13–20, 2015. doi: 10.1515/johh-2015-0008.
- [61] R. P. Benedict, N. A. Carlucci, and S. D. Swetz. Flow Losses in Abrupt Enlargements and Contractions. *Journal of Engineering for Power*, 88(1):73–81, 01 1966. ISSN 0022-0825. doi: 10.1115/1.3678482. URL <https://doi.org/10.1115/1.3678482>.
- [62] PL Spedding, Emmanuel Bénard, and GM McNally. Fluid flow through 90 degree bends. *Developments in chemical engineering and mineral processing*, 12(1-2):107–128, 2004.
- [63] K. Hilding Beij. Pressure losses for fluid flow in 90 degree pipe bends. 21, 1938.
- [64] H Ito. Pressure losses in smooth pipe bends. 1960.
- [65] Naomi Mary Crawford. *Pressure losses at bends and junctions*. PhD thesis, Queen’s University of Belfast, 2005.

- [66] RP Prickett, E Mayer, and J Hermel. Water hammer in a spacecraft propellant feed system. *Journal of Propulsion and Power*, 8(3):592–597, 1992. doi: 10.2514/3.23519.
- [67] Renaud Lecourt and Johan Steelant. Experimental investigation of waterhammer in simplified feed lines of satellite propulsion systems. *Journal of Propulsion and Power*, 23(6):1214–1224, 2007. doi: 10.2514/1.29269.
- [68] Marcos Lema, Johan Steelant, Fernando López Peña, and Patrick Rambaud. Multiphase fluid hammer in spacecraft propulsion systems. In *47th AIAA/ASME/SAE/ASEE Joint Propulsion Conference & Exhibit*, page 5683, 2011. doi: 10.2514/6.2011-5683.
- [69] Walter Tam, Gary Kawahara, Donald Jaekle, Jr, and Laurie Larsson. Design and manufacture of a propellant tank assembly. In *36th AIAA/ASME/SAE/ASEE Joint Propulsion Conference and Exhibit*, page 3444, 1997. doi: 10.2514/6.1997-2813.
- [70] Titanium ti-6al-4v (grade 5), annealed. <http://asm.matweb.com/search/SpecificMaterial.asp?bassnum=MTP641>. Accessed:06-01-2021.
- [71] Thomas Henry Gordon Megson. *Aircraft structures for engineering students*. Butterworth-Heinemann, Oxford, United Kingdom, 2013.
- [72] Titanium ti-6al-4v (grade 5), solution treated and aged. http://www.matweb.com/search/datasheet_print.aspx?matguid=b350a789eda946c6b86a3e4d3c577b39. Accessed:14-05-2021.
- [73] Aisi type 304l stainless steel. http://www.matweb.com/search/datasheet_print.aspx?matguid=e2147b8f727343b0b0d51efe02a6127e. Accessed:14-05-2021.
- [74] 301 stainless steel. <http://www.matweb.com/search/datasheet.aspx?matguid=0cf4755fe3094810963eaa74fe812895>. Accessed:14-05-2021.
- [75] Jason W Hartwig. A detailed historical review of propellant management devices for low gravity propellant acquisition. In *52nd AIAA/SAE/ASEE Joint Propulsion Conference*, page 4772, 2016. doi: 10.2514/6.2016-4772.
- [76] Jason W Hartwig. Propellant management devices for low-gravity fluid management: past, present, and future applications. *Journal of Spacecraft and Rockets*, 54(4):808–824, 2017.
- [77] W Tam, G Kawahara, K Wlodarczyk, H Gutierrez, and D Kirk. Review of atk diaphragm tanks—an update. In *Proceedings of the Space Propulsion Conference, 2018, Seville, Spain*, 2018.
- [78] Christian B Carpenter, Derek Schmuland, Jon Overly, and Robert Masse. Cubesat modular propulsion systems product line development status and mission applications. In *49th AIAA/ASME/SAE/ASEE Joint Propulsion Conference*, page 3760, 2013. doi: 10.2514/6.2013-3760.
- [79] Steven H Collicott, Emily A Beckman, and Praveen Srikanth. Conformal tanks: Small-sat propellant management technology. In *AIAA Propulsion and Energy 2019 Forum*, page 3874, 2019.
- [80] D Jaekle, JR. Propellant management device conceptual design and analysis: sponges. In *29th Joint Propulsion Conference and Exhibit*, 1993.
- [81] D JAEKLE, JR. Propellant management device conceptual design and analysis-vanes. In *27th Joint Propulsion Conference and Exhibit*, page 2172, 1991.
- [82] Peter Fortescue, Graham Swinerd, and John Stark. *Spacecraft systems engineering*. John Wiley & Sons, 2011.
- [83] Mylar (R) Polyester Film physical-thermal properties. http://usa.dupontteijinfilms.com/wp-content/uploads/2017/01/Mylar_Physical_Properties.pdf. Accessed: 31-08-2021.

- [84] Hydrazine - substance information. <https://echa.europa.eu/substance-information/-/substanceinfo/100.005.560>. Accessed:18-02-2021.
- [85] Robert L Bayt. Analysis, fabrication and testing of a mems-based micropropulsion system. Technical report, Aerospace Computational Design Laboratory, Dept. of Aeronautics ..., 1999.
- [86] Bradford ECAPS bradford ecaps - products - 100 mn hpgp thruster. <https://www.ecaps.space/products-100mn.php>, . Accessed: 1-Dec-2020.
- [87] Robert Masse, May Allen, Ronald Spores, and Elizabeth A Driscoll. Af-m315e propulsion system advances and improvements. In *52nd AIAA/SAE/ASEE Joint Propulsion Conference*, page 4577, 2016.
- [88] Busek busek green monoprop thrusters. http://busek.com/technologies_greenmonoprop.htm, . Accessed: 1-Dec-2020.
- [89] Busek bgt-x5 green monopropellant thruster (70008517e.pdf). http://busek.com/index_htm_files/70008517E.pdf, . Accessed: 1-Dec-2020.
- [90] Aro: Aurora resistojet one. <https://aurorapt.fi/downloads/ARO.pdf>, . Accessed:17-03-2021.
- [91] Moog: Cold gas thrusters. https://www.moog.com/content/dam/moog/literature/Space_Defense/spaceliterature/propulsion/moog-coldgasthrusters-datasheet.pdf, . Accessed:16-03-2021.
- [92] Valcor engineering pressure regulator valves. https://www.valcor.com/valcor-technical-datasheets/valcor_missiles_space_regulators_space.pdf. Accessed:17-01-2021.
- [93] Moog proportional flow control valve (pfcv). https://www.moog.com/content/dam/moog/literature/Space_Defense/spaceliterature/propulsion/moog-proportional-flow-control-valve-datasheet.pdf, . Accessed:17-01-2021.
- [94] Pelle Rangsten, Johan Bejhed, Håkan Johansson, Maria Bendixen, Kerstin Jonsson, and Tor-Arne Grönland. Advanced mems components in closed-loop micro propulsion applications. In *Proceedings of the 26th Annual AIAA/USU Small Satellites Conference, Logan, UT*, 2012.
- [95] Spv187 solenoid valve. <https://marotta.com/wp-content/uploads/2020/09/SPV187.pdf>. Accessed:01-05-2021.
- [96] Eui-Hyeok Yang, Choonsup Lee, Juergen Mueller, and Thomas George. Leak-tight piezoelectric microvalve for high-pressure gas micropropulsion. *Journal of Microelectromechanical systems*, 13(5):799–807, 2004. doi: 10.1109/JMEMS.2004.835767.
- [97] Michael Tsay, John Frongillo, Derek Lafko, and Jurg Zwahlen. Development status and 1u cube-sat application of busek's 0.5 n green monopropellant thruster. In *Proceedings of the 28th Annual AIAA/USU Small Satellites Conference, Logan, UT*, 2014.
- [98] Michael Tsay, Derek Lafko, Jurg Zwahlen, and William Costa. Development of busek 0.5 n green monopropellant thruster. 2013.
- [99] James A Richard. Slm produced hermetically sealed isolation valve. In *Aerospace Mechanisms Symposium*, 2014.
- [100] Juergen Mueller, Stephen Vargo, David Bame, Dennis Fitzgerald, and William Tang. Proof-of-concept demonstration of a micro-isolation valve. In *35th Joint Propulsion Conference and Exhibit*, page 2726, 1999. doi: 10.2514/6.1999-2726.
- [101] Arianespace space propulsion valves. <https://www.space-propulsion.com/brochures/valves/space-propulsion-valves.pdf>. Accessed:18-01-2021.

- [102] Juergen Mueller, Eui-Hyeok Yang, Amanda A Green, Victor White, Indrani Chakraborty, and Robert H Reinicke. Design and fabrication of mems-based micropropulsion devices at jpl. In *Reliability, Testing, and Characterization of MEMS/MOEMS*, volume 4558, pages 57–71. International Society for Optics and Photonics, 2001.
- [103] VACCO space products - low pressure latch valves. https://www.vacco.com/images/uploads/pdfs/latch_valves_low_pressure.pdf, . Accessed: 23-Jul-2021.
- [104] VACCO space products - high pressure latch valves. https://www.vacco.com/images/uploads/pdfs/latch_valves_high_pressure.pdf, . Accessed: 23-Jul-2021.
- [105] Omnidea-rtg product catalog. http://www.omnidea-rtg.de/site/images/stories/Downloads/Omnidea-RTG_Catalogue_Feb2016.pdf. Accessed:17-01-2021.
- [106] VACCO space products - low pressure fill/drain valves. https://www.vacco.com/images/uploads/pdfs/fd_low_pressure.pdf, . Accessed: 28-Jul-2021.
- [107] VACCO space products - low pressure fill/drain valves. https://www.vacco.com/images/uploads/pdfs/fd_low_pressure.pdf, . Accessed: 23-Jul-2021.
- [108] VACCO all metal filters. https://www.vacco.com/images/uploads/pdfs/VACCO_Filtration_Catalog_042121_FINAL_with_bookmarks_web.pdf, . Accessed: 28-Jul-2021.
- [109] Peter Friedhoff, Alisa Hawkins, John Carrico, Jonathan Dyer, and Kjell Anflo. On-orbit operation and performance of ammonium dinitramide (adn) based high performance green propulsion (hpgp) systems. In *53rd AIAA/SAE/ASEE Joint Propulsion Conference*, page 4673, 2017.
- [110] RS Pro iec mineral insulated thermocouples – 0.5mm grounded junction for fast response. <https://docs.rs-online.com/0a7f/0900766b815bb421.pdf>. Accessed: 17-08-2021.
- [111] GP50 miniature pressure transducer. https://www.gp50.com/wp-content/uploads/2021/07/A5SL-120_7000_RwA-1.pdf. Accessed: 17-08-2021.
- [112] Aerojet Rocketdyne cubesat mod prop-2sided. <https://www.rocket.com/sites/default/files/documents/CubeSat%20Mod%20Prop-2sided.pdf>. Accessed: 30-Nov-2020.
- [113] NanoAvionics cubesat propulsion system epss. <https://nanoavionics.com/cubesat-components/cubesat-propulsion-system-epss/>, . Accessed: 27-09-2021.
- [114] Vacco Space Products standard micro propulsion system. https://www.vacco.com/images/uploads/pdfs/MiPS_standard_0714.pdf, . Accessed: 2-Dec-2020.
- [115] Malte Wurdak, Friedolin Strauss, Lukas Werling, Helmut Ciezki, Dirk Greuel, Robert Lechler, Niklas Wingborg, Dov Hasan, and C. Scharlemann. Determination of fluid properties of the green propellant flp-106 and related material and component testing with regard to applications in space missions. In *Proceedings of the Space Propulsion Conference 2012 in Bordeaux, France*, 05 2012.
- [116] A Cervone, B Zandbergen, DC Guerrieri, M De Athayde Costa e Silva, I Krusharev, and H van Zeijl. Green micro-resistojet research at delft university of technology: new options for cubesat propulsion. *CEAS Space Journal*, 9(1):111–125, 2017.
- [117] Keita Nishii, Jun Asakawa, Kosei Kikuchi, Mariko Akiyama, Qihang Wang, Masaya Murohara, Yasuho Ataka, Hiroyuki Koizumi, Ryu Funase, and Kimiya Komurasaki. Flight model development and ground demonstration of water resistojet propulsion system for cubesats. *Transactions of the Japan Society for Aeronautical and Space Sciences*, 63(4):141–150, 2020.
- [118] Andrew D Ketsdever and Michael M Micci. *Micropropulsion for small spacecraft*. American Institute of Aeronautics and Astronautics, 2000.

- [119] Flightworks, inc. product datasheet - m-series (magnetic drive gear pumps) models 2212-m04c49/c50/c51. [https://products.flightworksinc.com/Asset/Product%20Data%20Sheet%20\(2212-M04C49.C50.C51\).pdf](https://products.flightworksinc.com/Asset/Product%20Data%20Sheet%20(2212-M04C49.C50.C51).pdf), . Accessed:2-04-2021.
- [120] Flightworks, inc. product datasheet - m-series (magnetic drive gear pumps) models 2212-m03c01/c03/c05. [https://products.flightworksinc.com/Asset/Product%20Data%20Sheet%20\(2204-M03C01.C03.C05\).pdf](https://products.flightworksinc.com/Asset/Product%20Data%20Sheet%20(2204-M03C01.C03.C05).pdf), . Accessed:22-04-2021.
- [121] Malte Wurdak, Friedolin Strauss, Lukas Werling, Helmut K Ciezki, Dirk Greuel, Robert Lechler, Niklas Wingborg, Dov Hasan, and Carsten Scharlemann. Determination of fluid properties of the green propellant flp-106 and related material and component testing with regard to applications in space missions. In *Space Propulsion Conference, Bordeaux, France*, 2012.
- [122] Anilkumar G. Gaonkar and Ronald D. Neuman. The uncertainty in absolute values of surface tension of water. *Colloids and Surfaces*, 27(1):1–14, 1987. ISSN 0166-6622. doi: [https://doi.org/10.1016/0166-6622\(87\)80324-4](https://doi.org/10.1016/0166-6622(87)80324-4). URL <https://www.sciencedirect.com/science/article/pii/0166662287803244>.
- [123] Steven P Berg and Joshua L Rovey. Assessment of multimode spacecraft micropropulsion systems. *Journal of Spacecraft and Rockets*, 54(3):592–601, 2017.
- [124] Royal Chemical Society silicon - element information, properties and uses | periodic table. <https://www.rsc.org/periodic-table/element/14/silicon>. Accessed: 11-08-2021.
- [125] Cubesat design specification 1-12u cubesats. <https://static1.squarespace.com/static/5418c831e4b0fa4ecac1bacd/t/5f24997b6deea10cc52bb016/1596234122437/CDS+REV14+2020-07-31+DRAFT.pdf>. Accessed:14-05-2021.



Requirements

A.1. Main Propulsion System Requirements

Req. ID	Type ¹	Identifier	Text	Rationale	Verif. method ²
PROP.010	FUN	Overall Δv	The propulsion system shall provide a minimum $\Delta v = 200 \text{ m}\cdot\text{s}^{-1}$ for station-keeping and orbital transfer.	From Δv budget (including all dictated margins as per ESA margin policy).	R
PROP.020	FUN	EOL Δv	The propulsion system shall allow for a minimum $\Delta v = 3 \text{ m}\cdot\text{s}^{-1}$ to remain available at the end of the mission for EOL manoeuvres.	From Δv budget and EOL strategy.	R
PROP.050	FUN	Max. thrust	The thrust delivered by each thruster shall be no more than 1000 mN.	For minimising transfer time without undesired unbalancing effects (Phase-0, CDF).	R, T
PROP.051	FUN	Number of thrusters	The number of main thrusters shall be 2, placed symmetrically with respect to the spacecraft principal axis of inertia.	To allow for compensation of misalignment effects.	R
PROP.052	FUN	Throttleability	Each thruster shall be throttleable within a range of no less than $\pm 10\%$ of the nominal thrust.	To facilitate compensation of undesired torques (such as those caused by misalignment effects).	R, T
PROP.053	FUN	Min. thrust	The thrust delivered by each thruster shall be more than 100 mN.	To allow for quasi-impulsive manoeuvres (from Phase-0 and CDF studies).	R, T
PROP.060	FUN	Thrust time	The propulsion system shall have a maximum thrusting time of 60 min per manoeuvre. Maximum manoeuvre time is the Stable Manifold Injection Manoeuvre (SMIM) with a Δv of $73 \text{ m}\cdot\text{s}^{-1}$.	Maximum estimated thrusting time for a quasi-impulsive manoeuvre. From Phase-0 and CDF studies. Can be split in shorter thrust times separated by non-firing intervals, if preferable.	R, A
PROP.070	OPS	Lifetime	The propulsion system shall have an operational life in space of at least 1.5 years.	Operational lifetime constraints.	R

¹FUN: Functional, DES = Design, OPS = Operations, ENV = Environmental, CON = Constraints, PHY = Physical

²R = Review-of-Design (ROD), A = Analysis (including similarity), T = Test (including demonstration), I = Inspection

Req. ID	Type	Identifier	Text	Rationale	Verif. method
PROP.080	ENV	External Environment	The propulsion system shall be able to operate in a vacuum external environment.	Environmental constraints.	R, A
PROP.090	ENV	Thermal Environment	The propulsion system shall be operational in the temperature range between 278 K and 323 K.	Required temperature range to allow safe operation of the thruster.	R, A
PROP.091	ENV	Non-Operational Temperature	The complete propulsion system shall withstand a non-operational temperature in the range between 273 K and 313 K, eventually using its own thermal control if the spacecraft thermal control is not sufficient.	Required temperature range to allow safe propellant storage.	R, A
PROP.100	CON	Volume	The propulsion system shall have a maximum volume of 5U (CubeSat form factor).	From spacecraft volume budget.	R, A
PROP.110	CON	Mass	The propulsion system shall have a wet mass of no more than 6 kg.	From spacecraft mass budget.	R, A
PROP.120	CON	Power Consumption	The propulsion system shall require a total power of no more than 10 W during firing, 25 W for preheating, and 1 W during standby.	From spacecraft power budget.	R, T
PROP.124	CON	Electrical Interface	The propulsion system shall operate at a voltage of no more than 32 V, and allow for switching to lower voltage to keep the thrust valve open (when needed).		R
PROP.130	FUN	Response Time	The propulsion system shall reach steady state conditions in less than 2 s after the thrust valve opening command is sent.	To ensure fast operations when required.	R, T
PROP.150	FUN	Number of Restarts	The propulsion system shall be able to be restarted for a minimum of 500 times.	Assuming one restart per day + margins.	R, A
PROP.160	CON	Maximum Pressure	The pressure in all components of the propulsion system shall be no more than 50 bar.	From launch and safety constraints.	R, A
PROP.161	CON	Pressure Drop	The pressure drop between propellant tank and thruster shall be less than 0.1 bar.	Typical pressure drop value in micro-propulsion systems.	R, A
PROP.162	CON	Burst Pressure	All propulsion system components shall be designed based on a burst factor of at least 2.5.	From safety constraints.	R, A
PROP.170	CON	Passivation	The propulsion system shall allow for spacecraft passivation, by releasing all remaining propellant.	From safety constraints.	R
PROP.180	CON	Tank Sensors	The propulsion system shall include sensors to continuously monitor the pressure and temperature in the propellant tank.	To allow for propulsion system telemetry.	R
PROP.190	CON	Propellant Toxicity	The propellants shall not include any substance that is classified as toxic according to the REACH regulations.	From safety constraints.	R

Req. ID	Type	Identifier	Text	Rationale	Verif. method
PROP.191	CON	Propellant compatibility	All propulsion system components shall be compatible to the propellants used by the system.		R
PROP.200	CON	Volume	Payload reserved volume not to be used by any propulsion system components: 3U in length (one quarter of the bus).	Payload volume reservation.	R

A.2. Reaction Control System Requirements

Req. ID	Type	Identifier	Text	Rationale	Verif. method
RCS.030	FUN	Overall Total Impulse	The RCS propulsion system shall provide a minimum Total Impulse for all RCS tasks of 110 Ns (if the Aurora ARM-A system is used), or 170 Ns (if the GomSpace 6DOF system is used). The custom system shall provide a worst-case total impulse of 170 N-s.	From Attitude control strategy (including all dictated margins as per ESA margin policy). Note that the required total impulse depends on the characteristics of the system used (thrust, placement of thrusters etc.)	R
RCS.050	FUN	Thrust	The thrust delivered by each RCS thruster shall be in the range 1-10 mN.	To allow for an optimum RCS strategy.	R, T
RCS.051	FUN	Number of Thrusters	The number of RCS thrusters shall be no less than 4.	Minimum number of RCS thrusters that theoretically allows for 3-axis operation. In practice, 6-12 RCS thrusters are probably preferable.	R
RCS.070	OPS	Lifetime	The RCS propulsion system shall have an operational life in space of at least 1.5 years.	Operational lifetime constraints.	R
RCS.080	ENV	External Environment	The RCS propulsion system shall be able to operate in a vacuum external environment.	Environmental constraints.	R, A
RCS.090	ENV	Thermal Environment	The RCS propulsion system shall be operational in the temperature range between 278 K and 308 K .	Required temperature range to allow safe operation of the thruster.	R, A
RCS.091	ENV	Non-Operational Temperature	The RCS propulsion system shall withstand a non-operational temperature in the range between 273 K and 313 K, eventually using its own thermal control if the spacecraft thermal control is not sufficient.	Required temperature range to allow safe propellant storage.	R, A
RCS.100	CON	Volume	The RCS propulsion system shall have a maximum volume of 1U (CubeSat form factor).	From spacecraft volume budget	R, A
RCS.110	CON	Mass	The RCS propulsion system shall have a wet mass of no more than 1 kg.	From spacecraft mass budget.	R, A
RCS.120	CON	Power Consumption	The RCS propulsion system shall require a power of no more than 25 W during operation, and no more than 0.5 W during standby	From spacecraft power budget.	R, T
RCS.124	CON	Electrical Interface	The RCS propulsion system shall operate at a voltage between 3.3 and 16V.		R
RCS.140	FUN	Impulse Bit	The RCS propulsion system shall be able to provide a minimum impulse bit of 2 mNs.	For precision manoeuvres (from Phase-0 and CDF studies).	R, T
RCS.150	FUN	Number of Restarts	The RCS propulsion system shall be able to be restarted for a minimum of 2000 times.	Assuming five restarts per day + margins.	R, A
RCS.160	CON	Maximum Pressure	The pressure in all components of the RCS propulsion system shall be no more than 50 bar.	From launch and safety constraints.	R, A

Req. ID	Type	Identifier	Text	Rationale	Verif. method
RCS.161	CON	Pressure Drop	The pressure drop between propellant tank and thruster shall be less than 0.1 bar.	Typical pressure drop value in micro-propulsion systems.	R, A
RCS.162	CON	Burst Pressure	All RCS propulsion system components shall be designed based on a burst factor of at least 2.5.	From safety constraints.	R, A
RCS.170	CON	Passivation	The RCS propulsion system shall allow for spacecraft passivation, by releasing all remaining propellant.	From safety constraints.	R
RCS.180	CON	Tank Sensors	The RCS propulsion system shall include sensors to continuously monitor the pressure and temperature in the propellant tank.	To allow for propulsion system telemetry.	R
RCS.190	CON	Propellant Toxicity	The propellants shall not include any substance that is classified as toxic according to the REACH regulations.	From safety constraints.	R
RCS.191	CON	Propellant Compatibility	All RCS propulsion system components shall be compatible to the propellants used by the system.		R
RCS.200	CON	Volume	Payload reserved volume not to be used by any propulsion system components: 3U in length (one quarter of the bus).	Payload volume reservation.	R

A.3. ECSS Requirements

A.3.1. Sourced From Tailored Requirements of ECSS-E-ST-35-01C

Req. ID	Type	Identifier	Text	Rationale	Verif. method
ECSS.020	CON	Fluid Hammer	Evaluation shall be performed to confirm no water hammer issues and ensure proper propulsion system functioning. This shall include assessment of worst case pressure transients.		R, A
ECSS.060	FUN	Separation of Blocks	If the flight version of the system is divided into independent blocks, they should be separated by safety barriers such as pyrovalves, latch valves or burst membranes.		R
ECSS.080	FUN	Draining	The system design shall allow for on-ground draining.		R
ECSS.090	CON	Draining	The location of fill-and-drain valves and piping layout shall prevent contact between dissimilar fluids.		R
ECSS.100	FUN	Filters	All filters used at system or component level shall be designed and positioned according to the results of contaminant control and reliability studies.		R, A
ECSS.110	FUN	Filters	Filters shall be installed immediately downstream of potential particle generating components and, depending on the result of the failure risk analysis, directly upstream of components sensitive to pollution or contamination. NOTE: For example: actuation valves, pressure regulators, injectors and thrusters.		R
ECSS.120	FUN	Propellant Tanks	To avoid propellant freezing and control propellant tank pressures, the tank and line temperatures shall be controlled during the whole mission.		R, A
ECSS.130	CON	Blow-Down	For propulsion systems working in blow-down mode, the ratio of pressurant volume between BOL and EOL shall be consistent with thruster specifications. NOTE: For example: Isp, combustion stability and mixture ratio shift.		R, A

A.3.2. Sourced From Tailored Requirements of ECSS-E-ST-35C Rev. 1

Req. ID	Type	Identifier	Text	Rationale	Verif. method
ECSS.140	FUN	Instrumentation	Redundant functional transducers shall be installed.		R

A.4. Miscellaneous Requirements

Req. ID	Type	Identifier	Text	Rationale	Verif. method
PLD.150	PHY	Maximum size	The maximum size of the payload shall be 98 mm X 98 mm X 290 mm.	Size constraint	T
SYS.040	CON	ITAR	The system shall be free of components as described in ITAR Regulations.	To comply with European law and allow exporting of the satellite.	R
SYS.050	CON	Total mass	The integrated system shall have a mass of ≤ 26 [kg] (TBC).	Estimate on maximum capacity of 12U XL deployers.	I
SYS.060	CON	12U Standard	In the launch configuration, the satellite shall comply with the 12U standard.	To be compatible with 12U deployers.	I

B

State-of-the-Art Propulsion Systems and Thrusters (COTS and Experimental)

#	Type ¹	Name	Company/ institute	I_{sp} (s) ²	F_T (N)	P_{el} (W) ³	Propellant	Ref.
1	CGT	SNAP1	SSTL, UK	43	0.05	n/a	Butane	[16]
2	CGT	CNAPS	UTIAS-SFL, CA	35	0.04	n/a	SF ₆	[16]
3	CGT	POPSAT-HIP1	Microspace Rapid, SI	43	0.001	n/a	Argon	[16]
4	CGT	MEMS CG	GOMSpace, DK	75	0.001	n/a	Methane	[16]
5	CGT	CPOD	VACCO, US	40	0.025	n/a	R134a	[16]
6	CGT	NANOPS	UTIAS-SFL, CA	45	0.05	n/a	SF ₆	[13]
7	CGT	MEMS	Aerospace Co. US	30	0.1	n/a	Xe	[13]
8	CGT	T3- μ PS	TNO/TUD/UT, NL	69	0.006	n/a	N ₂	[13]
9	CGT	MEPSI MiPS	VACCO, US	65	0.053	n/a	Isobutane	[13]
10	CGT	MiPS	VACCO, US	40	0.01	n/a	R134a	[13]
11	CGT	AFRL PUC	VACCO, US	47	0.0035	n/a	SO ₂	[13]
12	CGT	Custom	UTexas, US	64	0.11	n/a	R236fa	[13]
13	CGT	Microprop System	NanoSpace, SE	75	0.001	n/a	N ₂	[13]
14	CGT	MicroThruster	Marotta, IT	65	2.36	n/a	N ₂	[17]
15	CGT	Bevo-2 prop. sys	U. Texas, US	89	0.15	n/a	R236fa	[18]
16	CGT	58X125A	Moog, US	65	0.0044	n/a	N ₂	[14]
17	CGT	58E143-146	Moog, US	60	0.04	n/a	N ₂	[14]
18	CGT	58E142	Moog, US	57	0.12	n/a	N ₂	[14]
19	CGT	58E151	Moog, US	65	0.12	n/a	N ₂	[14]
20	CGT	58-118	Moog, US	65	3.6	n/a	N ₂	[14]
21	CGT	Butane Prop. Sys.	SSTL, UK	80	0.5	n/a	Butane	[17]
22	CGT	Nanoprop 3U	GomSpace/NanoSpace, DK	110	0.001	n/a	Butane	[17]
23	CGT	Nanoprop 6U	GomSpace/NanoSpace, DK	110	0.04	n/a	Butane	[17]
24	CGT	NanoProp 6DOF	GOMSpace, DK	50	0.01	n/a	Butane	[19]
25	CGT	MarCO MiPS	VACCO, US	40	0.025	n/a	R236fa	[20]

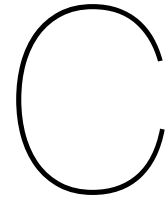
¹CGT = Cold Gas Thruster, CMP = Chemical Monopropulsion, CBP = Chemical Bi-propulsion, CHB = Chemical Hybrid, CSD = Chemical Solid, ETR = Electrothermal (resistojet), ESI = Electrostatic Ion, ESH = Electrostatic Hall, ESE = Electrostatic Electro spray/FEEP/Colloid, EDP = Electrodynamic Pulsed Plasma Thruster/Vacuum Arc Thruster/Magnetic Nozzle System.

²All reported I_{sp} are taken as vacuum values. For I_{sp} and F_T , the max. reported value is always taken.

³Power indicated as during firing/preheating/standby. n/a Indicates not available. Electric power consumption only considered for CMP (due to catalyst bed heating) and electric propulsion technology for preliminary review of technologies.

#	Type	Name	Company/ institute	I_{sp} (s)	F_T (N)	P_{el} (W)	Propellant	Ref.
26	CMP	GPIM	Aerojet, US	235	1.1	12/10/n/a	AF-M315E	[16], [21]
27	CMP	MPS-120 CHAMPS	Aerojet, US	215	0.26	11/0/10	Hydrazine	[16]
28	CMP	MPS-130 CHAMPS	Aerojet, US	235	0.25	11/0/10	AF-M315E	[16], [22]
29	CMP	HPGP 1N	ECAPS, SE	232	1	n/a/7.3/n/a	LMP-103s	[16], [23]
30	CMP	BGT-X1	Busek, US	214	0.1	n/a/4.5/n/a	AF-M315E	[16]
31	CMP	BGT-X5	Busek, US	225	0.5	n/a/20/n/a	AF-M315E	[16]
32	CMP	muprop system	VACCO/ECAPS, SE	258	0.1	n/a	LMP-103s	[13]
33	CMP	HPGP 0.1N	ECAPS, SE	200	0.1	n/a	LMP-103s	[13]
34	CMP	Hydros	Tethers Unl., US	258	0.6	n/a/10/n/a	Water	[13]
35	CMP	MR-103H	Aerojet, US	220	1.07	5/1.5/n/a	Hydrazine	[14]
36	CMP	HmNT	JPL, US	150	0.129	8/0.25/n/a	Hydrazine	[14]
37	CMP	MEMS	U. Cheng Kung, TW	162	0.00144	n/a	Hydrazine	[14]
38	CMP	Unnamed	ARC Seibersdorf, AT	153	0.8	n/a	H ₂ O ₂	[14]
39	CMP	Unnamed	U. Cheng Kung, TW	125	0.221	n/a/15/n/a	H ₂ O ₂	[14]
40	CMP	GR-1	Aerojet, US	231	1.42	8/14/n/a	AF-M315E	[17], [24]
41	CMP	GR-22	Aerojet, US	248	26.9	16/37/n/a	AF-M315E	[17], [24]
42	CMP	AMAC	Busek, US	225	0.425	n/a/20/n/a	AF-M315E	[17], [25]
43	CMP	MiPS	VACCO, US	190	0.4	0.055/n/a/15	LMP-103s	[17]
44	CMP	Integr. Prop. Sys.	VACCO, US	220	4	n/a	LMP-103s	[17]
45	CMP	ArgoMoon H-MiPS	VACCO, US	190	0.1	0.1/1/20	LMP-103s	[17], [26]
46	CMP	EPSS C1K	Nano Avionics, US	213	1	1/0.19/9.6	LMP-103s	[17], [27]
47	CMP	LFPS	GeorgiaTech, US	n/a	0.1	n/a	AF-M315E	[7]
48	CHB	Green Hybrid	Utah State, US	215	8	n/a	ABS, GOx	[17]
49	CHB	Unnamed	JPL, US	311	44	n/a	PMMA, GOx	[28]
50	CHB	Unnamed	Utah State, US	133	1	n/a	PMMA, GOx	[29]
51	CBP	MEMS	MIT, US	300	2.7	n/a	GOx, Ethanol	[14]
52	CBP	PM400	Hyperion Tech., NL	290	1	n/a	N ₂ O, Propane	[30]
53	CBP	PM200	Hyperion Tech., NL	285	0.5	12	Propene, N ₂ O	[31]
54	CSD	Isp30s	Aerospace Co. US	187	37	n/a	Al, NH ₄ ClO ₄	[16]
55	CSD	Star 4G	Orbital ATK, US	269	13	n/a	HIPEP-501A	[16]
56	CSD	CDM-1	DSSP, US	226	76	n/a	AP/HTPB	[16]
57	CSD	CAPS-3	DSSP, US	300	0.3	n/a	HIPEP-501A	[17]
58	CSD	STAR 5A	Orbital ATK, US	251	169	n/a	TP-H-3399	[14]
59	ETR	LPR	SSTL, UK	48	0.018	30	Xe	[16]
60	ETR	PUC	CU/Vacco, US	65	0.0054	15	SO ₂	[16], [32]
61	ETR	CHIPS	CU/Vacco, US	82	0.03	30	R134a, R236fa	[16]
62	ETR	AMR	Busek, US	150	0.01	15	Ammonia	[16]
63	ETR	CubeSat MEMS	NanoSpace, SE	92	0.001	2	Butane	[13]
64	ETR	FMMR	USC, US	79	0.000129	3.2	Water	[14]
65	ETR	ARM-A	Aurora, FI	100	0.004	20	Water	[33]
66	ESI	BIT-1	Busek, US	3200	0.00018	28	Xe, I ₂	[16]
67	ESI	BIT-3	Busek, US	2500	0.00115	75	I ₂	[16]
68	ESI	RIT- μ X	Airbus, DE	3000	0.0005	50	Xe	[16]
69	ESI	RIT-10-EVO	Airbus, DE	3200	0.025	145	Xe	[16]
70	ESI	MiXI	JPL, US	3100	0.0015	50	Xe	[13]
71	ESI	μ NRIT-2.5	Astrium, DE	2850	0.0005	35	Xe	[13]
72	ESI	MRIT	Penn. State. U., US	5480	0.00006	15	Ar	[14], [34]
73	ESI	1-COUPS	U. Tokyo, JP	1000	0.0003	38	Xe	[17], [35]
74	ESI	IFM Nano Thruster	Empulsion, AT	6000	0.0004	40	In	[17]
75	ESH	BHT-200	Busek, US	1390	0.0128	200	Xe, I ₂ , Kr	[16]
76	ESH	BHT-600	Busek, US	1530	0.0391	600	Xe, I ₂ , Kr	[16]
77	ESH	HT 100	Sitael, IT	1100	0.01	100	Xe, Kr	[16]
78	ESH	HT 400	Sitael, IT	1750	0.05	250	Xe	[16]
79	ESH	CHT	UTIAS-SFL, CA	1139	0.01	200	Xe, Ar	[16]

#	Type	Name	Company/ institute	I_{sp} (s)	F_T (N)	P_{el} (W)	Propellant	Ref.
80	ESH	SPT-30	Undefined	1370	0.013	258	Xe	[14]
81	ESH	Unnamed	MIT, US	865	0.0018	126	Xe	[14]
82	ESH	CHT 3.0	PPPL, US	1650	0.006	185	Xe	[14]
83	ESH	Halo	ExoTerra, US	1500	0.033	450 W	Xe	[36]
84	ESE	S-iEPS	MIT, US	1200	0.0001	1.5	Ionic liquid	[16]
85	ESE	TILE 5000	Accion, US	1800	0.0015	30	Ionic liquid	[16]
86	ESE	BET-1mN	Busek, US	800	0.0007	9	Ionic liquid	[16]
87	ESE	BET-100	Busek, US	1800	0.0001	5.5	Ionic liquid	[16]
88	ESE	IFM Nano	Enpulsion/Fotec, AT	6000	0.00035	40	In	[18]
89	ESE	ST-7	Busek, US	240	0.0000358	24.6	Ionic liquid	[14]
90	ESE	In-FEEp 100	ARC Seibersdorf, AT	12000	0.0001	10	In	[14]
91	ESE	GOCE MTA	ARC Seibersdorf, AT	12000	0.00065	52	In	[14]
92	ESE	In-FEEP 1000	ARC Seibersdorf, AT	12000	0.001	80	In	[14]
93	ESE	FEEP-5	Centrosazio, IT	9000	0.00004	2.7	Cs, In	[14]
94	ESE	FEEP-50	Centrosazio, IT	9000	0.0014	93	Cs, In	[14]
95	EDP	EO-1 PPT	Primex, US	1150	0.00014	12.5	PTFE	[16]
96	EDP	MPACS	Busek, US	830	0.000144	10	PTFE	[16]
97	EDP	BmP-220	Busek, US	536	0.00014	7.5	PTFE	[16]
98	EDP	μ CAT	GWU, US	3000	0.00002	10	Ni	[16]
99	EDP	UWE4 Arc Thruster	WU, DE	1100	0.00001	2	Ti, W	[16]
100	EDP	μ PPT	Busek, US	700	0.0005	2	PTFE	[13]
101	EDP	μ BLT	U. of Illinois, US	3000	0.000054	4	Al	[13], [37]
102	EDP	Dawgstar	U. Washington, US	266	0.000264	n/a	PTFE	[14]
103	EDP	PPTCUP	AAC-Clyde, UK	655	0.00004	2	PTFE	[17]
104	EDP	NanoSat PPT	AAC-Clyde, UK	640	0.00009	5	PTFE	[17]
105	EDP	Metal Plasma Thruster	Applied Sci. Corp., US	2400	0.0015	100	Al	[17]
106	EDP	RFT	Phase Four, US	498	0.00277	50	Xe	[13]
107	EDP	RFT	Phase Four, US	7852	0.00277	50	Water	[13]

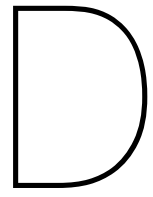


Flightworks, inc. Magnetically Coupled Micro-Gear Pumps

Data for continuous operation, heavy fuel, $\nu \approx 2 \text{ E-3 Pa-s}$ [56]. Determined graphically, some inaccuracies expected but data assumed sufficiently accurate for selection.

Model ID	Flow rate in ml/min, highest attainable Δp in psi (bar)		Mass (g)	Port diameter (mm)
	At ω_{min}	At ω_{max}		
2204-M03C01.C03.C05	1, 30 (2.068)	8, 30 (2.068)	65	3
2204-M03C40.C41.C42	2, 30 (2.068)	24, 30 (2.068)	75	3
2204-M03C58.C59.C60	2, 30 (2.068)	24, 30 (2.068)	90	3
2204-M03X05.X06.X07	2, 30 (2.068)	24, 30 (2.068)	105	3
2205-M03C01.C03.C05	1, 95 (6.550)	7, 125 (8.618)	65	3
2205-M03C40.C41.C42	1, 80 (5.516)	30, 125 (8.618)	70	3
2205-M03C58.C59.C60	1, 80 (5.516)	30, 125 (8.618)	90	3
2205-M03X05.X06.X07	1, 105 (7.240)	32, 125 (8.618)	105	3
2212-M04C01.C03.C05	12, 100 (6.895)	65, 100 (6.895)	125	3
2212-M04C10.C12.C15	1, 100 (6.895)	20, 200 (13.790)	140	3
2212-M04C40.C41.C42	25, 80 (5.516)	160, 80 (5.516)	130	3
2212-M04C49.C50.C51	1, 155 (10.687)	95, 250 (17.237)	175	3
2212-M04C58.C59.C60	1, 155 (10.687)	95, 250 (17.237)	150	3
2212-M04X01.X03.X04	1, 155 (10.687)	95, 250 (17.237)	175	3
2212-M04X05.X06.X07	1, 155 (10.687)	120, 180 (12.411)	160	3
2222-M04C10.C12.C15	20, 125 (8.618)	120, 125 (8.618)	140	3
2222-M04C49.C50.C51	25, 175 (12.066)	270, 175 (12.066)	175	3
2222-M04C58.C59.C60	25, 175 (12.066)	270, 175 (12.066)	150	3
2222-M04X01.X03.X04	30, 175 (12.066)	275, 175 (12.066)	180	3
2222-M04X05.X06.X07	65, 105 (7.240)	330, 105 (7.240)	160	3
2222-M04X10.X11	95, 175 (12.066)	350, 175 (12.066)	190	3
2232-M04C10.C12.C15	125, 80 (5.516)	225, 80 (5.516)	145	3
2232-M04C49.C50.C51	95, 125 (8.618)	490, 125 (8.618)	180	3
2232-M04C58.C59.C60	100, 105 (7.240)	500, 105 (7.240)	155	3
2232-M04X01.X03.X04	95, 125 (8.618)	490, 125 (8.618)	180	3
2232-M04X05.X06.X07	160, 40 (2.758)	575, 40 (2.758)	165	3
2232-M04X10.X11	170, 125 (8.618)	600, 125 (8.618)	195	3
2232H-M05C22.C23.C24	310, 100 (6.895)	440, 100 (6.895)	205	6
2232H-M05C49.C50.C51	240, 210 (6.895)	795, 210 (6.895)	210	6

Model ID	Flow rate in ml/min, highest attainable Δp in psi (bar)		Mass (g)	Port diameter (mm)
	At ω_{min}	At ω_{max}		
2232H-M05X01.X03.X04	325, 125 (8.618)	820, 125 (8.618)	225	6
2232H-M05X2	295, 225 (15.513)	795, 225 (15.513)	245	6
2232H-M05X10.X11	295, 225 (15.513)	795, 225 (15.513)	240	6
2232H-M05X12	295, 225 (15.513)	795, 225 (15.513)	290	6
2252-M05C49.C50.C51	520, 140 (9.653)	1300, 140 (9.653)	220	6
2252-M05X01.X03.X04	575, 65 (4.482)	1400, 65 (4.482)	235	6
2252-M05X02	500, 175 (12.066)	1300, 175 (12.066)	255	6
2252-M05X10.X11	520, 130 (8.963)	3400, 130 (8.963)	250	6
2252-M05X12	500, 175 (12.066)	1350, 175 (12.066)	300	6
2282-M05C49.C50.C51	950, 100 (6.895)	2300, 100 (6.895)	220	6
2282-M05X01.X03.X04	980, 60 (4.137)	2400, 60 (4.137)	235	6
2282-M05X02	900, 125 (8.618)	2400, 125 (8.618)	265	6
2282-M05X10.X11	900, 125 (8.618)	2400, 125 (8.618)	260	6
2282-M05X12	900, 125 (8.618)	2400, 125 (8.618)	300	6



CubeSat Standard

D.1. 12U CubeSat Design Specifications (Outer Dimensions)

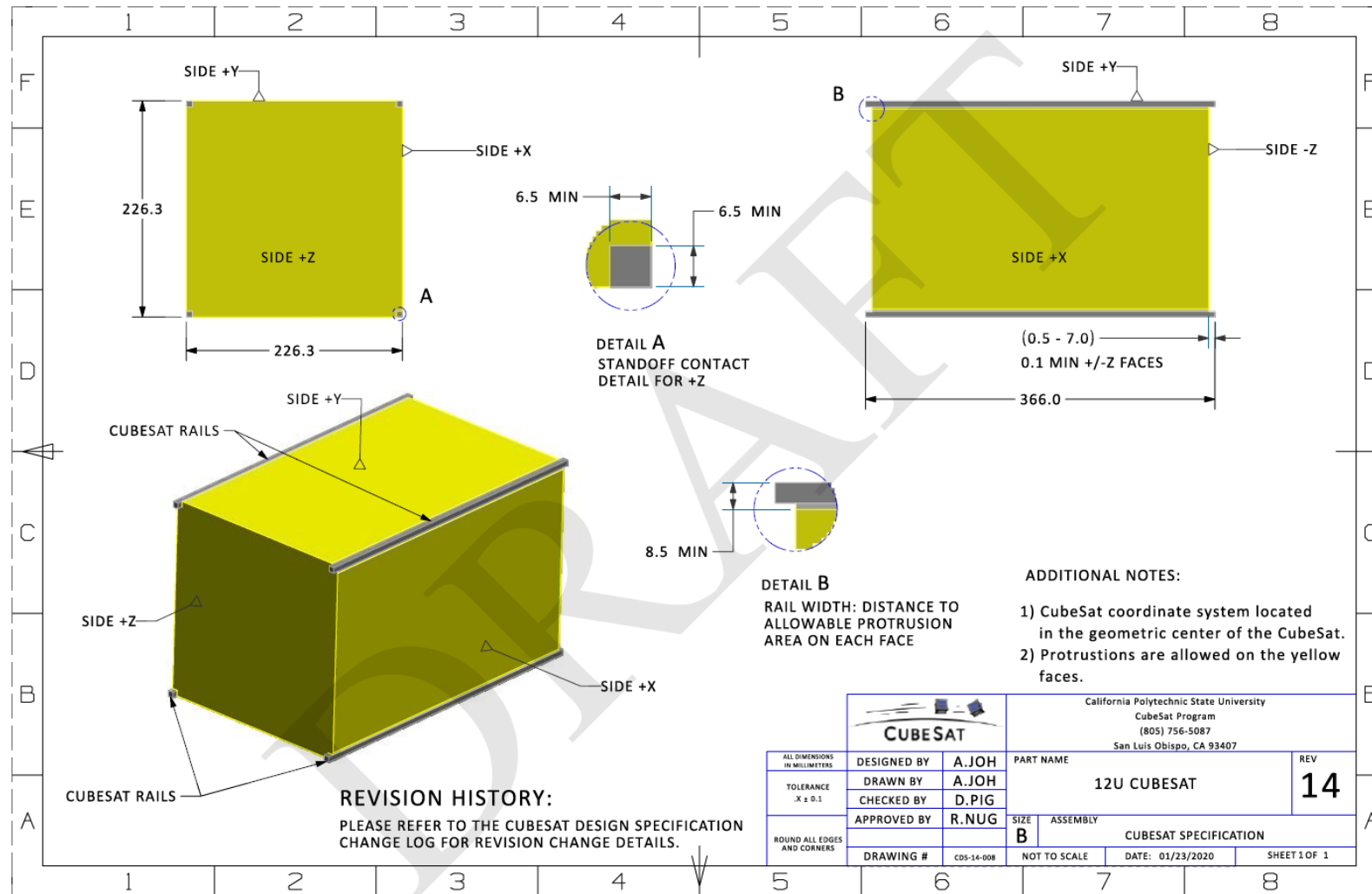


Figure D.1: CubeSat Design Specifications for a 12U CubeSat, captured from [125].

D.2. 12U CubeSat Design Specifications (Extra Volume)

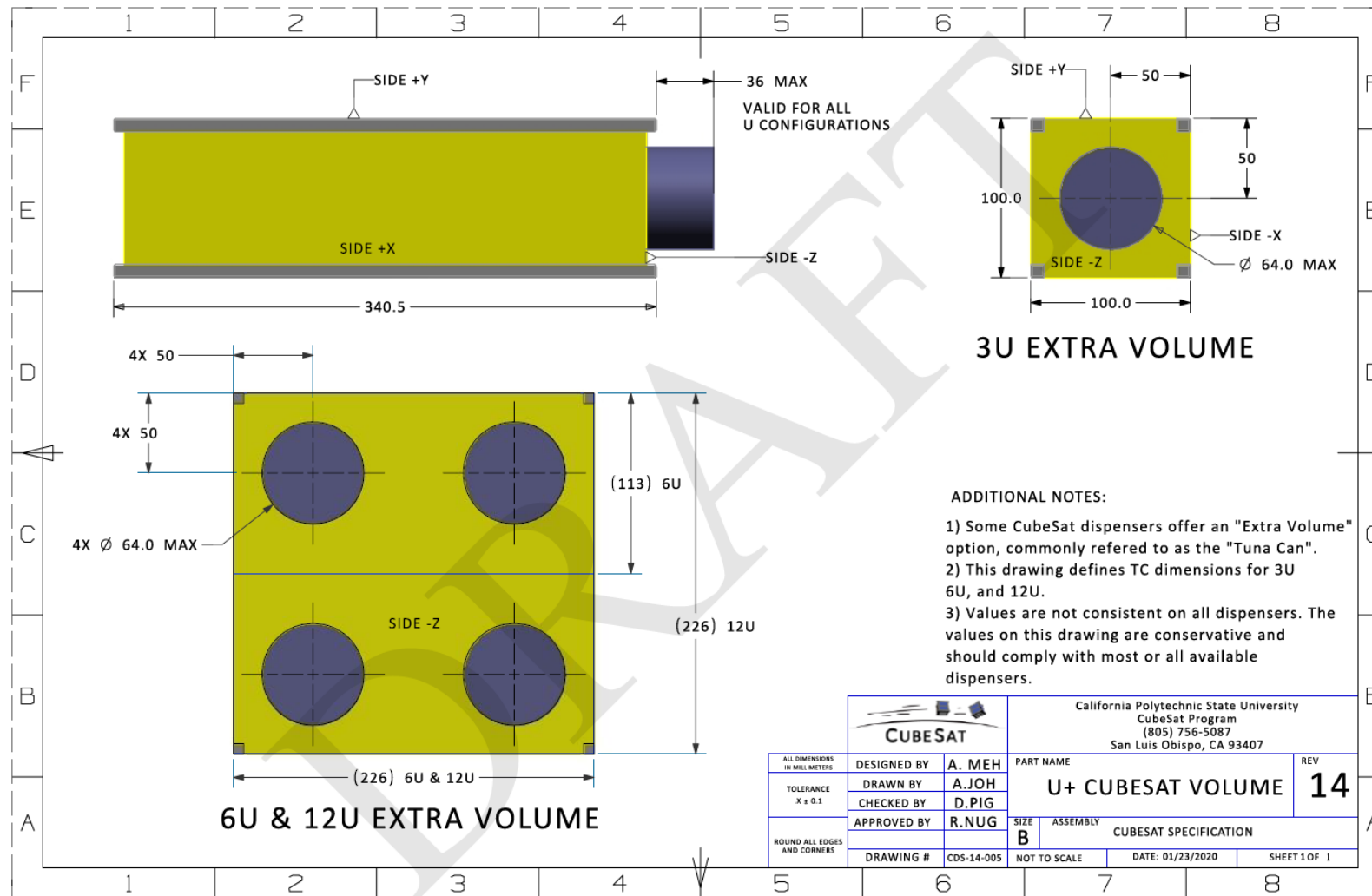
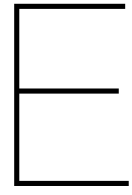


Figure D.2: CubeSat Design Specifications for CubeSats with extra volume, captured from [125].



Finite Element Analysis Results

E.1. Main Propulsion System

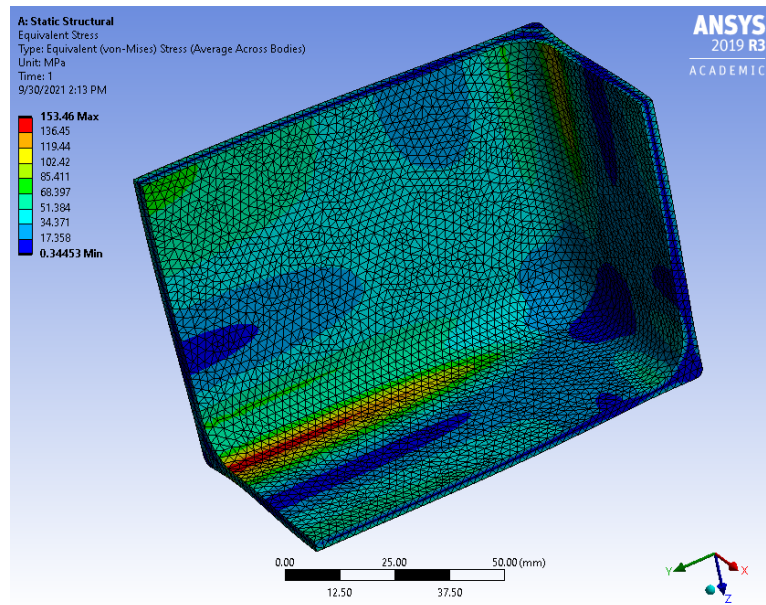


Figure E.1: Von Mises stresses. Maximum: 153.460 MPa, minimum: 0.344 MPa, ANSYS 2019.

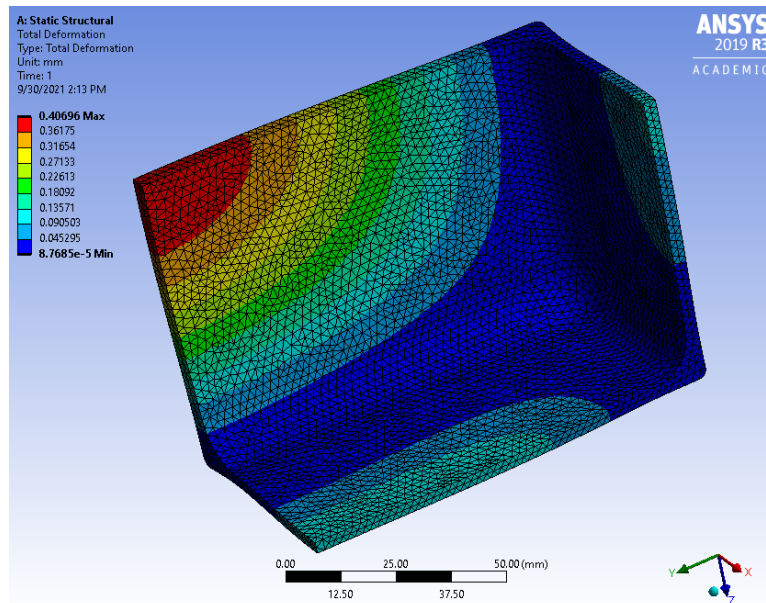


Figure E.2: Deformations. Maximum: 0.407 mm, minimum: 8.769 E-5 mm, ANSYS 2019.

E.1.1. Design Iteration: Reduction of Wall Thickness

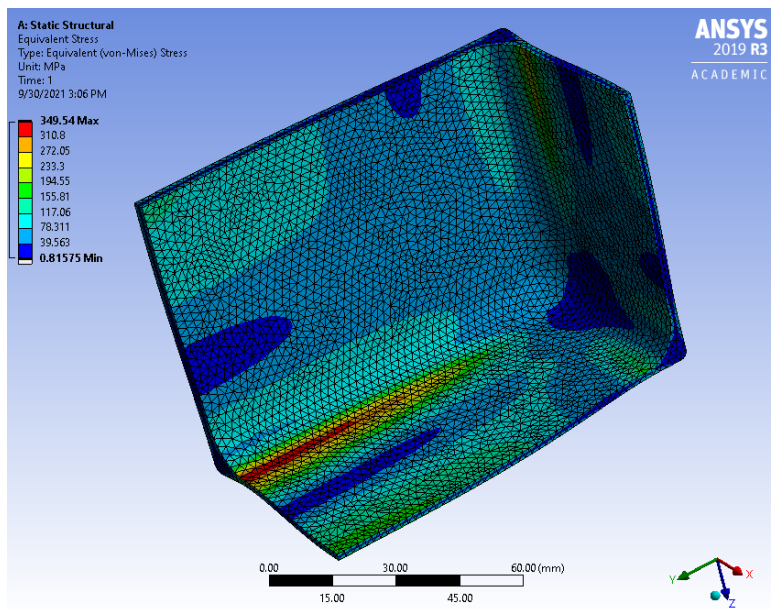


Figure E.3: Von Mises stresses after the first design iteration. Maximum: 349.540 MPa, minimum: 0.816 MPa, ANSYS 2019.

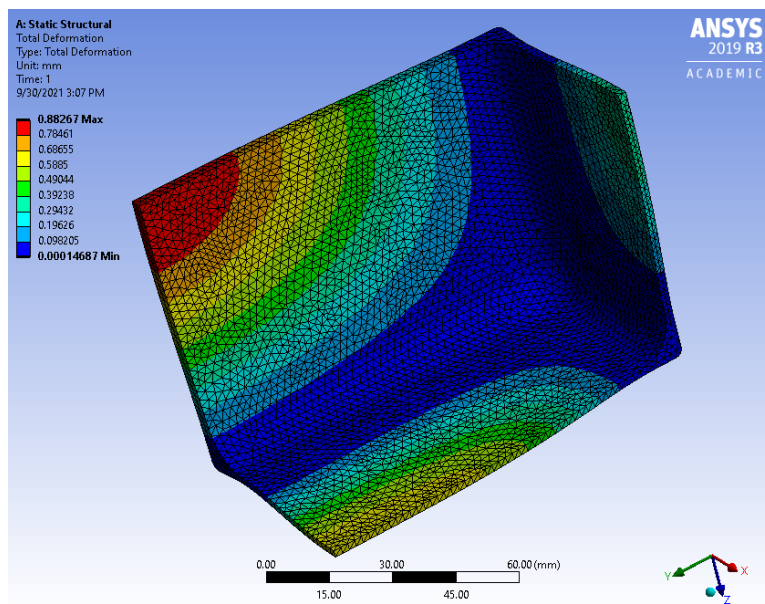


Figure E.4: Deformations after the first design iteration. Maximum: 0.883 mm, minimum: 1.467 E-4 mm, ANSYS 2019.

E.1.2. Sensitivity Analysis for FE-Analysis Element Size of 3 mm

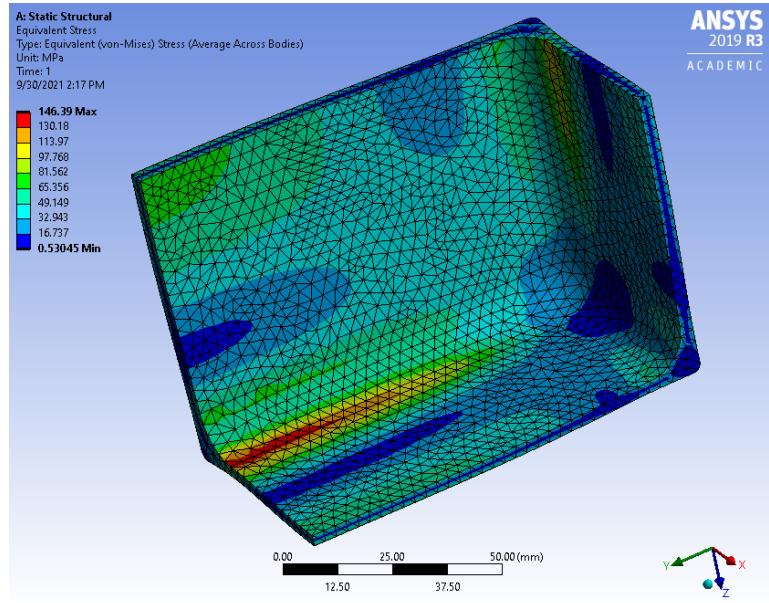


Figure E.5: Main Propulsion System tank FE-analysis Stress result for 3 mm element size, ANSYS 2019.

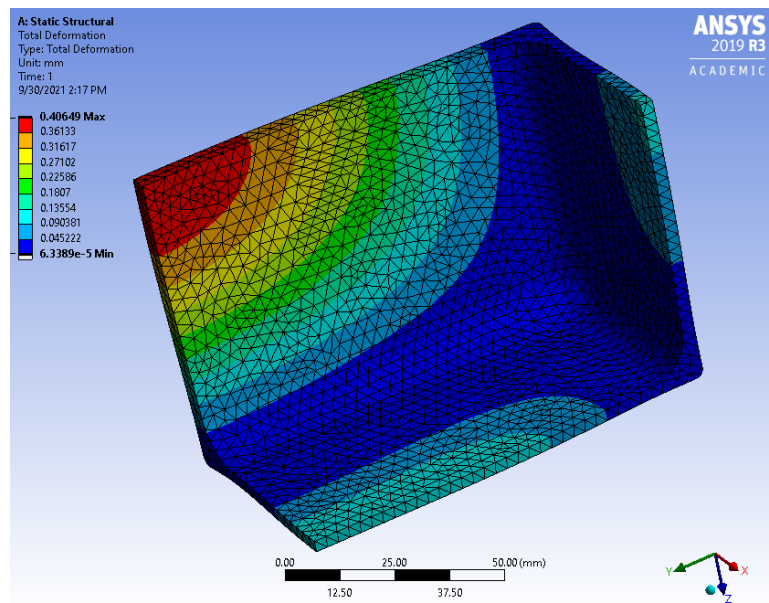


Figure E.6: Main Propulsion System tank FE-analysis Deformation result for 3 mm element size, ANSYS 2019.

Element Size of 5 mm

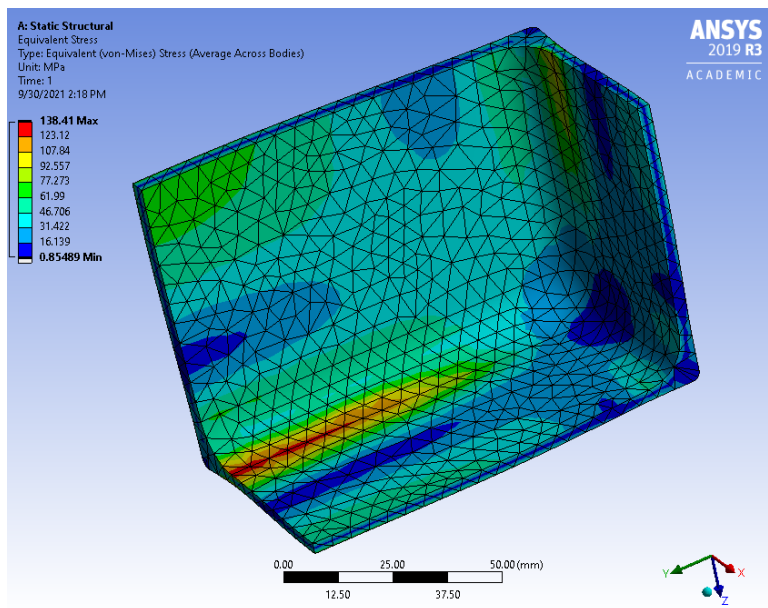


Figure E.7: Main Propulsion System tank FE-analysis Stress result for 5 mm element size, ANSYS 2019.

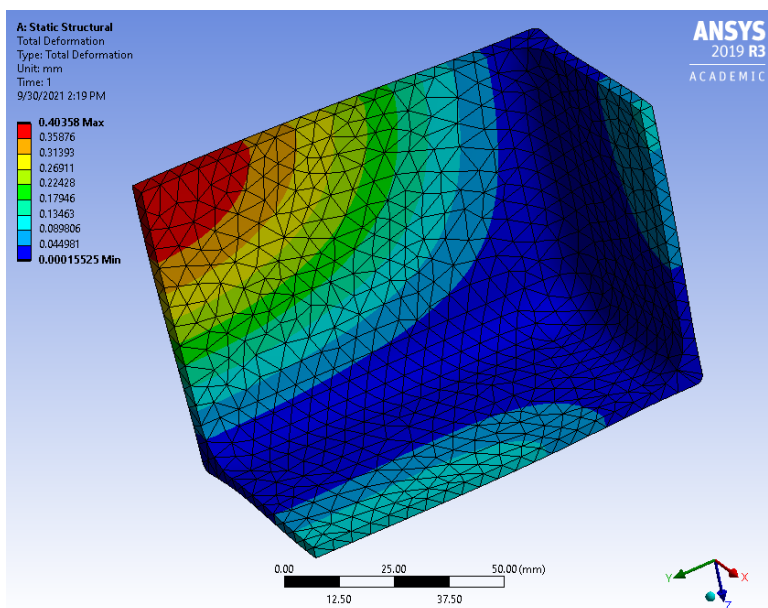


Figure E.8: Main Propulsion System tank FE-analysis Deformation result for 5 mm element size, ANSYS 2019.

Element Size of 10 mm

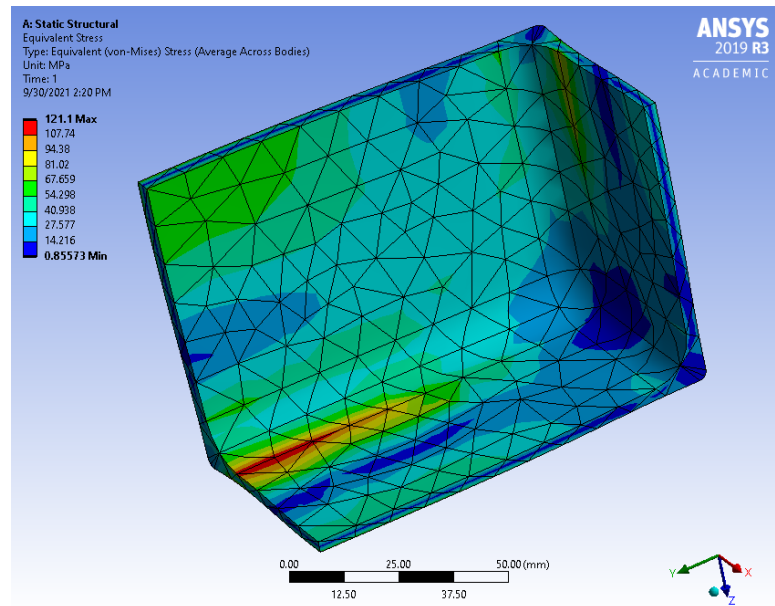


Figure E.9: Main Propulsion System tank FE-analysis Stress result for 10 mm element size, ANSYS 2019.

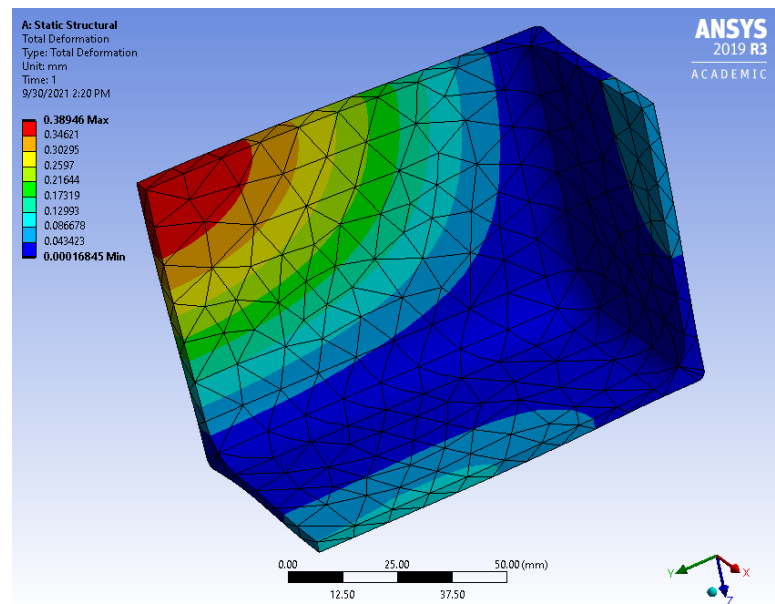


Figure E.10: Main Propulsion System tank FE-analysis Deformation result for 10 mm element size, ANSYS 2019.

Element Size of 3 mm - After Wall Thickness Reduction Iteration

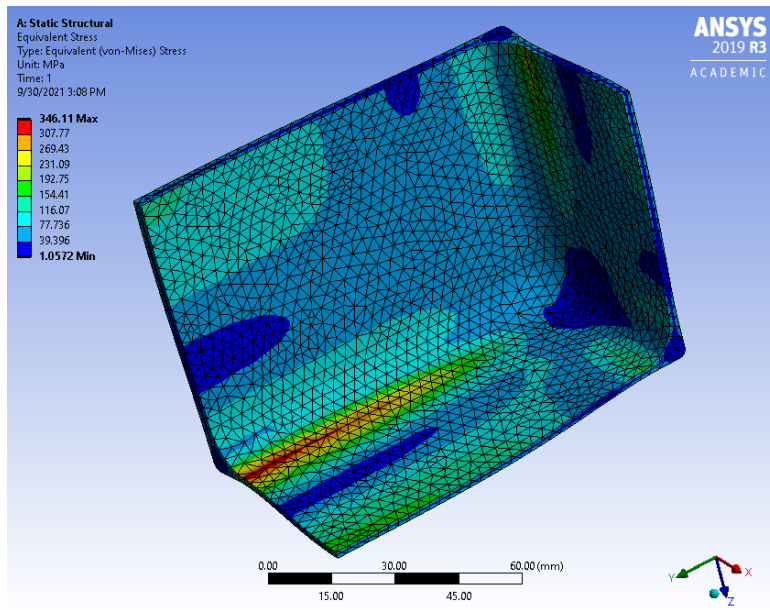


Figure E.11: Main Propulsion System tank FE-analysis Stress result for 3 mm element size, after the wall thickness reduction iteration, ANSYS 2019.

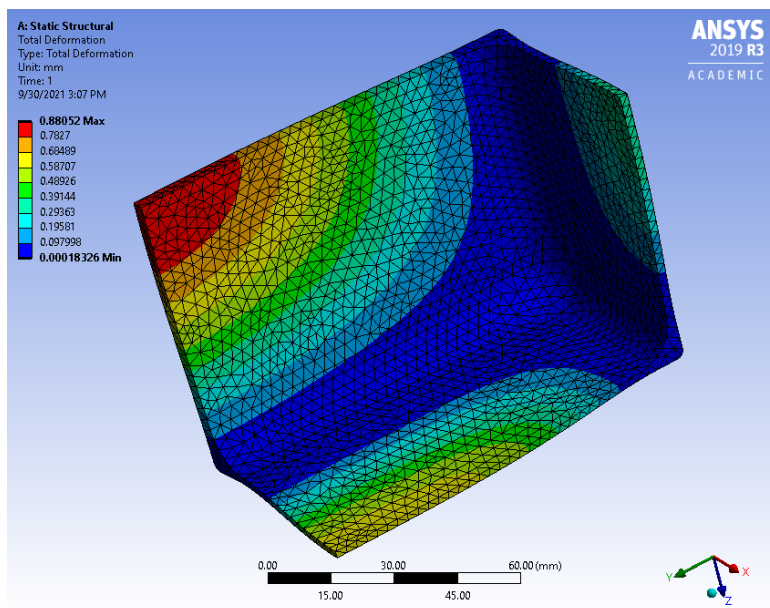


Figure E.12: Main Propulsion System tank FE-analysis Deformation result for 3 mm element size, after the wall thickness reduction iteration, ANSYS 2019.

Element Size of 5 mm - After Wall Thickness Reduction Iteration

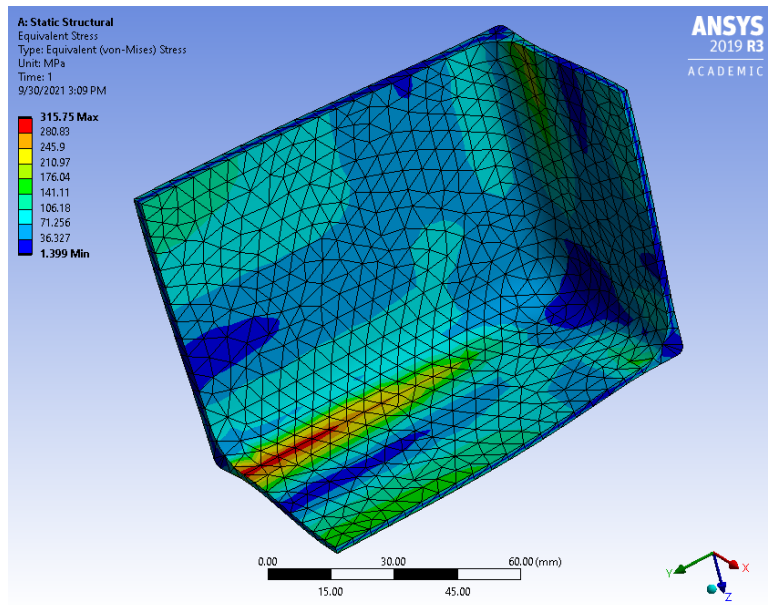


Figure E.13: Main Propulsion System tank FE-analysis Stress result for 5 mm element size, after the wall thickness reduction iteration, ANSYS 2019.

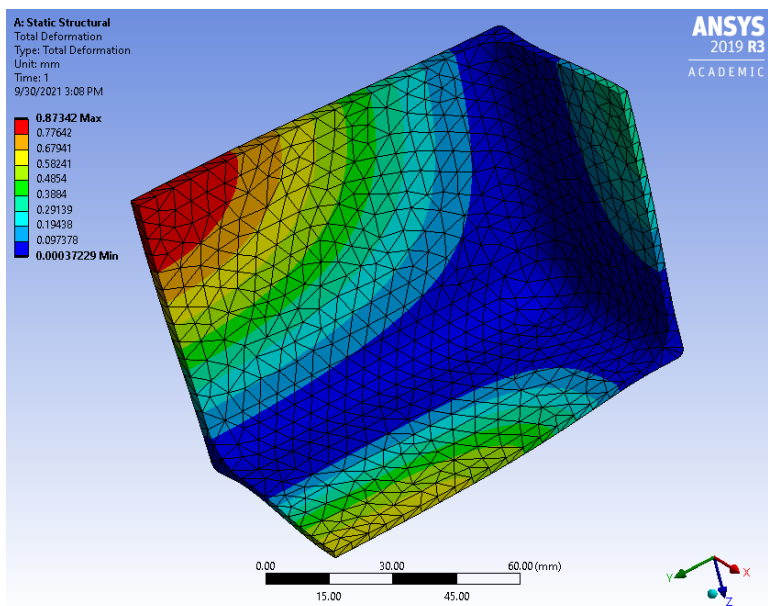


Figure E.14: Main Propulsion System tank FE-analysis Deformation result for 5 mm element size, after the wall thickness reduction iteration, ANSYS 2019.

Element Size of 10 mm - After Wall Thickness Reduction Iteration

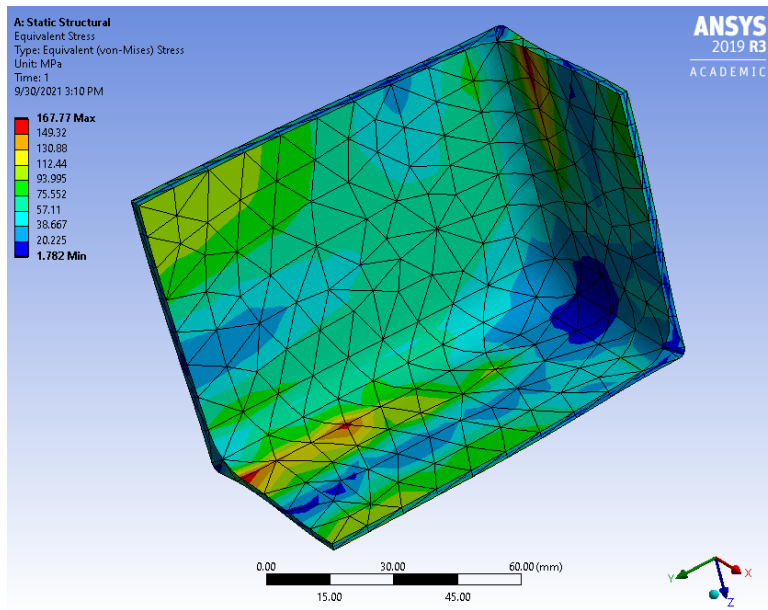


Figure E.15: Main Propulsion System tank FE-analysis Stress result for 10 mm element size, after the wall thickness reduction iteration, ANSYS 2019.

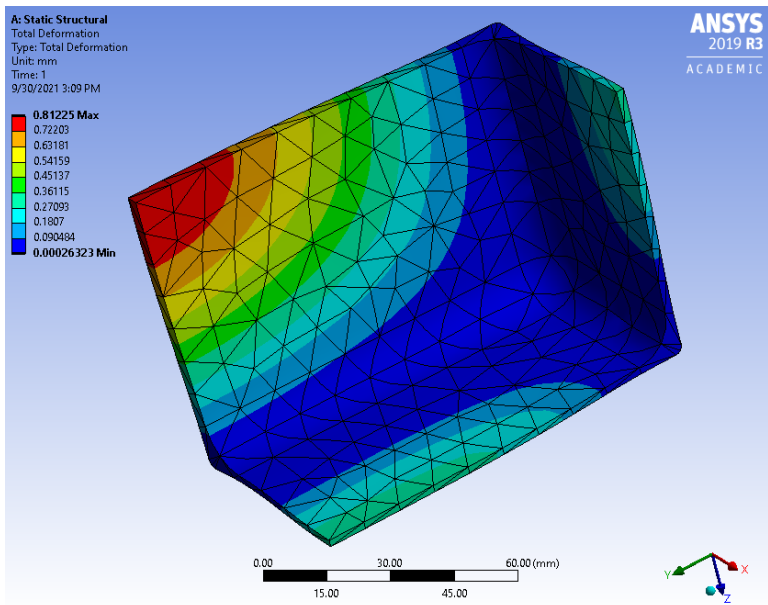


Figure E.16: Main Propulsion System tank FE-analysis Deformation result for 10 mm element size, after the wall thickness reduction iteration, ANSYS 2019.

E.2. Reaction Control System

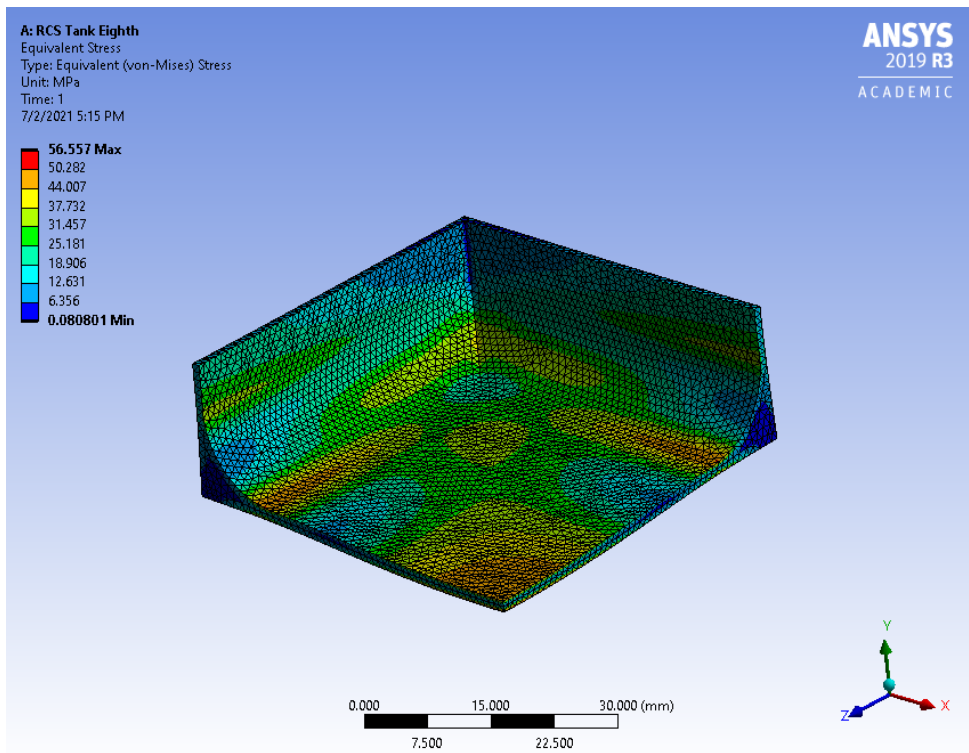


Figure E.17: Von Mises stresses. Maximum: 56.557 MPa, minimum: 0.081 MPa, ANSYS 2019.

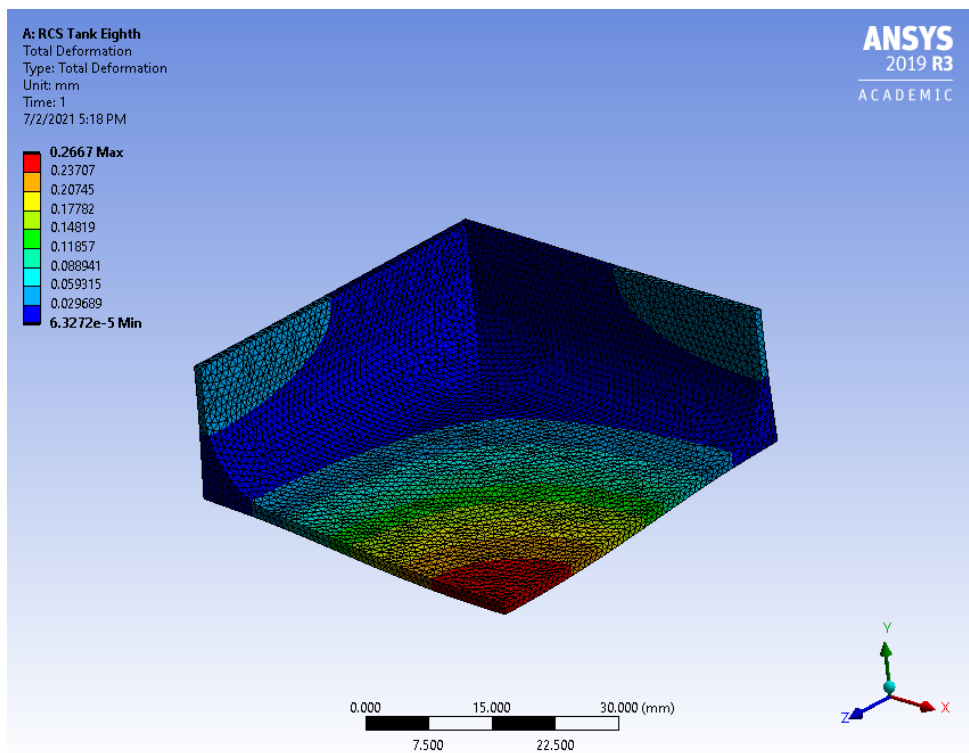


Figure E.18: Deformations. Maximum: 0.267 mm, minimum: 6.327 E-5 mm, ANSYS 2019.

E.2.1. Sensitivity Analysis for FE-Analysis 1 mm Element Size

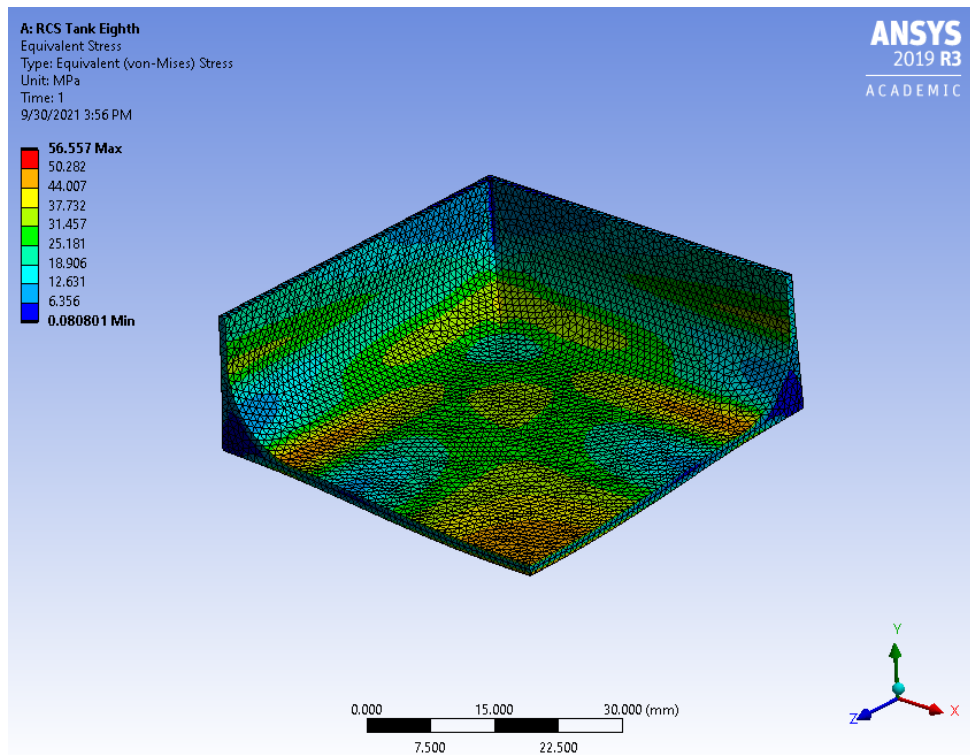


Figure E.19: Reaction Control System tank FE-analysis Stress result for 1 mm element size, ANSYS 2019.

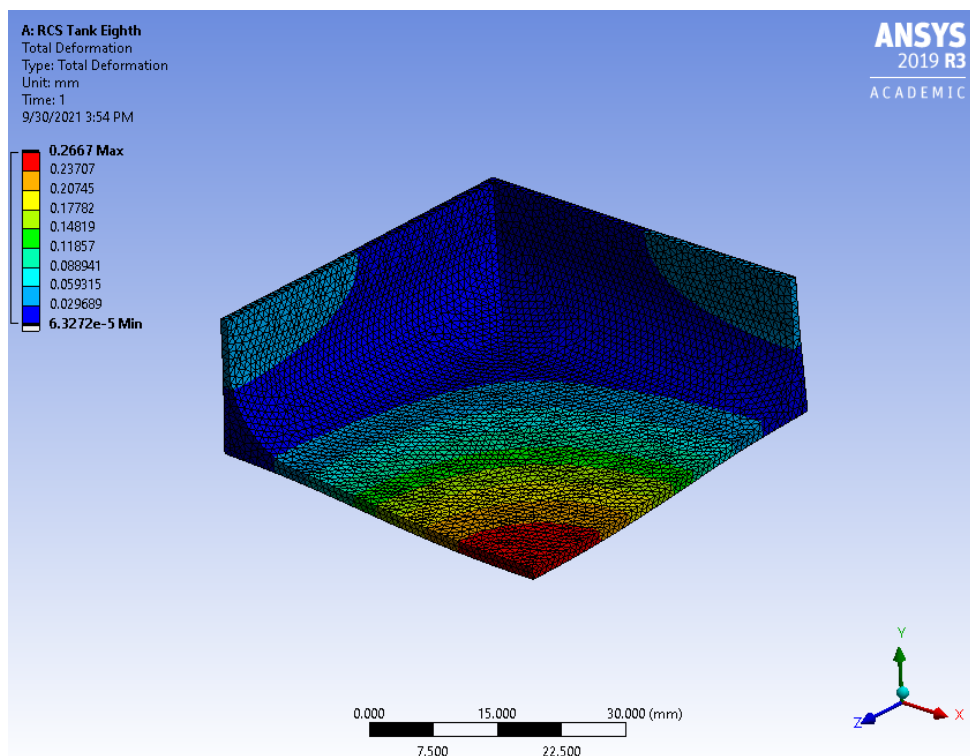


Figure E.20: Reaction Control System tank FE-analysis Deformation result for 1 mm element size, ANSYS 2019.

3 mm Element Size

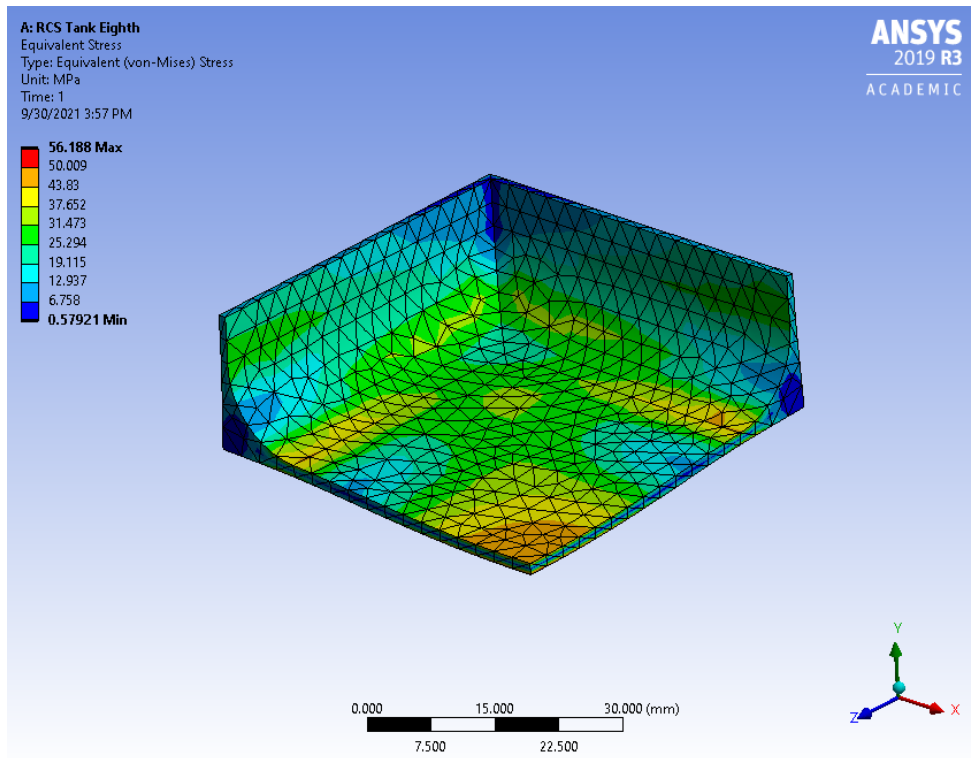


Figure E.21: Reaction Control System tank FE-analysis Stress result for 3 mm element size, ANSYS 2019.

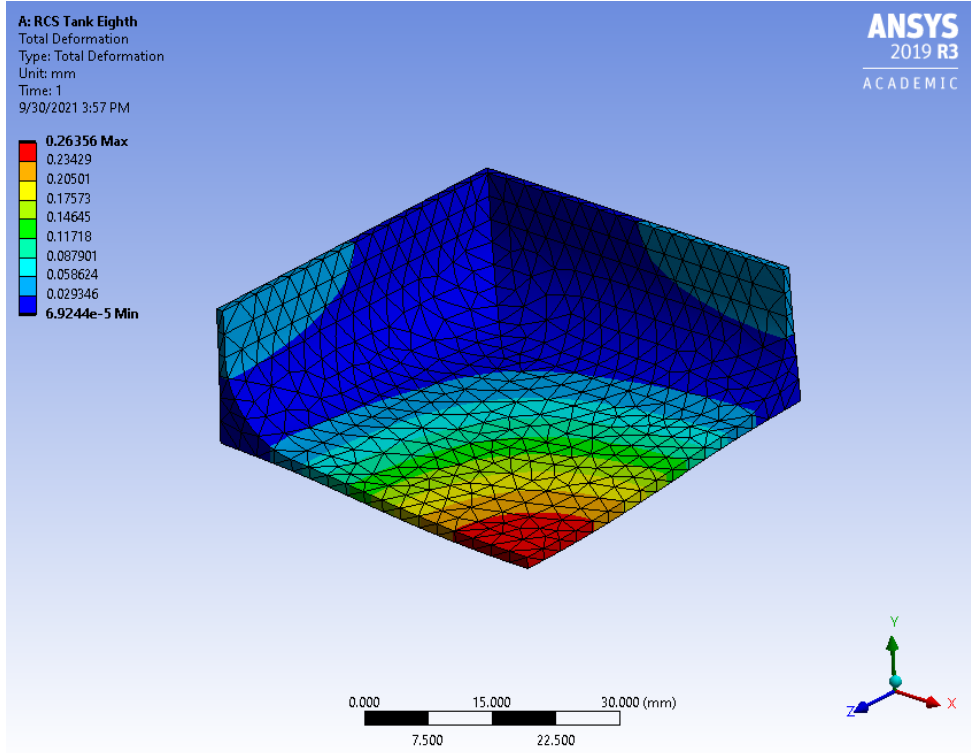


Figure E.22: Reaction Control System tank FE-analysis Deformation result for 3 mm element size, ANSYS 2019.

10 mm Element Size

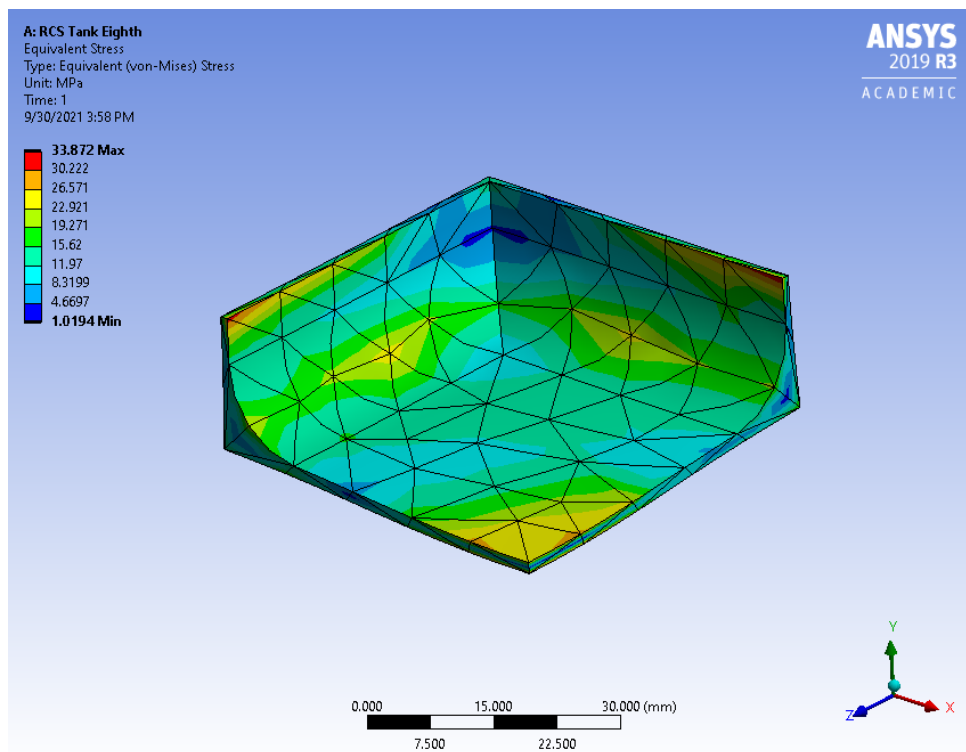


Figure E.23: Reaction Control System tank FE-analysis Stress result for 10 mm element size, ANSYS 2019.

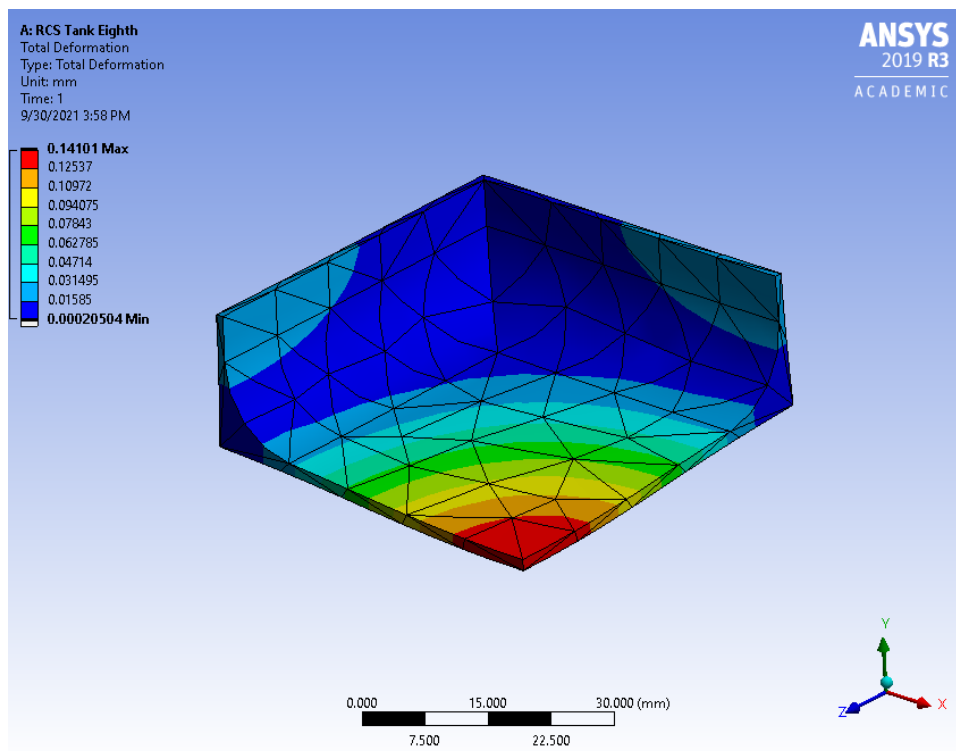


Figure E.24: Reaction Control System tank FE-analysis Deformation result for 10 mm element size, ANSYS 2019.